2019

The role of CD133 in mouse incisor tooth epithelium

Singer, Donald

UNIVERSITY OF PLYMOUTH

The role of CD133 in mouse incisor tooth epithelium

by

Donald Singer

A thesis submitted to the University of Plymouth
in partial fulfilment for the degree of

DOCTOR OF PHILOSOPHY

Peninsula Dental School

March 2019

Copyright Statement

Abstract

Mister Donald Singer

THE ROLE OF CD133 IN MOUSE INCISOR TOOTH EPITHELIUM

Since its discovery, CD133 has been used to identify, isolate and characterise many different stem cell types across a wide variety of tissues. Nonetheless, to date not much has been elucidated about its function in these cells. The continuously growing mouse incisor contains a large population of epithelial stem cells that drive the constant need for enamel generation. Using this model, this project aims to elucidate the role of CD133 in epithelial stem cell renewal and activation.

After validating the presence of CD133 in the developing mouse incisor epithelium, this project compared the dental epithelial stem cell dynamics of wildtype mice versus *CD133* KO mice. Mutant mice displayed significant anomalies across the whole dental epithelium, ultimately, leading to defects in the enamel, the product of fully differentiated ameloblasts.

Subcellular analysis of the dental incisor epithelium in *CD133* KO mice revealed disturbed primary cilia homeostasis. Primary cilia are crucial in interpreting extracellular cues and CD133 KO primary cilia specifically fail to transmit Shh-mediated signals. Further investigation of the functions of CD133 revealed that CD133 is important for the sequential recruitment of Arl13b and Hdac6 to the primary cilium regulating proper ciliogenesis.

Establishment of an *in vitro* cell culture model of dental epithelial cells allowed the investigation of nuclear CD133 under normal physiological conditions. To date, nuclear CD133 has been reported in a variety of cancers. This study provides insight into the formation of the CD133-Glis2 complex in the nucleus. This complex regulates the expression of Stat3, an important regulator of stem cells, in the dental epithelium.

In summary, this study has elucidated the importance of CD133 on primary cilium homeostasis, which in turn regulates stem cell renewal and activation in the developing incisor epithelium.

Table of Contents

Table of Figures

Table of Abbreviations

Abbreviation	Full name
AA	amino acid
AcTub	acetylated α-Tubulin
Ambn	Ameloblastin
AmelX	Amelogenin
Ant	Anterior
APC	Adenomatous polyposis coli
Arl13b	ADP ribosylation factor-like GTPase 13B
Arnt	Aryl hydrocarbon receptor nuclear translocator
ASPA	Animals Scientific Procedures Act 1986
Bmi1	B lymphoma Mo-MLV insertion region 1 homolog
BMP	Bone morphogenetic protein
bp	basepair
BrdU	5-bromo-2'-deoxyuridine
CD	Cluster of differentiation antigen
cDNA	Complementary deoxyribonucleic acid
CDS	Coding sequence
Cdt1	Chromatin licensing and DNA replication factor 1
CEP97	Centrosomal protein 97
ChIP	Chromatin immunoprecipitation
CLE	Cervical loop epithelial
CoIP	Co-immunoprecipitatation
CP110	Centriolar coiled-coil protein 110
CTGF	Connective tissue growth factor
DAPI	4',6-diamidino-2-phenylindole
DEPC	Diethylpyrocarbonate
DKK1	Dickkopf WNT signaling pathway inhibitor 1
DMEM	Dulbecco modified Eagle's medium
DNA	Deoxyribonucleic acid
DPLA	Duolink® proximity ligation assay
E	embryonic day
ECL	Extracellular loop
EGFP	Enhanced green fluorescent protein
EGFR	Epidermal growth factor receptor
ELK1	ETS transcription factor
EpCAM	Epithelial cell adhesion molecule
esiRNA	Endoribonuclease-prepared short interference RNA
EX	Extracellular
EYFP	Enhanced yellow fluorescent protein
FBS	Fetal bovine serum
FGF	Fibroblast growth factor
FITC	Fluorescein isothiocyanate
FSC	Forward scatter
FUCCI	Fluorescence-acquired ubiquitination cell cycle indicator

GapDH	Glyceraldehyde-3-phosphate dehydrogenase
GFP	Green fluorescence protein
Gli1	Glioma-associated oncogene homolog 1
Glis	Gli-similar
GSK3β	Glycogen synthase kinase 3 beta
H2B-GFP	Histone 2B-GFP
HBSS	Hank's balanced salt solution
HCC	Hepatocellular carcinoma
HDAC	Histone deacetylase
HERS	Hertwig's epithelial root sheath
Hh	Hedgehog
HIF1/2a	Hypoxia-inducible factors 1/2 alpha
HLA-DR	Major histocompatibility complex, class II, DR
Hox	Homeobox
HRP	Horseradish peroxidase
IC	Intracellular
ICD	Intracellular C-terminal domain
IGF1R	Insulin-like growth factor 1 receptor
IP	Immunoprecipitation
IR	Infrared
Irf1	Interferon regulatory factor 1
Jak	Janus kinase
kb	kilobasepair
kDa	kiloDalton
Ki67	Marker of proliferation Ki-67
KIF24	Kinesin family member 24
KLK4	Kallikrein-related peptidase 4
KO	Knockout
lacZ	β-galactosidase
LCM	Laser capture microdissection
Lef	Lymphoid enhancer binding factor
Lgr5	Leucine-rich repeat-containing G protein-coupled receptor 5
Lrp	LDL receptor related protein
MAP2K1	Mitogen-activated protein kinase kinase 1
MARK4	Microtubule affinity regulating kinase 4
MDCK	Madin-Darby canine kidney
MMP3	Matrix metalloprotease 3
MOB1	Mps one binder kinase activator-like 1
mRNA	messenger ribonucleic acid
MSX2	Msh Homeobox 2
Nanog	Nanog homeobox
ND	Not detected
NEDD9	Neural precursor cell expressed, developmentally down-regulated 9
NEK2	NIMA-related kinase 2
neo	Neomycin phosphotransferase

NLS	Nuclear localisation signal
NOD/SCID	Non-obese diabetic/severe combined immunodeficiency
NSCLC	Non-small cell lung cancer cells
Oct4	POU class 5 homeobox 1
P	Postnatal day
p53	Tumour suppressor protein p53
PAX2	Paired box 2
PBS	Phosphate-buffered saline
PCDH21	Protocadherin 21
PcG	Polycomb group
PCR	Polymerase chain reaction
PDGFR	Platelet-derived growth factor receptor
PDZ	PSD95/Dlg/ZO-1
PEN	Polyethylene naphthalate
PFA	Paraformaldehyde
PGR	Progesterone receptor
PI3K	Phosphoinositide 3-kinase
PIFO	Pitchfork
Pitx2	Paired-like homeodomain 2
PLA	Proximity ligation assay
PLK4	Polo-Like Kinase 4
Post	posterior
Prc	Plolycomb repressive complex
Pse	Posterior sex comb
PTCH	Patched
PVDF	Polyvinylidene fluoride
qPCR	quantitative polymerase chain reaction
RFP	Red fluorescence protein
ROI	Region of interest
RTK	Receptor tyrosine kinase
SEM	Scanning electron microscope
Shh	Sonic hedgehog
shRNA	short hairpin-ribonucleic acid
Smo	Smoothened
Socs3	Suppressor of cytokine signaling 3
Sox2	Sex-determining region Y-box 2
Spry	Sprouty
SSC	Sideward scatter
STAT	Signal transducer and activator of transcription
TEK	Tyrosine kinase, endothelial
Tgfβr	Transforming growth factor beta receptor
TTBK2	Tau tubulin kinase 2
UV	Ultraviolet
VDAC3	Voltage-dependent anion channel 3
Wnt	Wingless-Type MMTV integration site
WT	Wildtype

To

My mother

and

especially to

my partner

Lauren

and

my son

Jack

Acknowledgements

I would like to express huge thanks to my supervisors: Dr Bing Hu, Prof Christopher Tredwin, and Dr Denis Corbeil for their seemingly endless font of advice and enthusiasm; and Prof. Ophir Klein and Dr. Massimo Attanasio for their significant contributions.

I remain indebted to the BBSRC, Marie Curie Actions and NSFC for their kind provision of funds, without which this project would not have been possible.

My friends and family were a constant source of encouragement and support, as they always have been, and for this, I will always remain extremely thankful. My mother has always provided a reference point to aspire to and have shaped me into the person I am today.

Finally, I would like to thank my partner, Lauren, and my son Jack for their patience and forbearance during this long project, as well as their tolerance of my regular absence.

Authors Declaration

At no time during the registration for the degree of Doctor of Philosophy has the author been registered for any other University award without prior agreement of the Doctoral College Quality Sub-Committee.

Work submitted for this research degree at the University of Plymouth has not formed part of any other degree either at the University of Plymouth or at another establishment.

This study was financed with the aid of the European Union Marie Skłodowska-Curie actions (618930, OralStem FP7-PEOPLE-2013-CIG) a studentship from the Peninsula Dental School, University of Plymouth and carried out in collaboration with Technische Universität Dresden, University of California, UT Southwestern Medical Center, King's College London, and University of Oxford.

Publications (or presentation of other forms of creative and performing work):

Prominin-1 governs stem cell activation by orchestrating ciliary dynamics. The EMBO Journal (2018). DOI: 10.15252/embj.201899845

Presentation and Conferences Attended: ARSC 2014 Cornwall, BSODR 2015 Cardiff, ICDCSC 2016 Paris, ERSRAD 2016 Bradford, ARSC 2016 Cornwall, BSODR 2017 Plymouth, IADR 2018 London

Word count of main body of thesis: 51214

Signed…….

Date…….

Chapter 1. Introduction and Background

1.1 Stem cells

1.1.1 Definition and characteristics of stem cells

The existence of stem cells came to light from pioneering studies of Till and McCullogh on haematopoietic stem cells [1]. Since then, stem cells are defined as undifferentiated cells that are capable of giving rise to indefinitely more cells of the same type (self-renewal), and from which certain other kinds of cell arise by differentiation (potency, Figure 1)[2,3]. Factors that define 'stemness' are self-renewal or replication capacity, clonality, and potency [4,5].

Self-renewal

Most *in vitro* cultures of somatic cells are only capable of a finite number of population doubling eventually undergoing replication arrest or senescence [6,7]. Stem cells can create more stem cells. This phenomenon is called self-renewal and tissue homeostasis is dependent on the accurate regulation of stem cell activity to counter tissue damage and to proliferate according to tissue requirements [8].

Potency

Potency (Figure 1) refers to the capacity of stem cells to which they can differentiate into various cell types and is classified as follows:

A. Totipotency

Totipotent stem cells are considered as the only 'true' stem cells and are capable of differentiating into any cell type in the body as well as the extra-embryonic or

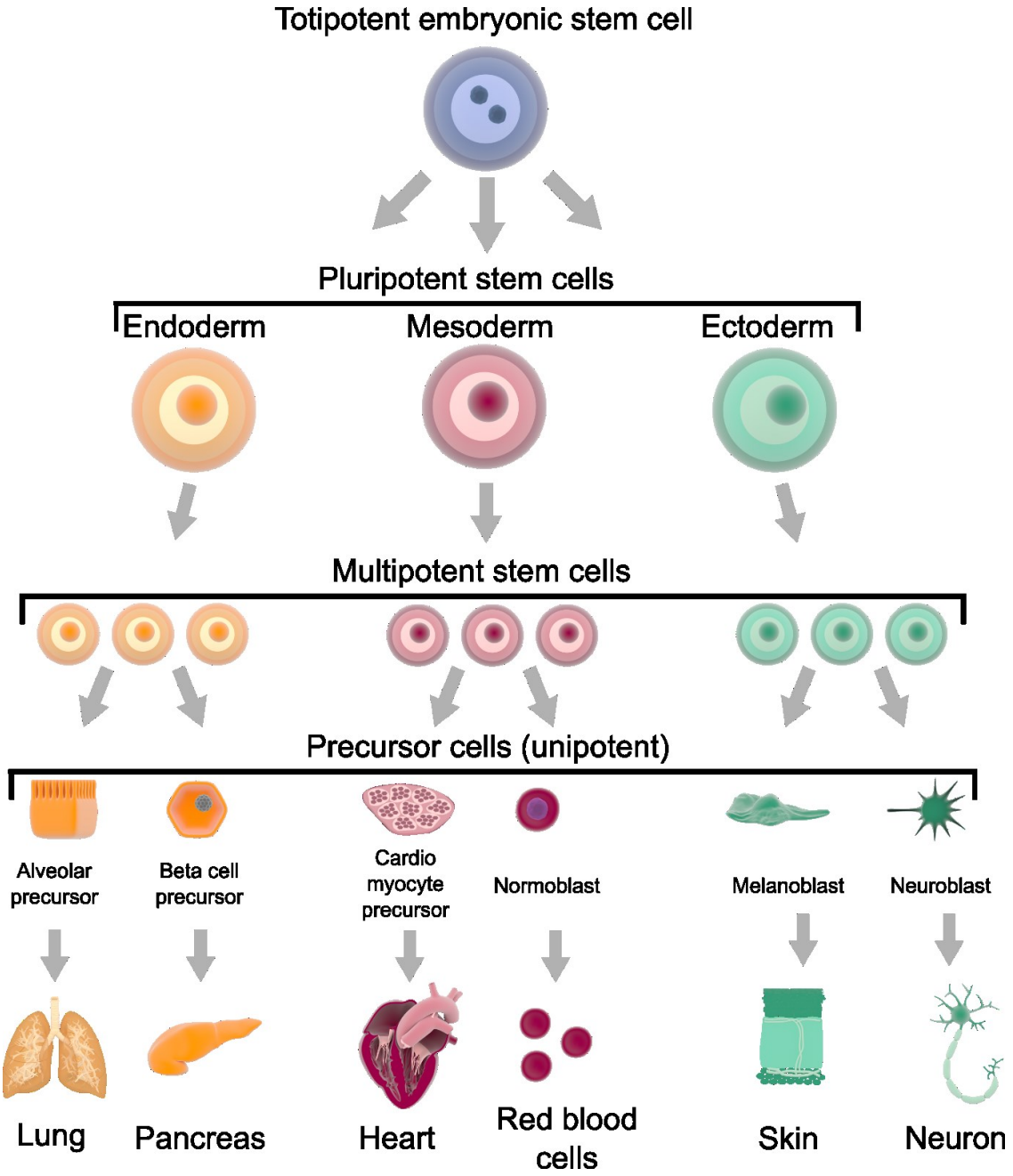

Figure 1: Potency of stem cells refers to its lineage differentiation potential.
Totipotent stem cells can generate all cells required to form an organism and its associated placenta. Pluripotent stem cells have the ability to produce cells that contribute to all three germ layers and are able to form a complete organism apart from the placenta. Multipotent stem cells are already committed to a specific germ layer and can only produce progeny of that germ layer. Unipotency refers to stem cells that can only lead to one type of specialised cell.

placental cells [9]. A zygote or fertilised egg and the blastocyst are the only source of totipotent stem cells that are capable of generating cells of all three germ layers (i.e., endoderm, mesoderm and ectoderm). Embryonic stem cells originate from the inner cell mass are currently being scrutinised as rapid progress in the stem cell field (i.e., cell reprogramming) are challenging these concepts[10].

B. Pluripotency

Pluripotent stem cells are derived from totipotent stem cells and can differentiate into any cell type of the organism except for extra-embryonic tissue. Embryonic stem cells derived from inner cell mass, embryonic germ cells and cord blood-derived stem cells are considered pluripotent and, therefore, capable of giving rise to tissues of all three germ layers[11–13].

C. Multipotency

Multipotent stem cells have a restricted differentiation potential compared to their pluripotent counterpart. Adult or somatic stem cells are considered multipotent as they can only generate cells of the tissue they reside in[14]. Examples include neuronal stem cells capable of generating neurons, oligodendrocytes and astrocytes, and haematopoietic stem cells which produce most blood cells[15,16].

D. Unipotency

Unipotent or precursor cells can only produce one cell type and have, therefore, a very limited differentiation potential. For example, cardiac precursor cells differentiate into cardiac muscle fibres only.

E. Induced pluripotency

In 2006, Yamanaka's lab showed that with the introduction of four transcription factors somatic cells could be reprogrammed to a more primitive state[17]. Since

then, different cell types and other combinations of reprogramming factors have been used to generate induced pluripotent stem cells[18]. Despite their enormous potential, the only clinical trial using induced pluripotent stem cells to treat macular degeneration was stopped after discovering that the used induced pluripotent stem cells carried potentially cancer-inducing mutations[19]. Currently, induced pluripotent stem cells provide an unlimited supply of once-inaccessible human tissues for research and are mostly used for modelling and investigating human diseases, on top of drugs screening.

1.1.2 Multipotent adult or somatic stem cells

Adult or somatic stem cells are undifferentiated cells, found in most organs of the body following development. They proliferate on appropriate cues to replenish dying cells and regenerate damaged tissues. Unlike embryonic stem cells, they can be found in juvenile as well as adult humans and animals. Scientific attention in somatic stem cells is focused on their ability to divide or self-renew for a prolonged period and produce all the cell types of the organ from which they derive. Unlike with embryonic stem cells, the use of human somatic stem cells in research and therapy is not considered controversial, as they are derived from adult tissue samples rather than human embryos.

Somatic stem cells are present throughout most tissues in the body, including but not limited to the bone marrow, the hair follicle, intestines and peripheral blood. They can be epithelial, nervous, adipose or mesenchymal in nature. The central view of a somatic stem cells, as with most other types of stem cells follows the traditional model that it is rare and spends the majority of its time in a ‘quiescent’, non-proliferative state as replication of its DNA carries the risk of mutation[20,21]. This can be experimentally distinguished from proliferating cells by the retention

of DNA labels[22,23]. However, the vast majority of cells in any tissue is in fact non-dividing. This dogma of a rare, quiescent stem cell capable of replenishing the whole tissue in a unidirectional manner stems from the haematopoietic stem cell, which was discovered in the 1960's[24].

The inhabitants of Nagasaki and Hiroshima who were exposed to low radiation fallout after the atomic bomb explosions died over time to a compromised haematopoietic system. Their weakened immune system did not allow the survivors to produce enough leukocytes to fight off infections or sufficient thrombocytes to prevent excessive bleeding. Follow up experiments on mice exposed to lethal radiation revealed that they could be saved when their spleen was protected from the lethal radiation[25]. In 1956, three research groups discovered independently the cause of regeneration of the haematopoietic system in the exposed mice. They determined that the transplanted cells were the progenitor cells responsible for the renewal of the haematopoietic system rather than acting indirectly by secreting factors that might enhance the repair of the compromised immune system of the host[26–28]. In the 1960's, increased use of radiation therapy to treat cancer sparked research into the sensitivity of bone marrow to radiation. Till and McCullogh used genetically labelled spleen cells to describe the two fundamental characteristics that are still used today to define adult stem cells: a quiescent cell with prolonged self-renewal capabilities and the ability to differentiate into all cells of the leukocyte and erythrocyte lineage (in the case of haematopoietic stem cells)[1].

Since then, the paradigm of a rare, quiescent haematopoietic stem cells that gives rise to all types of blood cells has served as a template to interpret experimental observations for all adult tissues. In addition to haematopoietic stem

cells in the bone marrow, the intestinal crypt and hair follicle have been widely used as a model to study somatic stem cells in self-renewal and activation.

The intestinal crypt as a model

The intestinal epithelium lining the crypt contains continuously proliferating Leucine-rich repeat-containing G-protein coupled receptor 5 (Lgr5) -positive stem cells that are located at the base of the crypt, whereas a 'backup' quiescent stem cell sits at position +4 counted from the crypt base[29]. Until recently, these +4 cells were thought to be the source of the proliferative Lgr5 cells but genetic tracing studies revealed a second alternative mechanism: +4 cells are daughters, which have left the cell cycle prior to terminal differentiation into secretory cells[30,31]. However, loss of the Lgr5+ stem cells after injury can persuade +4 cells to repopulate the Lgr5+ cells at the crypt's base and regain a stem cell phenotype. In normal homeostasis, these quiescent +4 cells are transient and short-lived as they will become secretory cells and die. In injury, these cells show remarkable plasticity and serve as a 'backup' stem cell pool to replenish the Lgr5+ multipotent stem cells. This observation challenges the concept of a unidirectional flow from stem cell to differentiated cell.

The hair follicle as a model

The hair follicle serves as an excellent model to study stem cell biology. Each hair follicle consists of a permanent part including the sebaceous gland, the dermal papilla (DP) and the bulge region, and a cycling segment that cycles through telogen (resting phase), anagen (growth phase) and catagen (retraction phase)[32].

Cells present in the bulge, a reservoir of epithelial stem cells, are able to retain Histone 2B-GFP signal and the majority of them express CD34, a well-known

stem cell marker. Grafting of these cells into nude mice resulted in the generation of entire hair follicles[33–35]. The mesenchymal dermal papilla at the base of the hair follicle signals to the quiescent stem cells in the bulge and regulates their activation. Interestingly, not all bulge stem cells become activated during the anagen phase, suggesting that this stem cell population is heterogeneous in terms of the cell cycle state and that not all cells are involved in regeneration of the hair follicle[36].

1.1.3 Somatic stem cells and the extracellular micro-environment

The extracellular micro-environment or niche impacts cell behaviour within a tissue, including stem cells. The extracellular micro-environment in which a stem cell resides affects the cells survival, self-renewal and differentiation[37]. Many components form part of the extracellular micro-environment including resident cells[38], secreted and membrane-bound factors[30,38–40] and insoluble matrix molecules[41,42] (Figure 2). All these features can lead to changes within the extracellular micro-environment (e.g. recruitment of immune cells) or stem cells itself such as proliferation, differentiation and apoptosis.

Resident niche cells

In most tissues, the stem cell niche holds many different cell types. This is clearly illustrated in the case of the haematopoietic system within the bone marrow. Osteoblastic, neuronal and endothelial cells, megakaryocytes, macrophages as well as other immune cells all contribute to defining distinct haematopoietic stem cell niches[43]. In the colon and intestine, critical players in maintaining the niche are the progeny of the stem cells. For instance, in the colon, goblet cells which express epidermal growth factor (EGF), c-KIT and NOTCH ligands co-localise with and thus support the stem cells in their niche[44]. In the small intestine, stem

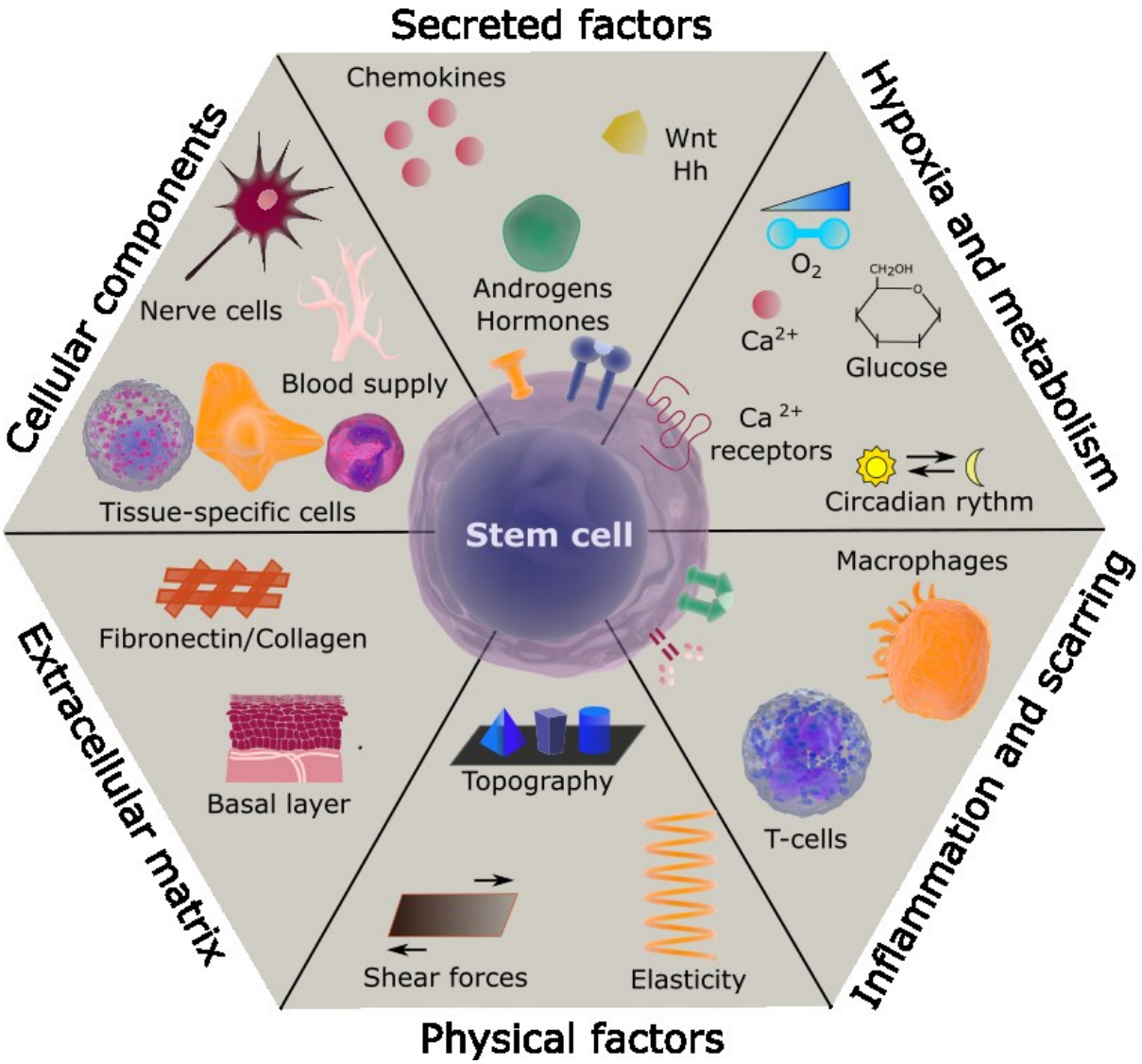

Figure 2: Factors in the extracellular microenvironment that affect stem cells.
The extracellular micro-environment is a complex, heterotypic and dynamic structure including different cellular components, secreted factors, immunological response, physical interactions and metabolic control. Stem cells and the extracellular micro-environment act in a bi-directional and reciprocal manner. Many features are shared between stem cells and their niches in different tissues (Adapted from [37]).

cells maintain their stemness partially through paracrine signalling of Wingless-Type MMTV Integration Site 3a (WNT3a), EGF and NOTCH[45,46]. Consequently, separate niches exist in different parts of the intestinal tract, which contribute to tissue homeostasis. In the hair follicle, neural Sonic hedgehog (SHH) is vital in maintaining the biological potential of the bulge stem cell in the telogen phase[47].

Inflammation

Endothelial cells, connective tissue and nerve cells are considered permanent residents within the stem cell niche. Whereas immune cells and cells, responding to tissue damage, would be more transient in nature to fight pathogens or to promote healing. Migration of cells of the adaptive and innate immune system can affect stem cell behaviour. Most stem cell niches are 'immune-privileged' meaning that mechanisms exist that protect the cells from immune response [48]. For instance, in the bone marrow, regulatory T-cells create pockets of immune privilege where haematopoietic stem cells reside to evade immune responses[49]. This protective mechanism is currently being exploited in clinical trials to prevent rejection of transplanted tissues.

Secreted factors

Communication between stem cells and other resident cells in the niche is partially facilitated by secreted factors including cytokines and hormones [50,51]. These factors control many processes during development including cell proliferation, differentiation, morphogenesis, tissue organization, and angiogenesis. Furthermore, in adult tissues, they are involved in wound healing, regulating metabolism and maintaining homeostasis[52]. Permanent activation of growth factor signalling is often seen in and tumourigenesis [53]. Two of the most

prominent secreted factors in controlling stem cell fate are WNT and Sonic hedgehog (SHH)[54].

Most stem cell populations are partially regulated by WNT signalling and changes in WNT activity in the stem cell compartment has inherent effects both on those cells and on other resident cells[55]. For instance, an increase in WNT activity in the epidermis leads to an increase in stem cell number and induces hair follicle differentiation, whereas the dermis takes on the features of neonatal dermis[56–58].

Another pathway that is important in the stem cell niche is hedgehog signalling. SHH is the best-studied ligand in hedgehog signalling and is a classic example of a morphogen. Typically, the secreted ligand diffuses through the surrounding tissues creating a concentration gradient. This gradient determines the patterning of organs such as the limb[59], midline structures of the brain [60] and teeth [61] and represents the process of differentiation of stem cells into different cell types.

Hypoxia and metabolism

Many stem cell populations exist in a hypoxic microenvironment that facilitates their survival and maintenance. Hypoxic cells undergo glycolysis instead of mitochondrial oxidative phosphorylation[62]. This switch in metabolism prevents the generation of reactive oxygen species in stem cells, thereby, minimizing the risk of DNA damage[63]. Indeed, *In vitro* culture of different mammalian stem cells under hypoxia promotes their proliferation, survival and functions after grafting. Likewise, in the bone marrow, hypoxia improves quiescence and renewal in haematopoietic stem cells[64,65]. It is clear that cellular metabolism plays a fundamental role in proliferation, differentiation and quiescence and the shift in glycolysis, mitochondrial oxidative phosphorylation and oxidative stress

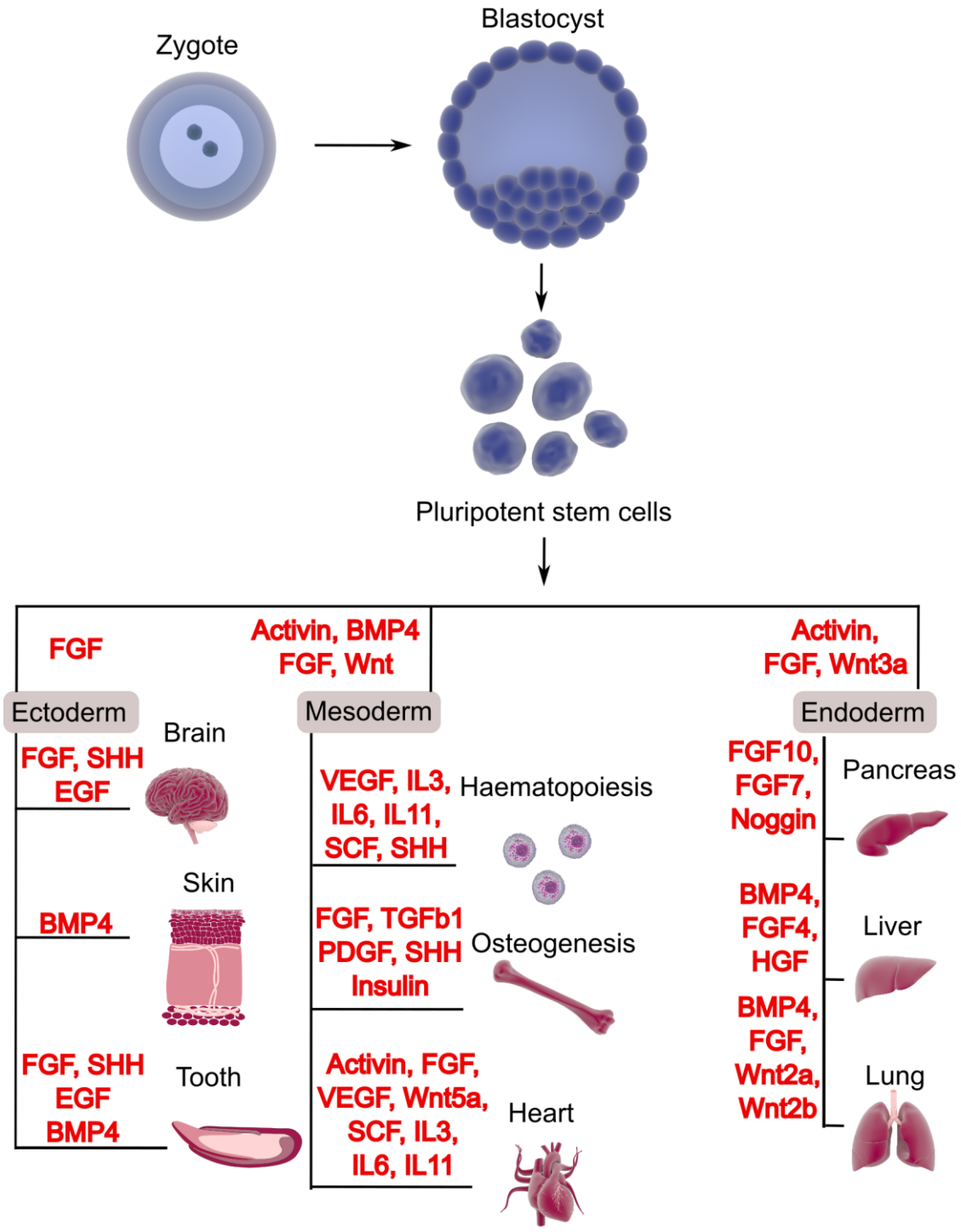

Figure 3: Role of secreted factors in specifying cell fate
Lineage relationship between secreted factors, and germ layer and tissue specification from pluripotent stem cells. Secreted factors are marked in red. Adapted from *Benvenisty et al*[450].

during the maturation of somatic stem cells can be used for novel metabolic therapies to enhance regeneration[66].

Extracellular matrix

The extracellular micro-environmentnis the 3D structure in which the stem cell resides and is a significant factor of the stem cell niche in virtually all tissues. Its composition and the nature of its interactions with stem cells differ substantially, even within the same tissue[67]. Extracellular micro-environment components are produced and secreted by resident cells and, typically, consists of an intertwining network of fibrous proteins and glycosaminoglycans.

It is well established now that the extracellular micro-environment tethers stem cells as well as direct their fate[68]. Anchoring of stem cells within the extracellular micro-environment leads to changes in intracellular signalling pathways of which many have been uncovered. The extracellular micro-environment also retains secreted factors, acting as a reservoir to increase the local concentration to which recipient cells are exposed [69]. Integrins are the major molecules involved in interactions between the cell and the extracellular micro-environment, and abnormal integrin signalling has been linked to many pathologies including cancer[70]. Integrins bind to their extracellular substrates, such as Laminins and Fibronectin, to direct differentiation of stem cells of all three germ layers and are to be considered as a candidate for *in vitro* differentiation of stem cells alongside the use of soluble factors to overcome the low success rate of generating mature cell types[71].

Physical factors

Historically, changes in stem cell behaviour, both *in vivo* and *in vitro*, has been ascribed predominantly to genetic and molecular factors such as growth factors

and transcription factors. Stem cell fate, however, also depends on signals from the extracellular micro-environment such as substrate elasticity and stiffness, shear forces and physical shape often mediated by Integrin substrate interactions. These mechanical forces have been used to expand stem cell populations, such as skeletal muscle stem cells and haematopoietic stem cells[72,73]. Chemical agents that affect the balance between elastic (e.g., cartilage, connective tissue) and rigid (e.g., bone) factors are already being used to treat metastatic bone cancers and osteoporosis. Also, distinctive niche topographies are known to promote cytoskeletal rearrangement in stem cells and this, in turn, induces specific differentiation signalling pathways[74,75].

1.1.4 Identification of somatic stem cells

Those extrinsic factors provided by the extracellular environment affect intracellular pathways or intrinsic factors within somatic stem cells leading to changes in its proliferation and differentiation. Intrinsic factors represent mainly transcription factors, which act to 'translate' the extracellular cues into appropriate gene transcription to facilitate renewal, proliferation or differentiation. The importance of transcription factors in achieving stem cell identity has been demonstrated more than ten years ago with the introduction of four transcription factors into murine embryonic fibroblasts pushing them into a pluripotent state[17]. Somatic stem cells express intrinsic factors in a tempo-spatial manner that makes them distinguishable from other cells within their niche.

One such factor is SOX2, a member of the SRY-related High Mobility Group family. SOX2 is essential during early embryonic development as has been demonstrated by the failure of SOX2 KO embryos to develop past the epiblast stage [76]. Moreover, it has been shown that SOX2 also marks long-lived somatic

stem cells to regulate homeostasis in a broad range of adult epithelial tissues including the stomach, cervix, testes, lens and several glands[77]. During development of the mouse incisor, SOX2 expression is universal during early tooth morphogenesis and becomes increasingly restricted to the proximal tip of the incisor, which has been shown to harbour label-retaining cells, a marker for quiescence. SOX2+ dental epithelial cells give rise to all epithelial lineages and persists throughout the animal's life[78]. SOX2 maintains stemness in concert with partner transcription factors in a tissue-specific way. A classic example is POU Class 5 Homeobox 1 (POU5F1, previously known as OCT3/4) which regulates the expression of genes necessary to maintain pluripotency and in embryonic development[79]. SOX2 is also implicated in chromatin remodelling in neural stem cells through binding to the ATPase Cadherin 7 (CDH7), member of the of the chromodomain helicase DNA-binding domain family of ATP-dependent chromatin remodellers.

Another chromatin remodeller associated with somatic stem cells is the polycomb group gene B Lymphoma Mo-MLV Insertion Region 1 Homolog (BMI1) that forms a complex to negatively regulate gene expression through ubiquitination of histone 2A. Only tri-methylated histones at lysine 27 are targets of the complex leading to the formation of heterochromatin[80]. However, recently it has been shown that BMI1 can positively influence gene expression independently of the complex[81]. In the continuously growing mouse incisor, BMI1+ cells mark the same region as SOX2+ cells and deletion of BMI1 results in fewer stem cells and aberrant enamel production due to derepression of the *Ink4a/Arf* locus and several homeobox genes[82]. Several pathways converge on BMI1 to regulate stem cell dynamics in a variety of tissues. For instance, hedgehog signalling is dependent on BMI1 to regulate stem cell renewal and proliferation in mammary

glands[83]. Whereas in the intestinal crypt, BMI1 is downstream of both Notch and WNT signalling and deletion of BMI1 leads to loss of the stem cell pool and increase of differentiation into goblet cells[84].

Lgr5, a class A G-protein coupled receptor involved in Wnt-signalling, has gained traction as a somaric stem cell marker when it was discovered that the receptor marks slow-cycling cells in the intestinal crypt, capable of generating all six differentiated epithelial cell types that line the crypt[451, 452] (see chapter 1.1.3: the intestinal crypt as a model). Since then its use as a somatic stem cell marker has expanded to other tissues including the mouse incisor. In the mouse incisor, LGR5 marks a subpopulation of Sox2+ stem cells and loss of Sox2 leads to a diminished LGR5+ cell population and reduction of the stem cell population in general. However, Sox2- cells within the stellate reticulum quickly replenish the Sox2+ stem cells including the LGR5+ subpopulation[454]. This phenomenom is also seen in the intestinal crypt where ablation of LGR5+ stem cells are rescued by a BMI1+ stem cell population to restore tissue homeostasis[412].Isolation of stem cells is often achieved using cell surface markers that are categorised as a cluster of differentiation antigens (CD). These cell surface markers have established the field of haematopoiesis and our understanding of existing subpopulations within blood[85]. CD antigens belong to different classes such as receptors, adhesion molecules, glycoproteins and integrins. Currently, there are 371 different proteins classed as CD antigens in humans (as of May, 2018)[86]. Different cell types display different CD antigens, and we are just beginning to understand the CD antigen signatures that are present in specific cell types. Several CD antigens are linked with human and mouse embryonic stem cells. CD9, a tetraspanin glycoprotein, is known to be highly expressed in mouse and human embryonic stem cells and rapidly lost upon differentiation. Its high expression in stem cells

is regulated via the LIF, Interleukin 6 Family Cytokine/ Signal Transducer And Activator Of Transcription 3 (LIF/STAT3) pathway[87]. Other CD antigens that are linked with pluripotent embryonic stem cells are CD24, CD30, CD90, CD133, CD200, and CD326[88–92]. In mesenchymal cell populations, it has been well established that ≥95% of the cells have to express CD73, CD90, and CD105 and ≤2% must not express CD34, CD45, CD14 or CD11β, CD79α or CD19 and Major Histocompatibility Complex, Class II, DR (HLA-DR)[93]. Despite their established expression profiles in a wide range of cell populations, only a fraction of CD antigens has been characterised. For instance, CD133 has been used as a stem cell marker in a wide variety of tissues. However, its function within those tissues has not been elucidated yet. In addition, in recent years its expression has also been shown to be in terminally differentiated cells questioning its use as a stem cell marker[94]. This observation might hold true for many CD antigens of which the function has not been determined yet.

1.1.5 Clinical relevance and limitations on the use of stem cells.

For over 40 years, the most widely used stem cell therapy is bone marrow transplant in patients suffering from leukaemia and lymphoma. This allows the patient to receive high dose treatment of chemo and radiation therapy. In recent years, other therapies have been approved including the production of skin grafts from adult hair follicle stem cells[95] or repairing corneal transparency using kerato-limbal stem cells[96]. These treatments are generally recognized as safe and effective in the medical field. Despite these advancements, there remain certain risks that currently limit the use of stem cells. These risks depend on many factors such as the source of stem cells as illustrated briefly in Table 1. Embryonic stem cells were initially the main type of stem cells used due to their ability to differentiate in every somatic cell type. However, embryonic stem cells being

allogenic in nature often required immunosuppressants to avoid rejection[97,98]. In addition, these cells also displayed a propensity to form tumours and its use in clinics is highly controversial because its generation involves the destruction of an embryo[99–101].

The use of induced pluripotent stem cells, another pluripotent stem cell type, in clinics is also limited. As with embryonic stem cells, induced pluripotent stem cells are likely to form teratomas in recipients[102]. Moreover, reprogramming efficiencies of somatic cells, albeit improved, remain low[17,103]. However, reprogramming efficiencies are currently undergoing intensive research as induced pluripotent stem cells avoid two drawbacks in the use of embryonic stem cells in clinics: ethical concerns and potentially immune rejection when autologous somatic cells are used. At present, the first clinical trial is underway using allogenic induced pluripotent stem cells that are reprogrammed to retinal cells. A similar clinical trial using autologous induced pluripotent stem cells was aborted in 2014 due to the presence of genetic abnormalities in cells prepared for the second patient[104].

Despite their potential in regenerative medicine, embryonic stem cells and induced pluripotent stem cells present issues that are difficult to overcome. Hence, they are underrepresented in clinical trials. Multipotent somatic stem cells are in essence already committed to a specific lineage, generating intended cell types is comparatively easy, and the possible risk for tumourigenesis is low.

Mesenchymal stem cells are the most common type of multipotent somatic stem cells and are of great interest to the scientific community, as they do not present the same ethical and immunological concerns as with induced pluripotent stem cells and embryonic stem cells. Mesenchymal stem cells are present in many

	Embryonic stem cells	Induced pluripotent stem cells	Somatic stem cells
Origin	Derived from inner cell mass of blastocyst	Derived from somatic cells	Isolated from adult tissue
Donor	Allogenic tissue	Autologous or allogenic tissue	Autologous or allogenic tissue
Potency	Pluripotent	Pluripotent	Multipotent
Differentiation potential	Can differentiate in cell types of all three germ lineages	Can differentiate in cell types of all three germ lineages	Can differentiate in limited cell types depending on the tissue of origin
Self-renewal capacity	Unlimited self-renewal	Unlimited self-renewal	Limited self-renewal
Hayflick limit	Indefinite growth	Indefinite growth	Limited lifespan (population doublings)
Teratoma risk	Significant	Significant	No
Ethics	Serious ethical issues	No ethical issues	No ethical issues
Immuno-privilege	Low level of MHC I and II	Not immuno-priviliged when derived from adult cells. Normal level of MHC I and II.	Mesenchymal stem cells have low immunogenicity and are immunomodulatory. Not known for other somatic stem cells.
Risk of immune rejection	Cell lines will be allogenic	HLA-matched induced pluripotent stem cells have less chance of immune rejection	Autologous somatic stem cells have less chance of immune rejection

Table 1: Characteristics and considerations of different stem cells in therapy

tissues including skin, bone marrow, adipose tissue, intestines and the umbilical cord and are, therefore, accessible. However, mesenchymal stem cells often make up only a fraction of the adult tissue and are, consequently, difficult to isolate but have the potential to differentiate into ectodermal and mesodermal lineages such as dopaminergic neurons, cartilage, hepatocytes, smooth muscle, pancreatic cells, cardiomyocytes, neuronal cells and osteoblasts[105]. Similar as with mesenchymal stem cells , epithelial stem cells have the same advantages and limitations in therapy and their use in forming skin grafts has saved lives of many severe burn victims[106]. In spite of this early success, epithelial stem cell isolation and *in vitro* expansion from other tissues has been met with considerable difficulties until recently as is demonstrated in the successful long-term engraftment of murine intestinal stem cells into damaged mouse colon[107]. Interestingly, Zhang *et al.* revealed that the transduction of a single gene could turn keratinocytes into corneal-like stem cells capable of replenishing the whole cornea in rabbits[108].

This finding necessitates further research to unravel other pathways and factors capable of altering stem cell fate and differentiation. Understanding both intrinsic and extrinsic cues that control stem cell behaviour in different contexts will lead to better treatments for a range of diseases. One organelle that is involved in processing extrinsic cues is the primary cilium. Indeed, primary cilia are mediators of extracellular signals into appropriate cellular responses and are inherently linked to the cell cycle, a process crucial to stem cell fate and differentiation.

1.2 The primary cilium

In some ways, we perceive our surroundings through cilia. For instance, the kinocilium in hair cells of the inner ear coordinates the stereociliary bundles that sense sound waves; the outer segments of photoreceptor cells are adapted cilia and cilia in the olfactory epithelium are involved in the detection of odours. Cilia are the oldest known cellular structure since its discovery in 1675 by Antony Van Leeuwenhoek[109], and up until the very end of the 20th century, most studies involving cilia only focused on the structure and motility. In 1898, a second type of cilia was discovered. These non-motile or primary cilia were regarded as vestigial organelles and were, therefore, mostly ignored by scientists[110]. It is only from the late 1990's that the importance of primary cilia was recognised as clinical studies have linked primary cilia function with diseases including cancer, neural tube defects and retinal degeneration[111–113].

1.2.1 Cilia Structure

The central core or axoneme of cilia consists of a nine parallel microtubule doublet core arranged radially around a central core[109]. Motile cilia ('9+2') possess two central microtubules linked by dynein arms, facilitating their mechanical function, with the microtubule doublets organised around it (Figure 4b). Primary cilia ('9+0') lack the two central microtubules and their associated dynein arms, which makes the primary cilium a static organelle (Figure 4d). Motile and primary cilia protrude from an adapted centriole or 'basal body', which is located intracellularly at the base of the cilium. The basal body offers the nine-fold symmetric model upon which microtubule doublets extend into the cilium[114]. This structure ensures the proper function of cilia by governing its position and orientation, act as a gateway for proteins and other molecules, and is involved in linking planar cell polarity signals with the axis of mitosis114.

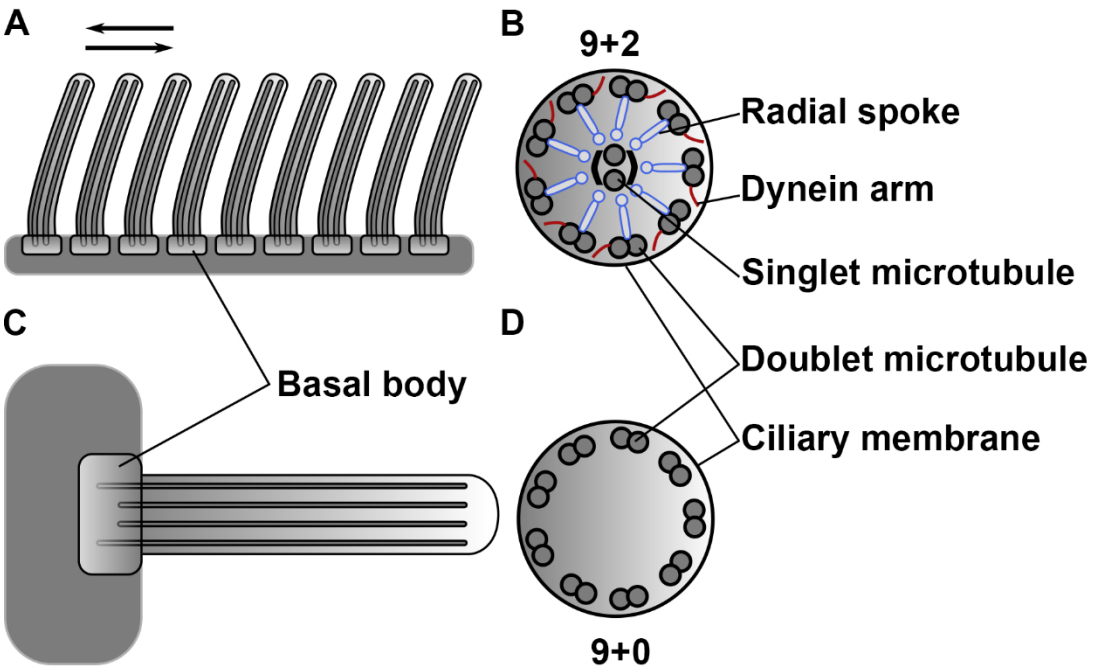

Figure 4: Structure of cilia.
A) Sagittal view of motile cilia. B) Topographical cross-section of a motile cilium displaying the typical '9+2' microtubule conformation. C) Sagittal view of a primary cilium. D) Topographical cross-section of a primary cilium showing the '9+0' microtubule conformation lacking the inner core.

Cilia display a number of sub-regions based on their microtubule composition. The proximal region of the cilium, termed the 'ciliary gate', consists of two structurally discrete sub-regions: the transition fibres and the transition zone[115]. Distal from the transition zone is where the axoneme of the cilium is formed. The axoneme extends from the transition zone and consists of a large part of a doublet zone, which contains motility-associated proteins. At the distal crown of the cilium, the doublet zone narrows into the singlet zone.

α-Tubulin is the main component of the axoneme and undergoes various post translational modifications such as, but not limited to acetylation, de-tyrosination and glutamylation[116]. Among these modifications, acetylation of lysine-40 (K40) is the best studied and plays a crucial role in the regulation of the primary cilium. During ciliogenesis, intraflagellar transport (IFT) complexes are responsible for the extension of the axoneme from the centriole. IFT complexes consist of 20 proteins that are organised in two subcomplexes termed IFT-A and IFT-B[117]. Bi-directional movement of the complexes along the axoneme is facilitated by two axoneme-based motor proteins: Kinesin-2 carries out anterograde transport of ciliary proteins to the ciliary tip whereas retrograde transport towards the cell body is driven by Dynein-1b[118]. IFT is necessary for ciliogenesis as it carries α-Tubulin to the tip of the axoneme. Subsequently, acetylation of K40 by α-Tubulin Acetyltransferase-1 stabilises α-Tubulin in the primary cilium. Indeed, deacetylation of α-Tubulin leads to retraction of the primary cilium. Histone deacetylase 6 (HDAC6) is a major player involved in all the known biological situations leading to a loss of the primary cilium including heatshock, mitosis and cancer[119–121]. The balance between ciliogenesis and resorption in any given cell is concomitantly linked with the cell cycle.

1.2.2 Ciliogenesis and the cell cycle

The formation of cilia and the cell cycle are connected as they both use the same machinery. In dividing cells, the basal body consists of a pair of centrioles, a mother and daughter centriole. The mother centriole is derived from the centrosome of the previous cell cycle and has distinctive ultrastructural and molecular features that separate it from the daughter centriole[122,123].

In the S-phase of the cell cycle, centrioles are duplicated once and migrate to opposite poles of the cell where they act as a microtubule organising centre to ensure proper chromosome segregation [124]. Consequently, after cell division, each daughter cell receives one pair of centrioles. During the G0/G1-phase, migration and docking of the centrioles to the plasma membrane defines the site of ciliogenesis. The mother centriole transitions into the basal body, acting as a scaffold for axoneme synthesis, whereas the daughter centriole remains docked at the proximal end of the mother centriole [125]. Prior to the fusion of the basal body with the plasma membrane, vesicles secreted by the Golgi apparatus are recruited to the distal appendages of the mother centriole to form the ciliary vesicle. The distal appendages of the basal body firmly attach to the plasma membrane and mark the beginning of the transition zone into which the axoneme protrudes. At the end of the G1-phase, the primary cilium is resorbed in two waves. The initial wave happens before the G1/S transition and is followed by a second, major wave before mitosis. Therefore, cells undergoing mitosis are devoid of primary cilia, with only a fraction of the ciliary membrane bound to the mother centriole 126. This ciliary resorption allows the centrioles of the basal body to act as centrosomes during mitosis. Hence, the suppression of cilia formation is critical in proliferating cells, and several signalling pathways linked to the cell cycle have evolved to control ciliogenesis.

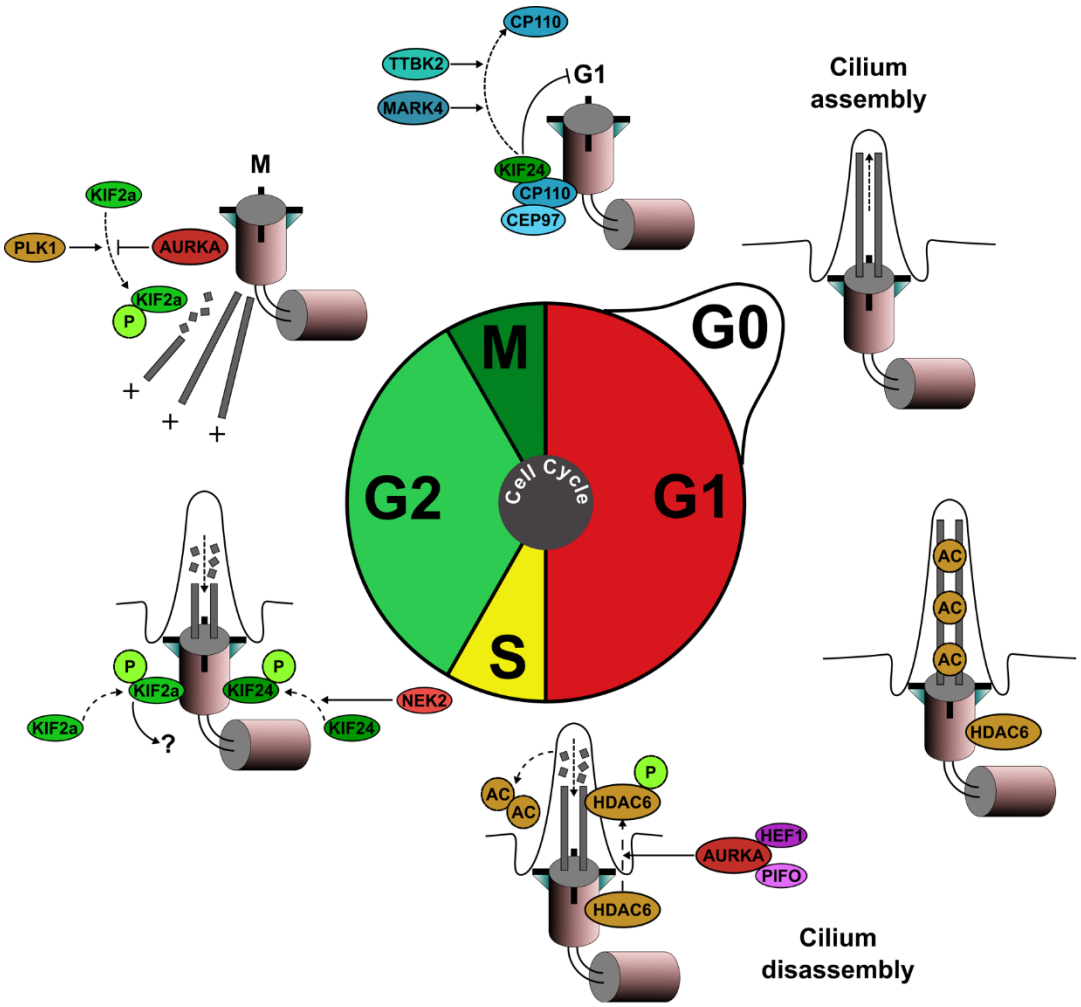

Figure 5: primary cilia formation and absorption is linked to the cell cycle.
Primary cilia assembly and associated proteins are dynamic throughout the cell cycle (G1, S, G2 and M phases), and in quiescence (G0 phase). The basal body is indicated by the double cylinders; microtubules are represented by the grey rods, only two doublet microtubules are shown for simplicity. Stable, acetylated tubulin is indicated at G1/G0 with acetyl groups (Ac) shown as brown circles. Proteins discussed in this chapter are highlighted in different colours: AURKA–HDAC6 disassembly pathway is shown in red and brown, respectively. KIF2A and KIF24 mediate microtubule depolymerisation and are coloured in green. 'P' in green circles indicates protein phosphorylation. Other centrosomal components are coloured in blue and purple. The function of KIF24 during the cell cycle is currently unclear, other proteins are assumed to be involved in the formation and regulation of the CEP97–CP110 scaffold. AURKA activates KIF2a during G1/S and in M-phase it negatively regulates it by phosphorylation. The arrows indicate activating effects, whereas bar-headed lines specify inhibitory effects. Dashed arrows refer to a post-translational modification of a protein or physical translocation.

How is the cell cycle linked to the formation and disassembly of cilia?

Microtubules are in a constant dynamic flux, and one mechanism to control ciliogenesis is to shift the equilibrium between formation and resorption of axonemal microtubules. Despite recent efforts, the mechanisms behind this are still not completely understood. A number of ciliary and centrosomal proteins are known to regulate this process, and their function often depends on negative regulation by cell-cycle kinases such as Polo-Like Kinase-4 (PLK4), Centriolar Coiled-Coil Protein-110 (CP110) and Voltage Dependent Anion Channel-3 (VDAC3)[127–129].

For instance, the CP110-Centrosomal Protein-97 (CEP97) complex is bound to the distal region of the mother centriole to prevent ciliogenesis during the cell cycle. When cells exit the cell cycle or complete mitosis this inhibitory complex is dissociated from the mother centriole for proper cilia formation (Figure 5). Microtubule Affinity Regulating Kinase-4 (MARK4) and Tau Tubulin Kinase-2 (TTBK2) are two protein kinases involved in the dissociation of CP110 and, therefore, initiation of ciliogenesis although the exact mechanism is still unclear[130,131]. The CP110-CEP97 complex also plays a role in sequestering a kinesin, Kinesin Family Member 24 (KIF24), at the distal tip of the mother centriole leading to the depolymerisation of centriolar microtubules, thus, suppressing cilia formation (Figure 5)[132]. NIMA Related Kinase-2 (NEK2), a S/G2-phase kinase interacts with and phosphorylates KIF24 to start microtubule depolymerisation[133]. Despite this, KIF24 remains present at basal bodies after cilia formation[132]. KIF2a, a promoter of mitotic spindle assembly, is also implicated in tubulin depolymerisation and is upregulated by the mitotic PLK1, and downregulated by Aurora kinase A (Figure 5)[134,135]. All these examples demonstrate the pivotal role of cell-cycle kinases as regulators of cilium formation.

The KIF2a–PLK1 signalling pathway seems to be partly redundant to the KIF24–NEK2 signalling pathway. Also, KIF2a instead localizes to the sub-distal appendages of the mother centriole. Taken together, it is more likely that KIF2a is involved in centrosomal or cytoplasmic microtubule depolymerisation rather than in axonemal depolymerisation, thus preventing cilia formation outside G0-phase[136]. This might represent a more general mechanism to allow regulatory inputs from the cytoskeleton to affect cell cycle and cilium outcome.

Aurora kinase A is also involved in a second mechanism of cilium resorption in cells entering the cell cycle. Aurora kinase A forms a complex with Neural Precursor Cell Expressed, Developmentally Down-Regulated-9 (NEDD9) and Pitchfork (PIFO), leading to the phosphorylation of HDAC6[137,138]. Activation of HDAC6 destabilises the ciliary axoneme through deacetylation of its microtubules (Figure 5). Several studies have pointed out that HDAC6 is crucial for proper cilia resorption[138–140]. Interestingly, HDAC6 mutant mice do not develop any cilia-related symptoms[141].

1.2.3 The primary cilium in stem cells

Despite the link between ciliogenesis and G0 or quiescent phase, the role of primary cilia and somatic stem cells has been understudied despite its observation in a range of stem cells[144-148]. In mesenchymal stem cells, primary cilia are crucial in proper lineage differentiation. Knockdown of Kinesin-like protein-3a (KIF3a) in mouse embryonic fibroblasts, which have a similar differentiation potential to mesenchymal stem cells, disrupted the primary cilium structure and stimulated canonical WNT signalling, a crucial component in chondrogenic and osteogenic differentiation[142,143]. In epidermal cells that have disrupted cilia display no altered WNT signalling despite many other phenotypical changes in KIF3a mutant mice such as increased epidermal ridging, hyper-proliferation of the basal

progenitor cells and aberrant differentiation into keratinocytes[144]. Knockdown of IFT88, a gene involved in ciliogenesis and autophagy, displays reduced differentiation potential upon exposure to chemical-induced differentiation media for adipogenic, chondrogenic and osteogenic cell types.as shown by reduced expression of early differentiation markers, PPARg, SOX9 and RUNX2, respectively[145]. This result indicates that the primary cilium regulates the chemo-sensitivity of cells.

The link between primary cilia and lineage specification of stem cells has been confirmed in neural stem cells where it is thought that asymmetric cell division is guided by the distribution of the centrioles. The mother centriole maintains the stem cell character of the daughter cell whereas, the daughter centriole directs the daughter cell to differentiation[126].

1.2.4 The primary cilium as a signalling centre

The primary cilium extends into the extracellular micro-environment and is, therefore, a prime candidate for the detection of signals produced within the tissue, suggested by the enrichment of various receptors in the ciliary membrane. In fact, there is evidence showing that the translocation of these receptors to the primary cilium is crucial for their proper function demonstrating that the primary cilium acts as a signalling centre[146–148]. In the last 15 years, many different pathways have been associated with the primary cilium including Notch[149], Sonic Hedgehog (SHH)[130], canonical and non-canonical Wingless-Type MMTV Integration Site (WNT)[150], Platelet-derived growth factor (PDGF)[147], and Hippo[151].

WNT

WNT molecules bind to different membrane-bound receptors to activate canonical and non-canonical WNT signalling pathways, which are different in

their downstream steps. Canonical WNT signalling leads to the stabilisation of cytosolic β-catenin, which then translocates to the nucleus and induces WNT target gene expression. Whereas downstream events of non-canonical WNT signalling lead to changes in cell morphology (actin dynamics, cell polarity and cell shape,) independent of β-catenin rather than transcription.

It has been reported that downregulation of cilia-related proteins *in vitro* or in zebrafish increases canonical WNT signalling and/or interrupts processes depending on non-canonical WNT signalling. Hence, the primary cilium was suggested to mediate the switch between canonical and non-canonical WNT signalling pathways[157, 158].

PDGF

The PDGF signalling pathway is involved in cell proliferation, survival and migration[152]. When cells exit the cell cycle, the PDGFRα, but not PDGFRβ, receptor translocates to the primary cilium in fibroblasts. This translocation makes the receptor susceptible to binding of its ligand Pdgf-aa and will, in turn, activate a downstream cascade of proteins including AKT, Mitogen-activated protein kinase-1/3 (MAPK1/3), and Mitogen-activated protein kinase kinase-1/2 (MAP2K1/2)[153]. Improper ciliogenesis causes inhibition of PDGF-aa signalling resulting in aberrant cell migration and chemotaxis of endothelial cells[154]. PDGFR is a receptor tyrosine kinase (RTK), and other RTK-signalling events have been shown to take place in primary cilia such as Epidermal growth factor receptor (EGFR), Insulin Like Growth Factor-1 Receptor (IGF1R) and Tyrosine Kinase, Endothelial (TEK) signalling[155].

Notch

Notch signalling is a process in multicellular organisms by which neighbouring cells communicate with each other. All multicellular animals use Notch signalling, and the pathway is involved in cell fate specification, differentiation, proliferation, and survival and contributes to the formation, growth, and homeostasis of tissues. The connection between Notch signalling and primary cilia has only been made recently. In early embryogenesis, components of the Notch signalling pathway, such as Notch 3 and Presenilin 2, are located within the primary cilium of E9.5 epidermal skin cells, and loss of primary cilia leads to impaired Notch signalling and negatively affects epidermal differentiation and skin barrier function[149]. Similar findings have been reported in corneal epithelial cells where loss of cilia negatively regulated Notch signalling leading to hyperproliferation and reduced differentiation[156]. Interestingly, disruption of the BBSome complex, which is responsible for the trafficking of proteins in and out of the primary cilium, leads to accumulation and, subsequent, increased activation of Notch *in vitro* and in zebrafish[157].

SHH

The connection between hedgehog (Hh) signalling and the primary cilium is the most investigated of all major pathways and Hh signalling mostly depends on proper ciliogenesis[130]. This is highlighted in mouse knockout models of key cilia markers such as Intraflagellar Transport 88 (IFT88) and KIF3a and members of the Hh pathway showing similar phenotypes[161]. Of the three ligands in the family SHH is the best characterised.

When SHH is absent in the extracellular micro-environment , the Hh-binding receptor Patched (PTCH) inhibits the translocation of Smoothened (SMO) to the

primary cilium[130]. This inhibition sustains a state of repression of members of the GLI family within the primary cilium. GLI forms a complex with SUFU and KIF7 maintaining a state of repression through PKA, GSK3β and CK1.Upon binding of SHH to the Ptch receptor, SMO is able to translocate to the primary cilium in an ADP ribosylation factor-like GTPase 13b (ARL13b) -dependent manner[162]. SMO will then interact with GLI, which will trigger a downstream cascade leading to the transcription of effector genes.

Currently, three members are known of the GLI family of transcription factors with GLI1, GLI2 and GLI3 all being involved in mediating the Hh signalling pathway. GLI1 and GLI2 are considered transcriptional activators whereas GLI3 is a transcriptional repressor[163]. So far, only GLI2 and GLI3 have been shown to be present within the primary cilium and their translocation to the nucleus to act as transcription factors is the defining moment in Hh signalling. Another family of proteins that are structurally similar to GLI and are involved in Hh-signalling is GLI-similar (GLIS). This family consists of three members: GLIS1-3, GLIS2, and GLIS3 have been shown to be present in the primary cilium. It has been proposed that GLIS members perform similar functions as GLI members in the primary cilium[164]. However, not much has been known yet about the particular mechanisms of and interaction partners with this family of proteins.

Besides these core-signalling pathways described in this chapter, new advances in proteomics have added more candidates to the list of cilia-related-signalling. The ‘ciliome’ consists of about 800 proteins and from recent efforts, it is clear that the cilium both interacts with numerous traditional molecular pathways, regulating and tweaking cellular outcomes[449]. One such candidate is CD133, a membrane protein often linked with stem and progenitor cells. CD133 clusters within

protrusions of the plasma membrane, e.g.: microvilli and primary cilia[172]. Despite its discovery in the 1990's not much has been elucidated about its functions, interactions with other proteins or its translocation to the primary cilium.

1.3 CD133

1.3.1 Discovery and Structure

CD133, also called Prominin-1 (Prom1), was identified in 1997 via immunisation of New Zealand Black mice with foetal liver CD34+ cells. This resulted in an immune response and subsequent antibody production against CD133 identified as the human orthologue of the murine Prominin-1[165,166]. Today there are several antibodies available targeting different epitopes of the receptor.

CD133 is a pentaspan membrane glycoprotein (Figure 6) often associated with plasma membrane protrusions such as primary cilia, hence, the name prominin from the Latin word *prominere* meaning 'to protrude'. It is the first member of a class of membrane receptors. The canonical sequence of CD133 cDNA encodes a transmembrane glycoprotein of 866 amino acids (AA) with a unique structure consisting of an extracellular N-terminus (105 AA), two extracellular domains (258, and 279 AA), five transmembrane domains (23 AA each), two intracellular domains of 29 and 21 AA, and a 59 AA intracellular N-terminal domain (Figure 6). This topology closely resembles that of mouse Prom1, an 858 AA protein identified by the mouse monoclonal antibody 13A4 [167] and expressed in kidneys and microvilli of the mouse neuroepithelium. Human CD133 and mouse Prom1 share roughly 60% homology. Based on the sequence, eight potential N-glycosylation sites have been identified (Figure 6). Indeed, incubation of whole cell protein lysates with PNGase F leads to removal of N-linked oligasaccharides from glycoproteins. Subsequent westernblotting of the lysates resulted in a reduction in molecular weight of CD133 from ~120kDa to 97kDa[168].

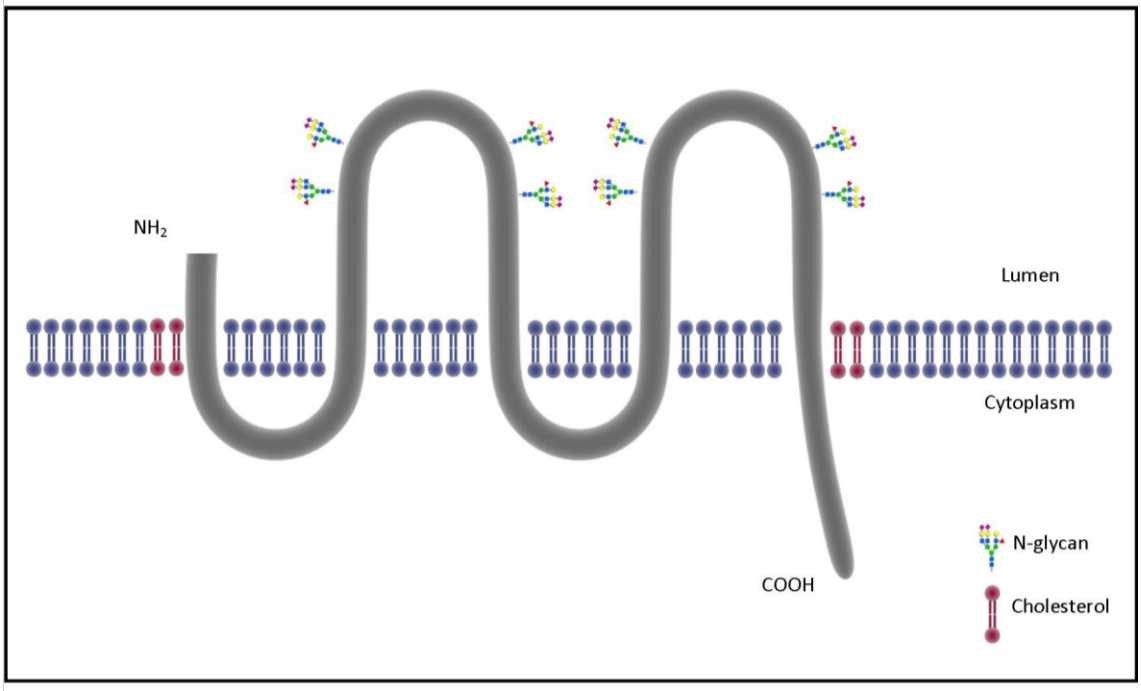

Figure 6: Membrane topology of CD133.
CD133 is a plasma membrane glycoprotein containing five transmembrane regions and two glycosylated extracellular loops with a molecular weight of 97-120 kDa. CD133's distribution in the plasma membrane is asymmetric as it favours cholesterol-rich lipid rafts.

1.3.2 Other members of the Prominin family

In 2003, a second member of the Prominin family, Prominin-2, was discovered. This protein has despite its low AA similarity of ~30% the same membrane topology as CD133. Also, the genomic makeup of CD133 and prominin-2 is nearly identical indicating that Prominin-2 is a paralogue of CD133[169]. *In vitro* studies of Prominin-2 have shown that it is co-localised with CD133 in plasma membrane protrusions of transfected Chinese hamster ovary cells. However, in Madin Darby Canine Kidney (MDCK) cells, Prom2 was also present on the basal and lateral membrane domains whereas CD133 is restricted to the apical side. Together with the observation that its tissue distribution largely overlaps with that of CD133 suggests that's Prominin-2 might have similar functions as CD133. This is confirmed by the observation that loss-of-function mutation of *CD133* results in retinal degradation of the eye but no other pathological effects in other organs[197]. Indeed, Prominin-2 has not been detected in the eye indicating that Prominin-2 expression might rescue the phenotypical outcome of loss-of-function mutations in CD133 in other tissues[173].

In 2011, a novel member of the Prominin family, Prominin-3, was discovered in *Xenopus laevis* and *Danio rerio,* but not in mammals[170].

1.3.3 Genomic organisation and transcriptional regulation of CD133

The *CD133* gene is a single copy gene and is located on chromosome 4p 15.32 in humans and 5B3 in mice. It comprises at least 37 exons of which up to ten alternative exons are located before the start codon[171]. The locus spans more than 152 kilobasepair (kb) and is under the control of five alternative tissue-specific promoters (P1 to P5) of which three contain CpG islands emphasising complex gene regulation[171,172]. Although, promoter activity of P4 has not been

demonstrated yet (Figure 7). The genomic makeup of both mammalian CD133 and Prominin-2 is strikingly similar despite significant differences in AA sequence homology. However, the structure of exons does not correlate with the protein structural domains as the coding regions of CD133 and Prominin-2 cover 28 and 23 exons, respectively[173].

The distal promoter P5 which is located outside the CpG island is under control of Hypoxia-inducible factors 1/2 alpha (HIF1/2a)[174]. Overexpression of both HIF1/2a in human embryonic kidney and colon cancer cell lines HEK293T and WiDr, respectively, leads to a five-fold increase of *CD133* expression through the ETS transcription factor (ELK1), an effector of MAPK signalling. This result provides a mechanism explaining the increased expression of *CD133* often seen in solid tumours as hypoxia is a hallmark of cancer[175,176]. Indeed, aberrant methylation of the CD133 promoter is frequently observed in several types of cancer such as glioblastoma and colorectal tumours whereas the promoter of CD133 is essentially unmethylated in healthy tissues 177,178. In vitro analysis of the CD133 promoter revealed conflicting results about its methylation status in glioblastoma cell lines177,179. Gopisetty showed that hypermethylation leads to diminished expression of CD133 in glioblastoma due to loss of Specificity protein 1 (Sp1) and Myc transcription factor binding sites177. Whereas, Tabu et al. show that increased CD133 expression due to hypomethylation is prevalent in high-grade glioblastoma179. In cancer cell lines, it has been revealed that there is a direct correlation between CD133 expression levels and promoter activity. Under stress conditions, the tumour suppressor protein p53 (p53) directly binds to promoter P1 to act as a negative regulator of CD133 expression in in vitro cultures. P1 activity has been demonstrated in most cancer cell lines. p53 serves as a

A

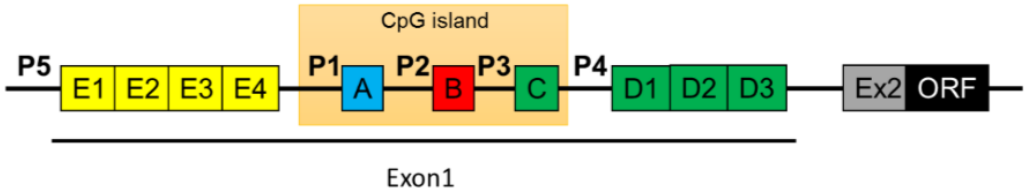

B

	P5	P1	P2	P3	P4
CD34+ HSC					
Liver					
Skeletal muscle					
Kidney					
Pancreas					
Brain					
Placenta					
Lung					
Spleen					
Thymus					
Prostate					
Testis					
Ovary					
Small intestine					
Colon					
Leukocytes					
Caco2					
NT2					
HEK293T					
WiDr					

Figure 7: Promoter organisation of human CD133.
A) Promoter distribution of exon 1 indicating the five currently known promoters of which P1-3 are present in a CpG island indicating the potential for epigenetic silencing. Exon 2 contains the start codon. B) Tissue-specific use of promoters in listed tissues is indicated in green. The activity of promoter 4 hasn't been demonstrated yet [171].

scaffold for Histone deacetylase 1 (HDAC1)-mediated Histone 3 deacetylation. Attenuation of CD133oncogenic transcription factors such as Nanog Homeobox (Nanog), Sex Determining Region Y-Box 2 (Sox2) and POU Class 5 Homeobox 1 (Oct4)[180].

1.3.4 CD133 isoforms

Since its initial discovery in 1997 by Yin and Miraglia, CD133 has been shown to be expressed in a wide variety of different tissues of both healthy and oncogenic nature. A total of 12 CD133 isoforms (s1–s12) have been identified in human and rodents[169,181–185,186]. The inclusion or exclusion of exons predominantly affects the N- terminal extracellular (EX) 1 and C-terminal intracellular (IC) 3 domains (Figure 8) In the N-terminal domain (EX1) the inclusion or exclusion of exon 3 (a 9 AA sequence) distinguishes CD133 s1 and s2 isoforms and might possibly alter affinity for different ligands. Interestingly, both isoforms can be detected by the human stem cell-associated AC133 antibody[166,188]. However, the most significant variability across isoforms is seen in IC3 where a total of 10 splice variants can be generated from the inclusion or exclusion of the last four facultative exons[189,190]. Sequence analysis of IC3 revealed that each isoform (minus s6 and s12) contain potentially one of three classes of PSD95/Dlg/ZO-1 (PDZ) domain. These domains are involved in anchoring receptor proteins in the membrane to the cytoskeleton. For instance, mouse s1, s2, s7, s8 and s11 contain the sequence PSQR which has the characteristics of class 1 PDZ-binding domain. Other isoforms carry different classes of PDZ domains in their IC3 such as s3, s4 and s5 containing a class 2 PDZ domain (HFTL) and s9 harbouring a class 3 PDZ domain (SVQC)[191,192].

A

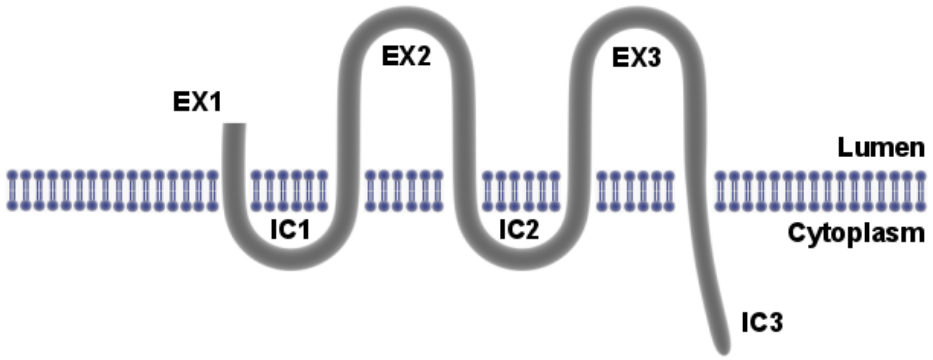

B

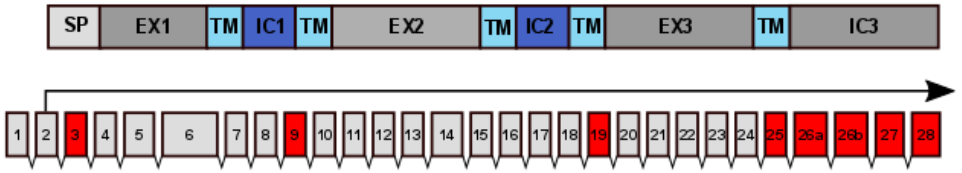

C

	Facultative exons included in the coding sequences									
Isoform	**3**	**9**	**19**	**25**	**26a**	**26b**	**27**	**28**	*Homo sapiens*	*Mus musculus*
s1	-	+	-	-	-	+	+	+	AF507034	AF026269
s2	+	+	-	-	-	+	+	+	AF027208	AF039663
s3	-	+	-	-	+	-	-	-		AF305215
s4	-	-	-	-	+	-	-	-		AY223521
s5	-	-	-	-	+	-	-	-		AY223522
s6	-	+	-	-	-	-	-	-		AY099088
s7	-	+	-	-	-	-	-	+	AY449690	AK029921
s8	+	+	+	-	-	-	-	+		BC028286
s9	-	+	-	+	-	+	-	-	AY449689	
s10	-	+	-	-	-	+	-	+	AY449691	
s11	-	+	-	-	-	-	-	+	AY449692	
s12	-	+	-	-	-	-	-	+	AY449693	

Figure 8: Facultative exons in CD133 isoforms.
A) Topological domains in CD133 B) Facultative exons (red) within the CD133 coding sequence C) The presence (+) or absence (-) of facultative exons in the 12 isoforms discovered in human and mouse. CD133 isoforms in human and mouse are identified by their GenBank accession number [187].

1.3.5 Expression of CD133 in tissues

Human CD133 messenger RNA (mRNA) transcripts are detected in many cell lines and in most tissues apart from mature peripheral blood leukocytes[171]. However, the human AC133 epitope, used initially to discover CD133, is restricted to stem- and progenitor cells that include endothelial progenitor cells[193], hematopoietic stem cells[165], foetal brain stem cells[194], embryonic epithelium[167,168], prostatic epithelial stem cells[195], myogenic cells[196] and are found in certain cancers such as retinoblastoma[166,197], teratocarcinoma[166] and leukaemia[198]. This discrepancy is again confirmed in mice where the murine counterpart of AC133, 13A4, detects approximately the same epitope in mouse CD133. Using this antibody, CD133 was detected in tubular epithelium of the kidney and in the ependymal epithelium in the brain[167,199] whereas CD133 mRNA is more widespread as is evident from the analysis of β-galactosidase (LacZ*)* reporter gene expression under the control of CD133 promoter in mutant mice[94,171]. This difference in mRNA and protein detection of mammalian CD133 could be explained by tissue-specific glycosylation, as AC133 antibody recognizes only a specific form of glycosylated CD133[165]. In contrast, it is known that 13A4 recognises both unglycosylated as well as glycosylated CD133[167]. Moreover, AC133 and 13A4 antibody may selectively bind to a unique alternatively spliced isoform of CD133. Together, these findings explain the earlier observations of CD133 expression restricted to stem and progenitor cells.

Haematopoietic stem cells

Perhaps one of the best-documented areas of CD133 expression has been in haematopoietic stem cells. Haematopoietic stem cells are the progenitors to all different cell types from the lymphoid lineages (NK-cells, B-cells, T-cells) to the

myeloid lineages (macrophages and monocytes, megakaryocytes/platelets, neutrophils, basophils, eosinophils, dendritic cells, erythrocytes)[200].

CD133 is known to mark a pluripotent population of haematopoietic stem cells derived from different sources such as human bone marrow, foetal liver and peripheral blood[201]. Yin *et al.* have shown that the receptor is downregulated to undetectable levels as the haematopoietic stem cell matures[165].

Approximately 0.52% of bone marrow and 0.16% of cord blood mononuclear cells express CD133[202]. CD133 is expressed on 83% of cord blood CD34+ cells and up to 70% in bone marrow CD34+ cells[165]. Analysis showed that CD133 is undetectable on committed precursors, such as red blood cells, granulocytes and pre-B-cells, and that populations of CD133+ cells consist mainly of long-term culture initiating cells, the most primitive human haematopoietic cells which can be assayed *in vitro*[203]. CD133+ cells appear to be precursors to CD34+ cells as Gallacher showed that CD133+ cells were the only subset of a CD34-CD38-lineage population from human umbilical blood that could generate CD34+ cells *in vitro* with a 400 fold increase of engraftment capability in NOD/SCID (Non-obese diabetic/severe combined immunodeficiency) mice than that observed in the CD133- subset[202].This was partially confirmed by Summers' work which produced CD34+ cells from CD133+ CD34- cells in culture[204]. As the cells differentiate, they first begin to express markers such as CD38 and finally express differentiation markers such as CD13 and CD33.

In vivo applications of CD133+ stem cells in tissue regeneration have already been shown to be beneficial. Umbilical cord blood or bone marrow-derived CD133+ cells have been applied to myocardial tissue regeneration after infarction. Two reports showed that CD133+ cells improved myocardium recovery through

an increase in angiogenesis and prevention of scar thinning and diastolic dilation[205,206].

Other stem cells

Within human tissue, CD133 expression is widespread and not solely restricted to haematopoietic stem or progenitor cells. CD133+ cells isolated from foetal liver, umbilical cord blood, bone marrow and mobilized blood were capable of *in vitro* differentiation to neuronal cells and astrocytes, oligodendrocytes and glial cells[207]. CD133+ cells from peripheral blood markedly improved angiogenesis, astrogliosis, axon growth and functional recovery in a mouse spinal cord injury model compared to CD133- cells[208].

Similarly, CD133+ cells isolated from the human foetal brain or skin tissues were capable of forming neurospheres *in vitro* and to differentiate into neurons and glia[194]. Moreover, when human CD133+ neurosphere cells were transplanted into neonatal NOD-SCID mice, they proliferated, migrated and differentiated into fully integrated neurons and glial cells[209].

Grafting of integrin $\alpha 2\beta 1^{hi}$/CD133+ prostate basal cells in immunodeficient mice are capable of forming fully differentiated acini structures with evidence of both secretory and squamous cells present whereas the CD133- population leads to the formation of fibromuscular stroma with a complete absence of functional glands[195].

CD133+ cells from the stroma of human cornea have the capacity to proliferate in vitro; colonies derived from CD133+ cells could be differentiated into fibroblastic cells, indicating that CD133+ cells represent stem cell of the corneal stroma[210].

Initial reports of CD133 expression in the kidney showed that its presence is restricted to the interstitium and that they lack the haematopoietic stem cell markers CD34 and CD45 but do express Paired Box 2 (Pax2) indicating their renal origin[211]. Interestingly, these cells are capable of differentiating into endothelial and epithelial cells expressing markers of both distal and proximal epithelium[211].

Furthermore, stem cell therapy involving CD133+ cells derived from bone marrow have been used in clinical trials for patients recovering from cardiac arrest[212], hepatic cirrhosis[213] and chronic total occlusion and ischemia[214]. As of February 2017, 17 clinical trials are ongoing using CD133+ cells in regenerative medicine[215]. It is clear from the highlighted cases that CD133+ cells possess tremendous benefits for tissue engineering but more research is required to understand the role of CD133 in these processes.

CD133 in differentiated cells

Despite the focus of most research on CD133 in stem and progenitor cells, there is considerable evidence of CD133 expression in terminally differentiated cells of glandular organs such as the salivary glands, pancreas, mammary glands and liver as well as in kidneys[216–218]. This comes as no surprise as CD133 mRNA transcripts, unlike the AC133 epitope, have been observed in Caco-2 cells that underwent enterocytic differentiation[219]. The lack of CD133 protein detection using the AC133 antibody is partly due to its dependence on the glycosylation status and could be circumvented with the rabbit antiserum αhE2 targeting amino acid residues Gly_{240}-Ser_{388}. Using this antiserum, CD133 has been detected in the parietal layer of Bowman's capsule of nephrons present in the juxtamedullary region of the cortex similar to 13A4 epitope detection in the adult mouse

kidney[167,216]. Immunoreactivity of αhE2 but not AC133 has also been detected on the apical side of lactiferous ductal epithelia in the mammary glands corresponding to high CD133 mRNA transcripts[216].

Immervoll and Corbeil both demonstrated for the first time that the human AC133 epitope, previously thought to be inversely correlated with differentiation, can also be detected in differentiated cells, namely at the differentiated apical/endoluminal face of ductal pancreatic epithelia with increasing expression towards the acini where CD133 staining was more cytoplasmic as opposed to the usual membrane detection. Although these cells express the pancreatic differentiation marker Carbonic anhydrase II it is believed that these cells positive for the AC133 epitope could be in fact dedifferentiated or transdifferentiated cells. However, given that approximately 30% of the ductal cells are positive for AC133, it is clear that this epitope is not a marker for stem and progenitor cells only.

1.3.6 Subcellular Localisation of CD133

Plasma Membrane

Many examples exist where CD133 and other members of the Prominin family are mainly detected in plasma membrane protrusions. For example, mammalian CD133 is targeted to the apical membrane, and more specifically, CD133 is highly concentrated in microvilli and primary cilia of polarised epithelial cells such as kidney proximal and intestinal crypt cells[167,168,220,221]. Although there is no specific retention motif in CD133's AA sequence, it is thought that this specific localisation is due to the direct binding of lipid raft-associated cholesterol to CD133[222–224]. Lipid rafts are characterised by their insolubility to non-ionic detergents such as Lubrol WX but remain soluble in Triton X-100[222]. Lipid rafts are plasma membrane microdomains that are enriched in specific glycosphingolipids,

gangliosides, and sterols[225]. CD133 potentially binds to other lipids present in lipid rafts such as GM1 and GD3 gangliosides as is evident from their co-localisation with CD133 in microvilli of epithelial cells[226].

Several but not all CD133 isoforms contain PDZ-binding domains in their C-terminal intracellular domain hinting at possible interactions with the cytoskeleton through other PDZ-containing proteins that act as adaptor/linker proteins between integral membrane proteins and the actin cytoskeleton[184,227]. Interestingly, the specific localisation of CD133 in plasma membrane protrusions is not regulated by the C-terminal intracellular domain since it is not prevented by deletion of this part[220]. In addition, localisation of CD133 to the microvilli is not affected when its cytoskeletal architecture is disturbed, as seen in Caco2 cells displaying diminished and morphologically altered microvilli upon downregulation of the actin-bundling protein Villin[222].

Extracellular vesicles

Proper communication between cells in tissues is critical for tissue formation and homeostasis. Exchange of extracellular vesicles between cells is one of many ways for them to communicate and can contain RNA, DNA and proteins[228]. Marzesco *et al.* showed for the first time in the developing mouse brain that CD133 immunoreactivity to 13A4 was not only detected at the luminal side of the neuro-epithelium but was also observed in the membrane of vesicles in the cerebrospinal fluid[167,229,230]. The same study also investigated various body fluids of the adult human and revealed the presence of CD133-containing vesicles of various sizes in seminal, saliva, urine and lacrimal fluids. Analysis of the properties of the vesicle membrane and the lack of specific extracellular vesicle markers such as CD63 for exosomes seem to suggest that these are a new type

of vesicle[230]. Indeed, these vesicles are now termed P2- and P4-type vesicles based on their size and are therefore pelleted at different at different centrifugal speeds. The largest vesicles, P2 which are released from the midbody, are between 0.5-1µm in diameter and appear electron-dense upon immunogold electron microscopy whereas the P4-type vesicles are between 50-80nm and electron translucent. Interestingly, the secretion of P2 and P4 vesicles is temporally linked with the cell's differentiation status. For instance, P2 vesicle release has been shown to be greater in stem cell-derived cell lines compared to differentiating, cancer-derived and immortalised cells. P4 vesicles, on the other hand, are only secreted in differentiated cells as is seen in confluent Caco2 cells or in chemical-induced differentiated haematopoietic stem cells[230–232].

The precise role for both P2 and P4 CD133-positive vesicles is still unclear. However, with keeping the biochemical properties of CD133 in mind, two probable roles for these vesicles can be hypothesised. Firstly, the plasma membrane is known to play an essential part in signal transduction and is asymmetrical in composition. The release of vesicles in a spatiotemporal manner might change membrane organisation and therefore affect signal transduction. Secondly, the release of CD133-positive vesicles might confer intercellular communication. For instance, between embryonic day (E) 10,5-12 when microvilli are abundant in the floor plate, a signalling centre in the developing nervous system, the release of P4 vesicles is increased. Similarly, the abscission of the midbody as P2 vesicles is likely to confer information to recipient cells about the type of cell division the donor cell underwent, i.e. asymmetric vs symmetric cell division[221].

Nucleus

Interestingly, nuclear CD133 has also been identified in triple-negative breast cancer, rhabdomyosarcoma cell lines and non-small cell lung cancer cells (NSCLC) [233–235]. Potentially, according to Cantile *et al.*, to function as a regulator of transcription. A minor fraction of cell lines and cancer cells are positive for nuclear CD133. Depending on the rhabdomyosarcoma cell line it ranges from 3.4% to 7.5% of cells that have CD133 in the nucleus [233]. In NSCLC, a cancer with high mortality rates, CD133 is expressed at high levels and present in ~55% of the tumours investigated. However, nuclear CD133 was only sporadically present in lung tumours [235]. The exact mechanism as to its nuclear translocation and its function remains to be elucidated as well as its nuclear presence under normal physiological conditions.

1.3.7 CD133 in Disease

Photoreceptor Degeneration

Despite the expression of CD133 in a wide range of tissues ranging from stem cells to differentiated cells of all germ layers, the most striking phenotype of loss-of-function mutation is disk dysmorphogenesis and retinal dystrophy in the eye[197,236]. Photoreceptor cells are part of the retina, a light-sensitive layer of tissue able to transform light into nerve signals, which can be interpreted by the brain.

CD133 is expressed in both photoreceptor cells, namely cones and rods. The latter is concerned with vision in dim light whereas cones are involved in vision in bright light as well as colour perception. In rods, CD133 is specifically expressed at the base where newly synthesised membrane evaginations or disks develop from the connecting cilium and move up the tract[197,237]. In cones, CD133 is

observed in the outer segment along the whole tract[236]. Interestingly, immunoreactivity of CD133 is different in rods versus cones. The epitope AC133 which is often used as a human stem cell marker is mainly detected in the outer segment of cones whereas CD133 in rods was detected using αhE2, an antiserum[216]. This might indicate that different forms of CD133 are present in photoreceptors.

To date, five mutations in the human PROM1 gene responsible for retinal dystrophy affecting both cones and rods have been discovered. Most mutations lead to the introduction of a premature stop codon, and all of them share many symptoms including but not limited to night blindness, gradual loss of peripheral vision and photoreceptor degeneration[197,238–242].

Studies in mice replicating loss-of-function of CD133 gave the first clues as to what the function of CD133 is. *CD133* KO mice displayed an age-dependent loss of photoreceptors. Indeed, by the age of one year, the entire photoreceptor layer of mice lacking CD133 was missing resulting in full blindness[236]. Mice carrying the human R373C *PROM1* gene have abnormally shaped disk membranes and excessively large outer segments by P16. At four months, photoreceptor disks were either misaligned and were of excessive size compared to wild-type mice or defects in outer segment membrane organisation[241]. Remarkably, eyecup cultures treated with cytochalasin-D, an inhibitor of actin polymerisation, display a similar phenotype. Other studies showed that non-functional CD133 leads to defects in new disk formation, i.e. disks protruding from the ciliary plasma membrane. The interaction between actin, CD133 and Protocadherin 21 (PCDH21) as shown by co-immunoprecipitation might be crucial for the proper formation of new disks. Indeed, PCDH21 and CD133 are both present in newly-

made disks and in R373C mice non-functional CD133 leads to mislocalisation of PCDH21 and its impaired proteolytic cleavage[197,241,243]. The role of actin with the CD133-PCDH21 complex is also not clear but might be important in the proper distribution of the complex in a temporospatial manner[241]. The localisation of CD133 in the outer segment of disk evaginations might prevent fusion of disks as is evident from the separation of disks in cones.

Tumour-initiating cells

The traditional model of carcinogenesis states that any dividing cell of the body can give rise to a tumour if enough mutations that permit unlimited proliferation potential occur in its genome. This dogma was overturned in the late 90's by the discovery of cells within myeloid lymphoma[244] that possess stem cell features and were capable of generating the typical heterogenic population seen in many tumours[245]. Later, these stem cell-like tumourigenic cells were also discovered in solid tumours. Expansion of mammary stem cells in mouse breast cancer models prior to cancer development represent a probable link between normal stem cells and tumour-initiating cells also called cancer stem cell[246]. Mainly these cells have been identified through the expression of cell-specific surface markers. Among the most frequently shared markers by tumour-initiating cells of different germlines are CD20, CD24. CD34, CD44, CD90, CD117, CD133, Aldehyde dehydrogenase (ALDH), nestin, β1-integrin and Epithelial cell adhesion molecule (EpCAM)[247].

One of the most commonly used tumour-initiating cell markers across different tumour types is CD133. Singh *et al*. took CD133+ cells from human brain tumours and was able to show that they exhibit stem cell-like features, by proving they were capable of self-renewal and replication of an original tumour when grafted

into an immunodeficient brain of NOD/SCID mice with as little as 100 cells. Injection of 100 CD133- cells showed no tumorigenic response[248]. Confirming this result, Chiou *et al*., revealed that in atypical teratoid rhabdoid tumours, a malignant tumour of the central nervous system, the metastasis, malignancy and radioresistant capabilities of CD133+ were substantially increased when compared to CD133- cells[249].

Interestingly, Rappa *et al.* investigated CD133 as a possible therapeutic target for metastatic melanoma. Retroviral-mediated knockdown of CD133 in FEMX-1 melanoma cells showed slower growth and reduced capacity to form spheres compared to control cells. This suggests that the cells have lost some of their oncogenic properties. Knockdown of CD133 severely reduced the capacity of the cells to metastasise indicating that CD133 may have a role in the capacity of tumour cells to migrate to other tissues[250]. Indeed, immunohistochemical analysis of human hepatocellular carcinoma samples (HCC) showed that the number of CD133+ CD44+ HCC cells is increased and linked with portal vein invasion[251]. This was partially confirmed by Horst *et al.* showing that high levels of CD133 correlate strongly with synchronous liver metastasis, but knockdown of the receptor indicated no change in colony formation or proliferation[252]. Contrary to these findings, different groups have expressed their concerns regarding CD133 as a tumour-initiating cell marker. Using $IL10^{-/-}CD133^{LacZ/+}$ mice, Shmelkov showed that both CD133+ and CD133- metastatic colon cancer cells were capable of long-term tumorigenesis in immunodeficient mice and that the latter formed larger tumours[94]. Interestingly, the same study showed that CD133 expression in adult $CD133^{LacZ/+}$ mice is not restricted to stem cells but is also present in luminal terminally differentiated cells such as but not restricted to the pancreas and kidney. Several studies have confirmed this work claiming that

expression of CD133 in colon cancer is not restricted to tumour-initiating cells [253]. Likewise, in healthy cells of the gastrointestinal tract CD133 is uniformly expressed throughout the tissue[94,254]. Ogden et al. and Yoshikawa et al. revealed that CD133 could be a biliary and progenitor cell marker *in vivo*, concluding that CD133 alone is not sufficient to detect tumour-initiating cells in human hepatocellular carcinoma cell lines[255,256]. Therefore, the validity of CD133 being an oncogenic marker is still controversial.

Another major therapeutic problem tumour-initiating cells present is their resistance to treatment such as radiation and various chemotherapy, which generally target homogeneous populations of rapidly proliferating, differentiating tumour cells. Alternative targets are being looked at. These include the drug Salinomycin, a potassium ionophore that can reduce the proportion of CD133+ subpopulations in human colorectal cancer cell lines HT29 and SW480. Furthermore, Salinomycin treatment decreases colony-forming ability and cell motility in HT29 cells and decreases vimentin expression and induces E-cadherin expression in HT29 cells[257].

It is, therefore, imperative to try to understand the mechanisms contributing to this resistance which can only be achieved by identifying the cancer stem cells, the signalling pathways and their regulatory mechanisms involved in tumour-initiating cell maintenance. As discussed earlier, radiation and chemotherapy resistance, as well as limited cell numbers, has been a major therapeutic problem for combating CD133+ tumour-initiating cells.

1.3.8 Interactions of CD133 and its functions

Currently, nearly 5000 papers involving CD133 have been published. Despite this vast number of publications, not much has been known about its regulation,

molecular binding partners and function within mammalian cells.

Mice carrying a deletion of exon 2 in CD133 develop blindness over time which is a consequence of a progressive degeneration of both cone and rod photoreceptors. Strikingly, lack of CD133 does not seem to affect retinal cell composition at P10, and it is, therefore, unlikely that CD133 is involved in retinogenesis[236,258]. Instead, CD133 seems to be required for normal morphogenesis of photoreceptors. More specifically, the outer segments and disks of cone and rod receptors. This seems to coincide with proper distribution of the visual pigment Opsin to the outer segment. CD133 preferentially localises at the basal part of the outer segment in rods where loss of CD133 leads to misalignment of disks and subsequent mislocalisation of Opsin. These phenotypes are shared with other models of retinal degradation[259,260]. These data suggest that CD133 acts as an essential regulator of outer segment morphogenesis and maintenance.

An additional phenotype observed in *CD133* KO mice is decreased branching morphogenesis of the mammary glands that is independent of the oestrus cycle but is overcome by pregnancy. *In vitro* studies on mammary epithelial cells shows that CD133 loss leads to hyper-proliferation. Whereas in the NKI295 breast cancer cell line CD133 levels were unaltered[261]. An established molecular mechanism of CD133 in the mammary gland is still undefined. During puberty, Prolactin and Progesterone are involved in side-branching via the Progesterone receptor (PGR). Furthermore, Matrix metalloprotease 3 (MMP3) directs the degradation of the basal membrane around the main ducts necessary for branching morphogenesis[262]. This is further confirmed by the similar phenotypes displayed by both PGR and MMP3 deficient mice. Moreover, both proteins are

downregulated in *CD133* KO mammary glands. Despite all this, a direct interaction between these molecules and CD133 has not been found yet.

Despite the variability between CD133 isoforms in their N-terminal intracellular domain (Figure 8) one conserved tyrosine residue (Y828) is present in all isoforms[263]. Y828, together with Y852 is potentially phosphorylated by Src family kinases in the human medulloblastoma cell lines Daoy and D283. Phosphorylation of Y838 is required for the docking of the p85 regulatory subunit of phosphoinositide 3-kinase (PI3K) to IC3 of CD133 leading to activation of the PI3K/Akt pathway. This interaction promotes self-renewal and tumour formation of glioma stem cells[264].

Two independent studies in cancer have found an interaction between CD133 and canonical Wingless-Type MMTV Integration Site (Wnt) signalling. Rappa *et al.* have shown that in the melanoma FEMX cell line, short hairpin RNA (shRNA)-mediated knockdown of CD133 leads to Dickkopf WNT Signaling Pathway Inhibitor 1 (DKK1)-mediated inhibition of Wnt signalling[250].

CD133 also interacts with β-catenin, the central molecule of the canonical Wnt-signaling pathway, via Histone deacetylase 6 (HDAC6) to form a complex leading to a two-fold reaction. First, it has been shown that the interaction leads to diminished CD133 degradation through negative regulation of the endosomal trafficking compartment. Second, the complex formation stabilises β-catenin, independent of Glycogen Synthase Kinase 3 Beta (GSK3β), resulting in the activation of its signalling targets[265].

The presence of CD133 within membrane protrusions suggest that CD133 is potentially involved in the regulation of the plasma membrane as an "organiser"

of its topology. CD133+ exosomes, also termed prominosomes, present in the ventricular fluid of the developing mouse neural tube concur with the regression of microvilli and the formation of large pleiomorphic on embryonic neuroepithelium[230]. Moreover, CD133 interacts directly with cholesterol which is a lipid distributed unevenly in the plasma membrane. Cholesterol-rich domains within the plasma membrane are termed ‘lipid rafts’ suggesting that CD133 might be involved in lipid raft organisation[183]. This is further confirmed by the work of Roper that CD133 becomes associated with lipid rafts in the trans-Golgi network prior to sorting to the plasma membrane[222]. Despite the evidence of CD133 association with lipid rafts, its role is not clearly defined yet. It is known that lipid composition and location affect cell signalling processes. CD133 might have a direct effect on these systems as a critical player regulating lipid raft formation, integrity and maintenance.

1.4 The mouse incisor as a model to study stem cell activation

1.4.1 General mechanisms and Morphology of Tooth Development

Teeth are typical organs for vertebrates, whereas in some species they have been lost during evolution. As with other ectodermal organs, initial stages in tooth development include thickening of the epithelium resulting in bud formation associated with the surrounding condensation of the mesenchyme. After this stage when morphogenesis begins each ectodermal organ develops differently. The more distinct tooth morphogenesis stages include folding and growth of the epithelium into the cap stage an intermediate step leading to the bell stage, which will finally create the shape of the tooth crown[266].

In many animals, teeth are replaced continuously throughout life. This is different in mammals where teeth develop only once, such as in rodents, or twice, as in humans, forming primary and secondary dentition. To understand the molecular mechanisms behind the formation of secondary dentition, researchers use the ferret as a model whereas in non-mammalian vertebrates such as fish their teeth are continuously renewed and replaced thus providing an excellent model to study tooth development[267–269]. In birds, evolutionary pressure led them to lose their teeth approximately 80 million years ago, but the genes regulating tooth development still exist in the jaw as their activation via transplanted mouse neural crest xenografts leads to tooth formation in chicken[270–273].

The dentition of rodents only consists of molars and incisors that are separated by an area called the diastema, thus lacking both canines and premolars. Interestingly, premolars are being formed during early tooth development but never gets past the bud stage where it is removed apoptotically[274,275].

Broadly, the tooth can be anatomically divided into a root and a crown. During development, the morphology of the crown is tightly regulated leading to, for instance, complex cusp patterning in the molars. Cusp number and location is dependent on the folding of the epithelium and the location of enamel knots, the epithelial signalling centres in the tooth[276,277]. The morphological differences between incisors and molars become evident during the late stages of development. The mouse enamel knot can be detected by histological means at around E14 as a bulging and thickening of the inner dental epithelium. This condensed area of epithelial cells expresses many secreted proteins along with cell cycle regulators and transcription factors such as SHH, Fibroblast growth factors (FGF), Bone Morphogenetic Proteins (BMP), WNT's, p21 and Msh Homeobox 2 (MSX2)[276–280]. The enamel knot is activated at the late bud stage by signals from the condensed mesenchyme. At this stage, mesenchymal BMP4 and Activin induces enamel knot marker genes, MSX2, Edar and p21 in the oral epithelium[278,281,282]. The enamel knot is finally removed as it undergoes apoptosis during the cap stage of tooth development[283,284]. Thus, crown morphology is decided in the bud and cap stage of tooth development.

The tooth crown is covered with enamel and the underlying dentine. Mesenchymal cells contacting the inner dental epithelium begin to differentiate into dentine-forming odontoblasts, and the remaining dental papilla cells form the dental pulp. The inner dental epithelium differentiates into enamel-depositing ameloblasts. Odontoblast and ameloblast differentiation is regulated by reciprocal and sequential interactions between the mesenchyme and epithelium. In humans, the epithelial stem cell-containing cervical loops lose their stellate reticulum and the remaining epithelium, consisting only of inner and outer dental epithelia and the basal lamina, forms the Hertwig's epithelial root sheath (HERS).

HERS facilitates root development and induces the formation of dentine and cementum, formed by cementoblasts differentiating from dental papilla. Later the HERS partially disappear and form epithelial cell rests of Malassez (ERM)[285]. Although, in some cases, HERS is not necessary for the formation of ERM, and regulation between the crown and root fate is flexible[286].

In addition to the root, other supporting tissues such as periodontal ligament, alveolar bone, gingiva and cementum are needed for the firm attachment of the tooth. The dental follicle gives rise to fibroblasts, which produces the extracellular matrix, eventually forming the periodental ligament. The periodental ligament connects the tooth root to the alveolar bone, but they also act as sensory organs[285]. In rodents, certain teeth grow continuously. For instance, mice have continuously growing asymmetrical conical incisors whereas the southern vole also has continuously growing molars[286]. The initial stages of the development and differentiation of the continuously growing incisor or molar are similar to that of the root-forming mouse molar but the expression of several signalling molecules, which are lost in the latter, are maintained in continuously growing teeth[286]. Interestingly, *in vitro* cultured mouse molar cells still express the typical gene expression pattern of continuously growing teeth suggesting that the molar epithelium still can grow continuously287.

1.4.2 Initiation of Tooth Development

The reciprocal and sequential interactions between the mesenchyme and epithelium governing tooth development regulate proliferation, differentiation and apoptosis. The dental lamina or odontogenic band, a horseshoe-shaped thickening of the epithelium, forms from cells derived from the first branchial arch and is supported by the adjacent neural crest-derived mesenchymal

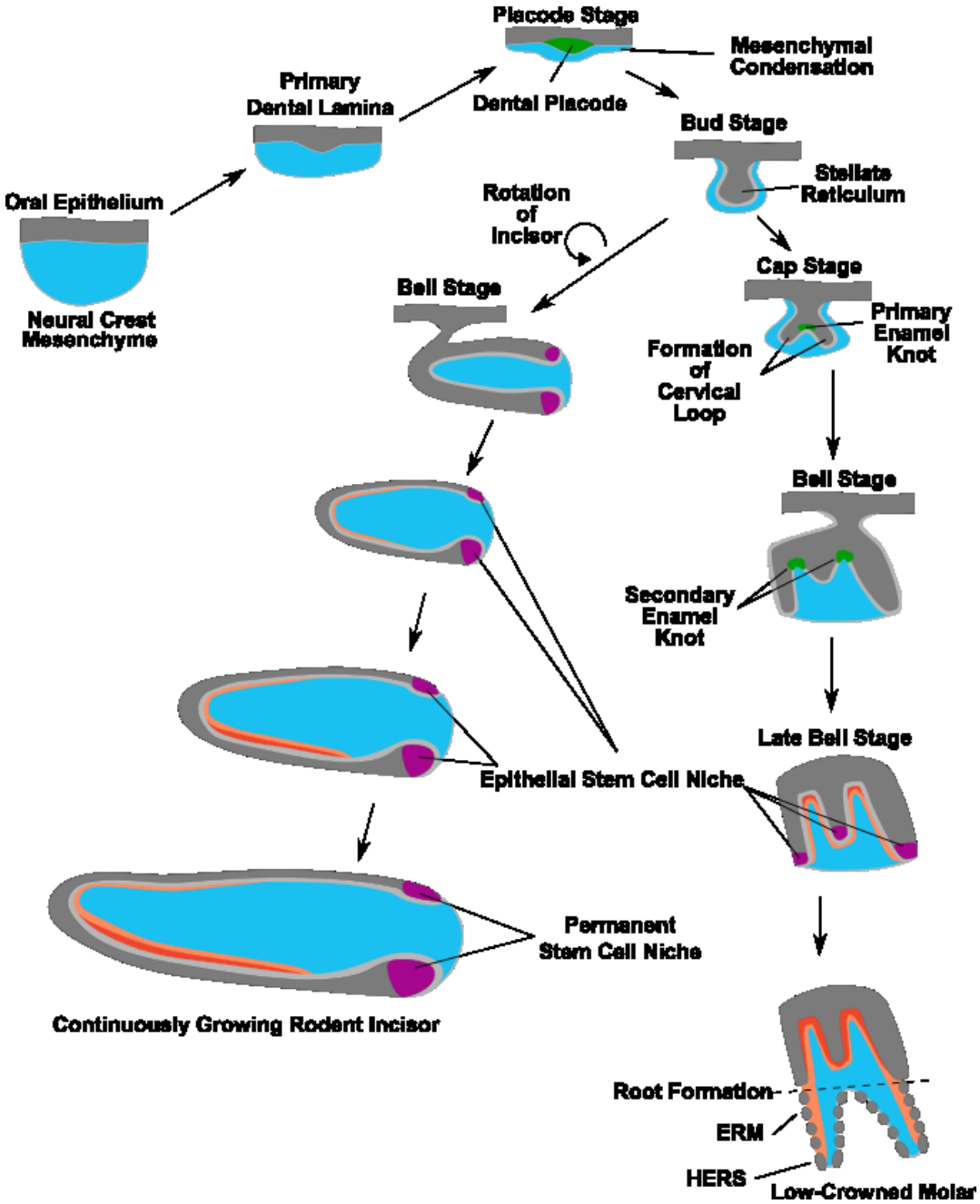

Figure 9: The developmental anatomy of early tooth morphogenesis in the rodent incisor and molar tooth types before eruption.
Penetration of the epithelium (grey) into the adjacent mesenchyme (blue) is the first step to the development of the primary dental lamina, which holds the dental placode (green). The condensation of the mesenchyme and subsequent budding of the epithelium follow the invasion of the epithelium. These initial steps are remarkably similar in the development of all ectodermal structures. During the cap stage, the epithelial bud will ultimately invaginate the mesenchymal dental papilla, and the stem cell-containing epithelial cervical loop (purple) is formed adjacent to the bud. The development of different tooth types depends on the different development cues from this point. The cervical loop in the epithelium persists in continuously growing teeth, whereas in root-forming teeth such as human teeth and molars in rodents, they completely disappear. Important stages in tooth development are regulated by signalling centres including the dental placode, and primary and secondary enamel knots. The enamel knots are characterised by the folding of the epithelium, which regulates crown morphogenesis. The secondary enamel knots determine cusp number and location. HERS, Hertwig's epithelial root sheath, ERM, epithelial cell rests of Malassez.

cells[288–290].The tooth only develops within this structure, and even development of ectopic teeth is limited to the dental lamina[237,291,292]. Interestingly, in mice with loss-of-function of Adenomatous Polyposis Coli (APC), a member of a protein complex targeting β-catenin to degradation, teeth can develop in some cases outside the lamina[293]. In mice, the tooth placode begins to form within the dental lamina at E11. Instructions to initiate tooth development come from the epithelium whereas during later stages the odontogenic potential changes to the dental mesenchyme[294].

1.4.3 Cap and bell stage of tooth development

Between E14 and E18 in embryonic mouse, the morphology of the first lower molar changes drastically and moves from the early cap to the bell stage. Five phenomena, controlled by epithelial-mesenchymal interactions, characterise this period: change in the cellular makeup of the mesenchyme, enlargement of the tooth germ; development of the cervical loop; maturation of the enamel organ and cusp formation due to the folding of the epithelial-mesenchymal junction[295–300].

During the cap stage at E14-E15, spatial variations in mitotic activity in dental epithelial cells and mesenchyme cause the enlargement of the tooth germ and changes in the shape of the epithelial-mesenchymal interface. This has been shown by the differential uptake of 3H-thymidine or 5-bromo-2'-deoxyuridine (BrdU) and changes in expression patterns of p21, an inhibitor of the cell cycle[278,295,301]. More specifically, this involves spatiotemporal control of apoptosis in the epithelium, changes in mitosis, alterations in cell adhesion and migration of both mesenchyme and epithelium. Moreover, other cell types are involved in the remodelling of basement membrane at the epithelial-mesenchymal junction and the invasion of exogenous cells in the dental pulp. At the epithelial-

mesenchymal interface, cell differentiation is induced first in the mesenchyme when pre-dentine is produced by the newly formed odontoblasts. This will induce differentiation in the inner dental epithelium into ameloblasts.

1.4.4 Maturation of Tooth Epithelial Cells

The subsequent and reciprocal interactions between cranial neural crest-derived mesenchyme and oral epithelium lead eventually to differentiation of both lineages and the production of teeth-specific mineralised tissues[302,303].At the epithelial-mesenchymal junction, odontoblasts responsible for dentine matrix production are derived from the mesenchymal part whereas ameloblasts, which produce the enamel matrix, are epithelial in origin. The first event in dental mineralisation is the differentiation of dental pulp cells into odontoblasts which secrete a collagen-like matrix that forms the mantle dentine[304]. Formation of this mantle dentine initiates the differentiation of epithelial cells into ameloblasts leading to enamel matrix deposition and mineralisation[305]. When the developing tooth still resides in the gum, ameloblasts go through four distinct stages during differentiation: the pre-secretory, the secretory, transition and maturation stage[306]. In the pre-secretory stage, before mantle dentine deposition, the bell stage of tooth development determines the shape of the crown. The cells from the inner dental epithelium which goes on to become ameloblasts are characterised by their cuboidal or low columnar shape with poorly developed Golgi complexes and centralised nuclei[307]. When the adjacent odontoblasts form the mantle dentine the inner dental epithelial cells elongate, and their nuclei move away from the dentine-facing side and become pre-ameloblasts. These cells further elongate and become post-mitotic, secretory ameloblasts. In the secretory stage, the rough endoplasmic reticulum of ameloblasts produces and secrete the majority

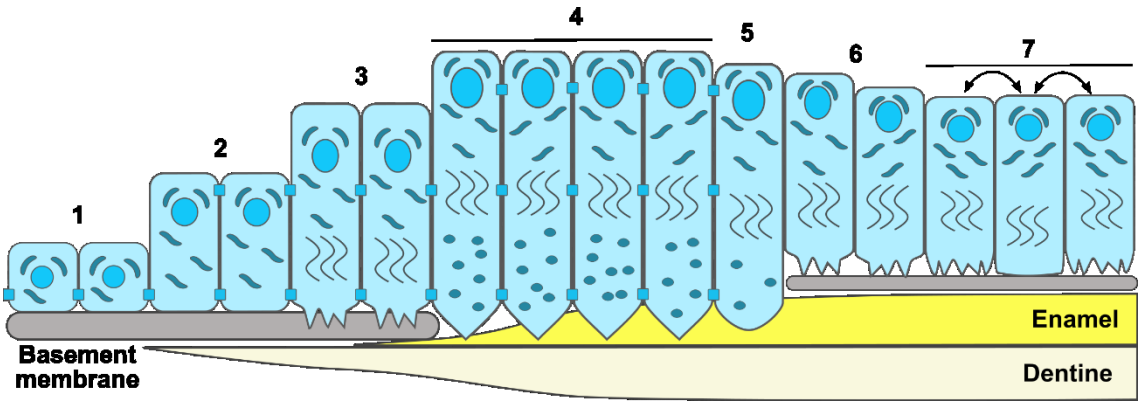

Figure 10: Ameloblast differentiation and enamel deposition.
The inner dental epithelial cells (1) contact the basal membrane. These cells transition into pre-ameloblasts upon contact with the mantle dentine matrix (2). Processes spread from the pre-secretory ameloblasts and penetrate the resorbing basement membrane to secrete enamel matrix proteins on the exterior of the mineralising dentine (3). After the establishment of the dentine-enamel junction and the initial layer of aprismatic enamel is deposited, the secretory ameloblasts grow Tomes' processes from which enamel proteins are secreted into the surrounding mineralisation front (4). A single enamel rod is produced by each ameloblast that elongates from the receding Tomes' process, and as the secretory stage ends, the ameloblasts have completely resorbed their Tomes' process and have produced full thickness immature aprismatic enamel (5). In the final transition stage, the ameloblasts become less columnar and adjust their secretome (6). Proteases are secreted and digest the protein matrix. Finally, ameloblasts are fully matured and interchange between smooth-ended and ruffled phases, which leads to maturation and hardening of the enamel layer (7).

of the enamel matrix which will support hydroxyapatite crystal growth and define the thickness of the fully mineralised enamel[305]. At the cusps, enamel can reach a thickness of about 2,5mm whereas it is at its thinnest where it borders the cementum at the cemento-enamel junction[307]. The enzyme alkaline phosphatase then initiates the first wave of mineralisation. The ameloblasts retreat from the dentino-enamel junction leading to the protrusion of Tomes' processes from the ameloblasts contacting the dentine. These processes are responsible for the hydroxylapatite crystal growth and are angled to allow for differences in crystallite orientation. Hence, increasing the strength of the forming enamel.

Initially, the secreted enamel matrix is composed of proteins such as Amelogenin (AmelX), Ameloblastin (Ambn) and Enamelin, and inorganic materials such as calcium and phosphate ions. The proteins form an extensive extracellular network where the inorganic material is incorporated to form hydroxyapatite crystals[308,309,310,311]. Once secretion of the enamel matrix is completed, ameloblasts in the maturation stage stimulate the thickening of the hydroxyapatite crystals and enamel rod formation. Simultaneously, the removal of the extracellular enamel proteins by proteases such as Matrix metalloprotease 20 (MMP20) in the secretory stage and Kallikrein-Related Peptidase 4 (KLK4) in the maturation stage is necessary to achieve the final hardness of fully developed enamel[312].

1.4.5 The dental epithelium in the continuously growing mouse incisor

In mice, each jaw quadrant consists of one continuously growing incisor and three molars separated by the diastema. The morphological events between the incisor and the molar are similar in early development. During the cap stage, the incisor

tooth germ orientates itself along the anteroposterior axis while the epithelial cervical loop develop asymmetrically with the labial cervical loop becoming larger than the lingual cervical loop[313,314].

The formation of the cervical loop and its maintenance throughout the animal's lifetime is critical for the renewal capacity of the incisor. The constant generation of dental hard tissues accompanies the continuous abrasion of the incisor tip. This requires both epithelial and mesenchymal tissues to form a gradient of differentiation from the cervical loop towards the incisor tip. The self-renewal and proliferation of epithelial stem cells take place in the cervical loop[78,315]. Currently, the exact origin of mesenchymal stem cells in the mouse incisor is still under debate[316–318]. The epithelial differentiating cells migrate towards the proximal incisor tip in a conveyor belt-like manner. They eventually differentiate into columnar, polarised ameloblasts, which produce and secrete enamel[319]. The incisor tooth is asymmetric in the generation of enamel, as the lingual side does not produce any enamel. Thus, only the labial cervical loop is capable of producing ameloblasts.

The cervical loop consists of a core of stellate reticulum surrounded by the basal epithelium which makes up outer dental epithelium, at the most apical side of the cervical loop, and the inner dental epithelium, bordering the mesenchymal dental pulp[320]. The stellate reticulum in the lingual cervical loop is mostly depleted in the adult incisor tooth and is therefore not capable of giving rise to ameloblasts. However, they are thought to be a source of epithelial rests of Malassez, an epithelial remnant of the root sheath[321].

Label-retaining experiments using $_3$H-Thymidine in the 1970's gave the first clue as to the location of epithelial stem cells in the incisors of rodents[322]. Whereas

others showed that BrdU-retaining cells are present in the stellate reticulum region of the mouse incisor labial cervical loop. Moreover, *in vitro* tissue-ablation experiments indicated that dissected cervical loop from P2 mice continues to produce dental tissues, showing that the cervical loop contains cells with significant growth and differentiation capabilities [315]. Recently, Histone 2B-GFP (H2B-GFP) technology, a marker for slow-cycling cells, indicated that label-retaining cells in the adult mouse labial cervical loop were located in the stellate reticulum and outer dental epithelium[323].

The molecular signature of the epithelial stem cells in the labial cervical loop contains typical stem cell markers such as Lgr5, Bmi1 and Gli1[82,323,324]. The lingual cervical loop appears to harbour slow-cycling stem cells as is shown by label-retention experiments. However, their numbers are low and are currently not well investigated[323].

1.4.6 Molecular regulation of labial cervical loop stem cells

Up until now, substantial progress has been made on how epithelial stem cells are maintained and regulated at the molecular level. It has become evident that the epithelial stem cells are controlled by complex and reciprocal interactions between the cervical loop epithelium and the surrounding mesenchyme, including several signalling pathways, transcription factors and cell adhesion molecules.

Mesenchymal Fgf3 and Fgf10 were the first extracellular ligands discovered that demonstrated the reciprocal control of epithelial stem cells[315]. Subsequent experiments involving mutant mice of both genes have shown that these mesenchymal signals affect the self-renewal and lineage differentiation of the stem cells[320,325]. Indeed, *Fgf3* and *Fgf10* KO mice do not develop enamel[320]. In agreement with this observation down-regulation of epithelial Fgfr2b, the receptor

for Fgf3 and Fgf10 exhibits similar phenotypes such as the impaired growth of the whole incisor and failure of enamel formation[326]. Interestingly, an increase in Fgf signalling via down-regulation of Sprouty genes (*Spry4* KO and *Spry2*$^{+/-}$) led to ectopic enamel formation on the lingual side of the incisor, thereby, creating as described by the authors a 'tusk-like' incisor tooth completely surrounded by enamel[327]. Loss of the mesenchymal Transforming Growth Factor Beta Receptor 1 (Tgfβr), a member of the Tgfβ superfamily, severely reduces stem cell maintenance and lineage differentiation and appears to be upstream of Fgf3 and 10 signalling[328].

Mesenchymal Tgfβ1 connects Fgf3 and 10 signalling with multiple conserved pathways in the control of dental epithelial stem cells. Tgfβ2r mediates Tgfβ1-dependent Fgf3 and 10 signalling in the mesenchyme which, in turn, leads to a decrease in LDL Receptor Related Protein 5/6 (Lrp5/6) signalling in the epithelium. The resulting reduction of Wnt5a signalling favours retention of stem cells in the cervical loop over differentiation of its progeny[329]. Bmp4, another well-known stem cell marker and under control of Tgfβ family members, reduces proliferation of the epithelial stem cells and their progeny while it promotes the differentiation of inner dental epithelial cells into ameloblasts. In line with this, overexpression of Noggin, an inhibitor of Bmp, in the dental epithelium leads to increased proliferation and lack of enamel due to the loss of ameloblasts [330]. The importance of Bmp signalling in tooth development is also demonstrated in conditional *Bmpr1a* KO mice that lack all teeth. More specifically, the development of all teeth is arrested at the bud stage [331]. Other examples of mouse genotypes that lack all teeth are Lymphoid Enhancer Binding Factor 1 (Lef1), Paired Like Homeodomain 2 (Pitx2), Pax9, Msx1/2 and Gli2/3 [332–336].

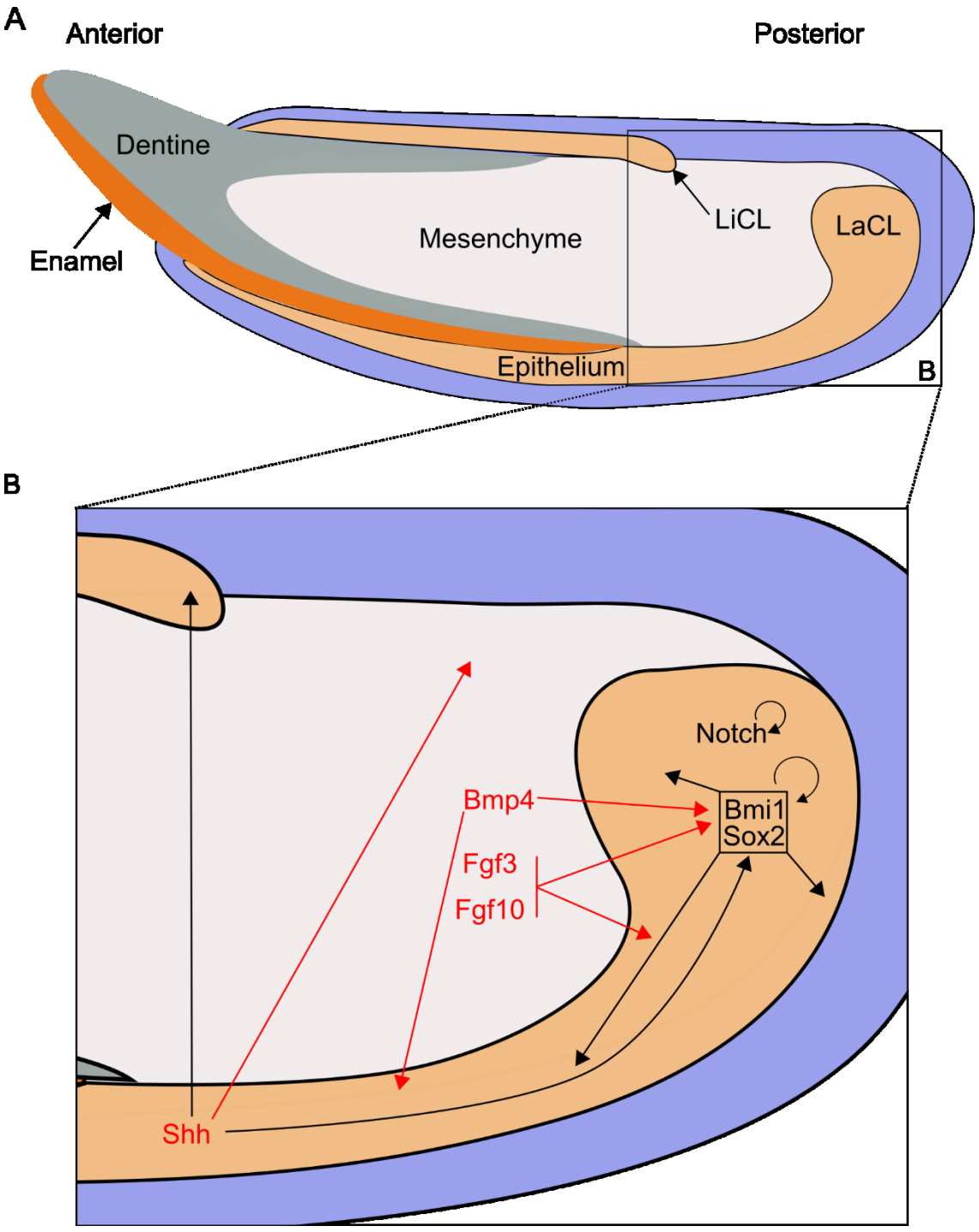

Figure 11: Overview of the adult mouse incisor and its regulation of stem cells in the labial cervical loop.
A) Schematic overview of the mouse incisor displaying the mesenchyme (light grey) and its associated dentine (dark grey), and the epithelium (light orange) responsible for enamel (dark orange) production. B) Gene regulatory network of epithelial stem cell homeostasis, proliferation and differentiation. Red arrows indicate epithelial-mesenchymal interactions whereas black arrows indicate epithelial factors. LaCL: Labial cervical loop, LiCL: Lingual cervical loop.

Previous examples illustrated how the mesenchyme affects epithelial stem cell maintenance and proliferation. There also exists a feedback loop in which epithelial progeny signal back to the cervical loop to promote lineage differentiation. Shh is a well-known mitogen involved in patterning events during development [337]. Despite the role of Shh in development, its part in adult stem cells is less clear as is evidenced by conflicting reports in haematopoietic stem cells [338–340]. *Shh* is known to be important in morphogenesis of teeth in the embryo [61,336,341]. Its expression in the progeny adjacent to the stem cell region in the labial cervical loop points at a role in lineage differentiation. Interestingly, not only cells in the labial cervical loop are Shh-responsive as shown by their expression of *Gli1* and *Ptch1* reporters but also cells in the mesenchyme and epithelial cells in the lingual cervical loop[323]. Inhibition of *Shh* led to a decrease in ameloblast differentiation but not the adjacent Stratum intermedium cells[323].

Bmi1, a polycomb group gene, is known to play a role in adult stem cell homeostasis in preventing arrested cell division via *Ink4a/Arf* and its expression is often linked with high expression of *CD133* in cancer[342–344]. In the mouse incisor tooth, an additional layer of regulation exists to prevent premature differentiation of stem cells. Indeed, negative regulation of Homeobox (*Hox*) genes rescues the phenotype caused by loss of *BMI1*[82].

Labial cervical loop stem cells also display Notch pathway activity, and a number of Notch receptors and its ligands are expressed in the cervical loop[315]. Notch signalling seems to be implicated in stem cell maintenance as its inhibition leads to smaller labial cervical loop[315,345]. *Sox2* is expressed in a wide range of stem cells including embryonic stem cells and is one of the four reprogramming factors used in generating induced pluripotent stem cells[17,346]. During mouse incisor

development, *Sox2* expression becomes progressively restricted during morphogenesis to the stem cell niche in the labial cervical loop[347]. Moreover, induced genetic fate mapping of Sox2+ cells in mouse incisor teeth have shown that these cells generate all cell types of the dental epithelium[78].

Collectively, these findings point out that the continuously growing incisor is a well-characterised organ that is suitable to investigate the role of CD133 in stem cells and their progeny.

2 Aims and objectives

Preliminary results in our group have confirmed that CD133 is expressed in the developing mouse incisor epithelium. Taken together with the literature study, we hypothesized that CD133 is important for incisor tooth development by affecting stem cell activation and fate.

2.1 Aims

- To test the function of CD133 in incisor epithelial stem cell maintenance, activation and differentiation.
- To examine the molecular binding partners of CD133 in mediating the transition of stem cells into transit-amplifying cells.

2.2 Objectives

Using mouse lower incisor teeth, I have performed experiments that cover the following steps:

Year 1. *CD133* expression in developing tooth, CD133 knockout mice tooth phenotype characterization and generation of Cervical Loop Epithelial cells.

- Assessment of RNA and protein expression of CD133 in Postnatal day 7 mouse lower incisors;
- Scanning electron microscopy analysis of *CD133* KO mice incisor tooth phenotype, including analysis of ameloblast differentiation marker expression;
- Definition of stem cells and transit-amplifying cells in the dental epithelium cervical loop including the transition zone between the two regions;

Year 2. *In vitro* and *in vivo* investigation of CD133's role on stem cell activation in the developing mouse incisor tooth.

- Generation and validation of cervical loop epithelial primary cells;

- Alteration of CD133 levels in *in vitro* cell culture and assessment of its effect on the cell cycle and stem cell activation;
- Comparison of cervical loop population size between WT and *CD133* KO mice;
- Generation of Ki67/FUCCI fluorescent cell cycle indicator system in cervical loop epithelial cells;

Year 3. Investigation of the role of CD133 in primary cilia dynamics

- Assessment of primary cilia dimensions in WT and *CD133* KO mice;
- Analysis of primary cilia markers Hdac6 and Arl13b in the context of CD133 expression;
- Examination of CD133 translocation to the nucleus;
- Analysis of Shh effectors in the dental epithelium of the mouse incisor tooth;

Year 4. Analysis of the role of CD133 in Shh signalling.

- Establishment of CD133 interaction with Glis2 and Arl13b;
- Determination of common pathways shared between Glis2 and CD133 using PCR array;
- Effect of Shh on cell fate with basal or reduced levels of CD133;
- Assessment of primary cilia dynamics and CD133 expression in *Bmi1*$^{GFP/GFP}$ mice;

3 Impact of the work

The importance of stem cells and their use in regenerative medicine cannot be understated. Damaged, dying or malfunctioning cells lead to injuries, diseases or aging. Replacement of these cells depends largely on the ability of stem cells to react to cues from the environment, facilitate a proper response leading to the generation of newly specialised cells, and simultaneously maintain the stem cell population to counteract future insults.

How stem cells communicate with the tissue environment is currently being subjected to extensive research. One organelle that is important for mediating extracellular signalling is the primary cilium, an antenna-like structure that protrudes from the cell membrane. Primary cilia in stem cells have been well investigated in *in vitro* cultures, however, this presents one major limitation. Typically, *in vitro* culture of cells involves maximum two different cell types to be investigated and this is not representative of the stem cell environment as illustrated in Section 1.1.3. This severely limits the research on extracellular signalling between different cell types and the roles primary cilia play in them. Our work studies the relationship between primary cilia and stemness of cells within the developing dental epithelium.

One protein that is predominantly found in primary cilia is CD133 and its discovery in stem cells happened right upon the advent of stem cell research 20 years ago. Initially, its expression was only seen in stem and progenitor cells in a wide range of tissues and was, therefore, a so-called stem cell marker. Indeed, since its discovery CD133 has been described in 5000 publications with nearly all of them of its use as a stem cell marker. Moreover, CD133 became clinically relevant when it was discovered that cancer stem cells harbouring CD133 have more tumourigenic capacity and are more resistant to treatment than their CD133-

negative counterparts are. Despite intensive research, the function of CD133 in primary cilia remains largely unknown. Our work shows the importance of CD133 in the dynamic regulation of primary cilia length and its relation to the stemness of the epithelial cells in the developing mouse incisor model. Moreover, we have proven that dysregulation of the primary cilia architecture leads to an altered stem cell response affecting homeostasis of the tissue investigated. Additionally, our results clearly indicate the potential of CD133 as a therapeutic target in cancer treatment.

4 Results

4.1 The developing mouse incisor as a model to investigate epithelial stem and transit-amplifying cells

The mouse incisor tooth continually grows throughout the animal's life. This continuous growth indicates that there might be stem cells present within the incisors. Indeed, previous reports suggest that epithelial stem cells of the incisor are presumably remaining in the cervical loop (Figure 12a), a specific epithelial structure located at the distal end of the tooth epithelium[315]. These cells express stem cell markers such as Leucine Rich Repeat-Containing G Protein-Coupled Receptor 5 (Lgr5) and Sex Determining Region Y-Box 2 (Sox2) and can differentiate into distinctive epithelial lineages under the instruction of mesenchymal cells[78,324]. B Lymphoma Mo-MLV Insertion Region 1 Homolog (Bmi1) and Glioma-Associated Oncogene Homolog 1 (Gli1) have also been shown to mark cells within the cervical loop that coincide with label-retaining cells[82].

Immunostaining of the cervical loop in postnatal day (P) 7 C57BL/6 mice revealed a large region of stem cells indicated by Sox2 (Figure 12b) which overlaps greatly with the stem cell markers mentioned earlier such as Bmi1 and Gli1[82]. Moreover, it has been shown that Sox2-positive cells give rise to all dental epithelial lineages[78]. Immediately adjacent to the stem cell region is the inner dental epithelium, a region that contains transit-amplifying cells which is highly positive for Marker Of Proliferation Ki-67 (Ki67), a well-known proliferation marker[348] (Figure 12b). Interestingly, both regions are connected by an area positive for both Sox2 and Ki67 indicating a transition zone where stem cells become activated and enter the cell cycle (Figure 12b).

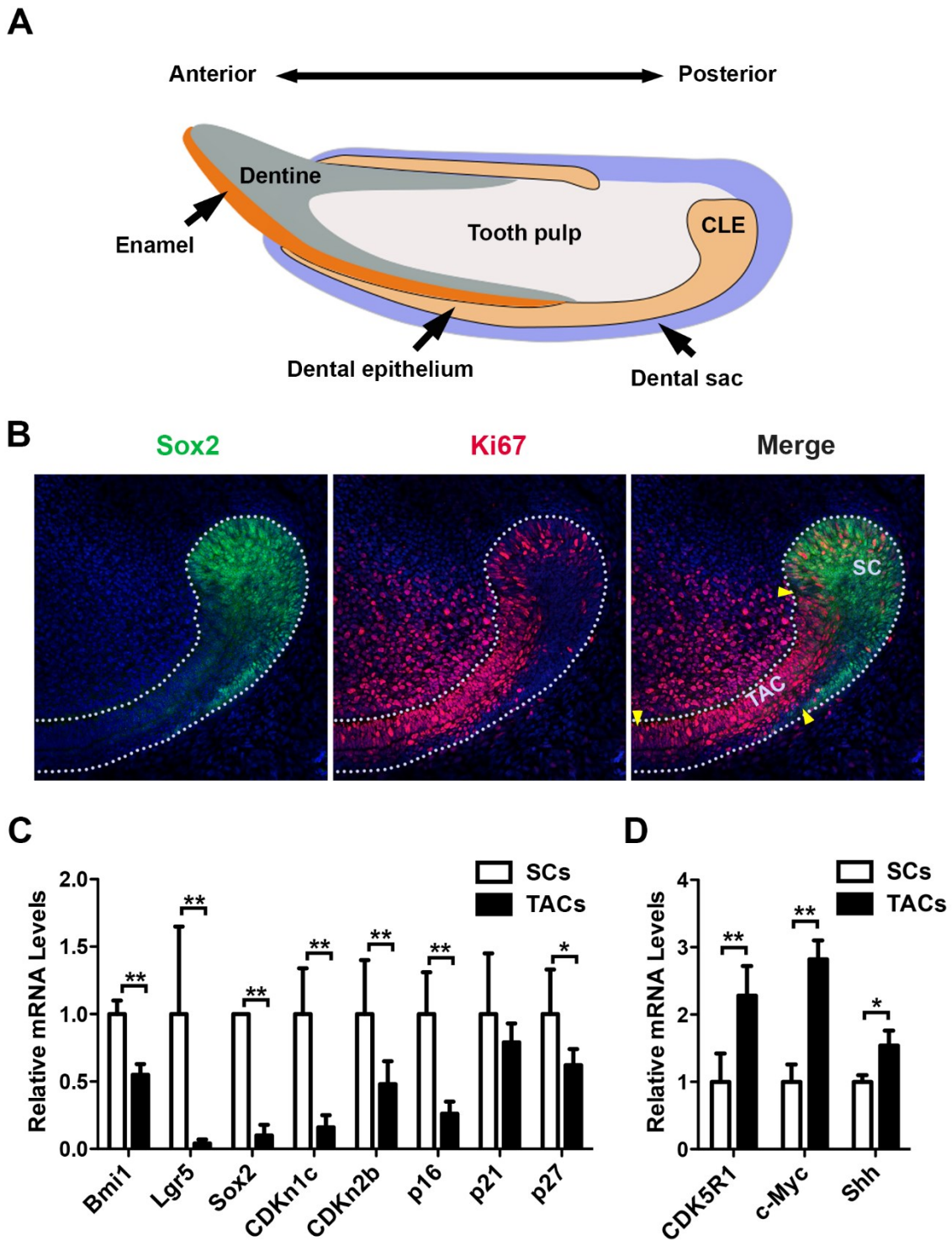

Figure 12: The mouse incisor tooth is an excellent model to study quiescent stem cell to transit-amplifying cell transition
A) Schematical overview of the lower mouse incisor tooth with the epithelium in orange and the mesenchyme in light grey. B) Sagittal view of the CLE region of P7 C57BL/6 mice. Yellow arrowheads mark the beginning and end of quiescent stem cell and transit-amplifying cell zones. Dotted lines mark the epithelium. C) Real-Time qPCR analysis of established stem cell and cell cycle inhibitor markers. D) Real-Time qPCR analysis of known mitogenic markers.

Laser Capture Microdissection (LCM) was then performed to extract total RNA from the Sox2- and Ki67-positive regions. Subsequent Real-Time quantitative Polymerase Chain Reaction (qPCR) analysis was done of specific markers associated with quiescence and proliferation confirming their quiescent stem cell and proliferating transit-amplifying cell status, respectively (Figure 12c & d). Our assessment of the cervical loop and its regions revealed two distinct zones based on quiescence and cell cycle status, which enables us to investigate the possible role and mechanisms of the stem cell marker CD133 in governing these regions.

4.2 Primary cilia dynamics are linked to the cell cycle in the cervical loop

The primary cilium is a dynamic organelle that is involved in chemical sensation, control of cell growth and signal transduction[130,349]. Its synthesis and resorption have been inherently linked with the cell cycle as they both share the same machinery. Indeed, the centriole that functions as the base from which the primary cilium protrudes into the extracellular matrix functions as a centrosome during mitosis. Therefore, it is well established that cell cycle progression and ciliogenesis are mutually exclusive within the same cell[350]. Currently, the precise mechanism of ciliogenesis in function of the cell cycle is complicated to investigate *in vivo* due to the heterogeneity of most tissues and the relatively low numbers of stem cells. Figure 12 has demonstrated that the mouse incisor tooth is enriched with stem cells and is, therefore, an excellent model to investigate primary cilium dynamics in the context of the cell cycle.

One of the most widely used markers to identify primary cilia is acetylated α-Tubulin (AcTub). AcTub is a stable form of microtubules that is only seen in primary cilia, the mitotic spindle and the midbody following mitosis[351]. Within the

primary cilium, AcTub is required for ciliogenesis where it is an integral part of the axoneme, a structural support for primary cilia. Clone 6-11B-1, a monoclonal antibody raised against acetylated α-Tubulin is the most commonly used antibody to detect and quantify primary cilia[352–354]. Using this antibody, our assessment of primary cilia within the stem cells and transit-amplifying cells of the lower mouse incisor tooth epithelium revealed interesting, but not entirely surprising, characteristics. AcTub immunofluorescence (IF) on 20μm cryo-sections of the cervical loop, containing stem cell and transit-amplifying cell populations, from P7 C57BL/6 mice confirmed that the stem cell population contains a higher density of positive staining compared to the transit-amplifying cell population (Figure 13a). Quantification of AcTub immunofluorescence using Imaris 9.0 software (Figure 13b) states that around 60% of stem cells have a primary cilium whereas in the transit-amplifying cell region this is decreased by approximately 50% to 30% of total cells (Figure 13c-d). In parallel with a higher primary cilium density, primary cilia in the stem cell population are longer and have an increased volume alongside a higher diameter at the base of the primary cilium compared to the transit-amplifying cells (Figure 13e-g). This is in line with the literature where it is well established that cells residing in G0 or quiescent phase, such as in our stem cell population, generally tend to have longer primary cilia compared to more proliferative cells[355].

4.3 CD133 mRNA is present in the developing mouse incisor tooth epithelium

CD133, also referred to as Prominin1, has been used previously to isolate and characterise stem and progenitor cells in many tissues of different germ layers including but not limited to the prostate, haematopoietic system and

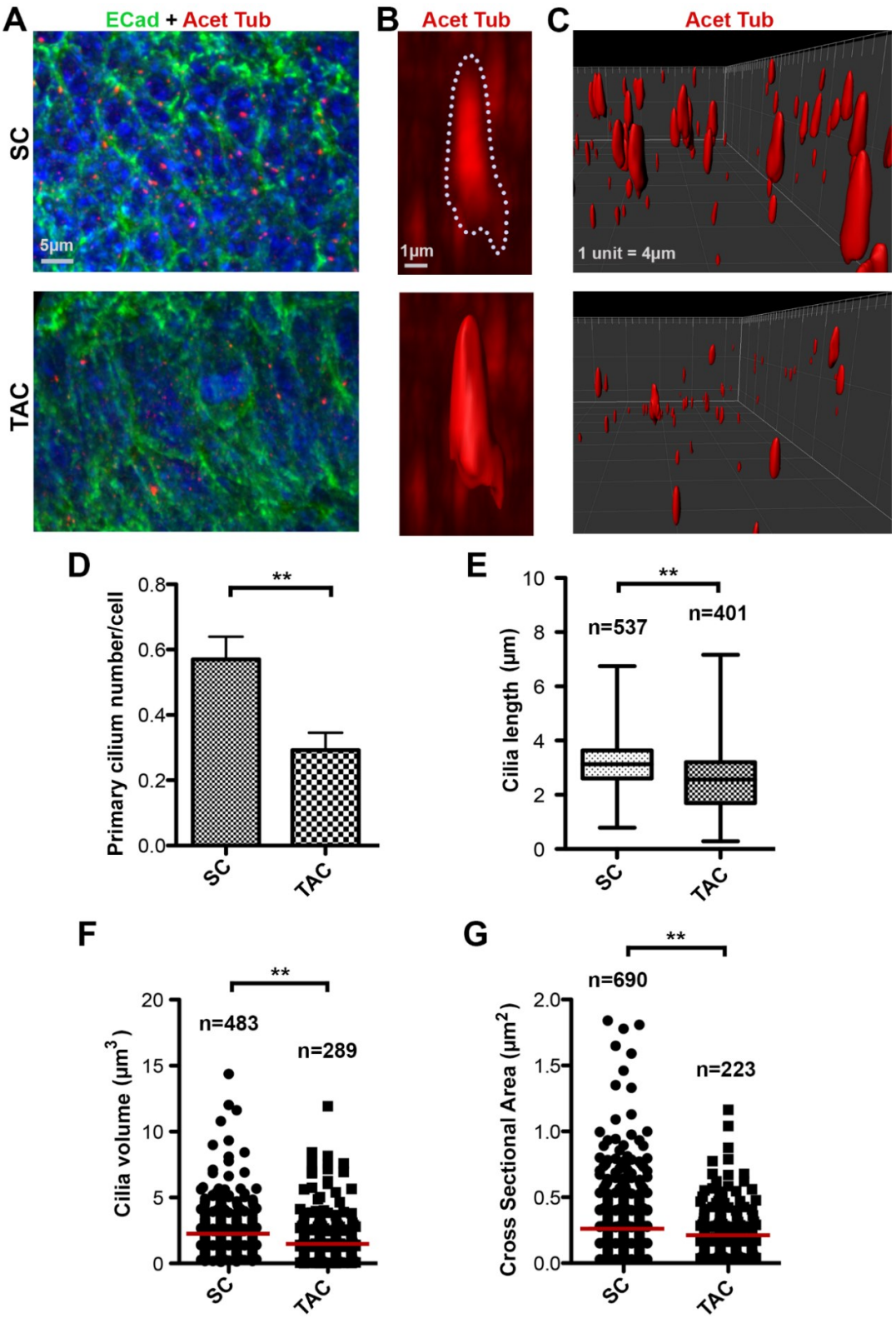

Figure 13: Primary cilium characteristics in the cervical loop of P7 C57BL/6 mice. A) AcTub (red) immunofluorescence shows the distribution of primary cilia in stem cells (top) and transit-amplifying cells (bottom), E-cadherin (green) used as a plasma membrane marker. B) Top: Example image of a primary cilium using AcTub as a marker, Bottom: 3D reconstruction of top image using Imaris software. C) transverse view of 3D reconstructed stem cells (top) and transit amplifying cells (bottom) D) Primary cilia quantification using AcTub immunofluorescence versus number of nuclei using 4',6-diamidino-2-phenylindole (DAPI) in stem cells compared to transit-amplifying cells E-F) Comparison of primary cilia dimensions in stem cell and transit-amplifying cell populations, n= number of primary cilia counted. ** $p<0.01$

kidney[165,195,211]. However, its usefulness as a stem cell marker has recently been challenged since its expression has also been detected in terminally differentiated cells[94]. CD133 mRNA in the cervical loop has been detected before by semi-quantitative PCR[356]. However, the presence of markers typically associated with mesenchymal tissues such as Sca1 suggests that their sample contained a fraction of the surrounding mesenchyme[357]. Therefore, the positive signal of CD133 mRNA could be derived from the surrounding mesenchyme rather than the epithelial cervical loop.

To answer the question whether CD133 is expressed in the cervical loop of the mouse incisor epithelium, we used LCM to isolate different populations of the mouse incisor tooth epithelium of P7 C57BL/6 mice. LCM enables us to avoid difficulties arising from analysis of heterogeneous tissues. The ability to isolate pure, homogenous cell populations allows the analysis of precise cellular and molecular interactions within the tissue microenvironment. Tissue extraction using LCM has been used successfully in many downstream applications such as RNA transcript profiling, next-generation sequencing, deoxyribonucleic acid (DNA) copy number and loss-of-heterozygosity analysis, mass spectrometry proteomics, and signal pathway analysis[358,359].

The LCM system is an inverted microscope with a built-in low power near-infrared (IR) laser and a high-power ultraviolet (UV) laser. Tissue sections are mounted on polyethylene naphthalate (PEN) membrane slides and are stained with methyl green for identification of tissue morphology and region-of-interest (ROI). The CapSure HS Cap coated with an ethylene–vinyl acetate film is then placed over the ROI. The IF laser provides enough energy to melt this thermoplastic film in a precise location, binding it to the targeted cells. The UV laser cuts the section at

a predetermined region, which separates the ROI from the surrounding tissue. The CapSure HS Cap and the collected samples are removed, and the remaining tissue is left behind on the PEN membrane slide. (For a video of this process, visit this site.) The ROI is then subjected to total RNA extraction protocol described in the Material and Methods section.

LCM was used to dissect the stem cell and transit-amplifying cell regions as defined in Figure 12 as well as the enamel-producing ameloblasts of three P7 mice (Figure 14a). Three to four consecutive 20µm cryo-sections per cervical loop were collected on PEN membrane slides and processed as described above within 20 minutes to minimise RNA degradation. RNA was pooled together and processed for complementary DNA (cDNA) conversion and analysis of CD133 mRNA expression using Real-Time qPCR. Primers directed against CD133 mRNA were carefully designed to include all known isoforms as well as to cross exons to eliminate amplification of contaminating DNA. Results showed that CD133 mRNA was detected with highest levels seen in stem cells and that transit-amplifying cells only had marginally lower levels of mRNA. Our Real-Time qPCR was not able to detect CD133 mRNA in the ameloblasts (Figure 14: CD133 mRNA levels in the mouse incisor epithelium of P7 C57BL/6 mice.

4.4 At least two different populations of CD133 exist within the mouse incisor tooth epithelium.

To validate the expression of CD133 at the protein level, we looked at the expression of two different epitopes: 13A4, which targets the 2nd extracellular loop (ECL) of CD133 and ORB129549, which targets the intracellular C-terminal domain (ICD) The 13A4 antibody has been used originally to describe CD133 in microvilli of the developing mouse neuro-epithelium. Moreover, it has been

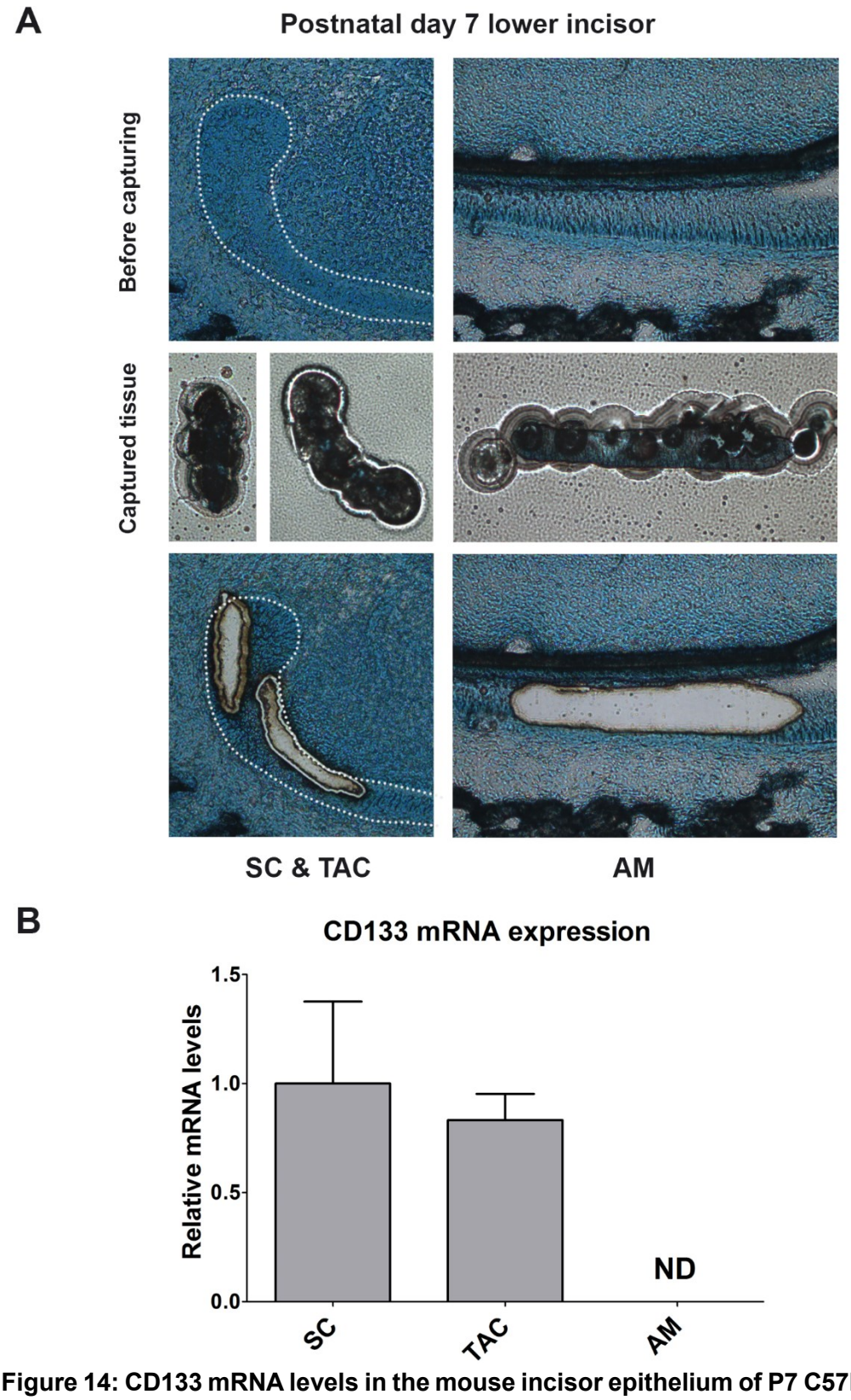

Figure 14: CD133 mRNA levels in the mouse incisor epithelium of P7 C57BL/6 mice
A) Top row: methyl green-stained sagittal section of cervical loop (left) and ameloblasts (right) region prior to cutting with UV laser. The dotted line represents the boundary of tooth epithelium. Middle row: Cut ROI on CapSure HS cap. Black circles are IF-melted film. Bottom row: methyl green-stained sagittal section of cervical loop (left) and ameloblasts (right) region after cutting with UV laser. Dotted line represents the boundary of tooth epithelium. B) Real-Time qPCR analysis of CD133 mRNA expression in stem cells, transit-amplifying cells and ameloblast populations. ND= not detected

shown that the antibody targets glycosylated and non-glycosylated CD133[167]. Despite its original observation in stem and progenitor cells in a variety of tissues, this epitope was also detected in post-mitotic ependymal cells and differentiated ductal and luminal epithelial cells in adult organs[94,199].

The ICD-targeting antibody was commercially generated using the following immunogen: CKYYRRMDSEDVYDD, which corresponds to a fragment within the ICD that is present in all known isoforms with no reported post-translational modifications yet. Assessment of CD133 protein expression within the mouse incisor using both antibodies revealed similar expression patterns. The ICD epitope is more broadly expressed in the whole cervical loop with increased expression in the transit-amplifying cells whereas the expression of CD133's ECL epitope is mostly restricted to transit-amplifying cells (Figure 15b&c). To date, most research on CD133 has been conducted in neural or epithelial tissues with few reports of CD133 expression in mesenchymal tissues and cells such as stromal stem cells in the bone marrow, mobilised peripheral blood and umbilical cord blood[360,361]. In our study, CD133 protein expression is also detected in the dental mesenchyme using the two antibodies (Figure 15b&c). Therefore, we were interested to see whether the mesenchymal cells in the mouse incisor are the source of CD133 protein expression in the dental mesenchyme. LCM was performed as described earlier in chapter 4.3 to extract four different populations of dental mesenchymal tissue from three p7 CD1 mice. Two extracts border the dental epithelium and are termed transit-amplifying cells and quiescent stem cells as they are directly adjacent to their epithelial counterparts. The dental pulp and pre-odontoblasts were also collected (Figure 16: CD133 mRNA expression in the dental mesenchyme.a). Of note, the dental pulp region also contains cells from the neurovascular bundle and is, therefore, not entirely mesenchymal in nature. RNA

extraction and cDNA generation were achieved as described in chapter 4.3 and the samples were then subjected to Real-Time qPCR to look at *CD133* mRNA expression levels. Our results indicate that *CD133* expression levels in the four mesenchymal extracts (black bars; Figure 16: CD133 mRNA expression in the dental mesenchyme.b) are much lower or non-existent compared to the inner dental epithelium (white bar; Figure 16: CD133 mRNA expression in the dental mesenchyme.b) and that the presence of CD133 protein in the mesenchyme is likely to be derived from the dental epithelium. Indeed, CD133 has been linked with exosomes, a type of vesicle and a means to transfer macromolecules between donor and recipient cells (see Chapter 1.3.6) where it is incorporated in the membrane and possibly is involved in exosome targetting to specific cells, cargo sorting and/or exosome stability. This phenomenom might explain the presence of CD133 protein in the dental mesenchyme despite the absence of its mRNA precursor.

Despite the central dogma in molecular biology, that mRNA translates into protein mRNA levels do not always equal similar amounts of protein expression. Indeed, several studies have pointed out that there is a weak correlation between mRNA and protein levels across many species[362,363]. First, there are many post-transcriptional modifications involved in mRNA translation into protein that is not yet completely understood. Second, proteins vary considerably in their *in vivo* half-lives. Finally, there is also the issue of experimental variance and technical difficulties between mRNA and protein experiments that restrict our ability to get a clear view.

A

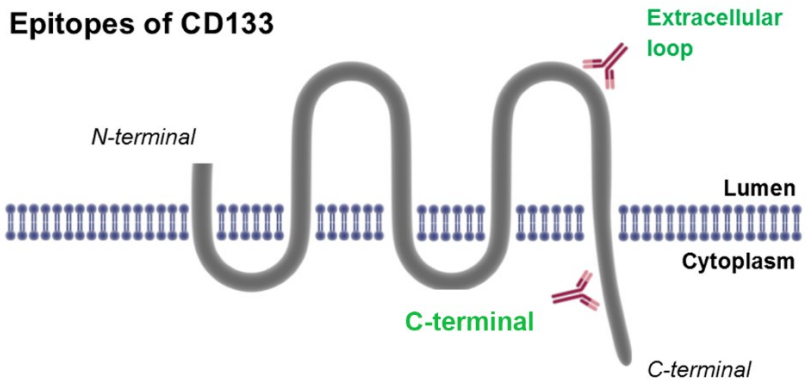

B

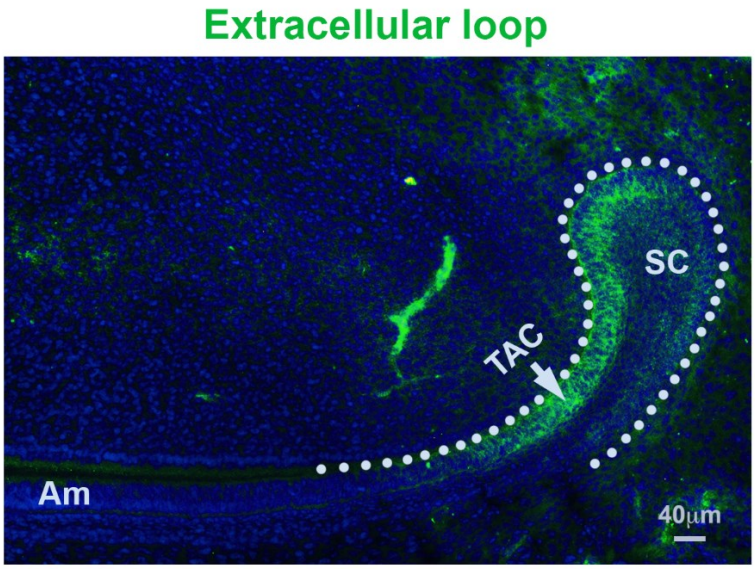

C

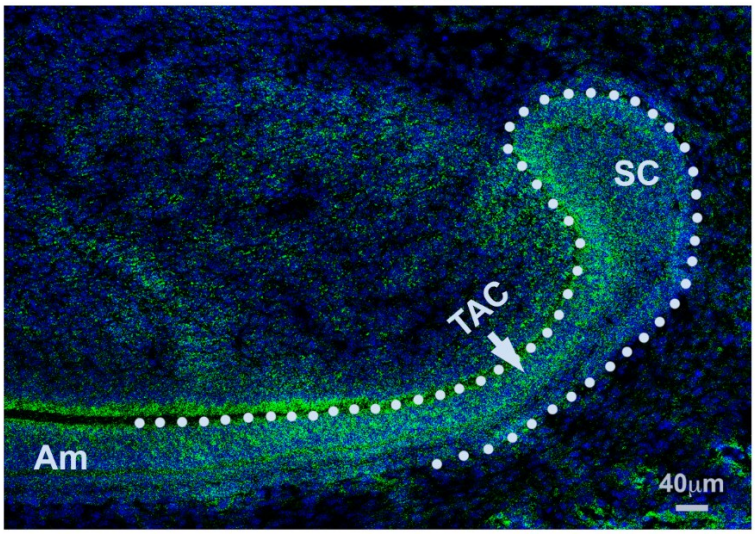

Figure 15: CD133 differential epitope expression in the mouse incisor.
A) Topographical overview of CD133 and its epitope locations. B) Representative immunofluorescence of CD133 (13A4) protein expression in P7 C57BL/6 mouse incisor tooth. C) Representative immunofluorescence of CD133 (ORB549) protein expression in P7 C57BL/6 mouse incisor tooth. White dotted lines mark dental epithelium border. SC: stem cell region, TAC: transit-amplifying region, Am: Ameloblasts.

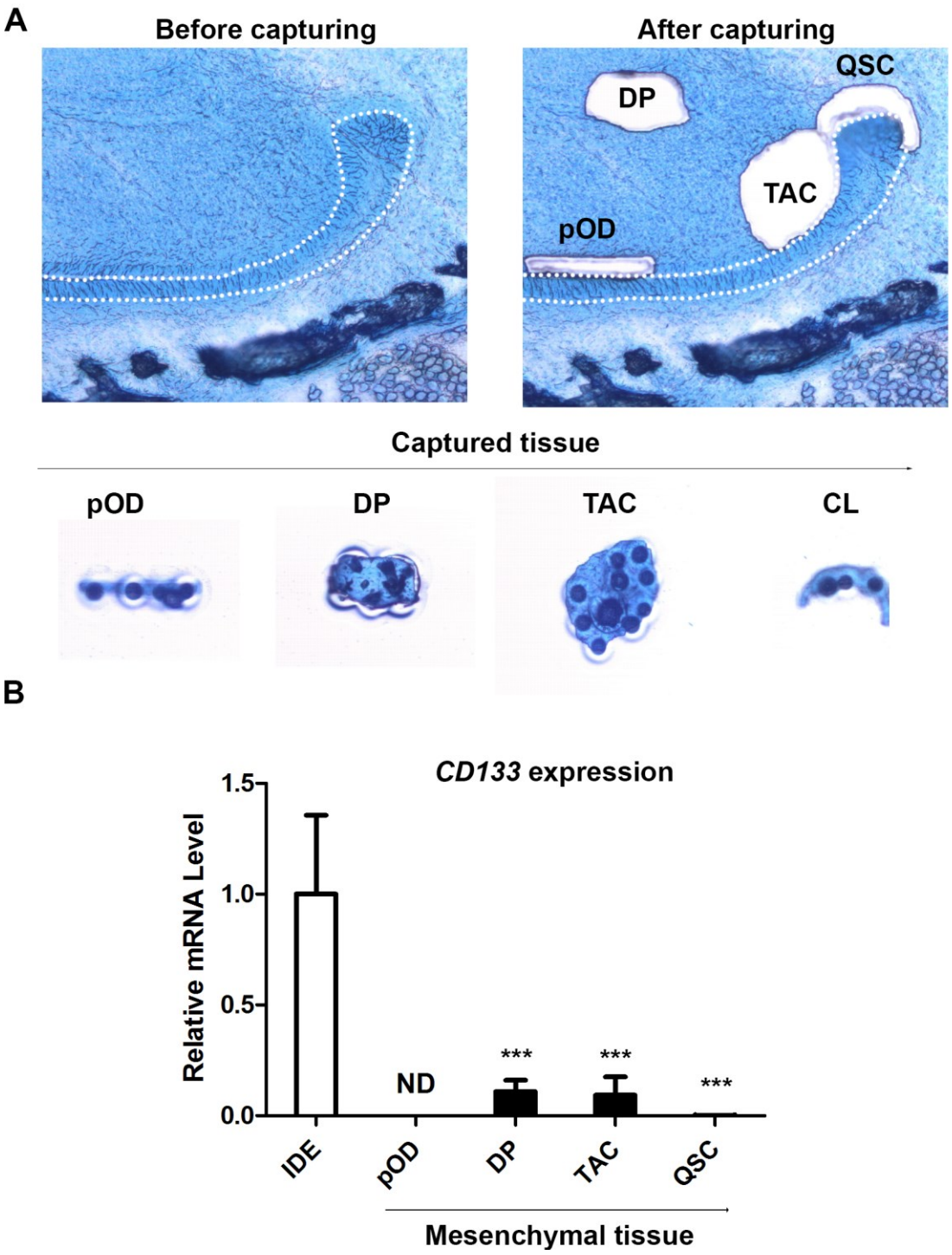

Figure 16: CD133 mRNA expression in the dental mesenchyme.
A) Representative images of LCM-captured mesenchymal dental tissues. Top left: methyl green-stained sagittal section of the mouse incisor tooth prior to LCM extraction. The dotted line represents the boundary of tooth epithelium. Top right: representation of ROI sites in the dental mesenchyme. Middle row: Cut ROI on CapSure HS cap. Black circles are IR-melted film. B) Real-Time qPCR analysis of CD133 mRNA expression in different mesenchymal extracts (black bars). Epithelial CD133 mRNA expression in the inner dental epithelium is represented as reference as white bar. ***: $p<0.001$; ND = Not detected.

4.5 CD133 C-terminal antibody validation

Despite the large overlap in CD133 protein detection, we sought to validate the ICD antibody both *in vivo* and *in vitro* to make sure that this recently produced antibody is specific. Firstly, CD133 ICD epitope expression patterns were analysed and compared to the ECL epitope in C57BL/6 wild type (WT) and *CD133* Knockout (KO) mice.

CD133 KO mice are viable and fertile but are affected with progressive retinal degradation due to delayed photoreceptor differentiation and survival leading eventually to blindness[236]. Knockout of *CD133* was achieved by replacing exon 2 containing the start codon with a neomycin phosphotransferase cassette. The knockout was validated at the DNA and protein level using Southern blot and Western blot, respectively[236].

Both the ICD and Ecl epitopes are absent in the transit-amplifying cell region in *CD133* KO mouse incisor compared to their WT counterparts (Figure 17: *In vivo* and *in vitro* validation of CD133 ICD antibody.a). Slight positive staining is still present, but this can be attributed to background noise. Specificity was also confirmed using short hairpin RNA (shRNA)-mediated knockdown of CD133 using three different shRNA sequences in dental epithelial cells (Figure 17b). *CD133* knockdown at the RNA level was verified using Real-Time qPCR and compared to the protein levels using the CD133 ICD antibody (Figure 17b&c). The Western blot result (Figure 17c) mimics the RNA expression result in Figure 17b. This confirms the result seen in Figure 17, thereby, strengthening the evidence that this antibody is specific for CD133.

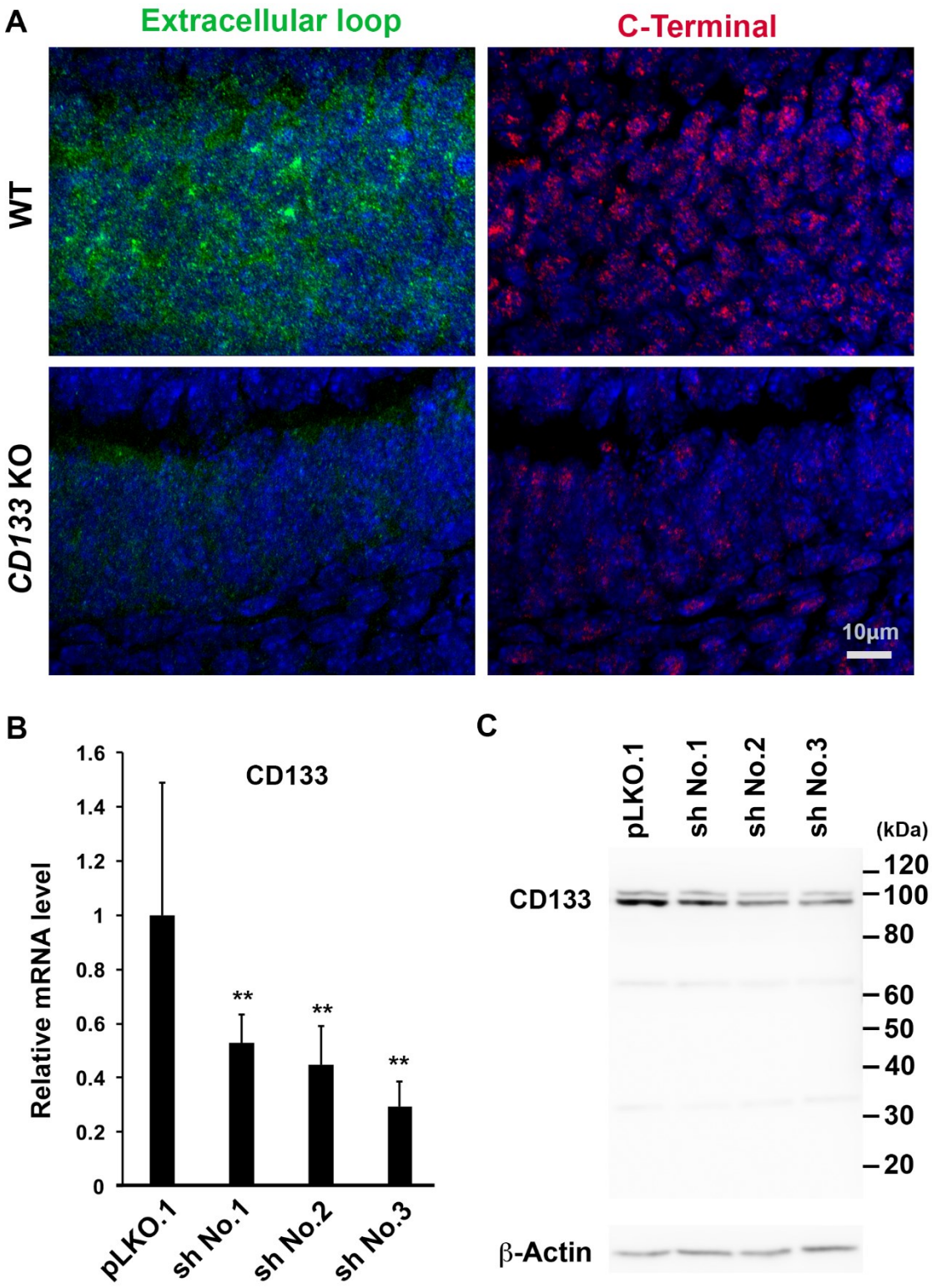

Figure 17: *In vivo* and *in vitro* validation of CD133 ICD antibody.
A) Representative image of CD133 positivity in the transit-amplifying cell region of C57Bl/6 WT (top panel) and CD133 KO (bottom panel) mouse incisor using CD133 ECL (left panel) and ICD (right panel) antibodies. B) Real-Time qPCR analysis showing downregulation of CD133 mRNA expression using shRNA. C) Western blot revealing CD133 ICD epitope expression in dental epithelial cells. **: $p<0.01$.

4.6 Mice lacking *CD133* exhibit enamel development defects

To investigate the biological consequences of losing CD133 in the dental epithelium, we examined mouse incisor teeth from 2-month old *CD133* KO mice. Macroscopic analysis showed that the tooth enamel developed dark spots in *CD133*-deficient mice (yellow arrowheads in Figure 18a). Further microscopic analysis of the dark spots using scanning electronic microscopy (SEM) revealed that this could be explained by the detachment of the enamel layer (Figure 18b). At higher magnification, enamel rods (yellow arrowheads) appear to be reduced around the Tomes' processes compared to their WT counterpart (Figure 18c). Enamel rods consist entirely of hydroxyapatite crystals and are the primary unit of the enamel. Its function is to provide rigidity and strength to the enamel, and any disorder affecting the enamel rods is called amelogenesis imperfecta[364]. Symptoms can vary from relatively mild such as hypersensitivity to temperature and discolouration up to very severe such as prone to breaking. Each enamel rod is synthesized from one ameloblast that secretes specific proteins within the enamel matrix[310]. The enamel proteins aid in the mineralization of the enamel matrix prior to being removed resulting in an inorganic enamel rod exclusively consisting of hydroxyapatite. Therefore, amelogenesis imperfecta is a manifestation of defects within the ameloblasts and, potentially, its precursors. Interestingly, the phenotypes are similar to other tooth epithelium phenotypes of small molecule-inhibition of Sonic hedgehog (Shh) and Wingless-Type MMTV Integration Site (Wnt) mutant mice[323,365].

Further analysis of the ameloblasts in *CD133*-deficient mice reveals multiple phenotypes that could potentially explain the amelogenesis imperfecta-like appearance of the enamel. Micro-computed tomography (μCT) is a high-resolution imaging technique capable of analysing hard tissues and an ideal tool

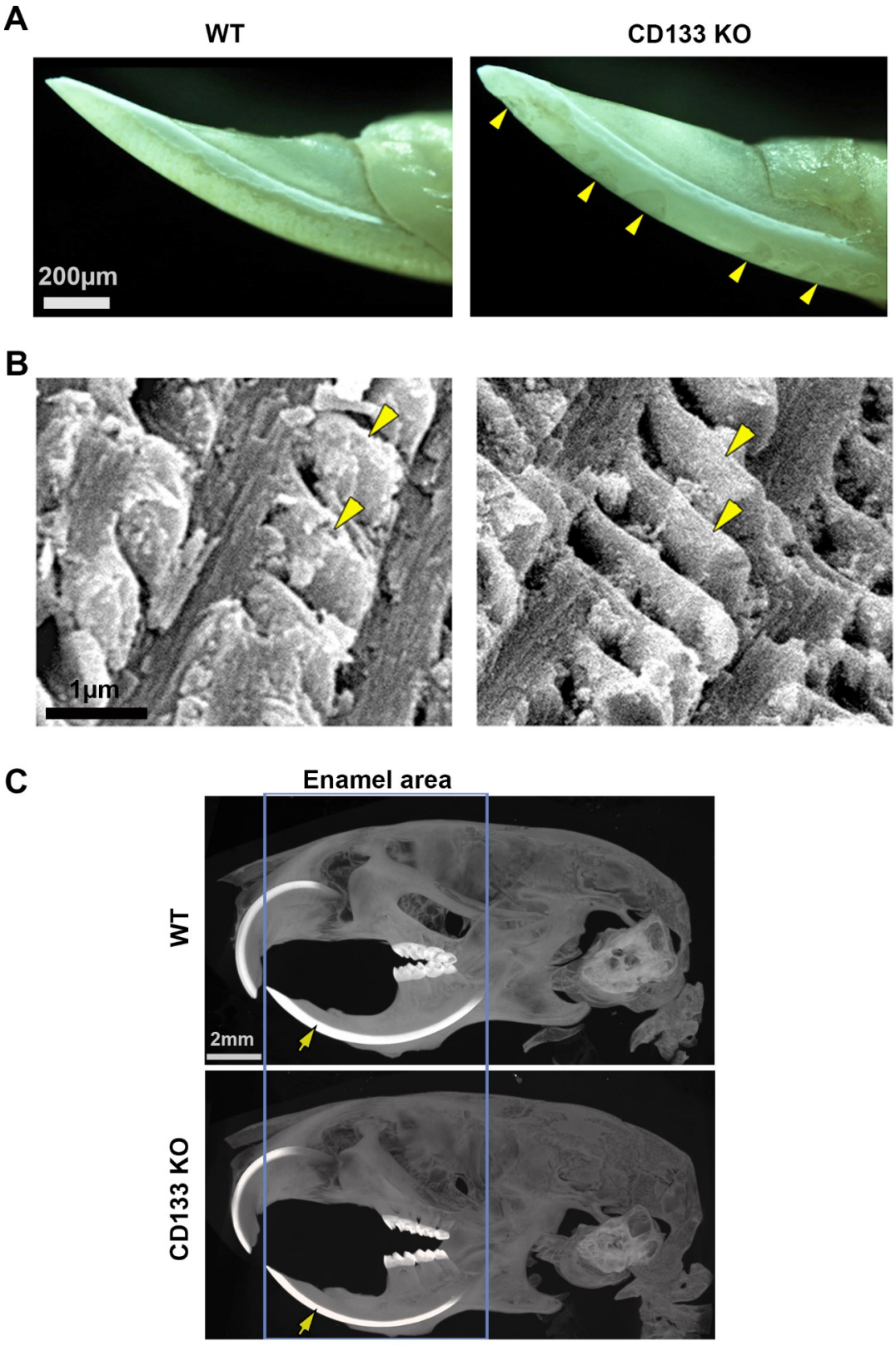

Figure 18: Macro and microscopic characterisation of *CD133* KO phenotype in the enamel.

A) Representative stereoscopic image of the lower incisor of 2-month-old WT and *CD133* KO mice. Yellow arrowheads indicate enamel defects in the *CD133* KO mice. B) High-magnification scanning electron microscopy analysis of the enamel layer. Samples indicated in A. Yellow arrowheads indicate enamel rods. C) Representative microCT analysis of enamel (yellow arrows) development of 4 months old female mice with indicated genotypes. Blue box represents start and endpoint of enamel tissue in WT mouse.

to analyse macroscopic properties of the enamel. Enamel is the hardest substance in the body, and it is, therefore, easy to differentiate from the surrounding bone structures. As a result of these properties, we sought to analyse enamel properties such as thickness and starting point of enamel secretion. Results show that CD133 KO mice develop shorter and thinner enamel tissues compared to WT mice (enamel length of WT incisor indicated by the blue box in Figure 18c).

Morphological evaluation of *CD133* KO ameloblasts showed that there was no difference in the elongation of the ameloblasts but that their nuclei were not polarised adequately compared to WT mice. In addition, *CD133* KO ameloblasts displayed increased vacuolation implying that exocytosis of the enamel matrix might be hampered (indicated by black arrows in Figure 19a). Indeed, CD133 has been shown to not only be associated with membrane protrusions but also with multivesicular bodies destined for exocytosis where it is present in the membrane of exosomes[366]. Therefore, ameloblasts that lack CD133 might lose the ability to secrete membrane vesicles into the extracellular matrix, in turn, possibly leading to hampered enamel rod maturation.

The ameloblast markers Ambn and AmelX are critical components in enamel matrix formation and mineralisation[367,368]. *Ambn* and *Amelx* KO mice display similar phenotypes as seen in our *CD133* KO mice such as ameloblast detachment in the case of *Ambn*-null mice[369] and cystic degeneration, as mentioned earlier, in *Amelx*-deficient mice[370]. Therefore, we sought to investigate the expression of these markers in our model. Immunostaining of ameloblasts revealed that protein levels of Ambn and Amelx are greatly diminished in CD133-deficient ameloblasts (Figure 19b).

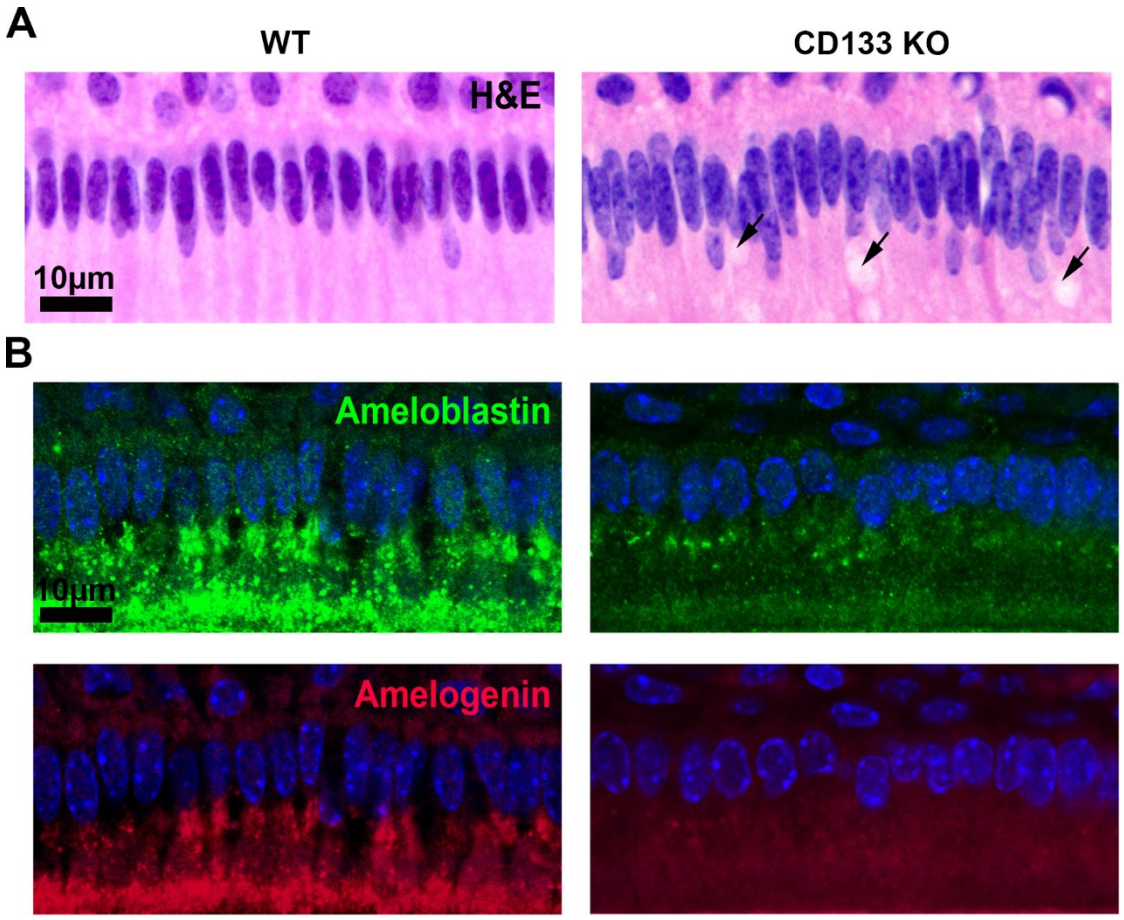

Figure 19: Phenotypical characterisation of *CD133* KO ameloblasts.
A) Representative H&E staining of ameloblasts in WT (left) and *CD133* KO (right) mice. Black arrows indicate the presence of vacuoles. B) Immunostaining of the ameloblast markers Ambn and Amelx in WT (left) and *CD133* KO (right) mice.

Taken together, our results show that the absence of CD133 affects the mouse incisor on multiple levels. First, the process of enamel matrix deposition is reduced (Figure 18b) leading to the detachment and, eventually, thinner enamel (Figure 18a&c). Underlying those issues are the ameloblasts that suffer from multiple defects including nuclear polarisation defects (Figure 19a), vacuole accumulation (Figure 19a), and deficiencies in the expression of essential enamel proteins (Figure 19b). We then wondered if ameloblast precursors, present in the stem cells and transit-amplifying cells of the dental epithelium, were also affected in *CD133* KO mice.

4.7 Volume of stem cell and transit-amplifying cells region is affected in *CD133* KO tooth epithelium.

The dental epithelium of P7 C57BL/6 mice and their *CD133* KO counterparts were cryosectioned coronally. All sections containing dental epithelium were kept and processed for immunostaining of Sox2 and Ki67, as in Figure 12b, to mark the stem cell and transit-amplifying cell region, respectively. The outline of the Sox2-positive region of every section was marked using Photoshop CC followed by digital reconstruction of the stem cell region in the cervical loop using the BioVis 3D 3.1 software (Figure 20a). The volume of each stem cell region (n>=3 mice) was then quantified using the software's measurement tool. Our result clearly demonstrates a significant decrease in volume in the absence of *CD133* compared to their littermate controls (Figure 20c). No significant change in cell size was detected (Figure 20f).

Interestingly, when we looked at the Ki67-positive fraction within the stem cell region, in other words, the stem cells that have entered the cell cycle and are, therefore, activated, we can see approximately 40% decrease in activated stem

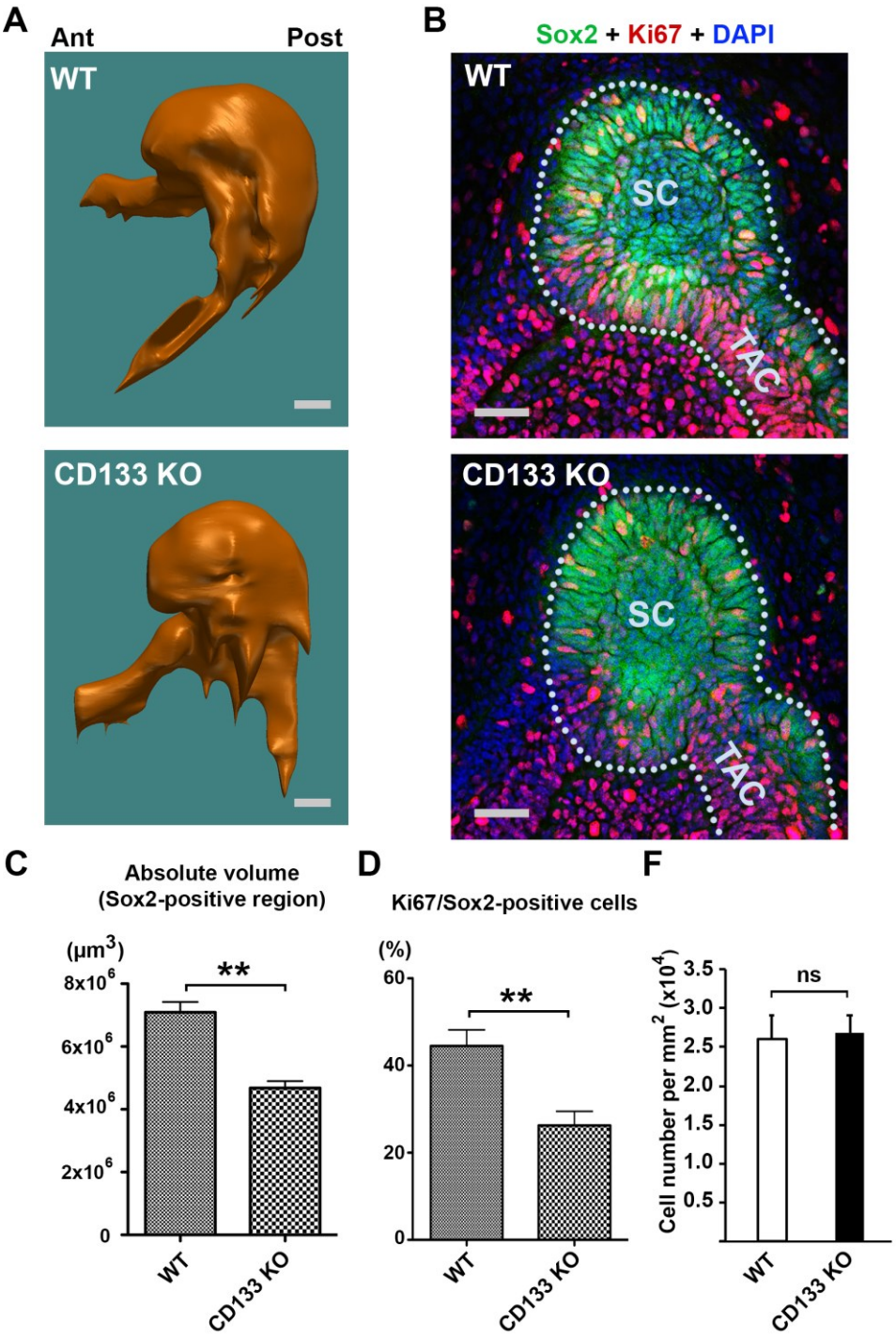

Figure 20: Phenotypical characterisation of the SC and TAC region in *CD133* KO dental epithelium.

A) Representative 3D reconstruction of Sox2-positive region in the CL of WT (top) and *CD133* KO (bottom) mice. Scale bar = 20µm. B) Frontal section of SC and TAC using Sox2 (green) and Ki67 (red) to distinguish between quiescence and proliferation in WT (top) and *CD133* KO (bottom), respectively. Dotted line marks the basement membrane. Scale bar = 20µm. C) Quantification of the volume of the Sox2-positive region using BioVis 3D measurement tool of WT (top) and *CD133* KO (bottom) mice. D) Manual quantification of Ki67-positive fraction within the Sox2-positive region. F) Average cell density in the SC region in WT and CD133 KO mice. Three animals were analysed per condition by quantifying DAPI-positive nuclei number. Ant: anterior; Post: posterior; ns: not significant, n>=3; mice, **: p<0.01.

cells (Figure 20b&d). Ki67-positive cells were counted manually and compared to the total number of nuclei present within the stem cell region using Fiji software. This decrease in both volume, as well as a reduced fraction of Ki67-positive cells, hints at a defect in the self-renewal as well as activation capacity of stem cells in the cervical loop. In the absence of *CD133,* the dental epithelium is significantly affected in all stages of its lineage. The stem cells, the adjacent transit-amplifying cells and partially overlapping transition zone are smaller, and these defects possibly culminate into the phenotypes observed in the mutant ameloblasts.

4.8 *CD133* KO primary cilia are more abundant and display altered dynamics compared to their WT counterparts

Stem cells rely on their entry into the cell cycle to become activated and contribute to lineage differentiation in tissues. Our observations (Figure 20b&d) have revealed that *CD133* KO stem cells display a lower frequency of self-renewal as well as activation. This led us to believe that primary cilia in *CD133* KO mice might be affected due to the shared machinery involved in primary cilia and cell division. Indeed, the centrioles which form the basal body from which the primary cilium protrudes into the extracellular matrix also take part in mitotic spindle formation and subsequent chromosome separation[123]. Consequently, mature primary cilia and cell cycle progression are, therefore, mutually exclusive.

As a result of these observations, we sought to investigate the effect of loss of CD133 on primary cilia in stem cells and transit-amplifying cells. Cryosectioning of the cervical loop was performed, and primary cilia were visualised using AcTub followed by digital reconstruction with Imaris as mentioned earlier in Chapter 4.2. Primary cilia length was measured in stem cell and transit-amplifying cell regions

of P7 WT and *CD133* KO cervical loops (Figure 21). Interestingly, primary cilia in the *CD133* KO stem cells were significantly shorter than their WT counterparts, whereas, primary cilia in the transit-amplifying cell region were longer. In fact, primary cilia in *CD133*-deficient transit-amplifying cells were longer than primary cilia present in WT stem cells (Figure 21c). WT stem cells showed the most significant variation in primary cilia length pointing at either a more heterogeneous population of stem cells in terms of their cell cycle state and/or a population of cells that is relatively homogeneous in their cell cycle state but have different needs from the extracellular matrix. Indeed, cilia length has been shown to be involved in different cellular responses with regards to mechanical forces in a variety of *in vitro* cell cultures[354]. This was partially explained by an increased anterograde intraflagellar transport but unchanged retrograde transport leading to a net influx of ciliary components into the primary cilium. It is not too farfetched to believe that a change in primary cilium components has an effect on the primary cilium response to cues from the extracellular matrix and, therefore, the cell fate decision of any given cell in a population.

To investigate the mechanism how CD133 regulates primary cilia length and function, we extracted the cervical loop and adjacent inner dental epithelium of P7 WT and P7 *CD133* KO mice.

4.9 Establishment of mouse dental epithelial primary cells

The isolation of cervical loop epithelial cells (CLE) from the labial cervical loop of P7 mice starts with the removal of the mandible from the animal. The mandibular bone is then removed to uncover the dental epithelium including the labial cervical loop (Figure 22a). The explant was then treated with Type1 Collagenase to dissociate the tissue before propagating them in culture. To favour the growth of

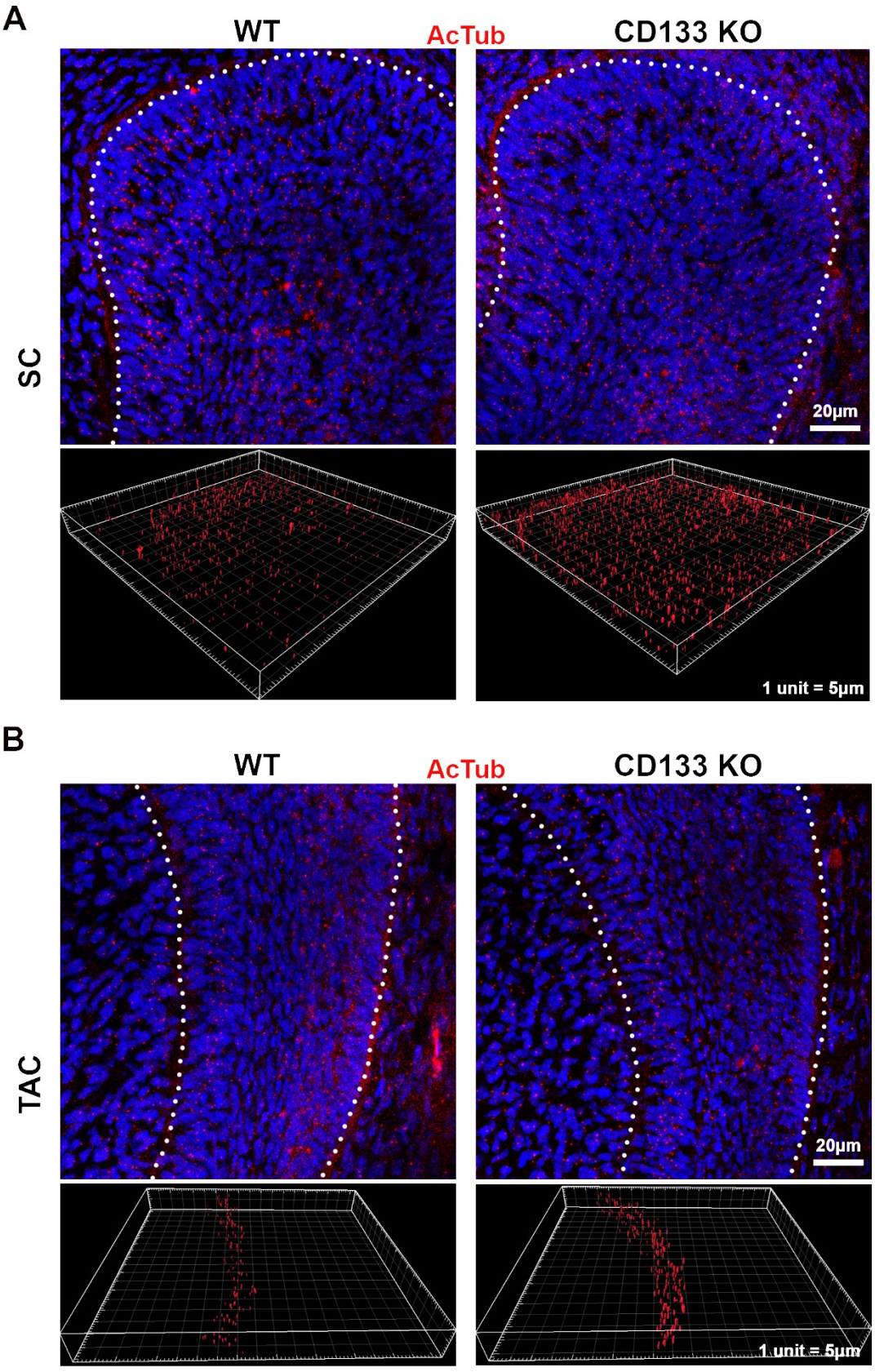
A
WT
AcTub
CD133 KO
SC
20μm
1 unit = 5μm
B
WT
AcTub
CD133 KO
TAC
20μm
1 unit = 5μm

C

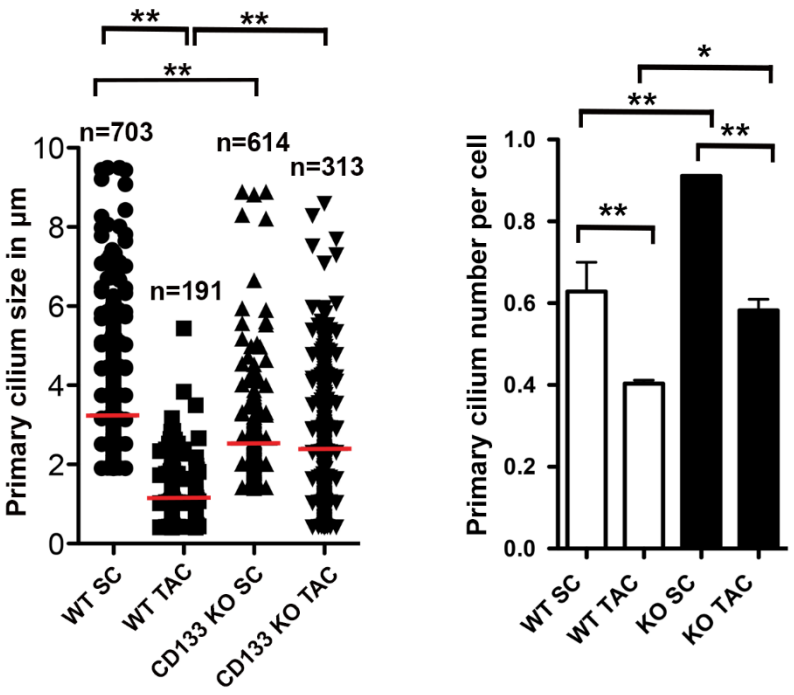

Figure 21: Primary cilia characteristics in WT versus *CD133* KO dental epithelium. A) Top: Representative confocal image of AcTub in the cervical loop of the dental epithelium in WT (left) and *CD133* KO (right) mice. Bottom: Corresponding 3D representation of primary cilia using Imaris for quantification. B) Top: Representative confocal image of AcTub in the transit-amplifying region of the dental epithelium in WT (left) and *CD133* KO (right) mice. Bottom: Corresponding 3D representation of primary cilia using Imaris for quantification. C) Quantification of primary cilia dimensions (left) and number (right) in indicated tissues., n>=3 mice, **: p<0.01, *: p<0.05.

epithelial rather than mesenchymal cells, we subjected the cells to DMEM/F12 supplemented with B27 supplement, 20ng/ml of EGF and 25ng/ml of FGF2 as described earlier[371].

After the first passage, morphological examination of the cells revealed the typical cobblestone-like colony formation often seen in many epithelial tissues (Figure 22b). To ensure that the cultures were purely epithelial in origin without contamination from the mesenchyme, gene expression profiling was performed after passage 1, the mesenchymal markers are not detectable in the epithelial cell culture.

Furthermore, we checked if our CLE cells were capable of differentiating along the dental lineage by looking at the expression of ameloblast markers *Ambn* and *Amelx.* Induction of differentiation was achieved using normal culture medium supplemented with 0.2mM $CaCl_2$ for 12 days (Figure 22g). $CaCl_2$ has been shown to restore in part ameloblast differentiation and function in fluoride-treated organ cultures[372]. Moreover, addition of $CaCl_2$ to *in vitro* culture of primary human ameloblast lineage cells leads to an increase of ameloblast differentiation markers such as Amelx and were capable of producing Von Kossa-positive nodules, an indication of enamel matrix production[373]. Our results indicate that the addition of $CaCl_2$ alone is enough to differentiate CLE cells along the dental epithelial lineage as is shown by increased expression of *Ambn* and *Amelx* (Figure 22g). Of note: consistent with previous observations, the expression of *Amelx* mRNA but absence of *Ambn* mRNA under normal cell culture conditions indicates the presence of pre-secretory ameloblasts but absence of fully differentiated, secretory ameloblasts[374].

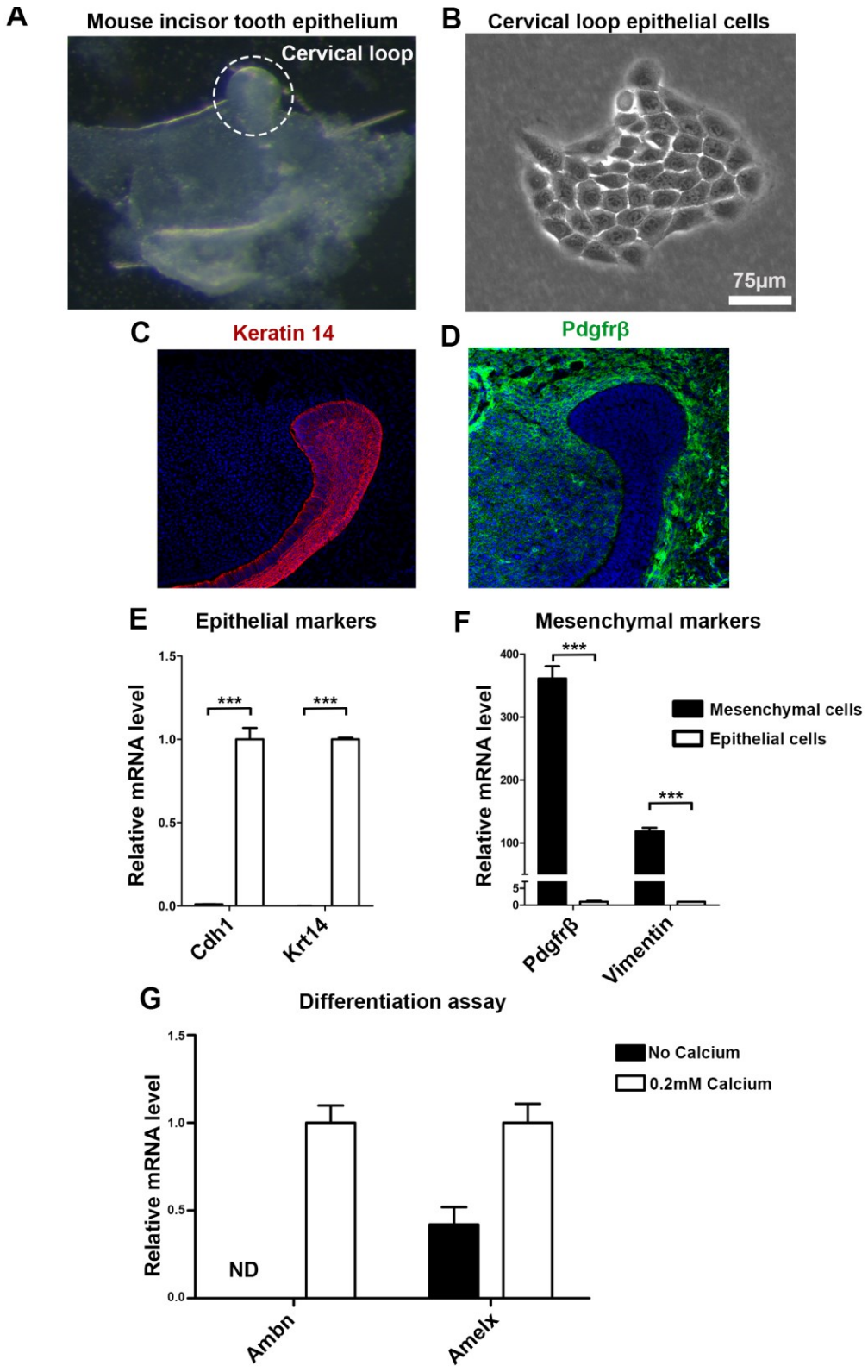

Figure 22: Isolation and cell culture of CLE primary cells.
A) Stereoscopic image of isolated dental epithelium with cervical loop at the top in a dashed circle. B) Morphology of p1 CLE colony. C&D) Immunofluorescence staining of Krt14 and Pdgfrβ as a marker for epithelial and mesenchymal tissue, respectively. E&F) qPCR analysis of Cdh1, Krt14, and Pdgfrβ and Vimentin expression in CLE cells (white bars) and mesenchymal cells (black bars). G) qPCR analysis of the ameloblast markers Ambn and Amelx on CLE cells. ***: $p<0.005$; ND = Not detected.

4.10 CD133 KO cells fail to survive *in vitro*

To investigate if the initial observation of smaller cervical loop in *CD133* KO mice was due to a failure in stem cell renewal, we performed a clonogenic assay with both WT and *CD133* KO CLE cells. This assay allows us to quantify the survival and proliferation rates of single cells to form colonies under specific conditions[375].

In our case, 4000 single cells were seeded in triplicates on a 12-well plate and maintained in normal conditions in the absence or presence of 100ng/ml Shh. Colonies were visualised with crystal violet. Stereoscopic images of each well were taken, and the number and size of colonies were quantified using ImageJ software. Interestingly, comparison of the different conditions showed that *CD133* KO cells fail to survive and proliferate in standard culture conditions compared to WT CLE cells (Figure 23a-c). Shh has been shown to play a role in cell survival as well as cell proliferation in the developing dental epithelium[341]. However, the addition of Shh failed to increase survival and proliferation in *CD133* KO cells (Figure 23a-c), thereby, strengthening our observation that Shh signalling is positively regulated by CD133.

Due to the sharp decline in survival rates in *CD133* KO as is evidenced by their failure to reach passage two *in vitro,* their use in dissecting the molecular mechanisms in which CD133 governs Shh signalling is severely limited. Therefore, we sought to use endoribonuclease-prepared short interference RNA (esiRNA) instead to induce a milder phenotype that does not entirely inhibit cell survival and proliferation. esiRNA is generated from a gene-specific cDNA template that is derived from the target mRNA. Subsequent reverse transcription into double-stranded RNA is followed by digestion with *Escherichia coli* RNase III to generate a mixture of siRNA that is specific to the target gene[376].

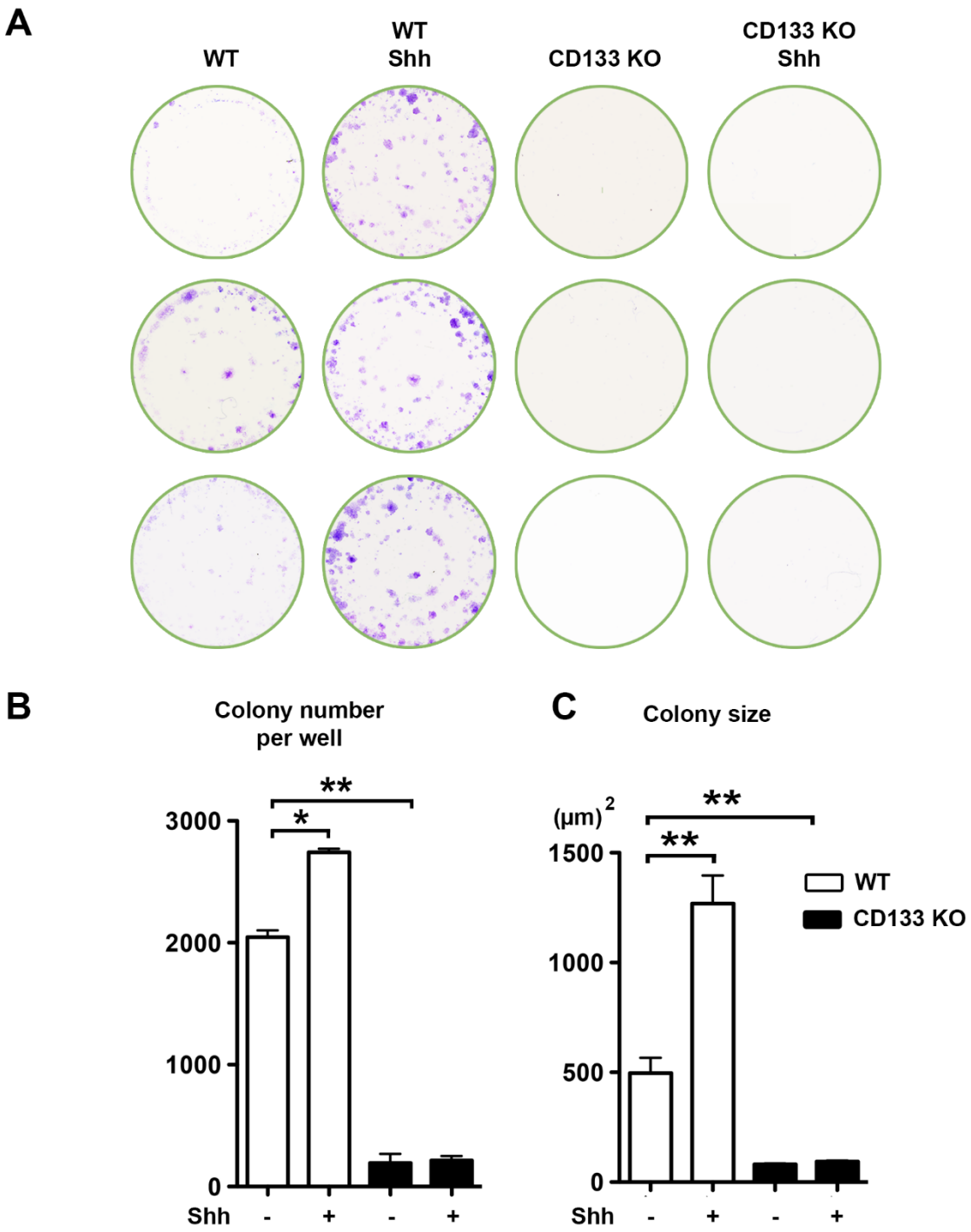

Figure 23: *CD133* KO CLE cells fail to survive and proliferate *in vitro.*
A) Clonogenic assay of WT and *CD133* KO cells (in triplicate) under normal culture conditions in the presence or absence of 100ng/ml Shh. B) Total number of colonies (>50 cells) in each condition. C) The average size of each colony in each condition. **p<0.01; *p<0.05.

Using this technique, WT CLE cells were transfected with 20nM esiCD133 or with esiRNA targeting *Renilla reniformis* Luciferase as a negative control. 24 hours later, transfected cells were either incubated in the absence or presence of Shh. Assessment of *CD133* mRNA levels revealed that esiRNA-mediated downregulation leads to a 70% reduction of *CD133* mRNA expression (Figure 25a). Low levels of CD133 is sufficient for CLE cells to survive and proliferate at the same level as the control cells (Figure 25b-d). Intriguingly, upon addition of Shh for 24h, cells expressing low levels of *CD133* form fewer colonies that are also smaller compared to no Shh treatment. Our observations reveal that CD133 directs the outcome of Shh signalling in CLE cells. Basal levels of CD133 favour Shh-mediated proliferation and survival *in vitro* which is completely abolished in *CD133* KO CLE cells. Whereas, CLE cells with low levels of CD133 leads to no changes in survival in the absence of Shh. However, upon addition of Shh, CLE cells show lower survival rates. In conclusion, CD133 acts as a molecular switch in the outcome of Shh-mediated survival and proliferation pathways.

4.11 Reduced levels of CD133 favour Shh-mediated apoptosis

The CD133-mediated changes in growth and apparent survival of CLE might also be due to increased rates of cell death. Therefore, we sought to investigate whether CD133 might regulate apoptosis in the dental epithelium. Apoptosis or programmed cell death is crucial in development and maintaining homeostasis in adult tissues and is a tightly regulated process that can be initiated via intra- and extracellular cues. Regardless of the source of the initiation signal, apoptosis culminates in the activation of executioner caspases, which mediate degradation of cellular components. Caspase 3 is such an executioner caspase and its cleavage will lead to its activation and is the last step before the initiation of

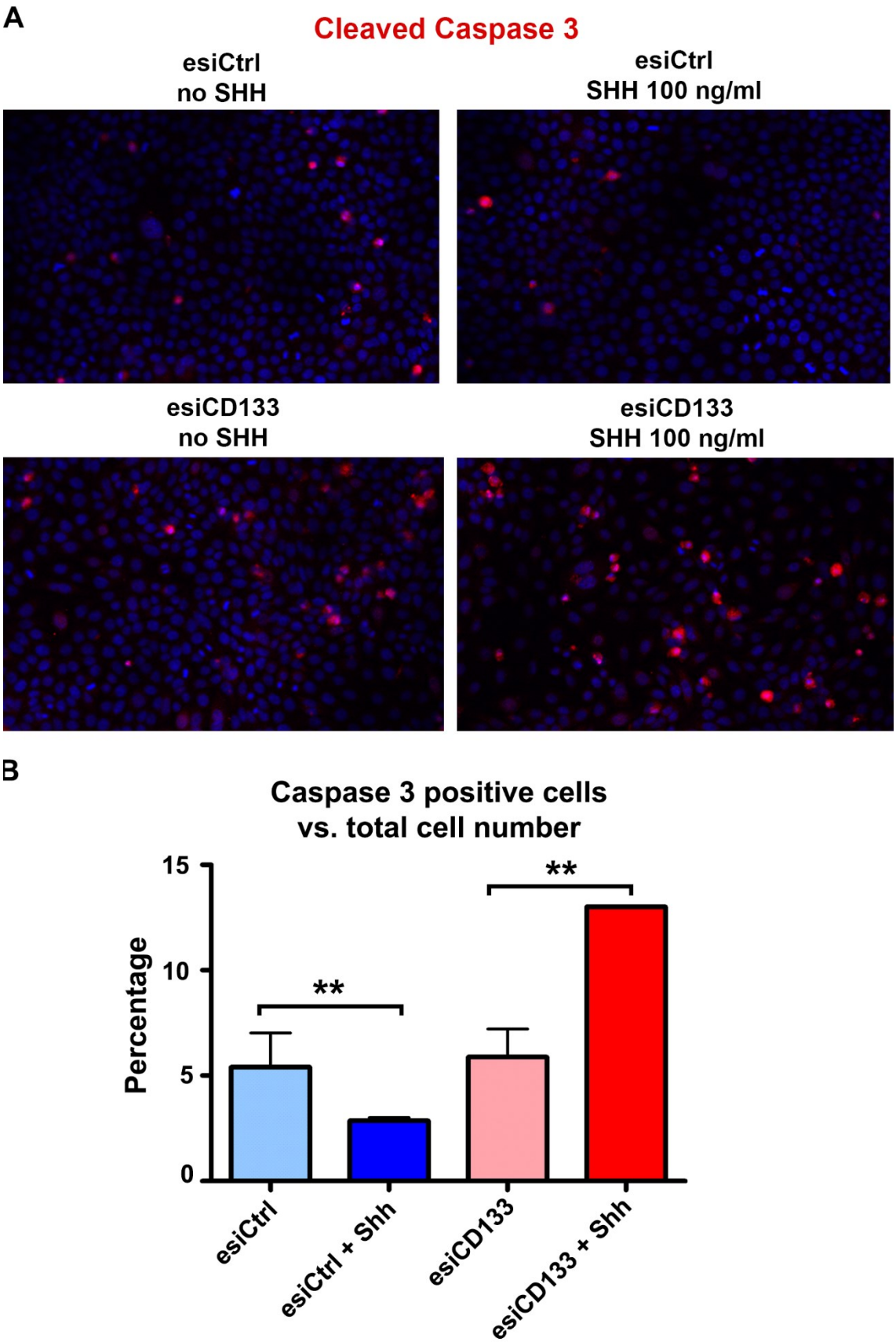

Figure 24: Downregulation of CD133 affects the outcome of Shh in CLE cells.
A) Representative confocal image showing cleaved caspase 3-positive cells (red) in CLE cells under different conditions. B) Percentage of cleaved Caspase 3-positive cells vs total cell population in respective conditions shown in A. **: $p<0.01$.

cellular degradation[377]. Therefore, cleaved caspase 3 is an often used and well-established marker of apoptosis.

When CLE cells are cultured in the absence of Shh, CD133 does not have any effect on the activation of cleaved Caspase 3 (Figure 24a&b). However, addition of Shh reduces apoptosis in normal WT CLE., whereas, the population of cells that is undergoing cell death is doubled when CD133 levels are low (Figure 24a&b). This leads us to believe that CD133 directs Shh-mediated cell fate decisions in the dental epithelium.

4.12 CD133 is involved in cell cycle progression

Our results so far have shown that different levels of CD133 affect proliferation and survival rates in CLE cells and, therefore, might play a role in cell cycle progression. Currently, there exist many systems to follow single cells' progress through the cell cycle. G1, S and G2 phases are part of the interphase, and typically cells spend the majority of their time in one of these phases to prepare for mitosis or cell division (Figure 26: Ki67p-FUCCI cell cycle indicatorb)[378]. Cells can go through an additional fifth phase called the quiescent or G0 phase where cells reside that exist in a non-cycling state and are withdrawn from the cell cycle in a reversible manner.

The fluorescence-acquired ubiquitination cell cycle indicator (FUCCI) has been developed initially to picture the precise transition of G1 to S phase[379]. This system uses the cell cycle-dependent ubiquitination pathway to generate an oscillating reporter system. It either favours the degradation of a truncated, inactive version of Geminin conjugated to green fluorescent protein (GFP) in the G1 phase or, in the S, G2 and M phase, the degradation of Chromatin Licensing And DNA Replication Factor 1 (Cdt1) coupled with red fluorescent protein (RFP).

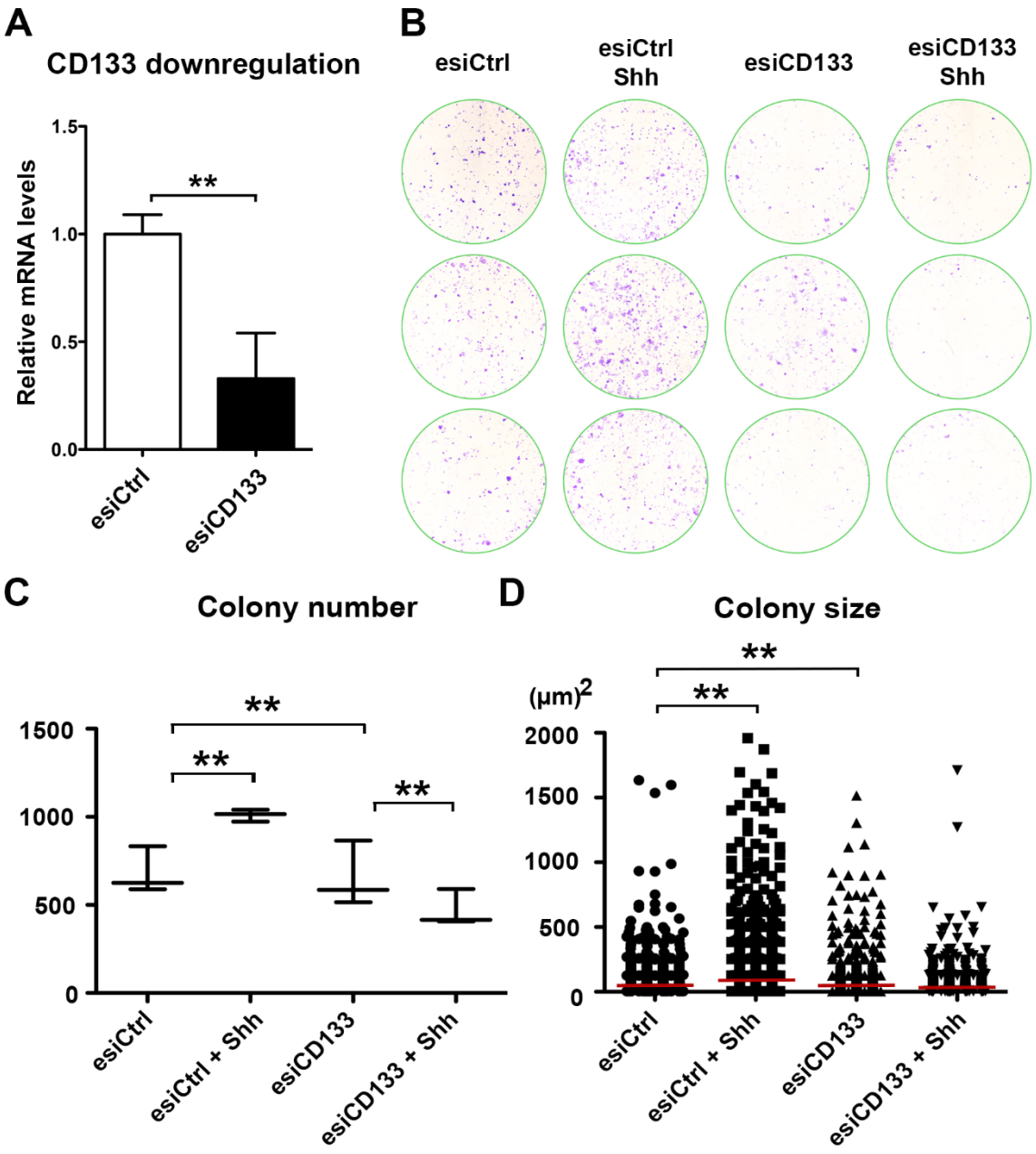

Figure 25: Knockdown of *CD133* leads to reduced proliferation and survival *in vitro.* A) Validation of *CD133* knockdown experiment. B) Clonogenic assay of WT CLE and CLE with reduced expression of *CD133* (in triplicate) under standard culture conditions in the presence or absence of 100ng/ml Shh. C) Total number of colonies (>50 cells) in each condition. D) The average size of each colony in each condition. **p<0.01.

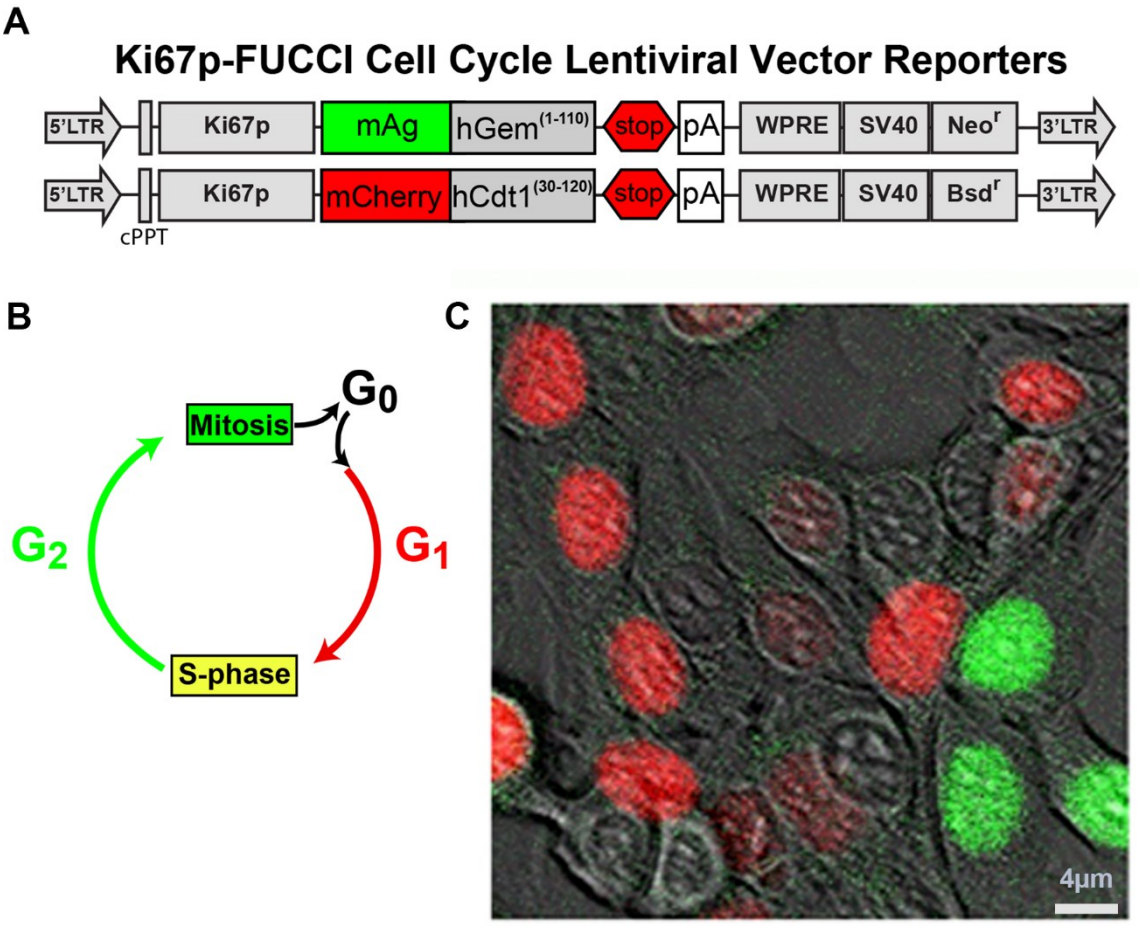

Figure 26: Ki67p-FUCCI cell cycle indicator.
A) Design strategy of the Ki67p-FUCCI cell cycle indicator system. B) Scheme demonstrating the various colours associated with cell cycle phase. C) Representative images of CLE harbouring the Ki67p-FUCCI system showing cells at different cell cycle phases.

The alternating degradation of these fluorophore complexes is regulated by the temporal activity of specific E3 ligases in a cell cycle-dependent manner leading to a robust system that allows the expression of RFP in the G1 and beginning of the S phase, and GFP in the S, G2 and M phase. However, there is no way to distinguish between cells in the quiescent G0 or G1 phase as Cdt1 is expressed in both phases.

Modifying the classical FUCCI system to incorporate a Ki67 promoter (Figure 26a) that controls the expression of the fluorophore complexes allows for the discrimination between the G0 phase with the rest of the cell cycle. Ki67 expression only occurs throughout the cell cycle and is absent in G0[380]. Therefore, expression of the fluorophore complexes only happens during the cell cycle leaving cells that do not express either fluorophore complex colourless (Figure 26a-c)[381]. To test this system, dual lentiviral infection of CLE cells was done by incubation of CLE cells with the viral supernatant. 48h after infection, cells were kept permanently under antibiotic selection. Confocal imaging of the Ki67-FUCCI system in CLE cells reveals the presence of four populations of cells depending on the cell cycle state (Figure 26c).

We then employed this system to check if altering levels of CD133 in the presence or absence Shh leads to changes in the colourless fraction or quiescent cell fraction. To monitor this, we used fluorescence-acquired cell sorting (FACS) to count cell population numbers in each cell cycle state. To determine the correct gate settings, we used WT CLE cells, isolated the single cell population and assessed the background fluorescence (Figure 27a-c). For each sample, the same gate settings (Figure 27c) were used except cell determination (Figure 27a) followed by doublet discrimination (Figure 27b) were done on a per sample basis.

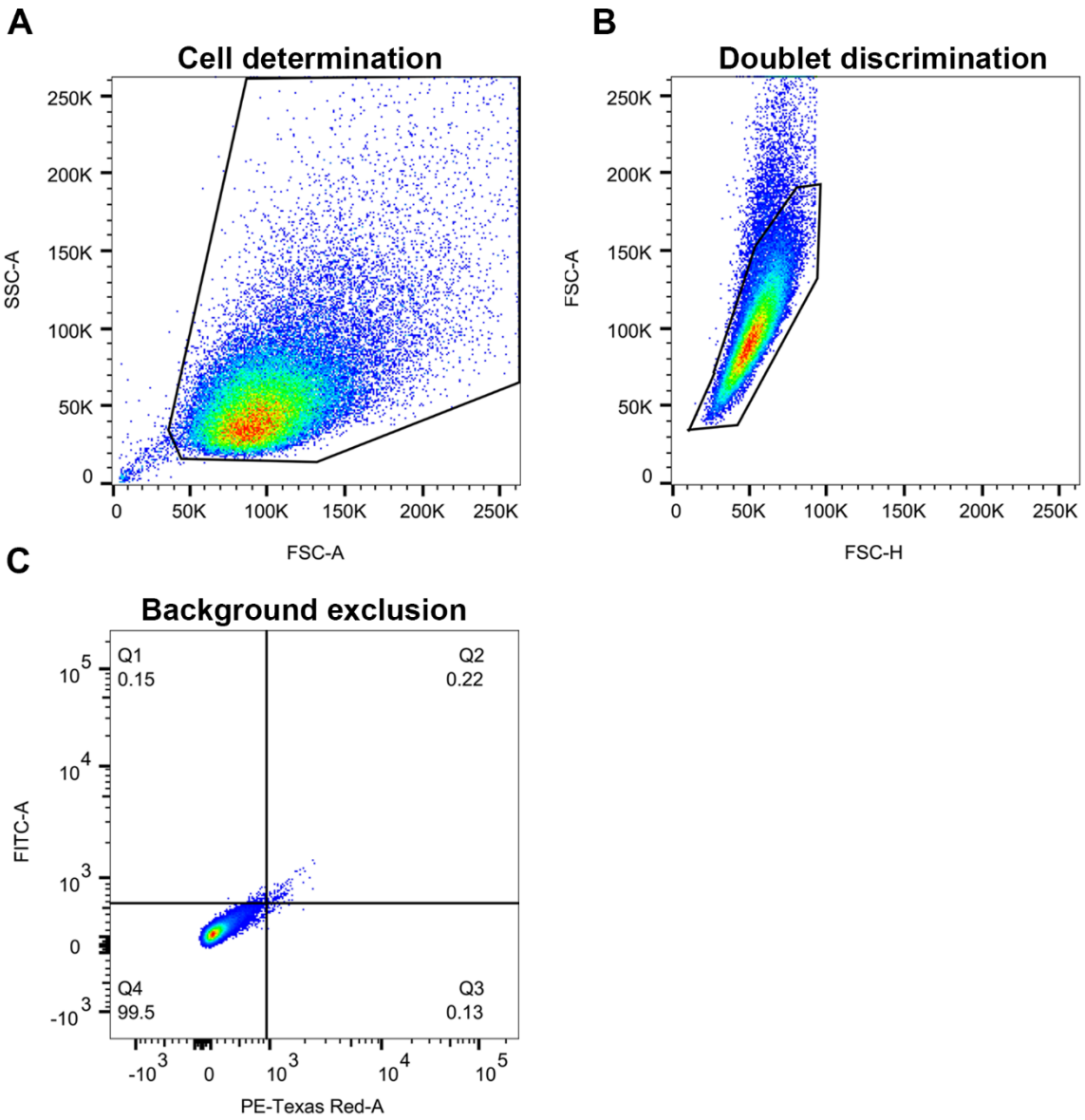

Figure 27: Gating strategy.
A) Use of FSC and SSC to isolate cell fraction from cell debris based on size and complexity, respectively. B) Separation of single cells from doublets using ratio of FSC-A over FSC-H. C) Gating of WT CLE to determine background fluorescence and setting of the gate to include the majority of WT CLE cells in the colourless fraction. PE-Texas Red: R-phycoerythrin-Texas Red.

Size and complexity were determined using forward scatter (FSC) and sideward scatter (SSC) parameters to separate cells from cell debris. The ratio between the area (FSC-A) and the pulse height (FSC-H) of FSC was used to mark the single cells in the previously isolated cell population. Fluorescence of every single cell was then plotted using the gate settings previously acquired with WT CLE. To assess the role of CD133 in cell cycle control, CLE Ki67-FUCCI were transfected using a polyethylimine derivative to deliver plasmid DNA into the cell. Overexpression of CD133 was achieved using the pRC/CMV-CD133 plasmid and the pRC/CMV backbone as a negative control for comparison[224]. Cells were then grown under standard conditions for 48h before FACS analysis. Overexpression of CD133 leads to a significant increase in cells that reside in the G0 phase and G2/M phase compared to its empty vector control as represented by the bottom and upper left quadrant, respectively (Figure 28a). Comparable results can be seen with cells grown in the presence or absence of Shh for 24h (Figure 28b). These results show that both CD133 and Shh are important in stem cell cycle control.

4.13 Arl13b and Hdac6 are expressed in primary cilia in the dental epithelium

Proper primary cilium-dependent communication of cells with their microenvironment depends on the precise and sequential coordination of events that leads to the growth and resorption of primary cilia and depends on a different set of proteins for each of these processes.

Arl13b is a mediator of Shh signalling and plays a critical role in several aspects of ciliogenesis[162,382]. Arl13b mutant mice have defects in Shh signalling in the neural tube where ligand-independent expansion of Shh signalling activity is seen,

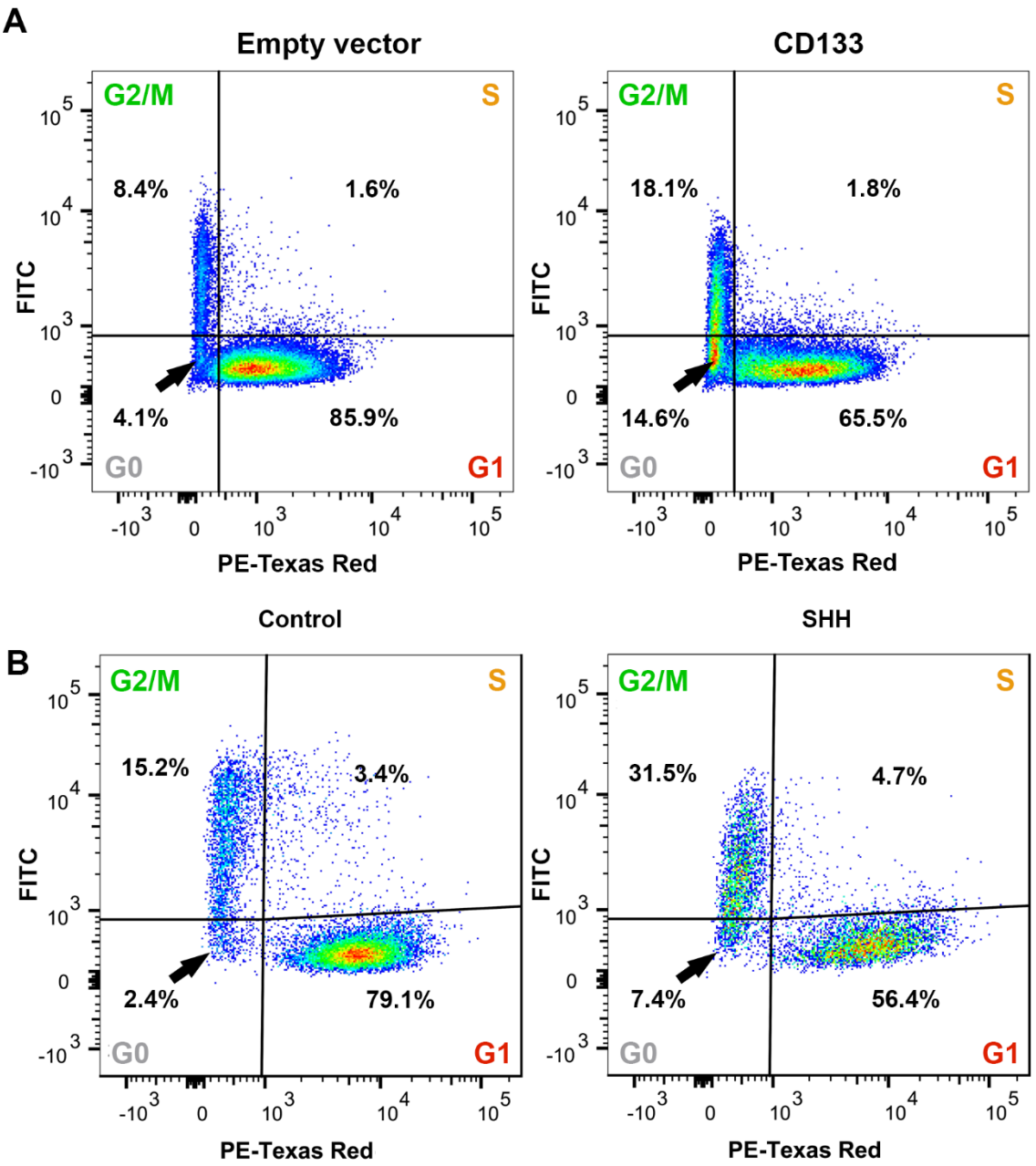

Figure 28: Effect of increased levels of CD133 and Shh on CLE cell cycle state. A) overexpression of CD133 (right panel) in CLE cells promotes cells to enter G0 and G2/M phases compared to empty vector control (left panel) using Ki67-FUCCI reporter system as revealed by FACS analysis. B) addition of Shh leads to a larger population of cells in the G0 phase using Ki67-FUCCI reporter system as revealed by FACS analysis.

however, basal levels of activity are not reached in the ventral neural tube[383]. At the molecular level, Arl13b regulates the entry of Smoothened (Smo), a transmembrane protein enriched in Shh-responding cilia, into the primary cilium which shifts the balance of Gli repressor proteins to the more activated form[384].

Downregulation of Arl13b *in vitro* leads to lower primary cilium numbers and length in a number of cell lines, whereas overexpression of Arl13b in cells results in increased primary cilia length indicating a vital role in primary cilia length control of Arl13b[162]. Aberrant primary cilia length in Arl13b-null cells is most likely due to a structural defect in the axoneme, which suggests a role for Arl13b to regulate tubulin modifications within primary cilia. This is confirmed in Arl13b^{hennin} mutant mice that have less acetylation of axonemal tubulin[383]. Hdac6, a class IIb enzyme, removes acetyl groups from substrates such as α-tubulin and plays, therefore, a central role in the destabilisation of the axoneme and subsequent resorption of the primary cilium. Its overexpression correlates with diseases such as the ciliopathies: chronic obstructive pulmonary disease, Joubert syndrome and polycystic kidney disease, and many cancers[385–387].

To investigate the mechanisms by which CD133 controls primary cilia length and function, we used Arl13b and Hdac6 to look for any anomalies in primary cilium dynamics in *CD133*-deficient dental epithelium. Tissues were processed as described earlier and protein expression levels of Arl13b and Hdac6 were compared in stem cell and transit-amplifying regions regions of WT and *CD133* KO mice. Both proteins were co-stained with AcTub to discriminate against primary cilium-associated and cytoplasmic Arl13b and Hdac6. Indeed, contrary to Arl13b, Hdac6 has also been shown to have roles in autophagy and ubiquitination within the cytoplasm, and its presence is, therefore, not exclusive

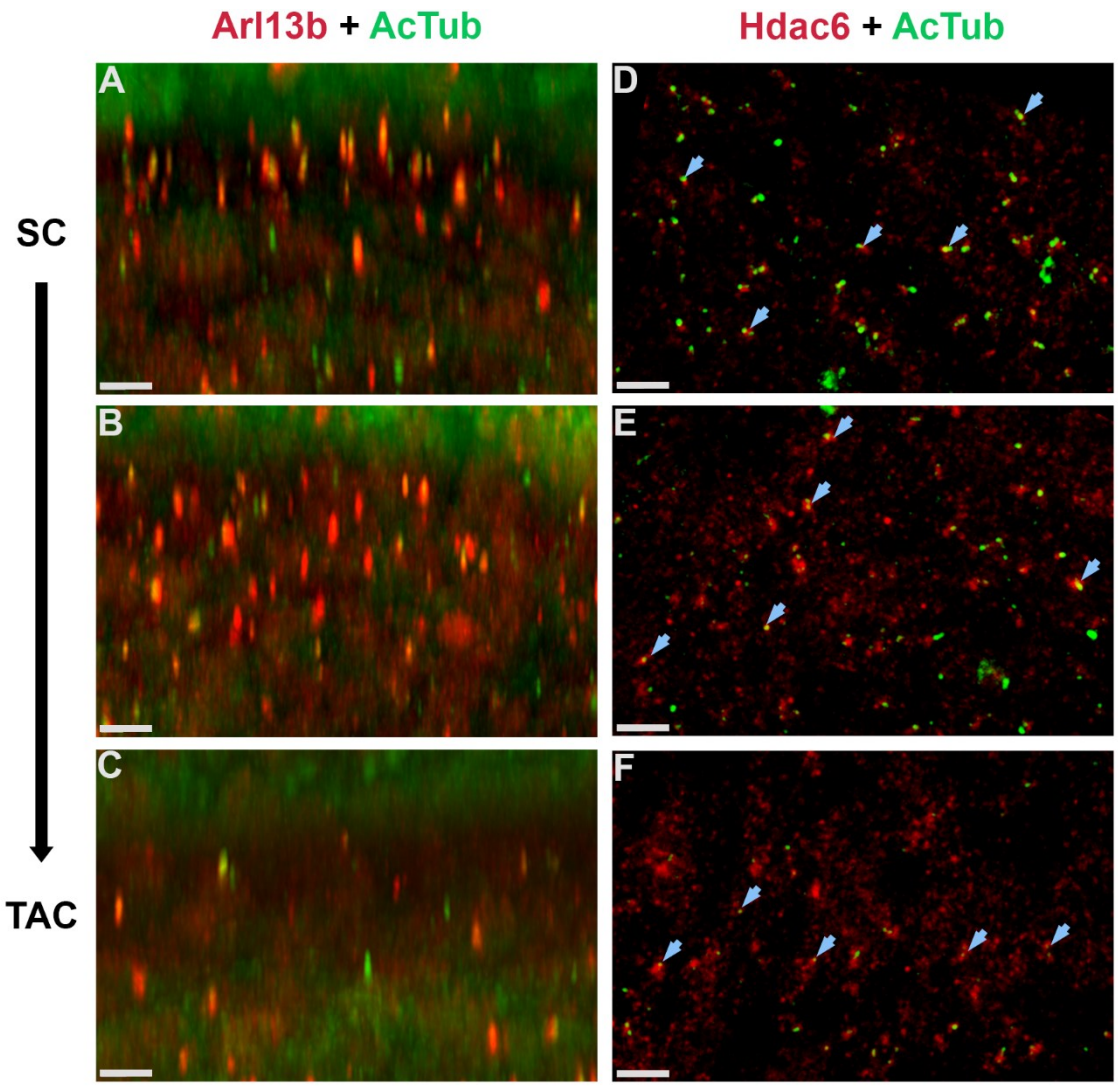

Figure 29: Arl13b and Hdac6 protein expression in the dental epithelium of P7 C57BL/6 mice.
A-C) Immunofluorescence analysis of Arl13b (lateral view) association with primary cilia (AcTub) in the stem cell region (A), transition zone (B) and transit-amplifying cell region (C). D-F) Immunofluorescence analysis of Hdac6 (top view, blue arrows point to primary cilia) association with primary cilia (AcTub) in the stem cell region (D), transition zone (E) and transit-amplifying cell region (F).

to primary cilia[388,389]. We found that Arl13b is present in most primary cilia of the stem cell region indicating that these primary cilia are still undergoing ciliogenesis and are increasing in length, and/or are more susceptible to Shh signalling (Figure 29a). Cells within the transition zone show a similar pattern of a high density of Arl13b-positive primary cilia (Figure 29b). Slower cycling cells within the transit-amplifying cells, specified by their more extended primary cilia, seem to retain Arl13b protein expression as opposed to cells with shorter primary cilia or the highly proliferating cells (Figure 29c). In contrast, Hdac6 was more tightly linked to primary cilia in transit-amplifying cells compared to stem cells (Figure 29d-f). These results confirm the previous *in vitro* observations of the role of Arl13b and Hdac6 in ciliogenesis and resorption, respectively[121,390].

4.14 CD133 and Arl13b are co-expressed in dental epithelial primary cilia

Previous studies on the subcellular location of CD133 has revealed that its expression is associated with curved plasma membrane protrusions on the apical often luminal side of epithelial cells. Apart from primary cilia, other membrane

protrusions expressing CD133 include the midbody, motile cilia and microvilli[167,219,254]. In our model, we sought to investigate whether CD133 co-localises with Arl13b in primary cilia. Immunofluorescence analysis on primary cilia in the dental epithelium revealed that CD133 (13A4 epitope) and Arl13b are present within the same cilia (Figure 30a&b). Interestingly, our experiment reveals that CD133 is asymmetrically distributed across the primary cilium membrane (Figure 30b, top view) whereas Arl13b is closely associated with the axoneme as visualised by AcTub staining (Figure 30b). The asymmetric distribution of CD133 is seen in all primary cilia investigated, however, the

distribution is not polarised and seems to be at random at the tissue level (Figure 30a).

4.15 *Arl13b* expression is decreased in *CD133* KO dental epithelium

Remarkably, a decrease in Arl13b expression is seen in most of the primary cilia in *CD133* KO stem cells compared to WT stem cells, which has Arl13b in nearly all primary cilia (Figure 31a). This observation might explain why primary cilia are shorter in the *CD133*-deficient stem cell region as Arl13b is known to be involved in ciliogenesis[162].

Western blot analysis of esiCD133-mediated knockdown in CLE cells leads to a decline in Arl13b protein levels of 80% in total lysates (Figure 31b&c). This explains that the decrease of Arl13b in the primary cilium is due to lower protein levels rather than mislocalisation to the primary cilium.

Nuclear and cytoplasmic protein extraction illustrates that Arl13b, which has been shown before[126], can translocate to the nucleus and that this shuttling between cytoplasm and nucleus happens independently from CD133 signalling given that the ratio between conditions did not change (Figure 31b&d). From our result, it is impossible to exclude the presence of ciliary proteins in the cytoplasmic extract.

The cytoplasmic part is obtained by disruption of the cell membrane using a hypotonic buffer that leaves the nuclear membrane intact. Therefore, the positive signal of Arl13b in the cytoplasm could well be the ciliary fraction.

Interestingly, our collaborators, Dr. Corbeil and Dr. Karbanova have demonstrated with Co-immunoprecipitation experiments that a fraction of human CD133 binds to Arl13b in Madin Darby Canine Kidney cells (MDCK). Moreover, this binding is interrupted in CD133 K138Q mutants (Figure 32a-c). The

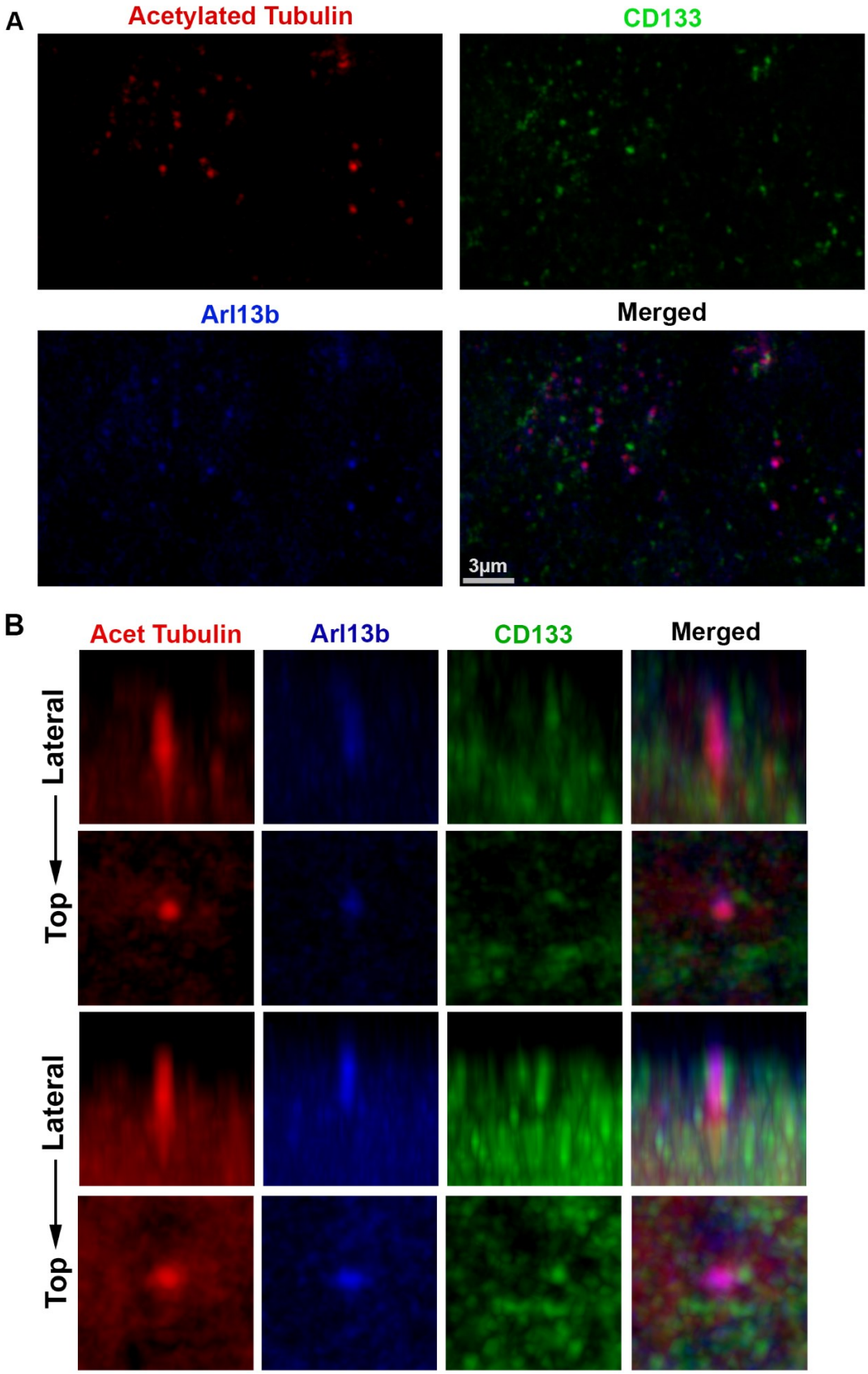

Figure 30: CD133 and Arl13b are co-expressed in primary cilia.
A) Representative immunofluorescent staining of CD133 (green) and Arl13b (blue) in the dental epithelium (top view). Primary cilia are visualised using AcTub (red). B) Two single primary cilia (top and lateral view) to illustrate Arl13b and CD133 co-expression.

substitution of lysine-138 with Glutamine leads to the neutralisation of the electric charge in the first intracellular domain of CD133 (Figure 32a&b). This mutation was initially described to inhibit the interaction between CD133 and Hdac6 in several cell lines leading to the destabilisation of β-catenin, the central molecule in canonical Wnt-signalling[391]. The absence of a positive band in WT MDCK cells can be explained that the human AC133 antibody does not detect endogenous levels of canine CD133. From these results, it appears that CD133, both, directly or indirectly controls Arl13b expression and binds to Arl13b. It is, however, not clear that this protein-protein interaction is required for a feedback loop on Arl13b expression or what isoform of CD133 binds to Arl13b as a sizeable portion of CD133 appears in the unbound fraction or flow-through (Figure 32a).

The observation that Arl13b and Hdac6, both key players in ciliogenesis and resorption, bind to the same domain in CD133, leads to the assumption that CD133 controls cilia length, as seen in Figure 21, and functions through competitive binding of these molecules.

4.16 Expression of Shh effectors in the mouse incisor tooth

Our results so far have indicated that CD133 partially mediates Shh signalling in the mouse incisor tooth epithelium. Gli proteins are members of the Kruppel family of zinc finger proteins and are the principal effectors of Shh signalling[392]. Gli2, 3 and Gli-similar (Glis) 2 have been shown to be present in the primary cilium where it is sequestered in an inactive form until it is activated via Smo[164,393]. Upon its activation, Gli translocates to the nucleus where it can act as a transcriptional repressor or activator[392]. Many target genes are currently known that affect many processes including proliferation and cell survival. In fact, in

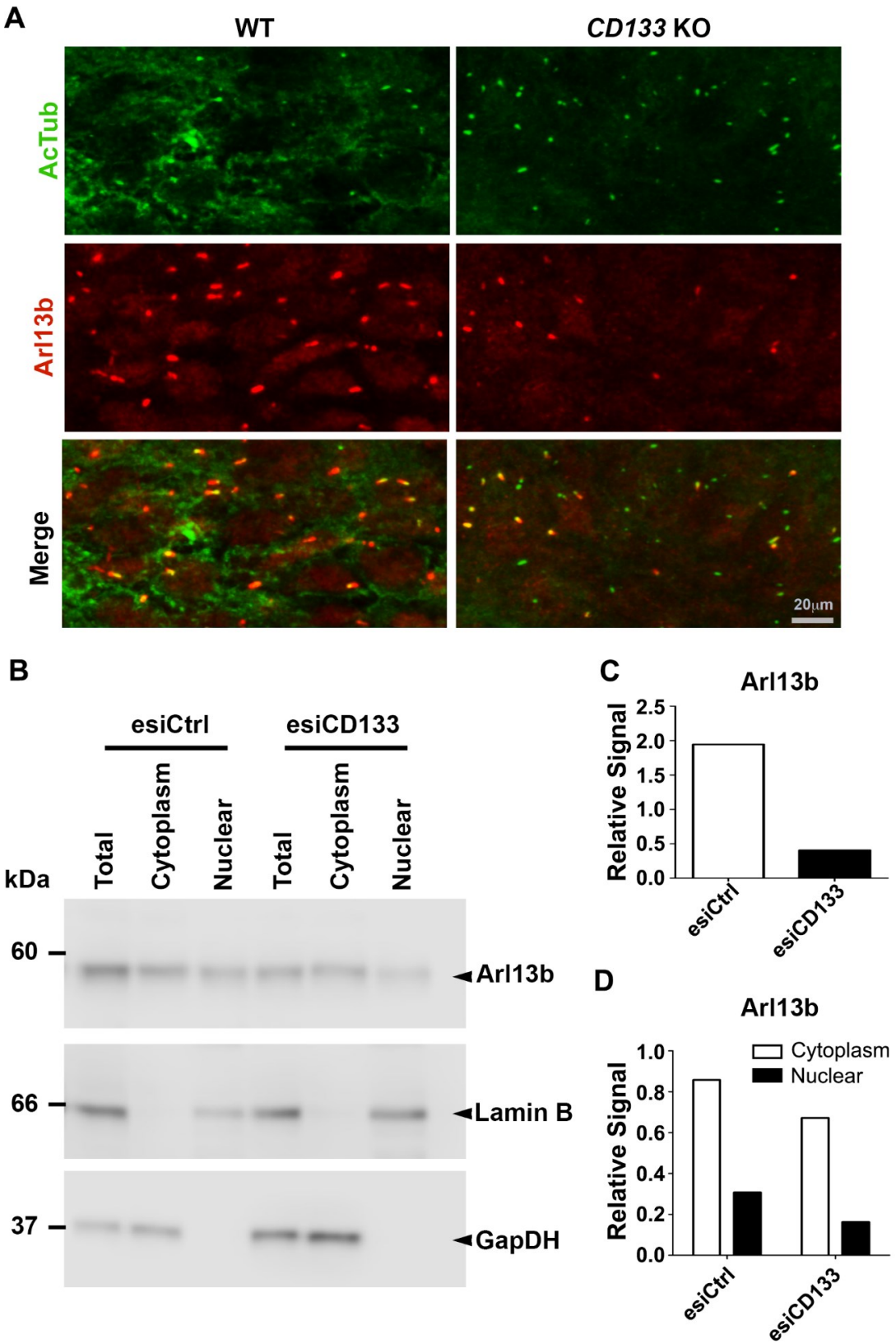

Figure 31: CD133 affects Arl13b expression in the dental epithelium.
A) IF staining on Arl13b in the WT SC region (left) and *CD133* KO SC region. B) Western Blot on Arl13b in total, cytoplasmic and nuclear fraction of esiCD133-mediated knockdown vs its control. Lamin B and Glyceraldehyde-3-Phosphate Dehydrogenase (GapDH) are used to indicate purity of nuclear and cytoplasmic fraction, respectively. C) Quantification of Arl13b in total lysates in esiCD133-mediated knockdown vs its control. D) Quantification of Arl13b in cytoplasmic (white) and nuclear (black) fractions in esiCD133-mediated knockdown vs its control.

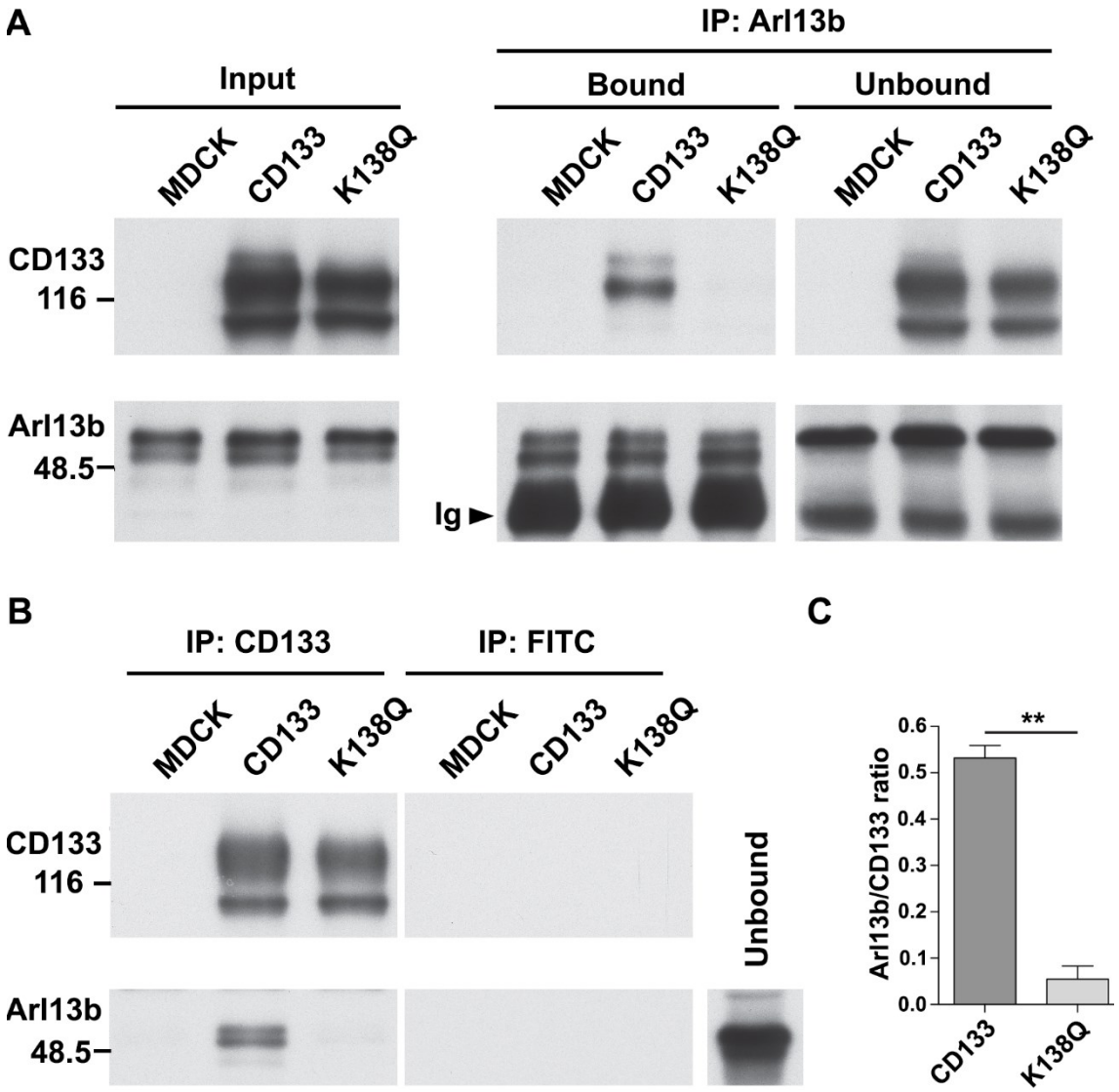

Figure 32: CD133 physically interacts with Arl13b through lysine-138 in MDCK cells.

A) Input panel shows CD133 and Arl13b expression in total lysates of WT MDCK, MDCK-hCD133 and MDCK-hCD133 (K138Q). Immunoprecipitation panel (IP) indicates the presence of CD133 in MDCK-hCD133 but not MDCK-hCD133 (K138Q) when using Arl13b as bait. B) IP using human AC133 antibosy as bait shows binding of Arl13b in MDCK-hCD133 only. Anti- Fluorescein isothiocyanate (FITC) antibody was used as negative control. Arrowhead: immunoglobulin. C) Quantification of Arl13b/CD133 ratio in MDCK-hCD133 versus MDCK-hCD133 (K138Q) was quantified. **: $p<0.01$.

oncogenesis pharmaceutical inhibition of Shh leads to a decrease in CD133+ cells and negatively affects tumourigenic capability[394].

To explore the mechanisms how CD133 directs the outcome of Shh signalling, we looked at the RNA expression levels of Gli family members: Gli1, Gli2 and Gli3 as well as members of the Gli Similar family: Glis1 and Glis2 in the stem cell and transit-amplifying cell region of the mouse incisor (Figure 33a). The stem cell and transit-amplifying cell region were captured as previously described in Figure 14. The results showed a higher expression of most Gli and Glis family members in the stem cell region compared to the transit-amplifying cell region. Interestingly, Glis2 expression is increased in the transit-amplifying cell region (Figure 33a).

This is confirmed at the protein level (Figure 33b) where its expression pattern is similar to that of CD133 (Figure 15). Due to the similar protein expression pattern of CD133 and Glis2 in the dental epithelium of the mouse incisor, we looked at Glis2 protein levels in CD133 KO mice. Immunofluorecence staining showed a clear co-localisation of Glis2 with AcTub in the transit-amplifying cell region of P7 WT mice (left panel, Figure 34a). This co-localisation is nearly completely lost in P7 *CD133* KO mice (right panel, Figure 34a).

Throughout the cervical loop, Glis2 immunoreactivity has been detected in the nuclei of P7 WT mice (Figure 34b) as reported earlier[164]. This might hint at a role for Glis2 in the transcriptional regulation of downstream effectors of Shh signalling in the dental epithelium. However, whether it represses and/or activates transcription is not yet clear at this stage.

A

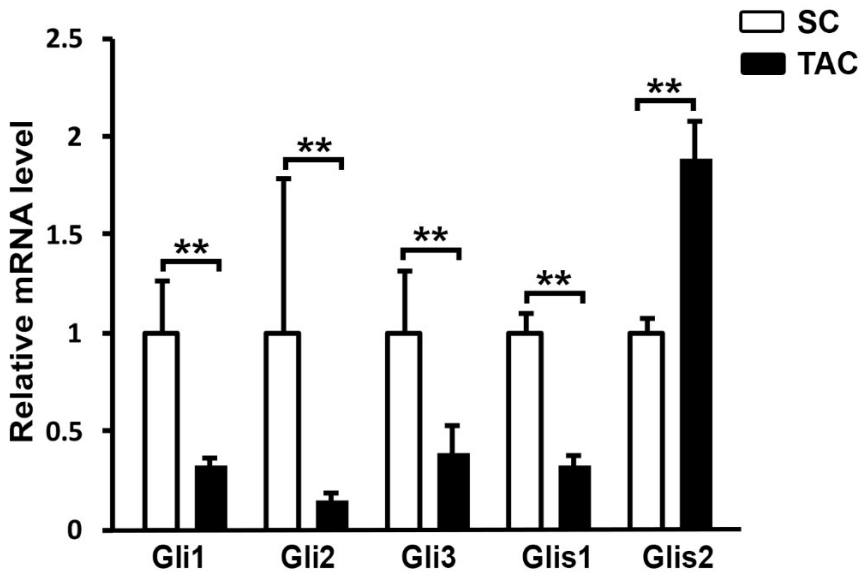

B

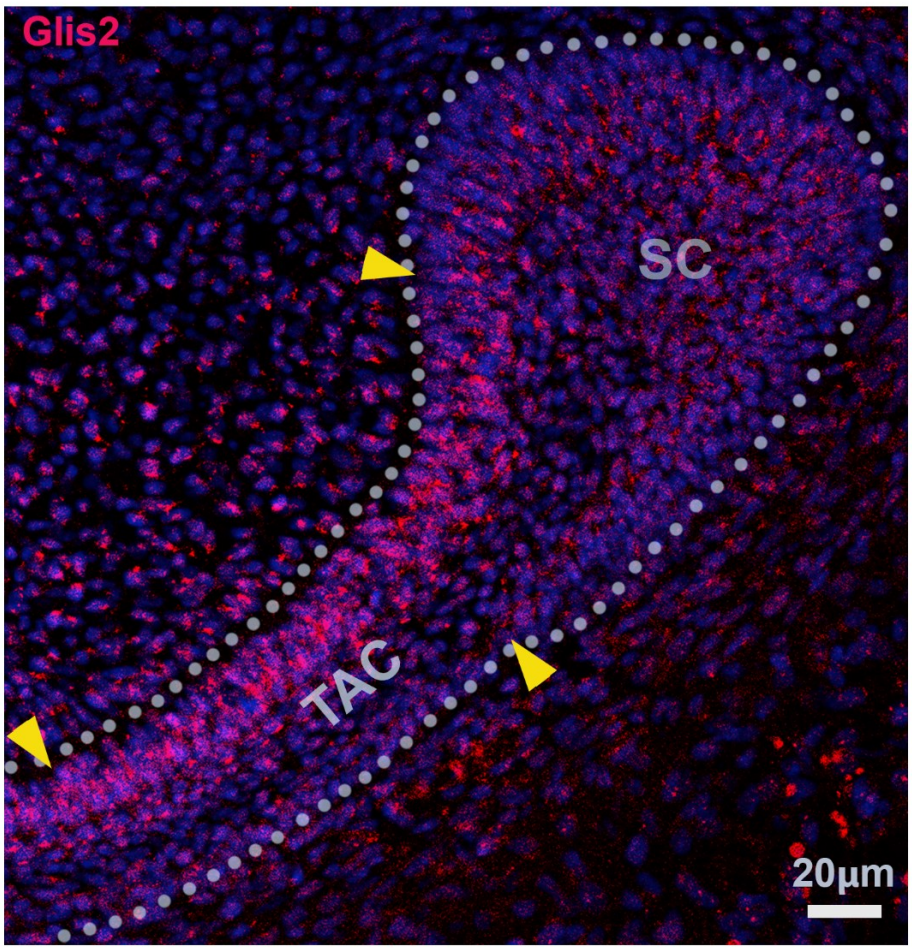

Figure 33: Expression of Gli and Glis family members in the stem cell and transit-amplifying cell region of the mouse incisor tooth.
A) RNA expression levels of Gli and Glis family members in stem cells (white bar) and transit-amplifying cells (black bar) region of P7 C57BL/6 mouse incisor tooth. B) Representative image of Glis2 protein expression in the mouse incisor tooth. Basement membrane separating mesenchyme and epithelium marked in dotted line. Yellow arrowheads indicate boundaries of the stem cell and transit-amplifying cell region.

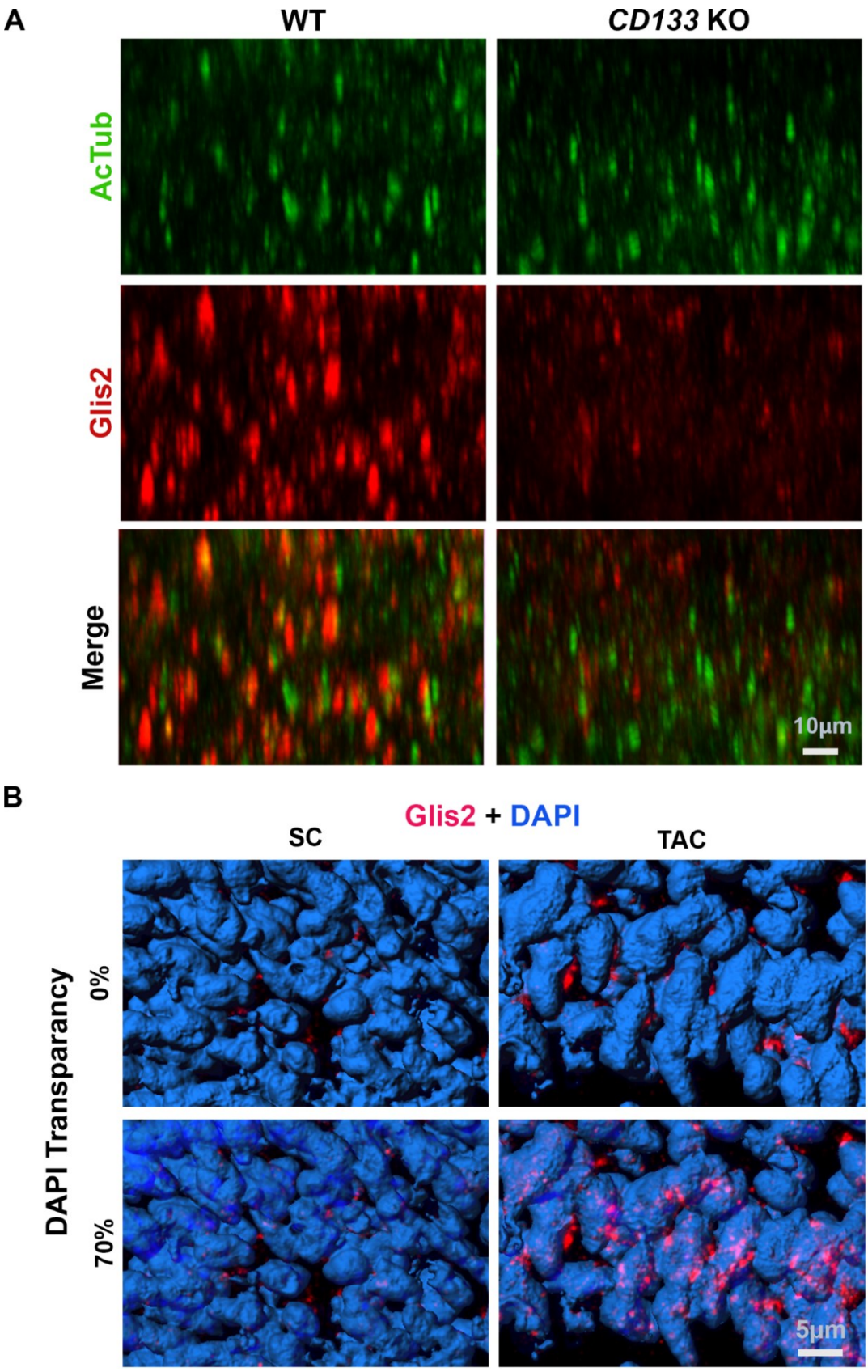

Figure 34: Subcellular localisation of Glis2 in the dental epithelium.
A) Representative immunofluorescence lateral view images of Glis2 and AcTub co-localisation in primary cilia in the stem cell region of P7 WT and CD133 KO mice. B) Glis2 immunoreactivity in the stem cell and transit-amplifying cell region of P7 C57BL/6 mice. 70% transparency nuclei (DAPI) was achieved using Imaris software.

4.17 CD133 translocates to the nucleus

A closer examination of the subcellular localisation of CD133 in the dental epithelium reveals that CD133 extracellular and c-terminal epitopes are both present in the nucleus (Figure 35). Presence of nuclear CD133 c-terminal epitope was also observed in CLE cells where a significant fraction of cells contains nuclear CD133 (Figure 35c). This result could not be replicated using the extracellular antibody of CD133. Potentially due to the epitope representing an isoform that does not translocate to the nucleus. Western blot analysis of CD133 c-terminal epitope in the nuclear protein fractions of two different batches of CLE confirms the nuclear presence (Figure 35d). The purity of the nuclear fractions was confirmed using Lamin A/C as a nuclear marker[395]. To our surprise, full-length CD133 is able to translocate to the nucleus. Proteins larger than 40 kiloDalton (kDa) cannot diffuse freely through the pores in the nuclear membrane and require the presence of a nuclear localisation signal (NLS) tag in their sequence to facilitate their import into the nucleus[396]. NLS comes in many forms, and currently, prediction websites exist to identify putative sequences within proteins. Using the NLS mapper website, examination of the amino acid sequence of mouse CD133 isoforms s1 and s2 but not others reveal the presence of a putative bipartite NLS signal (IKLAKYYRRMDSEDVYDDVETVPMKNLEI) in the intracellular c-terminus directly flanking the transmembrane sequence. Both NLS-containing isoforms are the longest isoforms, and this might explain the more pronounced higher kDa band seen in the nuclear fraction (Figure 35d). Currently, the band seen at 37kDa in both cytoplasmic and nuclear fractions cannot be explained. Theoretically, the cleaving of the c-terminal domain of CD133 would yield a fragment of approximately two to six kDa depending on isoform. Therefore, in addition to cleaving, an additional post-translational

modification such as phosphorylation should occur to explain a band of that size. Indeed, a previous publication has shown that human CD133 contains two phosphorylation sites that act as a substrate for Src and Fyn tyrosine kinases[397]. However, cleavage of the CD133 c-terminal domain has not been demonstrated yet. Our results clearly indicate that CD133 can translocate to the nucleus similar to Glis2.

4.18 Glis2 and CD133 physically interact in the nucleus

The golden standard for detecting protein-protein interactions is co-immunoprecipitation. The protein of interest is sequestered with a specific antibody, and binding partners are identified using Western Blot[398]. However, this technique comes with certain drawbacks. Due to the relatively harsh treatments of the sample, such as initial lysis and centrifugation steps, high-affinity interactions can only be detected with this technique. Dynamic *in vivo* interactions between proteins are also hard to reveal. Moreover, large amounts of sample are needed to counteract the relative insensitivity of Western Blotting as well as the inevitable loss of interactions during the processing of the samples. Also, co-immunoprecipitation does not allow to discriminate between direct and indirect interactions, i.e., the presence of bridging molecules such as DNA or scaffold proteins. *In vitro* interactions between endogenous CD133 and Glis2 could not be detected using standard co-immunoprecipitation protocol. Therefore, to circumvent the limitations listed above we employed a technique called Proximity Ligation Assay (PLA)[399]. There are two ways to perform the technique. The direct PLA requires the conjugation of DNA probes to the primary antibodies whereas the indirect PLA has the probes connected to secondary antibodies allowing for more targets to be investigated at the cost of sensitivity. When the PLUS and MINUS probe come together (30-40nm) the circular DNA acts as a primer for

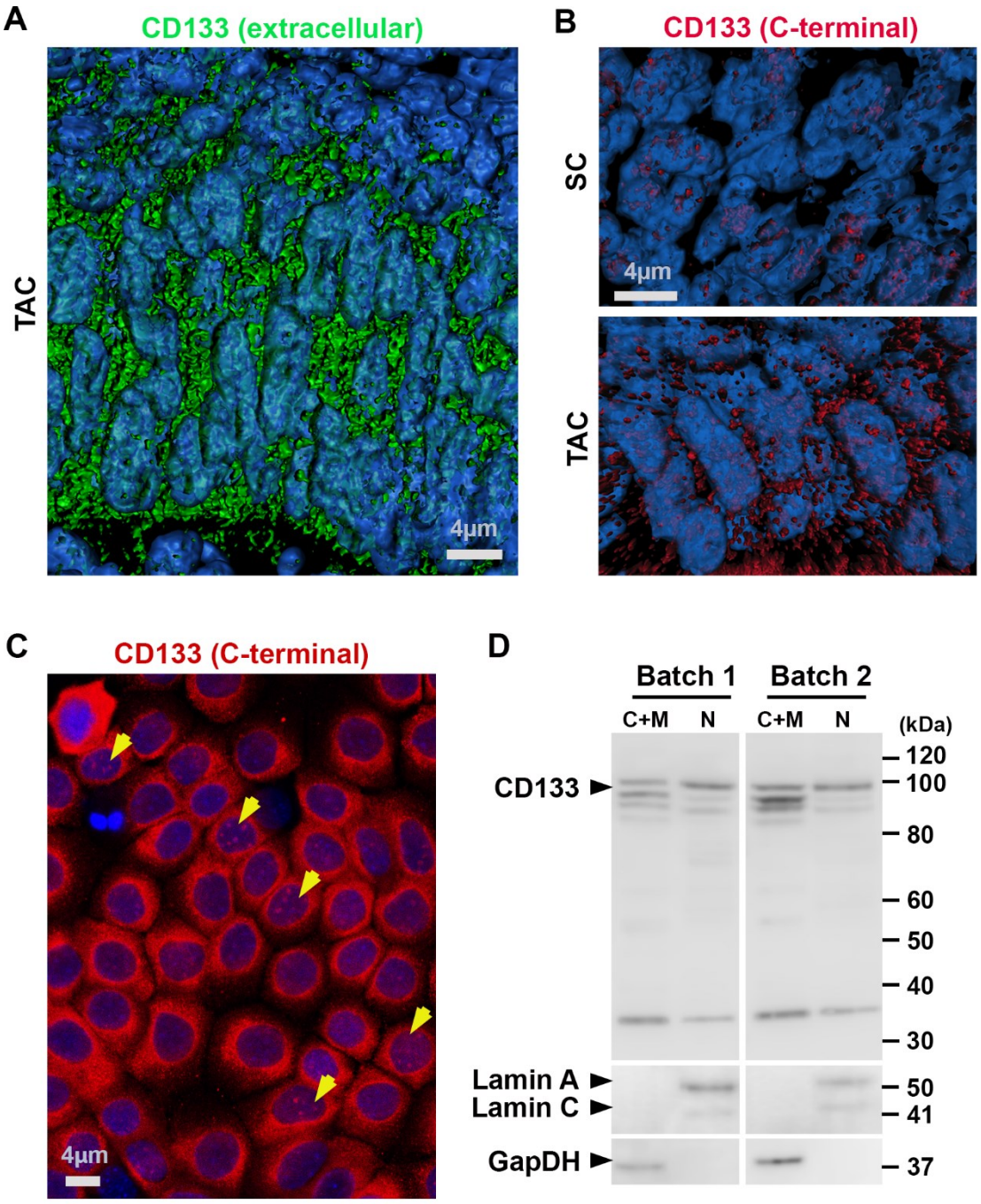

Figure 35: The presence of CD133 in the nucleus.
A) Immunoreactivity of CD133 extracellular epitope in the nucleus of TAC in the dental epithelium of P7 WT C57BL/6 mice. DAPI staining was made semi-transparent using Imaris software to indicate nuclear presence. B) Immunoreactivity of CD133 C-terminal epitope in the nucleus of SC and TAC in the dental epithelium of P7 C57BL/6 mice. DAPI staining was made semi-transparent using Imaris software to indicate nuclear presence. C) *In vitro* analysis of nuclear CD133 C-terminal epitope in CLE cells. Yellow arrowheads highlight cells with nuclear CD133. D) Western blot analysis on cytoplasmic and nuclear protein fractions on CD133 expression. Lamin A/C indicates nuclear purity and GapDH indicates cytoplasmic purity. C+M = cytoplasm + plasma membrane, N = nucleus.

rolling circle DNA amplification. Binding of fluorescently-labelled oligonucleotide probes to the amplified circular DNA provide a precise manner to visualise protein-protein interactions (Figure 36a). To detect the possible interactions of endogenous CD133 and Glis2 in vivo, we used the direct PLA method by initial incubation of CD133 C-terminal antibody and Glis2 to the MINUS and PLUS probes, respectively. P7 C57BL/6 mouse incisors were sectioned and processed as described earlier. Prior to incubation with both antibody-probe conjugates as per manufacturer's recommendations. It is evident from our results that CD133 and Glis2 interact mainly in the nuclei in a specific population in the stem cell region called the outer dental epithelium and transit-amplifying cell regions of the dental epithelium. Despite the presence of both proteins in the primary cilia, there is little interaction outside of the cell's nucleus. It is, therefore, possible that at least two different queues are necessary for the translocation of either protein into the nucleus. With the knowledge that Glis2 is a known transcription factor, we sought to investigate the downstream effector genes of this dual partnership.

4.19 CD133 and Glis2 are connected to Jak/Stat and p53 signalling pathways

To investigate the common effector genes of CD133 and Glis2 we used the RT^2 PCR array to assess the expression profile of 84 key regulators in 10 signal transduction pathways (See Appendix 7.5 for a complete list of genes and their associated pathways).

cDNA conversion of transit-amplifying cell regions of C57BL/6 WT, *Glis2* KO and *CD133* KO was achieved from the isolation of RNA using LCM as described in chapter 4.3. Real-Time qPCR analysis of these samples reveals that 61 out of 84 genes are expressed at detectable levels in all three samples (

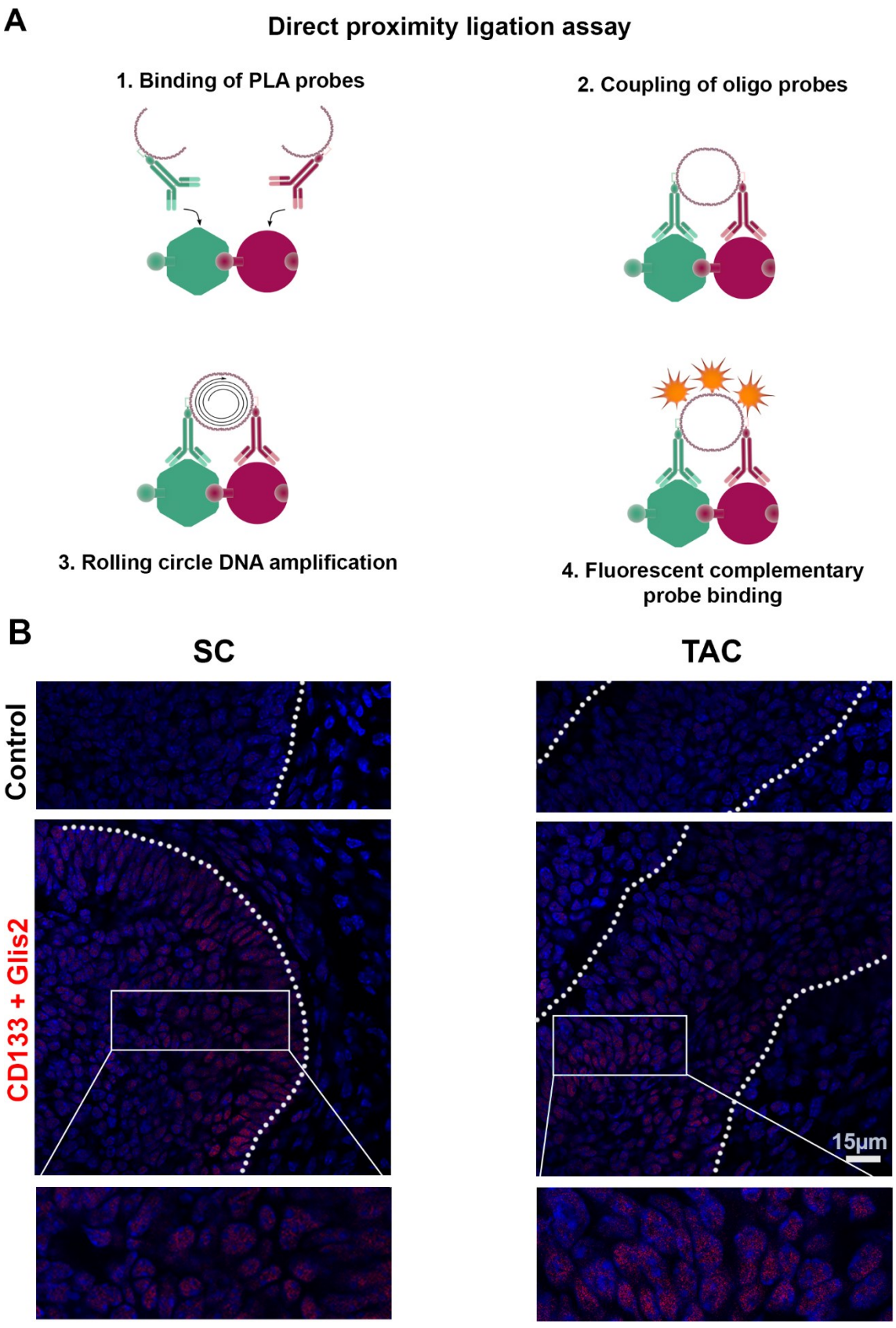

Figure 36: PLA reveals CD133-Glis2 interaction in the nucleus of the dental epithelium.
A) Diagram illustrating the four-step direct PLA workflow. B) Representative confocal images showing the interaction of CD133 and Glis2 in the nuclei of the dental epithelium of P7 WT C57BL/6 mice. Negative control is incubation of a single primary antibody with its conjugated probe.

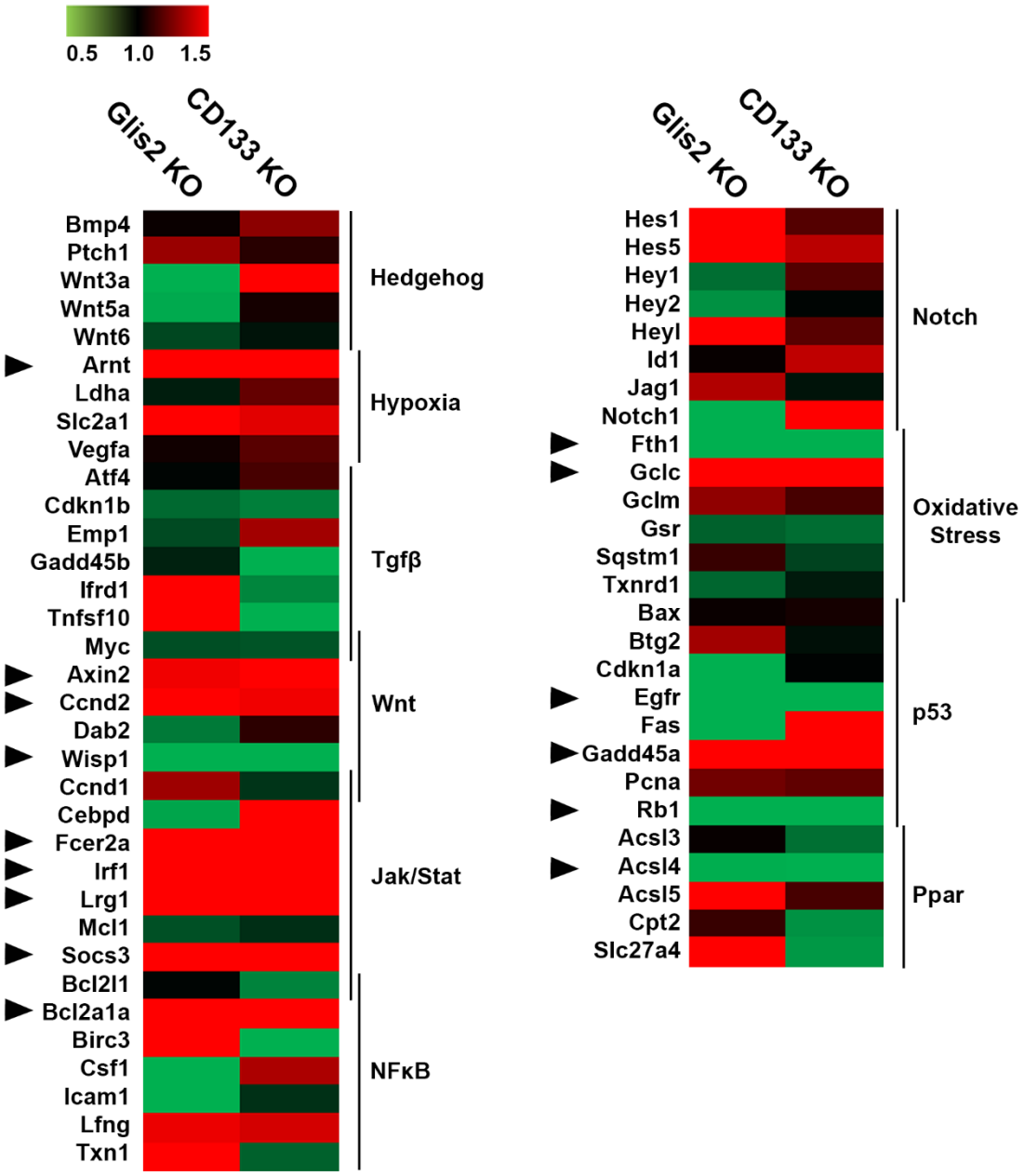

Figure 37: Heatmap of PCR array genes present in the mouse incisor.
Heatmap showing the differential expression of 61 out of 84 assayed genes and its associated pathway in C57BL/6 WT, *Glis2* KO, *CD133* KO mouse incisor. Gene expression of each gene in C57BL/6 WT was used to normalise its counterpart in each KO sample. Arrowheads indicate genes with similar trend and at least 50% differential expression compared to C57BL/6 WT.

Figure 37). After normalisation of the *Glis2* KO and *CD133* KO samples against the C57BL/6 WT control sample (not shown in

Figure 37), 15 genes remain that cover seven signal transduction pathways and show a similar trend in both KO samples of at least 50% difference in expression levels compared to the WT control sample (arrowheads,

Figure 37). Of these 15 genes, ten genes are upregulated, and five genes are downregulated compared to the WT control. However, due to the low number of technical replicates in the PCR array, we opted to repeat the experiment using the same samples but with primers designed for these 15 genes in our lab as the primer sequences of the PCR array are not disclosed. Gene expression of these 15 genes revealed differences compared to the result of the PCR array. Only six genes covering Wnt, hypoxia, Tumor protein p53 (p53) and Janus Kinase (Jak) Signal Transducer and Activator of Transcription (Stat) signal transduction pathways could be confirmed in that they show a similar trend for the KO samples as seen in the PCR array. The p53 and Jak/Stat signalling pathways have two members that could be confirmed. Whereas Wnt and hypoxia signalling pathways have one member each (Figure 38a).

To investigate the possible mechanisms in which Glis2 and CD133 cooperate to control the affected signal transduction pathways, we sought to confirm the results *in vitro*. Knockdown of CD133 and Glis2 was achieved using esiRNA and shRNA, respectively. Analysis of the *in vitro* samples revealed that only Interferon Regulatory Factor 1 (Irf1) and Suppressor of Cytokine Signaling 3 (Socs3) (Jak/Stat), and Aryl Hydrocarbon Receptor Nuclear Translocator (Arnt) (Hypoxia) show a similar trend compared to the *in vivo* assessments leaving them as the only candidates left to pursue (Figure 38a&b). We focused our attention on the

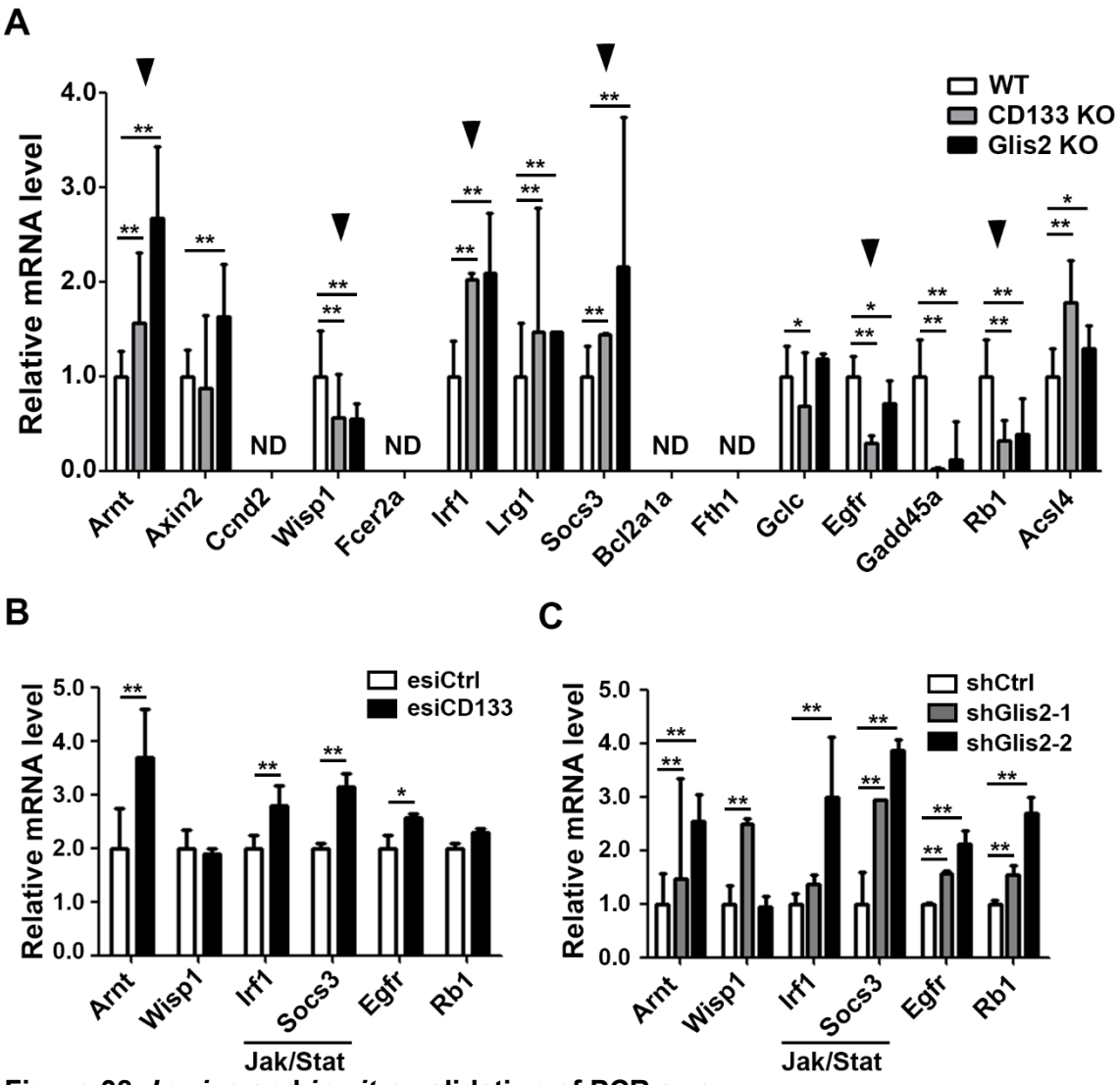

Figure 38: *In vivo* and *in vitro* validation of PCR array.
A) real-Time qPCR on selected genes in C57BL/6 WT, *Glis2* KO, *CD133* KO mouse incisor. ND= Not detected. B) *In vitro* validation of A in esiRNA-mediated knockdown of *CD133* in CLE cells. B) *In vitro* validation of A in shRNA-mediated knockdown of *Glis2* in CLE cells. **p<0.01

Jak/Stat signalling transduction pathway due to it being represented by two genes (Socs3 and Irf1) as opposed to the single gene in the case of Hypoxia signalling.

4.20 Assessment of the Jak/Stat signalling pathway in the mouse incisor tooth

The Jak/Stat signalling pathway is evolutionary conserved and has traditionally been linked to transmit extracellular signals, often cytokines and hormones, to the nucleus leading to changes in proliferation, differentiation, apoptosis and cell migration[400]. Loss of function mutations that lead to reduced activity of the pathway affect tissue processes such as haematopoiesis, mammary gland development and lactation, adipogenesis, and immune development. On the other hand, increased activity is linked with chronic inflammation, gigantism and several types of leukaemia[401,402]. Binding of a ligand to its receptor leads to the activation of receptor-bound Jaks. This in turn alters the cytoplasmic tail of the receptors creating docking sites for cytoplasmic Stats. Jak-mediated phosphorylation of Stats precedes the nuclear translocation and DNA binding of Stat resulting in transcription of its effector genes[403]. Currently, four Jaks and seven Stat family members are known in mammals.

Socs3, a gene that was overexpressed in our PCR array and our follow-up studies (Figure 37 & Figure 38), is involved in the suppression of infections and autoimmune diseases. Socs3 binds to both the cytokine receptor and Jak kinases resulting in the inhibition of Stat3 phosphorylation and activation. However, it has been shown that the phosphorylation of Stat is not always required for its nuclear translocation and subsequent transcriptional activity[400]. Additionally, Socs3 mediates the degradation of the cytokine receptor by ubiquitination leading to a decreased response to inflammation[404].

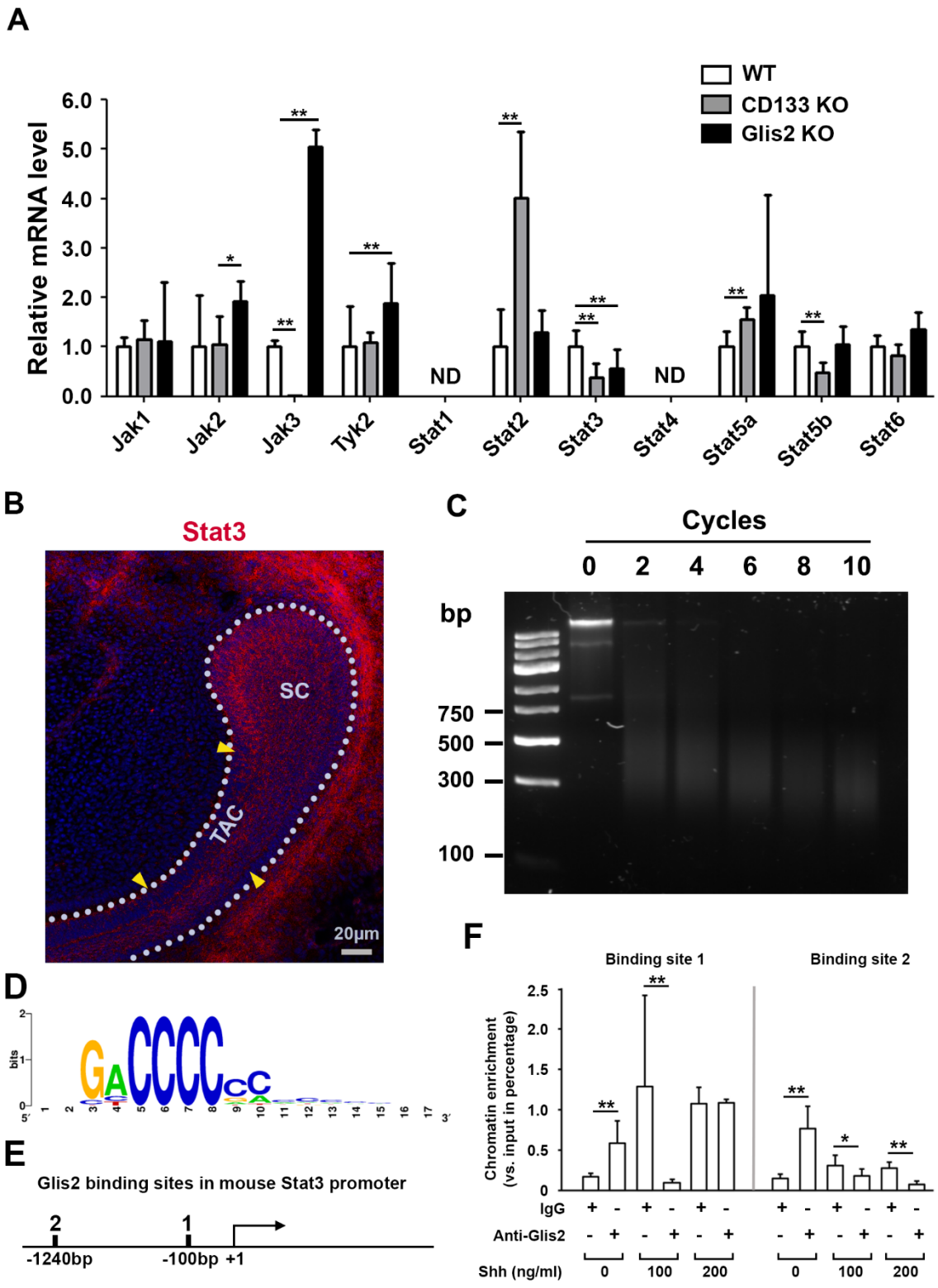

Figure 39: Jak/Stat expression in the dental epithelium of the mouse incisor tooth. A) Real-Time qPCR result of Jak/Stat family members in the transit-amplifying cell region of the mouse incisor epithetlium of P7 C57Bl/6 WT, *CD133* KO and *Glis2* KO mice. B) Representative immunofluorescence result of Stat3 in the labial cervical loop of the P7 C57Bl/6 WT mouse. Yellow arrowheads indicate boundaries between the stem cell and transit-amplifying cell region. D) Glis2 consensus sequence. E) Approximate positions of Glis2 DNA binding sites in the mouse Stat3 promoter sequence. F) Chromatin Immunoprecipitation (ChIP) -qPCR result indicating Glis2 binds to the promoter of Stat3. ND= Not Detected. **: p<0.01, *: p<0.05.

Irf1 plays a critical role in the immune response, inhibition of proliferation and induction of apoptosis where its expression is regulated by Stats[405]. Irf in itself is a weak transcription factor and depending on its binding partners regulates expression of Interferons[406]. Among its binding partners are several Jaks and Stats such as Jak 1, 2, and Stat1 and 3[407].

Due to the involvement of Irf1 and Socs3 in Stat signalling, we sought to assess the gene expression levels of all Jak and Stat members in the transit-amplifying cell regions of C57BL/6 WT, *Glis2* KO and *CD133* KO mouse incisor, which has not yet been reported previously. Real-Time qPCR analysis showed that all members the Jak/Stat familiy are expressed in the transit-amplifying cell region of the dental epithelium apart from Stat1 and 4. However, only Stat3 shows a similar downregulation in both KO samples compared to the WT control. We then looked at the Stat3 promoter, located on chromosome 11:100937600-100940601, to investigate whether it contains one or more Glis2 consensus sequence inits sequence. The promoter sequence is 3001 base pairs (bp) long and was retrieved using Ensembl (Release 91 - December 2017) and was then analysed for putative Glis2 transcription factor binding sites using the MatInspector module of the Genomatix Software Suite. Two possible Glis2 binding sites were uncovered using the consensus sequence determined by the Genomatix software (Figure 39d). Binding sites 1 and 2 are located 100 and 1240bp upstream of the transcription start site, respectively (Figure 39e) and primers were designed around those locations. Immunoprecipitation of Glis2 protein and associated DNA was done on CLE cells in the presence (100 and 200ng/ml) or absence of Shh for 24 hours. After crosslinking, nuclei were purified with mortar and pestle and then sheared by sonication for 6 cycles to achieve DNA fragments of 400-500bp (Figure 39c). Glis2-binding sequences were immunoprecipitated

and matching IgG isotype controls were used as a negative control. The presence of the putative Glis2 binding sites in the *Stat3* promoter was then assessed in the precipitated Glis2-positive DNA and its negative control using Real-Time qPCR.

Binding rates were calculated against the input sample. The exact same amount of chromatin was used for ChIP and generation of input signal. Our data reveals that our DNA samples are enriched with both binding sites compared to the IgG isotype controls when CLE cells are cultured in the absence of Shh (Figure 39f). Interestingly, Glis2 does not seem to bind to the *Stat3* promoter in CLE cells cultured with either 100ng/ml or 200ng/ml Shh for 24 hours. Of note, background signal seems to be relatively high in the Shh samples and this might mask the binding of Glis2 to the *Stat3* promoter.

Taken together, our results indicate that Glis2 only binds to the *Stat3* promoter in the absence of Shh and this fits with the observation that Stat3 expression is downregulated in the transit-amplifying cell region (Figure 39b) where Shh is highly expressed[323]. This also indicates that Glis2 is a positive regulator of *Stat3* transcription in the stem cell region in the cervical loop.

4.21 Bmi1 acts upstream of CD133-mediated ciliogenesis in the dental epithelium

Stem cell renewal, activation and distinct lineage differentiation patterns is only partially controlled by the equilibrium between different transcription factor networks[408]. In addition to these networks, gene expression can be influenced by epigenetic regulation of chromatin and has been shown to be crucial in the control of stem cell renewal and activation. Indeed, global and local changes in chromatin structure determine whether a stem cell will continue and differentiate or self-

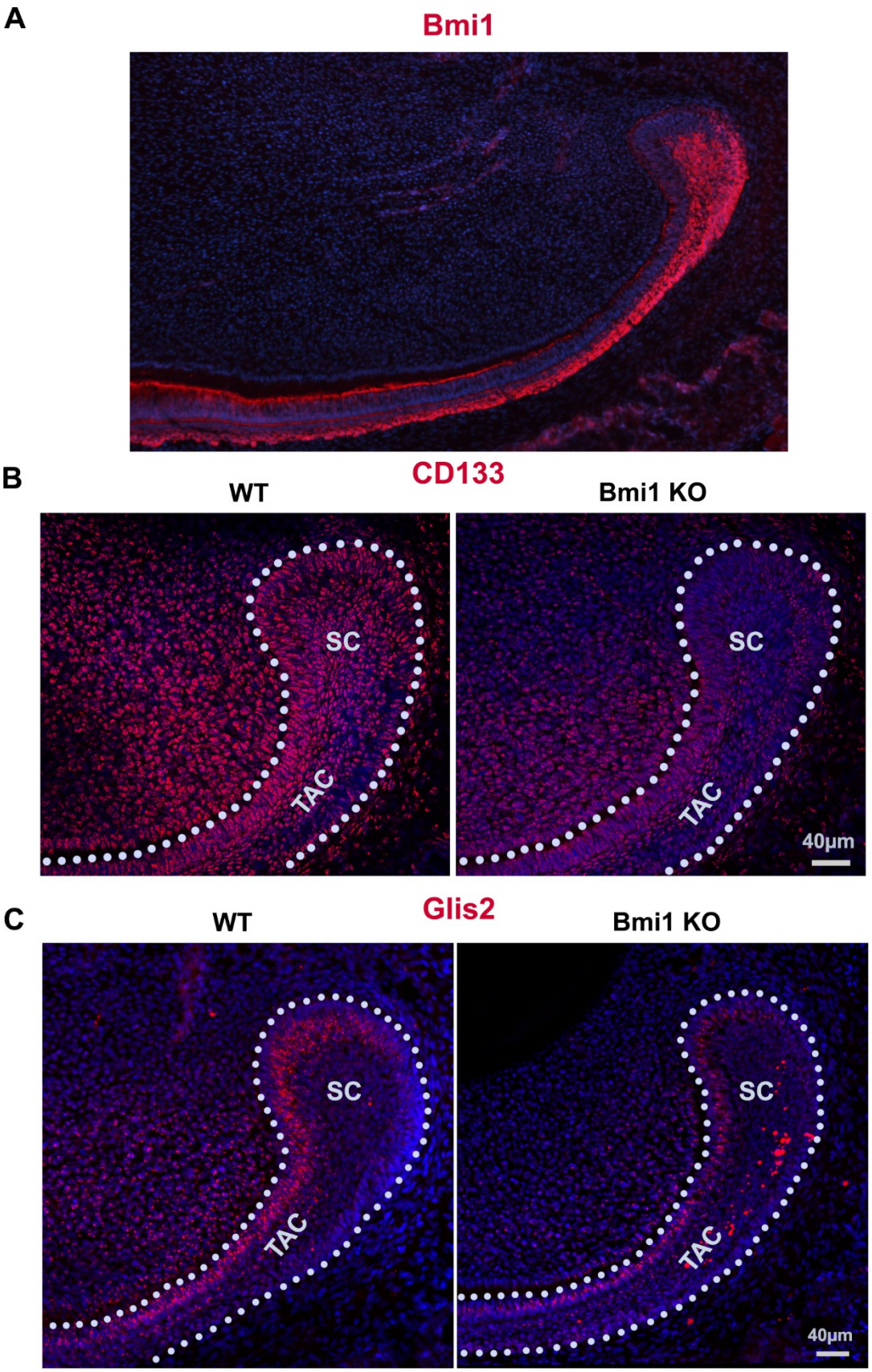

Figure 40: *BMI1* is expressed in the dental epithelium of P7 mouse incisor tooth and partially controls *CD133* and *Glis2* expression.
A) Representative immunofluorescence image of BMI1 expression in P7 mouse incisor tooth. B) Expression of CD133 ICD in the stem cell and transit-amplifying cell region of WT (left panel) and BMI1 KO mice (right panel). C) Glis2 expression in the stem cell and transit-amplifying cell region of WT (left panel) and BMI1 KO mice (right panel).

renew[409]. DNA can be directly modified by covalent modifications such as DNA methylation of CpG islands, or indirectly such as nucleosome remodelling and histone modifications, which controls the accessibility of the transcription machinery to DNA.

Histone modifications can act as scaffolds for protein complexes such as the Polycomb Group (PcG) family to alter gene expression. PcG proteins form protein complexes to maintain gene silencing during development, lineage commitment and differentiation. The PcG repressive complex (Prc) was initially identified in *Drosophila* and loss-of-function mutations lead to increased expression of Hox genes altering the body plan in these organisms[410]. Prc1 and Prc2 are the two canonical PcG complexes although their composition may vary depending on the context. Prc1 is built around the E3 ubiquitin-protein ligase Ring1-Posterior sex comb (Pse) heterodimer and one example of a Pse homologue in mammals is the *Bmi1* oncogene. *Bmi1* plays a crucial role in stem cell renewal and lineage differentiation during embryonic development and in adult organs[84,411]. The importance of BMI1 in adult tissue homeostasis is illustrated in the intestinal crypt.The intestinal crypt contains two stem cell populations: a rapidly cycling Lgr5-positive population and a quiescent Bmi1-positive population, and the latter is capable of replenishing the former after ablation of the Lgr5-positive population[412]. Expression of *BMI1* is often upregulated in cancers and BMI1-expressing tumours often display radio and chemo resistance resulting in poor prognosis for patients[81,413,414]. Inhibition of cell cycle repressors p16 and p19 by Bmi1 has been well studied and loss of Bmi1 has been associated with induction of senescence, an intrinsic tumour suppressor mechanism[415,416]. In the adult mouse incisor tooth, *Bmi1* expression is restricted to the outer dental epithelium and overlaps significantly with other stem cell markers such as H2B-GFP and

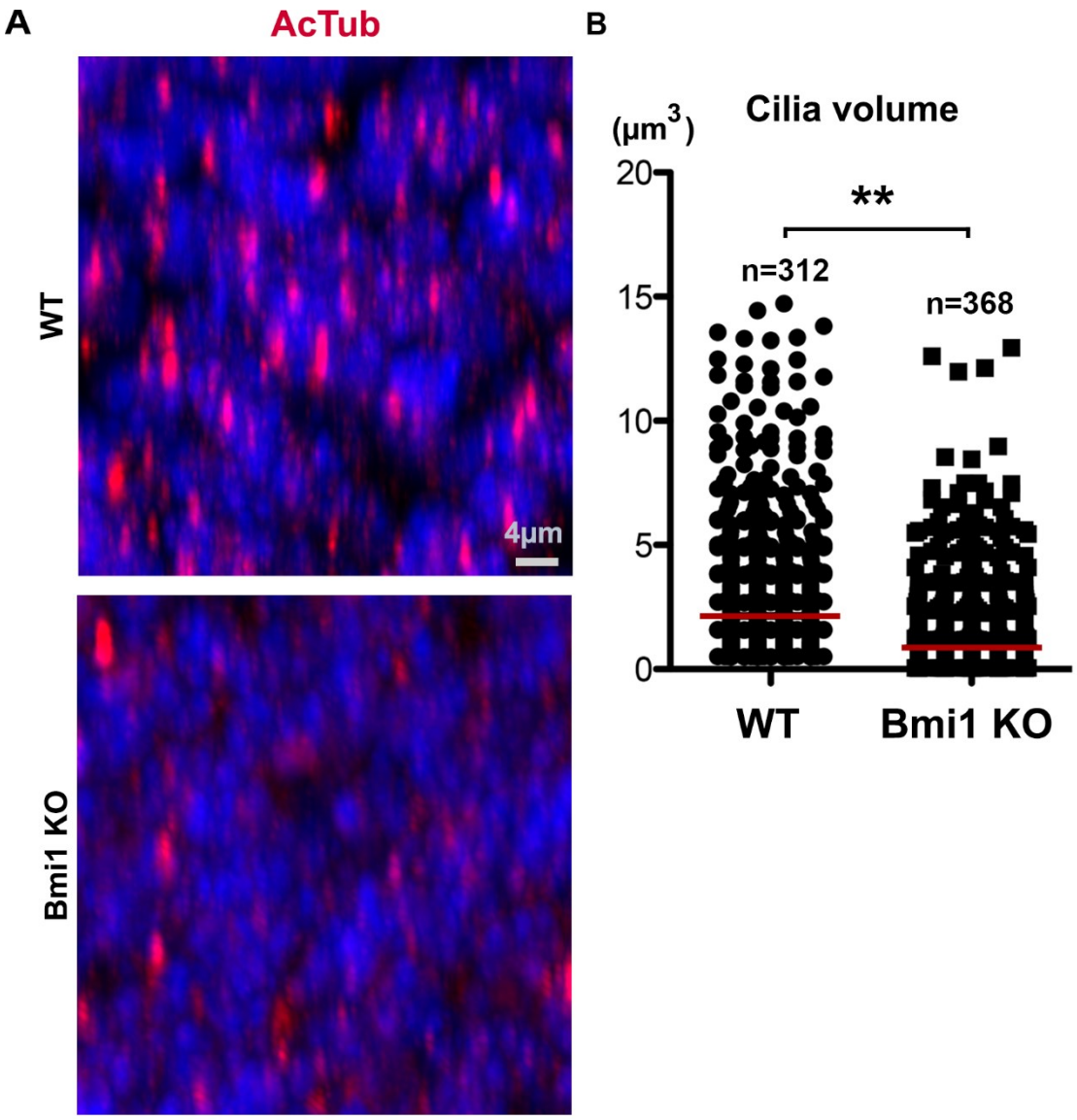

Figure 41: Phenotypical similarities in primary cilia dynamics between *Bmi1*^{GFP} and *CD133* KO mice.
A) Representative Immunofluorescence lateral view images of AcTub localisation in primary cilia in the stem cell region of P7 WT (top image) and *BMI1*^{GFP} (bottom image) mice. B) Comparison of primary cilium volume in stem cell populations P7 WT and *BMI1*^{GFP} mice. n= number of primary cilia counted. ** $p<0.01$

Gli1-LacZ[82]. As with the intestinal crypt, Bmi1-positive stem cells can generate all progeny in the incisor tooth.

In our model, we sought to investigate the protein expression pattern of *Bmi1* in P7 mice and its relation to CD133, Glis2 and primary cilium dynamics. Bmi1 is highly expressed in the outer dental epithelium, stellate reticulum and stellate intermedium of the developing dental epithelium (Figure 40a) as opposed to the adult dental epithelium where it is restricted to the outer dental epithelium[82].

Deletion of *Bmi1,* replaced through homologous recombination with the *GFP* gene[417], leads to diminished protein expression of both CD133 and Glis2 in the dental epithelium (Figure 40b&c). As expected, some expression remains as multiple transcription factors often control the expression of genes. Interestingly, expression of CD133 and Glis2 remains diminished in the transit-amplifying cell region where Bmi1 expression is very low. Bmi1 is commonly regarded as a transcriptional repressor suggesting that its control of CD133 and Glis2 expression is most likely indirect. However, recently, it has been shown that Bmi1 can act independently of the Prc1 complex as a transcriptional activator in prostate cancer[81]. This observation opens up the possibility of a direct control of *CD133* and *Glis2* expression by Bmi1.

If Bmi1 regulates directly or indirectly *CD133* and *Glis2* expression, we were wondering if *Bmi1*^{GFP} mice display similar phenotypical primary cilium characteristics as seen with *CD133* KO mice (Figure 21). Indeed, immunofluorescence staining of AcTub reveals lower primary cilia density in the cervical loop of *Bmi1*^{GFP} mice compared to their littermate controls (Figure 41a). Moreover, quantification of primary cilium size shows that the primary cilia are smaller in the mutant mice (Figure 41b).

Earlier reports have shown that adult *Bmi1*-deficient mice display smaller cervical loop due to depletion of stem cells in the outer dental epithelium of the cervical loop leading to enamel defects[82]. Ablation of CD133 leads to a similar phenotype further corroborating a molecular link between CD133 and Bmi1 (Figure 18-Figure 20). Our results indicate that Bmi1 acts upstream of CD133 to regulate ciliogenesis and lineage differentiation in the dental epithelium.

5 Discussion

Our study aims to look at the role of CD133 (Prominin-1) in dental epithelial stem cell maintenance, activation and lineage differentiation. In doing so, a novel pathway has been uncovered that mainly takes place in the primary cilium, an organelle that is present in nearly all cells and plays a crucial role in translating extracellular cues into appropriate cell responses. Remarkably, the relationship between the primary cilium and stem cell behaviour is understudied, especially in the epithelium, given its importance in regulating the cell cycle[362].

At present, CD133, a primary cilium component, is widely used as a stem cell marker to identify and isolate stem cells in a wide variety of tissues. However, its function remains poorly understood. Our work demonstrates that CD133 acts as a scaffold for the successive recruitment of Arl13b and Hdac6 in a cell status-dependent manner, i.e.: quiescent stem cell or transit-amplifying cell, respectively. The primary cilium architecture is cyclical in nature and changes in length depending on the cell cycle stage. Our *in vivo* CD133 KO experiments indicate that reduced primary cilium length renders cells less sensitive to the SHH morphogen, which requires the primary cilium for signal propagation into the cell. In the dental epithelium, SHH is expressed by transit-amplifying cells and acts in a positive feedback loop on the epithelial stem cells necessary to fuel the constant generation of enamel-secreting ameloblasts[323].

Loss of CD133 leads to a host of changes in primary cilia characteristics in the dental epithelium. First, primary cilia are shorter in the stem cell region, meaning that affected stem cells either have disturbed cell cycle dynamics, in this case, a shorter G0 and/or G1, the typical anagenic phases of ciliogenesis, or stunted primary cilium growth independent of the cell cycle. Second, primary cilia are

longer in the transit-amplifying zone than their WT's counterparts, indicating either that these cells spend more time in the G0-G1 phase or that primary cilium resorption is too slow leading to a slowdown of the cell cycle. In addition, primary cilium numbers were up in both CD133 mutant stem cell and transit-amplifying cell populations compared to wild-type controls implicating that a smaller fraction of affected cells resides in the M phase, the only cell cycle phase where primary cilia are completely resorbed.

These phenotypical changes contribute to a reduction in quiescent and activated stem cells as seen in the volume calculations of the Sox2-positive region (quiescence) of the cervical loop and the ratio of Ki67/Sox2 (activation) in control versus CD133 KO mice. Previously, it has been shown that Sox2-positive cells in the cervical loop can give rise to all cell types of the dental epithelium including the enamel-secreting ameloblasts[78]. Therefore, Sox2 is a true and validated stem cell marker in the dental epithelium. Ki67 is widely regarded as a proliferation marker that shows increasing protein expression levels in cycling cells with the highest expression seen in the M phase but whose expression is absent in quiescent G0 cells[418]. Hence, the use of both markers to carefully document changes in stem cell dynamics regarding its maintenance as well as activation in our study.

Ultimately, these defects are reflected in the stem cells' inability to become properly matured ameloblasts. CD133 KO ameloblasts are capable of producing and secreting enamel but do so less effectively. µCT data clearly shows that the onset of enamel deposition is delayed and that its final thickness is reduced compared to WT animals. Histological staining revealed that ameloblasts show expected elongation during differentiation but their nuclei are not properly

polarising away from the secreting front, phenocopied, albeit stronger, by Krt14-Cre: Shh mice[61]. Moreover, white vacuoles are present in KO ameloblasts hinting at inhibited secretion of enamel, which would explain the incomplete enamel rod maturation. Our study was not able to find out the role of CD133 in enamel secretion, but one possibility is the fact that complete differentiation of ameloblasts is not achieved as seen with the diminished expression of known ameloblast markers and, therefore, important components of the 'enamel production and secretion programme' are missing.

Interestingly, using antibodies targeting different epitopes of CD133 revealed different protein expression patterns. The entire dental epithelium is positive for the ICD epitope with the highest expression seen in the inner dental epithelium of the cervical loop, whereas, the ECL epitope is mostly restricted to the inner dental epithelium of the cervical loop. The ECL antibody has previously been shown to target both glycosylated and non-glycosylated forms of CD133[167]. However, it is likely that the antibody has different affinities for both forms of CD133. In addition, the second extracellular loop contains multiple possible N-glycosylation sites and it is, therefore, likely that the epitope is only recognised in its unglycosylated and a specific glycosylation pattern but not all possible glycosylation patterns. Our Western Blot results, using the ICD-targeting antibody, reveals there is at least four different full-length forms of CD133. This does not directly prove the existence of differently-glycosylated forms of CD133 in the dental epithelium as these size differences could also be due to different yet unknown post-translational modifications or even different isoforms. Indeed, according to the NCBI gene database, eight different murine isoforms have been confirmed with multiple predicted transcript variants. Whether, multiple transcript

variants are present within the dental epithelium and if these different isoforms perform different roles remains to be investigated.

Overall, the phenotype in the dental epithelium of *CD133* KO mice is relatively mild with fully functional, albeit thinner, enamel. In mammals, the Prominin family, of which CD133 is part of, contains an additional member: Prominin-2. The expression pattern of both members overlaps in most tissues apart from the eye where only CD133 is detected[173]. Given that the photoreceptor cells of *CD133* KO mice display an overt phenotype with the gradual loss of eyesight, it is likely that Prominin-2 rescues the phenotype in other *CD133*-expressing tissues. Indeed, elevated levels of Prominin-2 RNA has been detected in the developing mouse incisor tooth cervical loop[419]. Hence, a partial rescue by Prominin-2 is likely explaining the relatively mild phenotype. To date, research on Prominin-2 has been largely non-existent with only 17 publications so far and more research needs to be done on the mechanisms of the Prominin-2 rescue of *CD133* KO phenotype in different tissues including tooth development.

To understand the underlying mechanisms governing stem cell maintenance and activation, we isolated the dental cervical loop of P7 mice containing quiescent and activated stem cells, and the adjacent inner dental epithelium harbouring the transit-amplifying cells (CLE). To validate these cells, we used key epithelial (Krt14, Cdh1) and mesenchymal (Pdgfrβ, Vimentin) markers to determine their purified epithelial nature. In addition, these cells can express the ameloblast-specific differentiation markers, Ameloblastin and Amelogenin.

Addition of Shh to WT CLE cells leads to an increase in proliferation, which is completely prevented by simultaneously reducing *CD133* expression using esiRNA. Shh is important for growth control in tooth development. Indeed, Cre-

mediated deletion of Shh after epithelial placode formation (~E11.5-E12.5) leads to rudimentary tooth development, which does not affect enamel and dentine deposition, albeit structurally disorganised[61]. In addition, Shh decreases cell survival as seen by increased levels of activated Caspase 3, a critical executioner of apoptosis. Reduction of CD133 expression in the absence of Shh does not have any effect on colony size or number of CLE cells. However, complete loss *of CD133* leads to failure of CLE to form colonies independent of SHH. *In vivo* loss of *CD133* does not lead to such a strong phenotype, as the cervical loop is still present, although smaller, in two-month-old *CD133* KO mice and is likely due to epithelial-mesenchymal rescue mechanisms.

Whether Shh directly interacts with CD133 remains to be investigated. So far, Ptch1 is the only receptor known to directly bind to the ligand[420]. Given the strong phenotypes associated with changes in CD133 expression in Shh signalling and the importance of cholesterol in the correct membrane localisation and long range signalling of CD133[421] and Shh[61, 422], respectively, there is a possibility of both molecules directly interacting in a cholesterol-dependent manner. Of note: the recombinant Shh used in our *in vitro* experiments lack any sterol modifications but it is also possible it only requires CD133 bound to membrane-incorporated cholesterol. A follow-up study is necessary to prove both proteins can interact in a direct manner.

Our study does highlight an indirect role for CD133 in Shh signal propagation. Arl13b, a small GTPase responsible for cilia assembly, has also been implicated in the regulation of Shh signalling protein localisation to the primary cilium. Mouse embryonic fibroblasts (MEF) harbouring inactivating *Arl13b* mutations (hennin) show a similar phenotype to *CD133* KO mice in that their primary cilia are shorter

compared to WT. However, hennin mutant MEF are capable to be cultured *ex vivo* and respond to Shh unlike *CD133* KO through an increase in Smo, though less pronounced than in control cells, to the primary cilium. Hennin mutants also display ciliary Smo even in the absence of Shh[162,383]. This leads to a shallow gradient response to Shh as is confirmed with the hennin mutant's defective patterning during development[383]. Our *in vivo* study shows that Arl13b's localisation to the primary cilium is almost completely diminished in the absence of CD133 and that both molecules interact directly as shown in our CoIP experiments. It remains to be determined if the primary cilium localisation of Shh effector proteins is similarly affected in our model.

Arl13b binds to the same intracellular loop of CD133 as Hdac6, a key effector in cilia resorption. A previous study has shown that substitution of lysine with glutamate (K138Q) in CD133 neutralises the electric charge and prevents Hdac6 from binding to CD133 through its first intracellular loop[391]. Using the same K138Q construct, we confirmed that Arl13b loses its ability to bind to CD133. Arl13b and Hdac6 are responsible for cilium assembly and disassembly, respectively. This result opens up the possibility of a sequential binding mechanism between Arl13b and Hdac6, i.e.: cells present in the G0 or G1 will favour the CD133-Arl13b complex to stimulate primary cilium growth, whereas, from the S phase onwards, this complex dissociates and CD133 recruits Hdac6 to enable cilia resorption in preparation for mitosis. The question remains how exactly this transition happens. Several studies have shown that cells with long primary cilia were more receptive to mechano-transduction and fluid flow compared to cells with shorter cilia[354,423]. Our model demonstrates that this is also the case with chemo-sensation and that quiescent stem cells become more responsive over time to extracellular cues such as Shh stimulation.

Several Shh downstream effector genes are expressed in the dental epithelium. Gli proteins are the best-studied effectors of Hedgehog signalling. The family comprises of three members: Gli1, Gli2 and Gli3, and are all expressed in the developing dental epithelium of the incisor. Glis2, a member of the Gli similar family, has high sequence similarity with Gli proteins and acts in a similar fashion by translating extracellular cues into appropriate gene transcription. Profiling the expression of *Glis2* in the dental epithelium revealed that *Glis2* shows similar expression patterns as *CD133* at both the RNA and protein level. As with Gli2 and 3, Glis2 activation in primary cilia leads to its translocation to the nucleus where it acts mainly as a repressor of gene transcription with some evidence of promoting gene expression[424]. Loss of *Glis2* in human and mice leads to nephronophthisis, an end-stage autosomal recessive kidney disease. CD133 expression is particularly high in kidney as well[211]. So far, limited evidence exists linking Shh signalling to Glis2. Expression patterns of both molecules are remarkably similar in the developing kidney[425–427]. Moreover, in developing lungs, co-expression of both molecules points Glis2 to a role in branching morphogenesis and cell proliferation, a function attributed to CD133 in mammary glands[261,428]. However, Shh signalling is considered paracrine in nature, therefore, its exact co-localisation hints at an upstream role for Glis2 in Shh signalling. Glis2 has also been shown to interact with SuFu, which is involved in the activation of Gli proteins in primary cilia upon Shh stimulation. This interaction leads to ubiquitination of the complex in the kidney, which consequently leads to its degradation and negative regulation of Shh signalling[424].

Our study shows for the first time that CD133 can translocate to the nucleus under normal physiological conditions. Previous observations of nuclear CD133 was only reported in cancers. Indeed, this atypical localisation of CD133 has been

detected in non-small cell lung cancer, hepatocellular carcinoma, rhabdomyosarcoma and triple-negative breast cancer, and correlates with poor prognosis due to radio- and chemotherapy rsistance, and increased rates of metastasis[233–235,429]. Interestingly, this study illustrates that full-length CD133 is capable of nuclear translocation. In general, proteins that are larger than 60kDa cannot diffuse passively though the nuclear pore[430]. Instead, large proteins and macromolecules require an active transport mechanism to cross the nuclear pore barrier and relies on the presence of a special amino acid sequence, better known as the nuclear localisation signal, in the protein[431]. In general, this signal is made up of one or more short sequences of positively charged arginines or lysines, which are exposed on the protein surface and can be predicted using online resources[432]. CD133 lacks such classical sequences and it remains elusive as to how it translocates to the nucleus. Several alternative possibilities might explain its nuclear presence.

First, several nuclear localisation sequences exist, and new ones are being discovered regularly. Indeed, the recent discovery of the DFP motif being responsible for the Importin α5-mediated nuclear translocation of O-GlcNAc transferase attests to the divergent nature of the nuclear localisation sequence[433]. Interestingly, all murine and human isoforms of CD133 contain the motif in their extracellular N-terminal domain opening a future avenue for follow-up research. Second, the nuclear membrane in mammalian cells is a dynamic structure and is completely broken down during mitosis temporarily exposing the DNA to the cytosolic environment[434]. This event presents an opportunity for proteins to localise to the DNA periphery and, subsequently, to be encapsulated by the newly formed nuclear envelope during telophase of mitosis. Third, a previous report has implicated that a fraction of the resorbed primary cilium remains attached to the

mother centriole and governs asymmetric cell division. Therefore, the possibility of CD133 being part of the so-called ciliary remnant might be the principal mechanism of its nuclear translocation. In particular, the presence of Arl13b, a binding partner of CD133, in the ciliary remnant substantiates this hypothesis[229].

Finally, the interaction with Glis2 might facilitate its nuclear localisation. This has been shown previously to be the case with Type I insulin-like growth factor receptor that uses the Insulin receptor to translocate to the nucleus[435]. Regardless of the mechanism of translocation, this study conclusively proves that CD133 translocates to the nucleus under normal physiological conditions where, in the dental epithelium, it interacts with Glis2. This interaction could only be detected using the Proximity Ligation Assay but not classical co-immunoprecipitation. This indicates that the complex is only bound very weakly and that the interaction is disrupted due to the harsh conditions of co-immunoprecipitation. Another possibility is that binding of both proteins is also controlled by factors delivered by the extracellular environment (See chapter 1.1.3 Somatic stem cells and the extracellular micro-environment) as the Proximity Ligation Assay was performed on *in vivo* samples whereas the co-immunoprecipitation experiments were performed on *in vitro* CLE cells.

Investigation in the downstream signalling pathways that are controlled by CD133 and Glis2 leads to two major pathways commonly affected in the cervical loop of the two different mutants. *In vitro* assessment using siRNA on CLE cells could only confirm the *in vivo* observation of Jak/Stat signalling but not Hypoxia signalling. Hence, the focus of this study on Stat3. In addition to having Glis2 consensus sequences within the *Stat3* promoter, Stat3 is also an essential transcription factor involved in the regulation of stem cell maintenance and

activation[436,437]. In the cervical loop, Stat3 protein is highly expressed in the quiescent stem cell region whereas its expression is diminished in the transit-amplifying cell region where both CD133 and Glis2 are highly expressed. ChIP-qPCR confirmed that *Stat3* is a direct transcriptional target of Glis2. Together with the observation of Stat3 protein expression in the cervical loop, this study concludes that Glis2 is a negative regulator of *Stat3* in the dental epithelium. To find additional effector genes of the Shh-CD133-Glis2 axis, it would be beneficial to perform RNA-Seq on the dental epithelium as the PCR array only provides a limited scope on gene expression. In addition, the novel pathway should be verified in other model systems such as the kidney epithelium where both CD133 and Glis2 are highly expressed.

Finally, the present study shows that *CD133* and *Glis2* are both controlled by Bmi1, a master regulator of stem cells in a variety of tissues including the dental epithelium[82,412]. Not only does loss of *Bmi1* lead to diminished expression of *CD133* and *Glis2*, it also leads to a reduction in primary cilium length, which phenocopies *CD13*3 KO dental epithelium.

Taken together, this study provides insight in the control of stem cell maintenance and activation by the Shh-CD133-Glis2-Stat3 axis in the developing epithelium. Moreover, the discovery that CD133 directly mediates the Shh signal might have big implications in cancer therapy and treatment. Cells that contain low levels of CD133 show no gross phenotypes but favour apoptosis when exposed to excess Shh as seen in cancer. Currently, three models exist that describe Shh activity in cancer. Type I cancers are Shh ligand independent, such as basal cell carcinomas and medulloblastomas, and are characterised by activating mutations of Ptch and Smo. Type II tumours are autocrine (or juxtacrine) Shh

dependent, implicating that Shh is produced and responded to by the same (or neighbouring) cancer cells. Finally, type III tumours, which are paracrine Shh dependent where Shh is produced by the tumour and is received by the surrounding stroma, which in turn sends different signals back to the tumour to promote its growth and survival[438]. Within these three models, it would be worthwhile to investigate whether CD133 plays a role in the tumourigenic potential of Shh signalling.

6. Future research

Several avenues can be pursued to investigate the precise mechanisms of CD133 in governing the SHH signalling pathway in the dental epithalial stem cell renewal and activation. First, does SHH interact direcly with CD133 and if so, how is this binding facilitated? So far, only one receptor (Patched1) for SHH has been discovered. I propose to first perform a ligand-binding assay to establish/exclude direct binding of both proteins. However, due to technical limitations, such as limited resolution with *in vivo* ligand-binding assays, it is only feasible with *in vitro* cell cultures. Of note, it is well-established that both proteins require binding of sterols to function properly and it is essential to keep in mind that perhaps the interaction is also facilitated by cholesterol. Commercial recombinant SHH ligand conjugated with sterols is currently unavailable. Therefore, I propose to use primary cells that are capable of expressing and secreting SHH such as the CLE cells used in this study. It might well be that CD133 acts as a co-receptor to Patched1 or facilitates the translocation of Smoothened to the primary cilium to affect the SHH signalling pathway. To investigate these possible interactions co-immunoprecipitation or proximity ligation assays could be performed.

Second, how does CD133 translocate to the nucleus? The recent discovery of the DFP motif, which is present in all CD133 isoforms, is a good candidate to investigate as it directs Importin α5-mediated translocation to the nucleus. Again, direct interaction between Importin α5 and CD133 could be investigated using co-immunoprecipitation or proximity ligation assay combined with selective deletion of the DFP motif in the N-terminal domain of CD133. However, care needs to be taken when deleting the DFP motif as the N-terminal domain also contains te plasma membrane localisation signal.

It is also possible that CD133 translocates to the nucleus as a component of the ciliary remnant, which directs the outcome of the daugther cells, I.e.: stem cell renewal versus activation. This will require high-resolution time-lapse imaging of single cells undergoing mitosis as performed by Paridaen *et al*.

In our study, common downstream signalling pathways shared between Glis2 KO and CD133 KO inner dental epithelial cells were revealed using commercially available PCR arrays and led us to focus eventually on STAT3, a protein recently shown independently to be important in dental epithelial stem cell renewal and activation. It would be beneficial to cover the whole transcriptome using micro array or RNAseq to uncover all shared downstream signalling pathways.

The mouse incisor tooth phenotype observed in CD133 KO mice is relatively mild as CD133 KO teeth are still fully functional without discomfort to the animal. Prom2, a second member of the Prominin family is co- expressed with CD133 in nearly all tissues except photoreceptor cells. Our study has shown that Prom2 is also expressed in the dental epithelium of P7 CD1 and C57/BL6 mice, albeit at low levels. It would be interesting to generate double CD133-Prom2 KO mice to investigate the severity of the mouse incisor tooth phenotype. It is possible that double KO mice are embryonically lethal and, therefore, postnatal conditional deletion of CD133/Prom2 might be necessary to be able to investigate the cervical loop and enamel phenotype.

7 Materials & Methods

7.1 Mice

ICR (CD-1®) Mice (CD1) were purchased from Charles River UK Ltd. and CD1 mouse colonies were maintained at the Plymouth University Animal Facility with food and water provided *ad libitum*. CD1 mouse pups were euthanized humanely at postnatal day 7 by cervical dislocation in accordance to Home Office regulation under the UK Animals Scientific Procedures Act 1986 (ASPA). The heads were immediately submerged in dry ice-cooled 2-methylbutane (M32631, Sigma-Aldrich) for 10 minutes. Frozen heads were then removed and stored at -80°C.

Plymouth University Animal Welfare and Ethical Review Board granted ethical approval for all experiments.

BMI1$^{GFP/GFP\ 417}$, *CD133* KO[236], *Glis*$^{LacZ/LacZ\ 164}$ mice and their littermate controls used in this study were generated and kindly donated by our collaborators Prof. Ophir Klein (University of California, San Francisco), Dr. Denis Corbeil (Biotec, Dresden) and Dr. Massimo Attanasio (University of Iowa, Iowa city), respectively.

7.2 Extraction and culture of Cervical Loop epithelial cells

Cell culture media compositions are presented in Appendix section 7.1 and 7.2

Cervical loop epithelial cells (CLE) were extracted from incisor explants from p7 CD1 and *CD133* KO mice. The cervical loops were dissected under a Leica M80 stereomicroscope. Explants were incubated in 1% Collagenase I (C0130-1G, Sigma-Aldrich) in Hank's balanced salt solution (HBSS; 14175-053, Gibco) with 1% penicillin-streptomycin (SV30079.01, Hyclone) and 1% Fungizone® Antimycotic (15290-018, Gibco) for 60 minutes. Collagenase was deactivated with Dulbecco modified Eagle’s medium/F-12 (DMEM; 31331-028, Gibco)

containing 10% fetal bovine serum (FBS; F7524, Sigma-Aldrich) and 1% penicillin-streptomycin (SV30079.01, Hyclone). The cell suspension was then centrifuged at 1000rcf for 5 min before supernatant was removed and pellet was re-suspended and plated in DMEM/F-12 (31331-028, Gibco) containing B27 supplement minus vitamin A (12587-010, Gibco), with recombinant mouse carrier-free Egf (20ng/ml) (2028-EG-200, R&D Systems) and recombinant mouse carrier-free Fgf basic (25ng/ml) (3139-FB-025/CF, R&D Systems).

7.3 Passaging of CLE cells

CLE cells were passaged when reaching approximately 80% confluency. After removal of growth medium, CLE cells were washed with HBSS to remove trypsin-inhibiting components typically present in cell culture media. TrypLE Select (12563029, Gibco) was then added to the washed cells to dislodge them from the cell culture vessel. During this step, cells were incubated at 37^{o}C and 5% CO_2. TrypLE Select was then neutralised with equal volume of DMEM supplemented with 10% FBS and the resulting cell suspension was collected and spun down at 1500 rpm for 5 minutes. The cell pellet was resuspended in complete growth medium and re-plated at the appropriate density in a suitable culture vessel and incubated under normal growth conditions.

7.4 Freezing and thawing of CLE cells for long term storage

Dislodged CLE cells were collected and spun down as described in Section 6.3. The resulting cell pellet was then resuspended in chilled 90% FBS + 10% dimethyl sulfoxide (DMSO) (D2650, Sigma-Aldrich) and 1ml added to chilled cryovials (374080, Nunc). Cells were then slowly frozen to -80ºC. The following day, frozen cells were transferred to liquid nitrogen tanks for long-term storage.

Thawing of CLE cells was done at 37ºC and immediately diluted 10x with DMEM + 10% FBS. Cells were then spun down and plated as described in Section 6.3.

7.5 Knockdown of CD133 in CLE using esiCD133

Upon reaching 50-60% confluency, CLE cells were transfected with esiRNA using INTERFERin® (409-10, Polyplus) according to the manufacturer's specifications. In short, 20nM of esiRNA and INTERFERin® was prepared in normal growth medium and left to incubate for 20 minutes to allow for transfection complex formation. During incubation, fresh medium was applied to the CLE cells to stimulate growth and to enhance transfection. The transfected CLE cells were then left to incubate at 37°C and 5% CO_2 for 48h.

7.6 Colony Forming Assay

CLE cells at the exponential growth phase were harvested with TrypLE Select (12563029, Invitrogen) and counted using a Countess II Automate Cell Counter (AMQAX1000, Invitrogen). Following this, cells were diluted and seeded at 5000 cells per well of a twelve-well plate. After 48h incubation, cells were transfected with esiCD133 or esiRLUC. After incubation for 24h, cells were cultured with or without SHH-N (464-SH-025, Bio-techne) at a concentration of 100ng/ml for 24h. Cells were washed with HBSS twice, fixed with 10% neutral-buffered formalin (HT501128, Sigma-Aldrich) for 30', and stained with 1% crystal violet solution (V5265, Sigma-Aldrich) for 1 hour at room temperature.

7.7 Vector construction and site-directed mutagenesis of lysine 138

Construction of the human CD133 expression plasmid was achieved by introducing the full-length coding sequence (CDS) of human CD133 splice variant s2 (Genbank Accession number AF027208.1) into the enhanced Yellow

Fluorescent Protein (eYFP)-N1 plasmid (632445, Clontech). NotI and XhoI restriction sites were exploited for directional cloning of the CDS and excision of eYFP. Mutation of lysine 138 was achieved using the QuikChange® II Site-Directed Mutagenesis Kit (200523, Stratagene) according to manufacturer's directions. The forward and reverse primers were 5'-CGTTGCTGTAAC**C**AATGTGGTGGAG-3' and 5-CTCCACCACATT**G**GTTACAGCAACG-3', respectively. The single nucleotide modification from adenine to cytosine (underlined) leads to the translation of a glutamine residue. WT and mutated CD133 CDS expression vectors were sequenced in order to exclude the presence of any reading mistakes introduced by the cloning steps and/or DNA polymerase. Sequencing was performed using the Applied Biosystems 3730 Genetic Analyzer at the MPI-CBG facility (Dresden, Germany).

7.7 Lentiviral production, shRNA Knockdown and Selection

Two short hairpin RNA (shRNA) plasmids targeting the mouse gene sequence of CD133 (See appendix section 7.8 for sequence) were provided in the pLKO.1 plasmid (SHCLND-NM_008935, Sigma-Aldrich).

The Ki67-FUCCI system pLenti-mCherry-hCdt-2k7bsd and pLenti-mAG-hGem-Neo were a kind gift from Dr. Alexander Zambon (Pharmacology University of California).

Lentiviral shCD133 and Ki67-FUCCI plasmids were produced in 293FT cell line by co-transfection of pLKO.1 containing the different shRNA constructs and the Ki67-FUCCI plasmids with the MISSION lentiviral packaging mix (SHP001, Sigma-Aldrich). The viral supernatant was collected after 48h and passed through a 0.45µm filter to remove cell debris.

CLE cells were incubated for 2 hours at 37°C with the viral supernatant containing 10µg/ml polybrene (TR-1003-G, Millipore). After 2 hours, the viral supernatant was replaced with normal growth medium. CLE cells infected with shCD133 plasmids were continuously selected using 10µg/ml puromycin (P8833, Sigma-Aldrich). CLE cells infected with the Ki67-FUCCI system were selected using 250µg/ml Geneticin (10131-035, Gibco) and blasticidine S hydrochloride (15205, Sigma-Aldrich).

7.8 Generation of Ki67p-Fucci lentiviral reporters, cell transfection and infection

Ki67p-Fucci lentiviral reporter plasmids were kindly donated by Dr. Alexander Zambon (Keck Graduate Institute, Claremont). Generation of the lentiviral reporters was achieved using open reading frames of the mCherryhCdt1(30/120)-pCSII-EF-MCS and mAG-hGeminin(1/110)-pCSII-EF-MCS plasmids which were kindly supplied by Dr. Astsushi Miyawaki and were subcloned into the pENTR-D-Topo vectors (K240020 Life Technologies). Subcloning using Gateway recombination of the 1.5kb Ki67 proximal promoter (Ki67p) upstream of mAG and mCherry FUCCI reporters was performed into 2k7 lentiviral vectors, allowing for neomycin and/or blasticidine selection for cells expressing Ki67p-mAG-hGem(1-110) and Ki67p-mCherry-hCdt1(30-120), respectively[440,441].

The resulting Ki67p-Fucci vectors were transfected into the HEK293FT (R70007, Life Technologies) cell line together with pCMV-VSV-G (Envelope plasmid) and pCMV delta R8.2 (Packaging plasmid), producing lentiviral particles for cell infection. Viral supernatants were collected after 48h and 72 hours yielding two batches.

CLE cells were incubated with both viral supernatants containing the Ki67p-mAG-hGem (1-110) and Ki67p-mCherry-hCdt1(30-120) plasmids and 10µg/ml polybrene (TR-1003-G, EMD Millipore) for 2 hours under normal culture conditions. After 2 hours, the viral supernatant was removed, and cells were washed with HBSS prior to adding normal growth medium. After 24h, infected CLE cells (CLE-Ki67-FUCCI) were continuously selected using 10µg/ml blasticidine (15205, Sigma-Aldrich) and 250µg/ml G418 (11811023, Gibco).

7.9 Flow cytometry

For flow cytometry, CLE-Ki67-FUCCI were either transfected with the empty pRc/CMV vector or mouse pRc/CMV-CD133[167] and then harvested after 72 hours or cultured in the absence or presence of 100ng/ml carrier-free Shh for 24h (461-SH-025/CF, Bio-Techne). Treated CLE cells were then fixed in 4% paraformaldehyde (PFA) for 30min at room temperature followed by washing with Phosphate-buffered Saline (PBS; P4417, Sigma-Aldrich) for three times. Analysis was done using the BD FACSCanto™ II SOR (Beckman Coulter) and data was acquired using the blue laser (488 nm) for mAzamiGreen signal and theyellow-green laser (561 nm) for mCherry. Results were analysed using the FlowJo® software v10.3 (Tree Star Inc.).

7.10 Laser Capture Microdissection for RNA extraction

Frozen heads were cryosectioned at 10µm thickness on a Leica CM1850 cryostat. Sections were mounted onto PEN Membrane Glass Slides (LCM0522, Applied Biosystems) and immediately stained using 1% Methyl Green (67060, Fluka Analytical) in 0.1% diethylpyrocarbonate (D5758, Sigma-Aldrich) distilled water, then washed four times for 30 seconds in 0.1% diethylpyrocarbonate (D5758, Sigma-Aldrich) distilled water and then allowed to dry for 5 minutes. Laser

Capture Microdissection (LCM) was achieved using CapSure® Macro LCM Caps (LCM0211, Applied Biosystems) on an ArcturusXT™ LCM instrument within 30 minutes of sectioning. Samples were lysed in Tri-Reagent (T9424-100ML, Sigma-Aldrich) and stored at -80ºC until further processing.

7.11 RNA extraction & cDNA production

RNA was extracted and purified using the acid guanidinium thiocyanate-phenol-chloroform extraction protocol. The total RNA was extracted using Tri-Reagent. The samples were vortexed and incubated for 5 minutes at room temperature before addition of Chloroform (C2432, Sigma-Aldrich) at a ratio of 5:1 (lysate: chloroform). The samples were then incubated for a further 5 minutes before centrifugation for 15 minutes at 13000rpm. The aqueous phase was then collected and added 1:1 with 2-propanol (34965, Fluka Analytical) supplemented with 1µl GlycoBlue (AM9515, Ambion). The sample was incubated at -20°C overnight before centrifugation at 13000rpm for 15 minutes at 4°C. The subsequent pellet was then washed in 1ml 70% Ethanol (20821.321, VWR Chemicals) and centrifuged for 10 minutes at room temperature at 9000rpm. The resulting pellet was resuspended in 10µl of 0.1% diethylpyrocarbonate-treated (DEPC; D5758, Sigma-Aldrich) distilled water.

Purified RNA was quantified on a NanoDrop™ 2000 UV-Vis Spectrophotometer (Thermo Scientific). Quality control was assessed by analysis of the 260/280 and 260/230 ratios and corresponding graphs, which is an indicator for the presence of contaminants.

Reverse transcription was performed using High-Capacity cDNA Reverse Transcription Kit (4368814, Applied Biosystems) in accordance with the manufacturers protocol on a Veriti™ Thermal Cycler 96 well (Applied Biosystems).

1µg of total RNA was reverse transcribed using the Multiscribe™ Reverse Transcriptase polymerase and random hexamer primers. See appendix section 7.10.2 for programme details. Samples were then diluted in 180µl of DEPC-treated water and stored at -20°C.

7.12 Real-Time qPCR

Real Time qPCR was performed in triplicate. Samples were combined with LightCycler® 480 SYBR Green I master kit (4887352001, Roche Life Science) (diluted 1:1 with the water provided in accordance with the manufacturer's instructions) and appropriate primers in a ratio of 1:8:1 totalling 10µl. This equates to a final primer concentration of 1µM. The samples were analysed with each primer in triplicate as a technical control. Primers were designed against the CDS sequence for each gene, provided by NCBI gene (http://www.ncbi.nlm.nih.gov/gene/) using Primer 3 website (http://biotools.umassmed.edu/bioapps/primer3_www.cgi) and validated on UCSC In-SilicoPCR (http://genome.ucsc.edu/cgi-bin/hgPcr?command=start). Primers were designed to give an amplicon length that reduces the risk of dimers and hairpins. If possible, the primers were also designed to cross an exon to negate the problems of genomic DNA contaminants being amplified. To reduce the risk of RNA degradation leading to non-binding of primers, primers were designed to bind towards the centre of the cDNA. Primers (listed in appendix section 7.9) were all validated against cDNA extracted from mouse embryonic fibroblasts, to ensure that they can detect cDNA and that the amplicons produced are of the anticipated length. The instrument used was a Roche Lightcycler® 480 Instrument II 384-well block real-time PCR machine, used according to the manufacturer's instructions. Programme details are explained in appendix section 7.10.1. Results were analysed using Comparative Ct methods. PCR

amplification was checked to ensure appropriate amplification curves and annealing temperature was obtained. Results were exported into Prism (version 5.04).

7.13 Immunofluorescence

Frozen heads were cryosectioned at 20µm thickness for immunofluorescence application on a Leica CM1850 UV cryostat (Leica, Germany). Sections were mounted onto Polysine™ Microscope Adhesion Slides (J2800AMNZ, Thermo Scientific) and allowed to air dry for 30 minutes. Fixation of cryosections and CLE cells was dependant on the protein of interest being analysed. Typically, fixation was performed for 30 minutes and then washed three times in washing buffer (PBS or PBS with 0.1% Triton-X100, Sigma-Aldrich) for 5 minutes per wash. To prevent non-specific binding of antibodies, fixed and washed cryosections or CLE cells were blocked using 5% donkey serum (D9663, Sigma-Aldrich), 0.25% cold water fish gelatine (G7765, Sigma-Aldrich) and 0.25% Albumin from Bovine Serum (BSA; A2153, Sigma-Aldrich) in washing buffer for 12 hours at room temperature. Primary antibodies were diluted in blocking buffer and incubated overnight at 4ºC (See appendix section 7.6 and 7.7 for experimental details regarding each antibody). The following day, samples were washed three times in washing buffer at room temperature. Incubation with secondary antibodies, diluted in blocking buffer, was done for 2 hours at room temperature obscured from light. Samples were then washed three times for 5 minutes at room temperature. Nuclei were counterstained with 2µg/ml 4',6-diamidino-2-phenylindole (DAPI; D9542, Sigma-Aldrich) for 10 minutes. Finally, cryosections were mounted and sealed using DAKO mounting medium (S3023, Dako) and slides were stored at 4ºC for minimum 2 hours before imaging to allow the mounting medium to polymerise.

7.14 Confocal imaging

Immunofluorescence images were captured using a Leica DMI6000 confocal microscope with a Leica TCS SP8 attachment at a resolution of 2048x2048. The microscope runs on LAS AF software from Leica. Post-imaging processing was conducted using Adobe Photoshop CC.

7.15 Three-dimensional reconstruction of primary cilia

Fluorescence z-stack images were acquired using the Leica DMI6000 confocal microscope with a Leica TCS SP8 attachment with a Z-step size of 1µm. Imaris 8.3 (Bitplane) was used to generate a 3D reconstruction of primary cilia from the acquired images using acetylated Tubulin as a primary cilium marker. Measurements of primary cilium dimensions were performed manually using the Imaris Measurement Pro tool in Imaris 8.3. When required, 3D-reconstructed primary cilium images were rotated to render a cross-section appropriate for quantification.

7.16 Three-dimensional reconstruction of the cervical loop

Volume analysis of the P7 mouse incisor tooth cervical loop was achieved by outlining the structure based on the basement membrane from approximately 20 consecutive 20µm thick coronal sections of the apical side of the mouse incisor tooth (n = 3 animals per genotype). Rendering of the Sox2-positive region within the cervical loop was done using BioVis 3D software (version: 3.1.1.11; BioVis3D) and allowed us to calculate the volume.

7.17 Total protein extraction

Total protein content was collected as follows. CLE cells were washed with ice-cold HBSS to remove cell debris. Cells were then collected using a cell scraper in 1ml HBSS. Collected cells were then spun down at 10,000rpm for 10 minutes

at4ºC. Supernatant was removed and the remaining cell pellet was resuspended in ice-cold Radioimmunoprecipitation assay (89901, Pierce) buffer supplemented with Protease & Phosphatase Inhibitor Cocktail (78442, Pierce). The cell suspension was then incubated for 30 minutes on ice with periodical vortexing and the lysate was then spun down at 10,000rpm for 10 minutes at 4ºC to pellet the cell debris. The supernatant was then transferred to a new, chilled tube and stored at -20ºC until protein quantification.

7.18 Cytoplasmic and nuclear protein extraction

Approximately $10x10^6$ CLE cells were washed once with ice-cold HBSS and then collected. Cells were spun down at 10000rpm for 10 min. Supernatant was removed and pellet was used to extract nuclear and cytoplasmic protein fraction according to NE-PER™ Nuclear and Cytoplasmic Protein Extraction (78833, Pierce). In brief, the pellet was resuspended in lysis buffer 1 (CER I) and vortexed to obtain a homogenous mixture. The lysate was then incubated on ice for 10 minutes before addition of lysis buffer 2 (Cer II) at a ratio of 200:11 (Cer I: Cer II) for 1 minute on ice. Intact nuclei were then pelleted at 16,000rcf for 5 minutes. The cytoplasmic protein-containing supernatant was then transferred into a new tube and stored at -80ºC until protein quantification. The insoluble, intact nuclei fraction was then subjected to a third lysis step (Ner) to release the nuclear proteins into solution before nuclear debris was pelleted at 16,000rcf for 5 minutes. The nuclear protein-containing supernatant was then transferred to a chilled tube and stored at -80ºC until further processing.

7.19 Protein quantification

Total, nuclear and cytoplasmic protein fractions were quantified using BCA Protein Assay (23225, Pierce). A standard curve was generated from a set of

nine protein standards, which were prepared as follows. Protein standards were made from an BSA Standard (2mg/ml) and serially diluted in PBS to give the following protein concentrations: 0 (100% PBS); 25; 125; 250; 500; 750; 1000; 1500; 2000µg/ml. 25µl of each standard was used to determine the standard curve of the assay. At the same time, 2,5µl of each protein sample was added to 22,5µl of PBS to minimise the usage of sample as well as to mimic the protein standard diluent as close as possible. The BCA Working Reagent was then prepared as described in the manufacturer's protocol, added to the samples and standards and allowed to incubate for 25 minutes at 37°C. Following incubation, the absorbance of each well was measured at 562nm using a FLUOstar® Omega platereader (Firmware version: 1.43) and the Omega software (Software version: 5.11). The absorbance readouts of the standards were used to plot the linear regression line and its associated equation. The equation was then used to calculate the protein concentration of each sample.

7.20 Western blotting

Western blotting of total, nuclear and cytoplasmic lysates were processed as follows. All samples used were normalised based on their concentration obtained according to section 6.19. Normalised samples were then supplemented with 4x NuPAGE® Lithium Dodecyl Sulphate (LDS) Sample Buffer (NP0007, Invitrogen) and 10x NuPAGE® Reducing Agent (NP0004, Invitrogen) to linearize and reduce the net charge of individual proteins within the samples. Finally, distilled water was added up to 20 or 25µl depending on the well size of the running gel. Samples were then incubated at 37°C for 30 minutes when blotting for CD133 or at 95°C for 5 minutes for all other epitopes. Samples were then cooled on ice and spun down to collect all sample components. In the meantime, NuPAGE® MOPS running buffer (NP0001, Invitrogen) was prepared according to manufacturer's

instructions. 4-12% NuPAGE® Novex™ Bis-Tris gels were used in all Western Blotting experiments. XCell SureLock® Mini-Cell (EI0001, Invitrogen) was assembled with a 4-12% NuPAGE® Novex™ Bis-Tris gel and dummy cassette to create a closed circuit consisting of an inner and outer chamber. 200ml and 600ml of NuPAGE® MOPS running buffer was added to the inner and outer chamber, respectively. Samples and protein ladders were then added into the wells and protein separation was initiated at 200V for ~50 minutes. PageRuler™ Prestained Protein Ladder (SM0671, Fermentas) was used to assess protein migration and transfer during the experiment. Novex™ MagicMark™ XP (LC5602, Invitrogen) protein ladder was used to assess to assess protein size after development. During the running step, NuPAGE® Transfer Buffer (NP0006, Invitrogen) was prepared as per manufacturer's recommendations and supplemented with 100% methanol (322415, Sigma-Aldrich) up to 10% of the total transfer buffer volume.

When protein separation was completed, the gel was removed from its casing and the blot module was assembled in the following order from top to bottom in the cathode core: two blotting pads, filter paper, gel, methanol-activated Polyvinylidene fluoride (PVDF) membrane (0,45µm; LC2005, Invitrogen), filter paper, two blotting pads. After assembly, the blot module was then filled with transfer buffer and inserted into the XCell SureLock® Mini-Cell. The protein content was then transferred onto the PVDF membrane at 36V for approximately 1 hour 45 minutes until the high kDa bands of the PageRuler™ ladder are transferred on to the membrane. Following transfer, the membrane was washed in distilled water to remove methanol residue.

Detection of proteins was performed using the iBind™ Flex Western Device (SLF2000S, Invitrogen) and the iBind™ Flex Solution (SLF2020, Invitrogen) was used as a blocking buffer, washing buffer and antibody diluent throughout the process. During the assembly of the iBind™ Flex Western Device, the membrane is blocked in the iBind™ Flex Solution for 5 minutes at room temperature. Antibody solutions are prepared in the iBind™ Flex Solution and concentrations are listed in appendix section 7.6 and 7.7. Following the blocking step, the membrane is laid protein side down on to the iBind™ card. The mechanical force exerted by the lid allows for lateral sequential flow of the antibody and wash solutions over the protein side of the membrane. After the run, the membrane is washed three times in distilled water to remove non-bound antibodies.

Detection of Horseradish Peroxidase-conjugated (HRP) secondary antibodies was achieved with incubation of WesternSure™ PREMIUM ECL substrate (926-95000, Li-Cor) for 5 minutes at room temperature. The membrane was then digitally imaged ON the C-DiGit® Chemiluminescent Western Blot Scanner (3600-00, Li-Cor) using the Image Studio™ software (version: 3.1; Li-Cor).

7.21 Duolink® Proximity Ligation Assay

In situ protein interactions were detected by the proximity ligation assay kit Duolink® II (DUO92101, Sigma-Aldrich). The Duolink® proximity ligation assay (DPLA) probe anti-rabbit minus binds to the CD133 antibody, whereas the PLA probe anti-rabbit plus binds to the GLIS2 antibody. The DPLA secondary antibodies only generate a signal when the two DPLA probes have bound, which only takes place if both proteins are closer than 40nm, indicating their interaction[442].

Frozen CD1 mouse heads were prepared as described in section 6.7. After blocking, conjugated CD133 and GLIS2 antibody were added to the slides at a concentration of 1:100 in antibody diluent. Incubation was done overnight in a humidity chamber at 4°C. Slides were washed two times in Wash Buffer A for 5 min to remove unbound conjugated antibodies. The samples were incubated with the Ligation Solution consisting of Duolink® II Ligation stock (1:5) and Duolink® Ligase (1:40) diluted in high purity water for 30 min at 37 °C. After ligation the Duolink® Amplification and Detection stock, diluted 1:5 with addition of polymerase (1:80), was applied to the slides for 100 min. DAPI was used as described in section 6.13 to identify the nuclei. After the final washing steps using Wash Buffer A and B the slides were dried and cover slips were mounted using Fluorescence Mounting medium (S3023, DAKO).

7.22 Co-Immunoprecipitation

Co-Immunoprecipitatation (CoIP) was achieved using the µMACS™ isolation procedure (Miltenyi Biotec). 16 hours prior to protein extraction, Madin-Darby Canine Kidney (MDCK) cells were supplemented with 10 mM sodium butyrate. Cells were then lysed for 30 minutes on ice in lysis buffer containing (0.2% Triton X-100, 150mM NaCl, 20mM Tris/HCl, pH 7.5) containing Complete™ protease inhibitor cocktail (04 693 159 001, Roche Diagnostics), 2mM sodium orthovanadate (P0758, New England Biolabs), 10mM sodium fluoride (P0759, New England Biolabs) and 10mM β-glycerophosphate (G9422 Sigma-Aldrich). Cell debris was pelleted by centrifugation for 10 minutes at 16,000rcf at 4°C and the supernatant was collected in a chilled tube and pre-cleared by incubation with magnetic Basic MicroBeads (130-048-001, Miltenyi Biotec) for 30 minutes. The lysate was then passed through a MS column (130-042-201, Miltenyi Biotec) to remove proteins that non-specifically bind to magnetic beads. Pre-cleared lysates

were incubated with either 65µl anti-CD133–magnetic MicroBeads (130-097-049, Miltenyi Biotec) or 130µl anti-FITC–magnetic MicroBeads (130-048-701, Miltenyi Biotec) as negative control for 1,5 hours at 4°C before proceeding to magnetic separation using MS columns. For Arl13b CoIP, pre-cleared lysates were incubated first with 3.5µl of anti-Arl13b polyclonal antibody at 4°C for 30 minutes. Followed by incubation with 100µl µMACS Protein A MicroBeads for 1 hour at 4°C. Retained magnetic beads were washed 6 times with 1ml of ice-cold PBS containing 2mM EDTA and 0.1% Triton X-100. Followed by elution with pre-heated (95°C) Laemmli sample buffer. Flow-through samples were collected and subjected to methanol/chloroform precipitation and re-suspended in Laemmli sample buffer.

7.23 Chromatin Immunoprecipitation

Chromatin Immunoprecipitation (ChIP) assays were performed using Chip-IT® Express (53008, Active Motif) according to the manufacturer's instructions. Pre-treated cells were fixed with 40µl of 37% (wt/vol) formaldehyde (Sigma-Aldrich) per 1ml of overlaying medium for 10 minutes at room temperature, followed by 5 minutes of glycine stop-fix solution. Cells were washed twice with ice-cold PBS, PBS was poured off and discarded and cells were scraped, pelleted by centrifugation for 10 minutes at 2000rcf at 4°C. Cells were resuspended in 400µl of ice-cold ChIP-It® lysis buffer followed by 30 minutes incubation on ice. Nuclei release was further enhanced using an ice-cold dounce homogeniser and visually checked using a phase-contrast microscope. Pellets were spun down for 10 minutes at 2400rcf, resuspended in 350µl of Shearing Buffer and transferred to 1.5ml Bioruptor® microtubes (C30010016, Diagenode). Chromatin was sheared using Bioruptor® pico (B01060001, Diagenode) with the following optimised settings to generate DNA fragments of approximately 500 bp: 15'' ON/ 30'' OFF;

10 cycles. Sheared chromatin was cleared by centrifugation at 18000 rcf for 10 minutes at 4°C. For each ChIP, 60µl of the total sonicated chromatin was used. Immunoprecipitations were performed overnight at 4°C with 2µl of the Glis2 antibody (kindly gifted by Dr. Massimo Attanasio). Chromatin–antibody complexes were captured using Protein G magnetic beads (101945, Active Motif) and chromatin was eluted as described in manufacturer's instructions. The cross-links were reversed, and DNA purified by proteinase K. DNA was analysed by real-time qPCR (See appendix section 7.10.1 for programme details).

7.24 Scanning Electron Microscopy

Four-week-old C57BL/6 WT and *CD133* KO mice were killed and their lower jaws dissected and fixed in ethanol at increasing concentrations: 50%, 70%, 90%, 95% for 5 minutes each and then then three times 100% for 30 minutes. After fixation for 24 hours, a segment of the erupted part of the incisors was cut off with a watercooled diamond wheel, air-dried and glued to brass cylinders with cyanoacrylate glue[443]. The incisor segments were sputter-coated with a 50nm layer of gold-palladium in order to protect the enamel surface from the subsequent acid etching. All segments were ground transversely (at the incisal end), some also longitudinally, tangentially, or oblique transversely (at the apical end), using 3M waterproof silicon carbide paper and a specially designed apparatus[444] operated under a stereomicroscope. After grinding, the specimens were cleaned by light brushing under running tap water and etched for three times 10 seconds in 0.1 % nitric acid. The specimens were air-dried, sputter-coated with 30nm gold-palladium and observed in a Philips XL20 operated at 15kV, using a specially designed holder allowing multiangular viewing of the specimens[445].

7.25 X-Ray microscopy-based microCT analysis

Mouseheads were scanned at the Small Animal Imaging Core of the University of Iowa using the Zeiss Xradia 520 Versa (Pleasanton, CA). The 3D X-ray source acquisition settings were 10W, 120kV, and 0.4x magnification. Source distance from the mouse heads was 27mm, and the detector distance was 170mm. A total of 1,601 projections with a 1s exposure time over 360 degrees of rotation were acquired using the Reconstructor Scout-and-Scan software (Zeiss, Pleasanton, CA), projections were reconstructed with downsampling of 1, with beam hardening correction to yield a pixelsiye of 25μm. The generated DCOM files were reconstructed into 3D images and analzsed in Imaris software programme. (9.0, Bitplane).

7.26 Statistics

Statistical analyses were performed using GraphPad Prism® version 5.00. For box-whisker plots, the boxes represent data between 25th-75th percentiles and all data is contained within the whiskers. Median values are represented by the horizontal lines within the box. Unpaired t-test with Welch's correction was applied to all measurements involving primary cilium dimensions, except for primary cilium length measurements in the stem cell and transit-amplifying regions of WT and mutant mice where one-way ANOVA was applied. Unpaired t-test was applied to cervical loop volume measurements. All quantification and real time RT-PCR results were presented using style of Mean and Standard Deviation (error bars). Observed differences were regarded as significant if the calculated p-values were $\leqslant 0.05$. *, $p < 0.05$; **, $p < 0.01$; ***, $p < 0.001$.

8 Appendices

8.1 B27 Serum-free Medium Composition

Component	Concentration (per L)[446]
Vitamins	
Biotin	125mg
DL Alpha Tocopherol Acetate	50mg
DL Alpha Tocopherol	50mg
Proteins	
BSA, fatty acid-free fraction V	125g
Catalase	125mg
Human Recombinant Insulin	156.25mg
Human Holo-Transferin	250mg
Superoxide Dismutase	375.000 U
Other Components	
Corticosterone	1mg
D-Galactose	750mg
Ethanolamine HCl	50µg
Glutathione (reduced)	50mg
Linoleic Acid	50mg
Linolenic Acid	50mg
Progesterone	315µg
Putrescine 2HCl	805mg
Sodium Selenite	625µg
T3 (triodo-l-thyronine)	100µg
L-Carnithine HCl	100mg

8.2 DMEM/F12 Medium Composition

Components	Concentration (mg/L)[447,448]
Amino Acids	
Glycine	18.75
L-Alanine	4.45
L-Alanyl-L-Glutamine	542
L-Arginine hydrochloride	147.5
L-Asparagine-H2O	7.5
L-Aspartic acid	6.65
L-Cysteine hydrochloride-H2O	17.56
L-Cystine 2HCl	31.29
L-Glutamic Acid	7.35
L-Histidine hydrochloride-H2O	31.48
L-Isoleucine	54.47
L-Leucine	59.05
L-Lysine hydrochloride	91.25
L-Methionine	17.24
L-Phenylalanine	35.48
L-Proline	17.25
L-Serine	26.25
L-Threonine	53.45
L-Tryptophan	9.02
L-Tyrosine disodium salt dihydrate	55.79
L-Valine	52.85
Vitamins	
Biotin	0.0035
Choline chloride	8.98
D-Calcium pantothenate	2.24
Folic Acid	2.65
Niacinamide	2.02
Pyridoxine hydrochloride	2
Riboflavin	0.219
Thiamine hydrochloride	2.17
Vitamin B12	0.68
i-Inositol	12.6
Inorganic Salts	
Calcium Chloride	116.6
Cupric sulfate	0.0013
Ferric Nitrate	0.05
Ferric sulfate	0.417
Magnesium Chloride	61
Magnesium Sulfate	100
Potassium Chloride	311.8
Sodium Bicarbonate	2438
Sodium Chloride	6995.5

Components (continued)	Concentration (mg/L)
Sodium Phosphate dibasic	134
Sodium Phosphate monobasic	62.5
Zinc sulfate	0.432
Other Components	
D-Glucose (Dextrose)	3151
Hypoxanthine Na	2.39
Linoleic Acid	0.042
Lipoic Acid	0.105
Phenol Red	8.1
Putrescine 2HCl	0.081
Sodium Pyruvate	55
Thymidine	0.365

8.3 Gene list RT^2 Pathway finder

GeneBank	Symbol	Description	Pathway
NM_009741	Bcl2	B-cell leukemia/lymphoma 2	Hedgehog Signaling
NM_007553	Bmp2	Bone morphogenetic protein 2	Hedgehog Signaling
NM_007554	Bmp4	Bone morphogenetic protein 4	Hedgehog Signaling
NM_008957	Ptch1	Patched homolog 1	Hedgehog Signaling
NM_021279	Wnt1	Wingless-related MMTV integration site 1	Hedgehog Signaling
NM_009520	Wnt2b	Wingless related MMTV integration site 2b	Hedgehog Signaling
NM_009522	Wnt3a	Wingless-related MMTV integration site 3A	Hedgehog Signaling
NM_009524	Wnt5a	Wingless-related MMTV integration site 5A	Hedgehog Signaling
NM_009526	Wnt6	Wingless-related MMTV integration site 6	Hedgehog Signaling
NM_009627	Adm	Adrenomedullin	Hypoxia Signaling
NM_009709	Arnt	Aryl hydrocarbon receptor nuclear translocator	Hypoxia Signaling
NM_139305	Car9	Carbonic anhydrase 9	Hypoxia Signaling
NM_007942	Epo	Erythropoietin	Hypoxia Signaling
NM_010699	Ldha	Lactate dehydrogenase A	Hypoxia Signaling
NM_008871	Serpine1	Serine (or cysteine) peptidase inhibitor, clade E, member 1	Hypoxia Signaling
NM_011400	Slc2a1	Solute carrier family 2 (facilitated glucose transporter), member 1	Hypoxia Signaling
NM_009505	Vegfa	Vascular endothelial growth factor A	Hypoxia Signaling
NM_008390	Irf1	Interferon regulatory factor 1	JAK1 & JAK2/STAT1-Induced
NM_013517	Fcer2a	Fc receptor, IgE, low affinity II, alpha polypeptide	JAK1 & JAK3/STAT6-Induced
NM_008091	Gata3	GATA binding protein 3	JAK1 & JAK3/STAT6-Induced
NM_009742	Bcl2a1a	B-cell leukemia/lymphoma 2 related protein A1a	NFκB Signaling
NM_007464	Birc3	Baculoviral IAP repeat-containing 3	NFκB Signaling
NM_013653	Ccl5	Chemokine (C-C motif) ligand 5	NFκB Signaling
NM_007778	Csf1	Colony stimulating factor 1 (macrophage)	NFκB Signaling
NM_010493	Icam1	Intercellular adhesion molecule 1	NFκB Signaling
NM_008337	Ifng	Interferon gamma	NFκB Signaling
NM_009283	Stat1	Signal transducer and activator of transcription 1	NFκB Signaling
NM_013693	Tnf	Tumor necrosis factor	NFκB Signaling
NM_009743	Bcl2l1	Bcl2-like 1	NFκB Signaling, STAT3/STAT5-Induced
NM_008235	Hes1	Hairy and enhancer of split 1 (Drosophila)	Notch Signaling
NM_010419	Hes5	Hairy and enhancer of split 5 (Drosophila)	Notch Signaling
NM_010423	Hey1	Hairy/enhancer-of-split related with YRPW motif 1	Notch Signaling
NM_013904	Hey2	Hairy/enhancer-of-split related with YRPW motif 2	Notch Signaling

GeneBank	Symbol	Description	Pathway
NM_013905	Heyl	Hairy/enhancer-of-split related with YRPW motif-like	Notch Signaling
NM_010495	Id1	Inhibitor of DNA binding 1	Notch Signaling
NM_013822	Jag1	Jagged 1	Notch Signaling
NM_008494	Lfng	LFNG O-fucosylpeptide 3-beta-N-acetylglucosaminyltransferase	Notch Signaling
NM_008714	Notch1	Notch gene homolog 1 (Drosophila)	Notch Signaling
NM_010239	Fth1	Ferritin heavy chain 1	Oxidative Stress
NM_010295	Gclc	Glutamate-cysteine ligase, catalytic subunit	Oxidative Stress
NM_008129	Gclm	Glutamate-cysteine ligase, modifier subunit	Oxidative Stress
NM_010344	Gsr	Glutathione reductase	Oxidative Stress
NM_008706	Nqo1	NAD(P)H dehydrogenase, quinone 1	Oxidative Stress
NM_011018	Sqstm1	Sequestosome 1	Oxidative Stress
NM_011660	Txn1	Thioredoxin 1	Oxidative Stress
NM_015762	Txnrd1	Thioredoxin reductase 1	Oxidative Stress
NM_010442	Hmox1	Heme oxygenase (decycling) 1	Oxidative Stress, Hypoxia Signaling
NM_007527	Bax	Bcl2-associated X protein	p53 Signaling
NM_133234	Bbc3	BCL2 binding component 3	p53 Signaling
NM_007570	Btg2	B-cell translocation gene 2, anti-proliferative	p53 Signaling
NM_007669	Cdkn1a	Cyclin-dependent kinase inhibitor 1A (P21)	p53 Signaling
NM_007912	Egfr	Epidermal growth factor receptor	p53 Signaling
NM_007987	Fas	Fas (TNF receptor superfamily member 6)	p53 Signaling
NM_007836	Gadd45a	Growth arrest and DNA-damage-inducible 45 alpha	p53 Signaling
NM_011045	Pcna	Proliferating cell nuclear antigen	p53 Signaling
NM_009029	Rb1	Retinoblastoma 1	p53 Signaling
NM_001033606	Acsl3	Acyl-CoA synthetase long-chain family member 3	PPAR Signaling
NM_019477	Acsl4	Acyl-CoA synthetase long-chain family member 4	PPAR Signaling
NM_027976	Acsl5	Acyl-CoA synthetase long-chain family member 5	PPAR Signaling
NM_009949	Cpt2	Carnitine palmitoyltransferase 2	PPAR Signaling
NM_017399	Fabp1	Fatty acid binding protein 1, liver	PPAR Signaling
NM_138648	Olr1	Oxidized low density lipoprotein (lectin-like) receptor 1	PPAR Signaling
NM_011989	Slc27a4	Solute carrier family 27 (fatty acid transporter), member 4	PPAR Signaling
NM_009166	Sorbs1	Sorbin and SH3 domain containing 1	PPAR Signaling
NM_007707	Socs3	Suppressor of cytokine signaling 3	STAT3/STAT5-Induced
NM_007679	Cebpd	CCAAT/enhancer binding protein (C/EBP), delta	STAT3-Induced
NM_029796	Lrg1	Leucine-rich alpha-2-glycoprotein 1	STAT3-Induced
NM_008562	Mcl1	Myeloid cell leukemia sequence 1	STAT3-Induced
NM_009716	Atf4	Activating transcription factor 4	TGFβ Signaling
NM_009875	Cdkn1b	Cyclin-dependent kinase inhibitor 1B	TGFβ Signaling

GeneBank	Symbol	Description	Pathway
NM_010128	Emp1	Epithelial membrane protein 1	TGFβ Signaling
NM_008655	Gadd45b	Growth arrest and DNA-damage-inducible 45 beta	TGFβ Signaling
NM_022331	Herpud1	Homocysteine-inducible, endoplasmic reticulum stress-inducible, ubiquitin-like domain member 1	TGFβ Signaling
NM_013562	Ifrd1	Interferon-related developmental regulator 1	TGFβ Signaling
NM_009425	Tnfsf10	Tumor necrosis factor (ligand) superfamily, member 10	TGFβ Signaling
NM_015732	Axin2	Axin2	WNT Signaling
NM_009829	Ccnd2	Cyclin D2	WNT Signaling
NM_023118	Dab2	Disabled homolog 2 (Drosophila)	WNT Signaling
NM_010235	Fosl1	Fos-like antigen 1	WNT Signaling
NM_010810	Mmp7	Matrix metallopeptidase 7	WNT Signaling
NM_011145	Ppard	Peroxisome proliferator activator receptor delta	WNT Signaling
NM_018865	Wisp1	WNT1 inducible signaling pathway protein 1	WNT Signaling
NM_007631	Ccnd1	Cyclin D1	WNT Signaling, STAT3/STAT5-Induced
NM_010849	Myc	Myelocytomatosis oncogene	WNT Signaling, TGFβ Signaling

8.4 Primary antibodies used in this study

Target	Immunofluorescence (Diluting	Western Blotting	Company	Cat. No.	Lot	Representative publications (showing PMID only)	Validation in this study
Acetylated Tubulin	1/5000	1/2000	Sigma-Aldrich	T7451		20972424, 21307093	
Acetylated Tubulin	1/200		Cell Signaling	5335S	Lot4 ref03/2015	26931735, 27002170	
Active Caspase 3	1/200		Cell Signaling	9661	43	28443644, 28289704	
Ameloblastin	1/200		Santa Cruz	sc-33100		27146703	
Amelogenin	1/200		Santa Cruz	sc-32892		21514442	
ARL13b	1/250	1/400	Proteintech	17711-1-AP	00043031	23150559, 27153923	
beta-Actin		1/1000	Cell Signaling	8457	Lot1 ref04/2014	28569748, 27951586	
BMI1	1/100		Santa Cruz	SC-10745	E0316	26788137, 15171791	
CD133 (C-terminal)	1/1000	1/500	Biorbyt	Orb129549	I8429		Figure 16
CD133 (13A4; Extracellular Loop)	1/50		eBioscience	14-1331-82	e04033-1631	9356465, 15908947, 15316084	
ECadherin	1/200		Bio-Techne	BAF748	CXW0315091	24317254, 15994295	
GapDH		1/1000	Santa Cruz	SC-32233	K1216	29042957, 28855737	
GLIS2	1/200		Dr Massimo Attanasio	N/A		16326862, 17289029	
HDAC6 (BH*)	1/200		Dr Tso-Pang Yao	N/A		12024216, 17938201	
Ki67	1/200		Abcam	ab15580	GR1349163-4	28492284, 28281529	
LaminA/C	1/200	1/500	Cell Signaling	4777S	lot1 ref02/2014	24525530, 23319590	
LaminB1	1/200	1/500	Abcam	ab16048	GR302354-1	27391408, 26304990	
Sox2	1/200		R&D Biosystems	AF2018		28226240, 28566702	
STAT3	1/500		Cell Signaling	12640	lot4 ref10/2016	28301550, 26194464	

8.5 Secondary antibodies used in this study

Target	Immunofluorescence (Dilution factor)	Western blotting (Dilution factor)	Company	Cat. No.	Lot
anti-mouse HRP		1/2000	Cell Signaling	7076P2	
anti-rabbit HRP		1/2000	Cell Signaling	7074P3	
anti-rabbit Alexa Fluor 405	1/250		Life Technologies	A31556	1661251
anti-rabbit Alexa Fluor 568	1/500		Life Technologies	A10042	1826664
anti-rat Alexa Fluor 488	1/300		Life Technologies	A21208	1789917
anti-mouse Alexa Fluor 488	1/300		Life Technologies	A21202	
anti-goat Alexa Fluor 488	1/300		Life Technologies	A11055	1182671
anti-mouse Alexa Fluor 488 IgG1	1/500		Life Technologies	A21121	
anti-mouse Alexa Fluor 546 IgG1	1/500		Life Technologies	A21123	
anti mouse Alexa Fluor 488 IgG2b	1/600		Life Technologies	A21141	
anti mouse Alexa Fluor 546 IgG2b	1/600		Life Technologies	A21143	
anti mouse Alexa Fluor 647 IgG2b	1/600		Life Technologies	A21242	
anti rabbit Alexa Fluor 546	1/500		Life Technologies	A21085	

8.6 esiRNA and shRNA sequences used in this study

esiRNA (Sigma)	Sequence
CD133 EMU055321	ATCGCAGGATGGATTCAGAGGATGTATACGACGATGTTG AGACTGTGCCCATGAAAAATTTGGAAATCGATAGTAATG GTTATCATAAAGATCATTTATATGGTGTTCACAATCCTGT TATGACAAGCCCGTCTCGATACTGACAACTGGAGTTGAA GCTGCTTGAACAACAAGATAGTCAACATGGAAAGCATCA CAGATTTTGGATAGTTTCTGAGTCTTCTAGAACGTTCCAA GTGCAGAAGAAACCTGGTGGAGACTCAGGCGGGCACTA GGAACATGGCATCAGTGGTCTTAGGGATGCACTTTGTCA GGAATGAACAGTCATCATGGTTATAAGCCACATATCCATT GCAACTCATGAATGATTCTCTCCTGTTTTGTTTTTAACTTT TCTTTTTACACTGATTTTCTATTTAGACACTAAAACATATA GGGGTGCTTATTCCCCCTGGATACATTTACCTGTGAACC AGCTATTCCGGT
RLUC EHURLUC	GATAACTGGTCCGCAGTGGTGGGCCAGATGTAAACAAAT GAATGTTCTTGATTCATTTATTAATTATTATGATTCAGAAA AACATGCAGAAAATGCTGTTATTTTTTTACATGGTAACGC GGCCTCTTCTTATTTATGGCGACATGTTGTGCCACATATT GAGCCAGTAGCGCGGTGTATTATACCAGACCTTATTGGT ATGGGCAAATCAGGCAAATCTGGTAATGGTTCTTATAGG TTACTTGATCATTACAAATATCTTACTGCATGGTTTGAACT TCTTAATTTACCAAAGAAGATCATTTTTGTCGGCCATGAT TGGGGTGCTTGTTTGGCATTTCATTATAGCTATGAGCATC AAGATAAGATCAAAGCAATAGTTCACGCTGAAAGTGTAG TAGATGTGATTGAATCATGGGATGAATGG

shRNA (Sigma)	Clone ID	Legacy Clone Name	Target Sequence
shCD133-1	TRCN0000115316	NM_008935.1-3396s1c1	CCTGCGGTTTAGAAATAGAAT
shCD133-2	TRCN0000115319	NM_008935.1-1442s1c1	GCTGGAAGAATATGACTCGTA
shCD133-3	TRCN0000115320	NM_008935.1-1800s1c1	CTATTCAATAACCCAGACATT

8.7 Primers used in this study

Gene name	Forward primer ('5-'3)	Reverse primer ('5-'3)	Size
Acsl4	agaagggaagcaagggtgat	gattacaaagaggggcgtca	198
Arnt	ccatcgttgtgtggctactg	aaggagctcgttctcatcca	201
Axin2	taatgctaggcggaatgaag	aacccattacaagcaaacca	192
Bmi1	ccgctctttccgggatcttt	tgttcaggagtggtctggtt	237
Cdk5r1	taacaggattccagctttgc	ctagcggtcgttcctttaca	201
Cdkn1c	tctaggggaatggttgttga	gatttttgttgggcctcttt	189
Cdkn2b	cattttctgcagctggatct	ttcacaggggaaggtactga	228
cMyc	ccagatccctgaattggaaa	tcgtctgcttgaatggacag	93
Egfr	gtgatccaagctgtcccaat	cttggaacttttggcagacc	198
Gadd45a	tgcgagaacgacatcaacat	tcccggcaaaaacaaataag	200
Gclc	aacacagacccaacccagag	ccgcatcttctggaaatgtt	201
Gli1	atagggtctcggggtctcaa	cggctgactgtgtaagcaga	137
Gli2	aggcagtcagtgcctgggtat	accgcagccagggatga	246
Gli3	tgccgctggcttgattgt	tggcccgatctgaagcat	241
Glis1	ctccaagcatccacactgtt	gacaggatgcctgaagcaag	128
Glis2	caacgaccatcatgtcaagc	cggttgtggatcttcaggtt	198
Irf1	cctgggtcaggacttggata	ttcggctatcttcccttcct	202
Jak1	catgactcgctgcatgaact	tcaaccttcccaaagtgacc	201
Jak2	gtccacccgtggaatttatg	gaagggaaaggtccctgaag	198
Jak3	gtggcatcctgcctgtttat	ggatggcactggtcaaatct	204
Lgr5	ccttccctgtgactgggtta	cactgttgccgtcgtcttta	201
Lrg1	tcccatgtcagtgtgcagat	tcagcctaggagccgtttta	203
p16	caagagcggggacatcaagacatc	agctctgctcttgggattggcc	175
p21	cttgtcgctgtcttgcactc	tctcttgcagaagaccaatctg	142
p27	ttgggtctcaggcaaactct	tctgttggccctttgtttt	152
Prom1	tgtggatgtcatcaaagacg	gggcagctcctggtttaagt	149
Rb1	gcctcctaccttgtcaccaa	tgtcccaaatgattcaccaa	199
Shh	tccactgttctgtgaaagca	gtccaggaaggtgaggaagt	188
Slc2A1	aaacatggaaccaccgctac	gagaagcccataagcacagc	202
Socs3	gccccttttgtagacttcacg	aacttgctgtgggtgaccat	232
Sox2	aaccccaagatgcacaactc	ctccgggaagcgtgtactta	202
Stat3	tgatcgtgactgaggagctg	tggcggcttagtgaagaagt	203
Stat3 ChIP neg ctrl 1	gcaattcgacaacaaaagaaa	ttgagaagggtgttgtttcc	250
Stat3 ChIP neg ctrl 2	gacacatggttcacattctcc	agtcacttgatggcacctgt	164
Stat3_s1	cactgcagtacgcagagttca	tccacactttcccactactgc	218
Stat3_s2	cagcaggacattccgctaat	gcgagcgctgtacttcctaa	209
Stat5a	gtgaagcgctcaacatgaaa	gaaccactgccagaaggtgt	200
Stat5b	cccaagtcatggggagagta	agcatgcagataggggacac	199
Stat6	ccctgttcaagaacctgctc	agctttggcgttgttgtctt	200
Tyk2	acatggtcccttggatgtgt	tagcttgatgaaggggttgg	199
Wisp1	agatatgtgcccagcagctt	ttgtacctgcagttgggttg	199

8.8 PCR programme details

8.8.1 Real-Time qPCR

	Column1	Temperature (°C)	Duration (mm:ss)	Cycle (n°)
Step1	Initial denaturation	95	05:00	1
Step 2	Denaturation	95	00:10	45
	Annealing	60	00:20	
	Elongation	72	00:10	
Step 3	Final denaturation	95	00:05	1
	Start melting curve	65	01:00	1
	End melting curve	up to 96	Continuous	1

8.8.2 cDNA Reverse Transcription PCR

	Temperature (°C)	Duration (mm:ss)
Annealing	25	10:00
Elongation	37	120:00:00
Denaturation	85	05:00
Final hold	4	∞

9 List of References

1. Till, J. E. & Mc, C. E. A direct measurement of the radiation sensitivity of normal mouse bone marrow cells. *Radiat Res* **14,** 213–222 (1961).

2. Weissman, I. L. The road ended up at stem cells. *Immunol. Rev.* **185,** 159–74 (2002).

3. Scadden, D. T. Nice Neighborhood: Emerging Concepts of the Stem Cell Niche. *Cell* **157,** 41–50 (2014).

4. Melton, D. 'Stemness': Definitions, Criteria, and Standards. *Essentials Stem Cell Biol.* 7–17 (2014). doi:10.1016/B978-0-12-409503-8.00002-0

5. Aponte, P. M. & Caicedo, A. Stemness in Cancer: Stem Cells, Cancer Stem Cells, and Their Microenvironment. *Stem Cells Int.* **2017,** 5619472 (2017).

6. Hayflick, L. The longevity of cultured human cells. *J. Am. Geriatr. Soc.* **22,** 1–12 (1974).

7. Sherr, C. J. & DePinho, R. A. Cellular senescence: mitotic clock or culture shock? *Cell* **102,** 407–10 (2000).

8. Weissman, I. L., Anderson, D. J. & Gage, F. Stem and Progenitor Cells: Origins, Phenotypes, Lineage Commitments, and Transdifferentiations. *Annu. Rev. Cell Dev. Biol.* **17,** 387–403 (2001).

9. De Los Angeles, A. *et al.* Hallmarks of pluripotency. *Nature* **525,** 469–478 (2015).

10. Denker, H.-W. Stem cell terminology and 'synthetic' embryos: a new debate on totipotency, omnipotency, and pluripotency and how it relates to recent experimental data. *Cells. Tissues. Organs* **199,** 221–7 (2014).

11. McGuckin, C. P. *et al.* Production of stem cells with embryonic characteristics from human umbilical cord blood. *Cell Prolif.* **38,** 245–255 (2005).

12. Harris, D. T. & Rogers, I. Umbilical cord blood: a unique source of pluripotent stem cells for regenerative medicine. *Curr. Stem Cell Res. Ther.* **2,** 301–9 (2007).

13. Ivanovic, Z. Human Umbilical Cord Blood-Derived Very-Small-Embryonic-Like Stem Cells with Maximum Regenerative Potential? *Stem Cells Dev.* **21,** 2561–2562 (2012).

14. Plasticity of Adult Stem Cells. *Cell* **116,** 639–648 (2004).

15. Gage, F. H. Mammalian Neural Stem Cells. *Science (80-.).* **287,** (2000).

16. Orkin, S. H. Diversification of haematopoietic stem cells to specific lineages. *Nat. Rev. Genet.* **1,** 57–64 (2000).

17. Takahashi, K. & Yamanaka, S. Induction of Pluripotent Stem Cells from

Mouse Embryonic and Adult Fibroblast Cultures by Defined Factors. *Cell* **126,** 663–676 (2006).

18. Singh, V. K., Kalsan, M., Kumar, N., Saini, A. & Chandra, R. Induced pluripotent stem cells: applications in regenerative medicine, disease modeling, and drug discovery. *Front. cell Dev. Biol.* **3,** 2 (2015).

19. Takahashi. Clinical study of autologous induced pluripotent stem cell-derived retinal pigment epithelium (RPE) cell sheets for exudative age-related macular degeneration (AMD). (2015).

20. Cheung, T. H. & Rando, T. A. Molecular regulation of stem cell quiescence. *Nat. Rev. Mol. Cell Biol.* **14,** 329–40 (2013).

21. Sancar, A., Lindsey-Boltz, L. A., Ünsal-Kaçmaz, K. & Linn, S. Molecular Mechanisms of Mammalian DNA Repair and the DNA Damage Checkpoints. *Annu. Rev. Biochem.* **73,** 39–85 (2004).

22. Kanda, T., Sullivan, K. F. & Wahl, G. M. Histone–GFP fusion protein enables sensitive analysis of chromosome dynamics in living mammalian cells. *Curr. Biol.* **8,** 377–385 (1998).

23. Goldman, B. Magic marker myths. *Nat. Reports Stem Cells* (2008). doi:10.1038/stemcells.2008.26

24. Becker, A. J., McCulloch, E. A. & Till, J. E. Cytological demonstration of the clonal nature of spleen colonies derived from transplanted mouse marrow cells. (1963).

25. Jacobson, L. O., Marks, E. K., Robson, M. J., Gaston, E. & Zirkle, R. E. The effect of spleen protection on mortality following X-irradiation. *Jour Lab Clin Med* **34,** 1538–1543 (1949).

26. NOWELL, P. C., COLE, L. J., HABERMEYER, J. G. & ROAN, P. L. Growth and continued function of rat marrow cells in x-radiated mice. *Cancer Res.* **16,** 258–61 (1956).

27. FORD, C. E., HAMERTON, J. L., BARNES, D. W. & LOUTIT, J. F. Cytological identification of radiation-chimaeras. *Nature* **177,** 452–4 (1956).

28. GENGOZIAN, N., URSO, I. S., CONGDON, C. C., CONGER, A. D. & MAKINODAN, T. Thymus specificity in lethally irradiated mice treated with rat bone marrow. *Proc. Soc. Exp. Biol. Med.* **96,** 714–20 (1957).

29. Clevers, H. The Intestinal Crypt, A Prototype Stem Cell Compartment. *Cell* **154,** 274–284 (2013).

30. van Es, J. H. *et al.* Dll1+ secretory progenitor cells revert to stem cells upon crypt damage. *Nat. Cell Biol.* **14,** 1099–1104 (2012).

31. Buczacki, S. J. A. *et al.* Intestinal label-retaining cells are secretory precursors expressing Lgr5. *Nature* **495,** 65–69 (2013).

32. Fuchs, E. & Segre, J. A. Stem Cells: A New Lease on Life. *Cell* **100,** 143–

155 (2000).

33. Tumbar, T. *et al.* Defining the Epithelial Stem Cell Niche in Skin. *Science (80-.).* **303,** 359–363 (2004).

34. Blanpain, C., Lowry, W. E., Geoghegan, A., Polak, L. & Fuchs, E. Self-Renewal, Multipotency, and the Existence of Two Cell Populations within an Epithelial Stem Cell Niche. *Cell* **118,** 635–648 (2004).

35. Sidney, L. E., Branch, M. J., Dunphy, S. E., Dua, H. S. & Hopkinson, A. Concise Review: Evidence for CD34 as a Common Marker for Diverse Progenitors. *Stem Cells* **32,** 1380–1389 (2014).

36. Waghmare, S. K. *et al.* Quantitative proliferation dynamics and random chromosome segregation of hair follicle stem cells. *EMBO J.* **27,** 1309–1320 (2008).

37. Lane, S. W., Williams, D. A. & Watt, F. M. Modulating the stem cell niche for tissue regeneration. *Nat. Biotechnol.* **32,** 795–803 (2014).

38. Katayama, Y. *et al.* Signals from the sympathetic nervous system regulate hematopoietic stem cell egress from bone marrow. *Cell* **124,** 407–21 (2006).

39. Greenbaum, A. *et al.* CXCL12 in early mesenchymal progenitors is required for haematopoietic stem-cell maintenance. *Nature* **495,** 227–30 (2013).

40. Méndez-Ferrer, S., Lucas, D., Battista, M. & Frenette, P. S. Haematopoietic stem cell release is regulated by circadian oscillations. *Nature* **452,** 442–7 (2008).

41. Extracellular matrix: A dynamic microenvironment for stem cell niche. *Biochim. Biophys. Acta - Gen. Subj.* **1840,** 2506–2519 (2014).

42. Williams, D. A., Rios, M., Stephens, C. & Patel, V. P. Fibronectin and VLA-4 in haematopoietic stem cell-microenvironment interactions. *Nature* **352,** 438–41 (1991).

43. Morrison, S. J. & Scadden, D. T. The bone marrow niche for haematopoietic stem cells. *Nature* **505,** 327–34 (2014).

44. Rothenberg, M. E. *et al.* Identification of a cKit(+) colonic crypt base secretory cell that supports Lgr5(+) stem cells in mice. *Gastroenterology* **142,** 1195–1205.e6 (2012).

45. Sato, T. *et al.* Paneth cells constitute the niche for Lgr5 stem cells in intestinal crypts. *Nature* **469,** 415–8 (2011).

46. Barker, N. Adult intestinal stem cells: critical drivers of epithelial homeostasis and regeneration. *Nat. Rev. Mol. Cell Biol.* **15,** 19–33 (2014).

47. Brownell, I., Guevara, E., Bai, C. B., Loomis, C. A. & Joyner, A. L. Nerve-derived sonic hedgehog defines a niche for hair follicle stem cells capable of becoming epidermal stem cells. *Cell Stem Cell* **8,** 552–65 (2011).

48. Niederkorn, J. Y. See no evil, hear no evil, do no evil: the lessons of immune privilege. *Nat. Immunol.* **7,** 354–359 (2006).

49. Fujisaki, J. *et al.* In vivo imaging of Treg cells providing immune privilege to the haematopoietic stem-cell niche. *Nature* **474,** 216–9 (2011).

50. Heo, H.-R. *et al.* Hormonal regulation of hematopoietic stem cells and their niche: a focus on estrogen. *Int. J. stem cells* **8,** 18–23 (2015).

51. Collins, F. L., Rios-Arce, N. D., McCabe, L. R. & Parameswaran, N. Cytokine and hormonal regulation of bone marrow immune cell Wnt10b expression. *PLoS One* **12,** e0181979 (2017).

52. Burdon, T., Smith, A. & Savatier, P. Signalling, cell cycle and pluripotency in embryonic stem cells. *Trends Cell Biol.* **12,** 432–438 (2002).

53. Martin, G. S. Cell signaling and cancer. *Cancer Cell* **4,** 167–174 (2003).

54. WNT-SHH Antagonism Specifies and Expands Stem Cells prior to Niche Formation. *Cell* **164,** 156–169 (2016).

55. Holland, J. D., Klaus, A., Garratt, A. N. & Birchmeier, W. Wnt signaling in stem and cancer stem cells. *Curr Opin Cell Biol* **25,** 254–264 (2013).

56. Silva-Vargas, V. *et al.* Beta-catenin and Hedgehog signal strength can specify number and location of hair follicles in adult epidermis without recruitment of bulge stem cells. *Dev. Cell* **9,** 121–31 (2005).

57. Driskell, R. R. *et al.* Distinct fibroblast lineages determine dermal architecture in skin development and repair. *Nature* **504,** 277–281 (2013).

58. Collins, C. A., Kretzschmar, K. & Watt, F. M. Reprogramming adult dermis to a neonatal state through epidermal activation of β-catenin. *Development* **138,** 5189–99 (2011).

59. Riddle, R. D., Johnson, R. L., Laufer, E. & Tabin, C. Sonic hedgehog mediates the polarizing activity of the ZPA. *Cell* **75,** 1401–16 (1993).

60. Rash, B. G. & Grove, E. A. Patterning the Dorsal Telencephalon: A Role for Sonic Hedgehog? *J. Neurosci.* **27,** 11595–11603 (2007).

61. Dassule, H. R., Lewis, P., Bei, M., Maas, R. & McMahon, A. P. Sonic hedgehog regulates growth and morphogenesis of the tooth. *Development* **127,** 4775–85 (2000).

62. Oxygen in Stem Cell Biology: A Critical Component of the Stem Cell Niche. *Cell Stem Cell* **7,** 150–161 (2010).

63. Jena, N. R. DNA damage by reactive species: Mechanisms, mutation and repair. *J. Biosci.* **37,** 503–17 (2012).

64. Muscari, C. *et al.* Priming adult stem cells by hypoxic pretreatments for applications in regenerative medicine. *J. Biomed. Sci.* **20,** 63 (2013).

65. Forristal, C. E. *et al.* Pharmacologic stabilization of HIF-1α increases hematopoietic stem cell quiescence in vivo and accelerates blood recovery after severe irradiation. *Blood* **121,** 759–69 (2013).

66. Shyh-Chang, N., Daley, G. Q. & Cantley, L. C. Stem cell metabolism in tissue development and aging. *Development* **140,** 2535–2547 (2013).

67. Gattazzo, F., Urciuolo, A. & Bonaldo, P. Extracellular matrix: a dynamic microenvironment for stem cell niche. *Biochim. Biophys. Acta* **1840,** 2506–19 (2014).

68. Hall, P. A. & Watt, F. M. Stem cells: the generation and maintenance of cellular diversity. *Development* **106,** 619–33 (1989).

69. Brizzi, M. F., Tarone, G. & Defilippi, P. Extracellular matrix, integrins, and growth factors as tailors of the stem cell niche. *Curr. Opin. Cell Biol.* **24,** 645–51 (2012).

70. Desgrosellier, J. S. & Cheresh, D. A. Integrins in cancer: biological implications and therapeutic opportunities. *Nat. Rev. Cancer* **10,** 9–22 (2010).

71. Wang, H., Luo, X. & Leighton, J. Extracellular Matrix and Integrins in Embryonic Stem Cell Differentiation. *Biochem. insights* **8,** 15–21 (2015).

72. Gilbert, P. M. *et al.* Substrate Elasticity Regulates Skeletal Muscle Stem Cell Self-Renewal in Culture. *Science (80-.).* **329,** 1078–1081 (2010).

73. Holst, J. *et al.* Substrate elasticity provides mechanical signals for the expansion of hemopoietic stem and progenitor cells. *Nat. Biotechnol.* **28,** 1123–1128 (2010).

74. McBeath, R., Pirone, D. M., Nelson, C. M., Bhadriraju, K. & Chen, C. S. Cell shape, cytoskeletal tension, and RhoA regulate stem cell lineage commitment. *Dev. Cell* **6,** 483–95 (2004).

75. Kilian, K. A., Bugarija, B., Lahn, B. T. & Mrksich, M. Geometric cues for directing the differentiation of mesenchymal stem cells. *Proc. Natl. Acad. Sci.* **107,** 4872–4877 (2010).

76. Avilion, A. A. Multipotent cell lineages in early mouse development depend on SOX2 function. *Genes Dev.* **17,** 126–140 (2003).

77. Arnold, K. *et al.* Sox2+ Adult Stem and Progenitor Cells Are Important for Tissue Regeneration and Survival of Mice. *Cell Stem Cell* **9,** 317–329 (2011).

78. Juuri, E. *et al.* Sox2+ Stem Cells Contribute to All Epithelial Lineages of the Tooth via Sfrp5+ Progenitors. *Dev. Cell* **23,** 317–328 (2012).

79. Tapia, N. *et al.* Dissecting the role of distinct OCT4-SOX2 heterodimer configurations in pluripotency. *Sci. Rep.* **5,** 13533 (2015).

80. Abdouh, M., Hanna, R., Hajjar, J. El, Flamier, A. & Bernier, G. The

Polycomb Repressive Complex 1 Protein BMI1 Is Required for Constitutive Heterochromatin Formation and Silencing in Mammalian Somatic Cells * □ S. (2015). doi:10.1074/jbc.M115.662403

81. Zhu, S. *et al.* BMI1 regulates androgen receptor in prostate cancer independently of the polycomb repressive complex 1. **91012138,**

82. Biehs, B. *et al.* BMI1 represses Ink4a/Arf and Hox genes to regulate stem cells in the rodent incisor. *Nat. Cell Biol.* **15,** 846–852 (2013).

83. Liu, S. *et al.* Hedgehog Signaling and Bmi-1 Regulate Self-renewal of Normal and Malignant Human Mammary Stem Cells. *Cancer Res.* **66,** 6063–6071 (2006).

84. López-Arribillaga, E. *et al.* Bmi1 regulates murine intestinal stem cell proliferation and self-renewal downstream of Notch. *Development* **142,** 41–50 (2015).

85. Herzenberg, L. A. *et al.* The history and future of the fluorescence activated cell sorter and flow cytometry: a view from Stanford. *Clin. Chem.* **48,** 1819–27 (2002).

86. Molecule Information. Available at: http://www.hcdm.org/index.php/molecule-information. (Accessed: 17th November 2017)

87. Oka, M. *et al.* CD9 is associated with leukemia inhibitory factor-mediated maintenance of embryonic stem cells. *Mol. Biol. Cell* **13,** 1274–81 (2002).

88. Shakiba, N. *et al.* CD24 tracks divergent pluripotent states in mouse and human cells. *Nat. Commun.* **6,** 7329 (2015).

89. Herszfeld, D. *et al.* CD30 is a survival factor and a biomarker for transformed human pluripotent stem cells. *Nat. Biotechnol.* **24,** 351–357 (2006).

90. Draper, J. S., Pigott, C., Thomson, J. A. & Andrews, P. W. Surface antigens of human embryonic stem cells: changes upon differentiation in culture. *J. Anat.* **200,** 249–58 (2002).

91. Tang, C. *et al.* An antibody against SSEA-5 glycan on human pluripotent stem cells enables removal of teratoma-forming cells. *Nat. Biotechnol.* **29,** 829–834 (2011).

92. Sundberg, M. *et al.* CD marker expression profiles of human embryonic stem cells and their neural derivatives, determined using flow-cytometric analysis, reveal a novel CD marker for exclusion of pluripotent stem cells. *Stem Cell Res.* **2,** 113–124 (2009).

93. Dominici, M. *et al.* Minimal criteria for defining multipotent mesenchymal stromal cells. The International Society for Cellular Therapy position statement. *Cytotherapy* **8,** 315–7 (2006).

94. Shmelkov, S. V *et al.* CD133 expression is not restricted to stem cells, and

both CD133+ and CD133- metastatic colon cancer cells initiate tumors. *J. Clin. Invest.* **118,** 2111–20 (2008).

95. Chen, M., Przyborowski, M. & Berthiaume, F. Stem cells for skin tissue engineering and wound healing. *Crit. Rev. Biomed. Eng.* **37,** 399–421 (2009).

96. Atallah, M. R., Palioura, S., Perez, V. L. & Amescua, G. Limbal stem cell transplantation: current perspectives. *Clin. Ophthalmol.* **10,** 593–602 (2016).

97. Kfoury, C. Therapeutic cloning: promises and issues. *Mcgill J. Med.* **10,** 112–20 (2007).

98. Stuckey, D. W. & Shah, K. Stem cell-based therapies for cancer treatment: separating hope from hype. *Nat. Rev. Cancer* **14,** 683–91 (2014).

99. Hentze, H. *et al.* Teratoma formation by human embryonic stem cells: Evaluation of essential parameters for future safety studies. *Stem Cell Res.* **2,** 198–210 (2009).

100. Ramos-Zúñiga, R., González-Pérez, O., Macías-Ornelas, A., Capilla-González, V. & Quiñones-Hinojosa, A. Ethical implications in the use of embryonic and adult neural stem cells. *Stem Cells Int.* **2012,** 470949 (2012).

101. Marión, R. M. *et al.* Common Telomere Changes during In Vivo Reprogramming and Early Stages of Tumorigenesis. *Stem Cell Reports* **8,** 460–475 (2017).

102. Lee, A. S., Tang, C., Rao, M. S., Weissman, I. L. & Wu, J. C. Tumorigenicity as a clinical hurdle for pluripotent stem cell therapies. *Nat. Med.* **19,** 998–1004 (2013).

103. Maza, I. *et al.* Transient acquisition of pluripotency during somatic cell transdifferentiation with iPSC reprogramming factors. *Nat. Biotechnol.* **33,** 769–774 (2015).

104. Mandai, M. *et al.* Autologous Induced Stem-Cell–Derived Retinal Cells for Macular Degeneration. *N. Engl. J. Med.* **376,** 1038–1046 (2017).

105. Augello, A. & De Bari, C. The Regulation of Differentiation in Mesenchymal Stem Cells. *Hum. Gene Ther.* **21,** 1226–1238 (2010).

106. O'Connor, N., Mulliken, J., Banks-Schlegel, S., Kehinde, O. & Green, H. Grafting of burns with cultured epithelium prepared from autologous epidermal cells. *Lancet* **317,** 75–78 (1981).

107. Yui, S. *et al.* Functional engraftment of colon epithelium expanded in vitro from a single adult Lgr5+ stem cell. *Nat. Med.* **18,** 618–623 (2012).

108. Ouyang, H. *et al.* WNT7A and PAX6 define corneal epithelium homeostasis and pathogenesis. *Nature* **511,** 358–61 (2014).

109. Satir, P. Landmarks in cilia research from leeuwenhoek to US. *Cell Motil.*

Cytoskeleton **32,** 90–94 (1995).

110. Wheatley, D. N. Landmarks in the first hundred years of primary (9+0) cilium research. *Cell Biol. Int.* **29,** 333–9 (2005).

111. Toftgård, R. Two sides to cilia in cancer. *Nat. Med.* **15,** 994–996 (2009).

112. Vogel, T. W., Carter, C. S., Abode-Iyamah, K., Zhang, Q. & Robinson, S. The role of primary cilia in the pathophysiology of neural tube defects. *Neurosurg. Focus* **33,** E2 (2012).

113. Ibañez-Tallon, I., Heintz, N. & Omran, H. To beat or not to beat: roles of cilia in development and disease. *Hum. Mol. Genet.* **12 Spec No 1,** R27-35 (2003).

114. Chapter 1 Basal Bodies: Platforms for Building Cilia. **85,** 1–22 (2008).

115. Dean, S., Moreira-Leite, F., Varga, V. & Gull, K. Cilium transition zone proteome reveals compartmentalization and differential dynamics of ciliopathy complexes. *Proc. Natl. Acad. Sci. U. S. A.* **113,** E5135-43 (2016).

116. Magiera, M. M. & Janke, C. *Post-translational modifications of tubulin*. (2014). doi:10.1016/j.cub.2014.03.032

117. Cole, D. G. *et al.* Chlamydomonas kinesin-II-dependent intraflagellar transport (IFT): IFT particles contain proteins required for ciliary assembly in Caenorhabditis elegans sensory neurons. *J. Cell Biol.* **141,** 993–1008 (1998).

118. Scholey, J. M. Intraflagellar transport motors in cilia: moving along the cell's antenna. *J. Cell Biol.* **180,** 23–29 (2008).

119. Prodromou, N. V. *et al.* Heat shock induces rapid resorption of primary cilia. *J. Cell Sci.* **125,** 4297–4305 (2012).

120. Pugacheva, E. N., Jablonski, S. A., Hartman, T. R., Henske, E. P. & Golemis, E. A. HEF1-Dependent Aurora A Activation Induces Disassembly of the Primary Cilium. doi:10.1016/j.cell.2007.04.035

121. Gradilone, S. A. *et al.* HDAC6 Inhibition Restores Ciliary Expression and Decreases Tumor Growth. *Cancer Res.* **73,** 2259–2270 (2013).

122. Vorobjev, I. A. & Chentsov YuS. Centrioles in the cell cycle. I. Epithelial cells. *J. Cell Biol.* **93,** 938–49 (1982).

123. Nigg, E. A. & Stearns, T. The centrosome cycle: Centriole biogenesis, duplication and inherent asymmetries. *Nat. Cell Biol.* **13,** 1154–60 (2011).

124. Bornens, M. The centrosome in cells and organisms. *Science* **335,** 422–6 (2012).

125. Al Jord, A. *et al.* Centriole amplification by mother and daughter centrioles differs in multiciliated cells. *Nature* **516,** (2014).

126. Paridaen, Judith; Wilsch-Brauninger, michaela; Huttner, W. Asymmetric Inheritance of Centrosome-Associated Primary Cilium Membrane Directs Ciliogenesis after Cell Division. *Cell* **155,** 333–344 (2013).

127. Plk4-Induced Centriole Biogenesis in Human Cells. *Dev. Cell* **13,** 190–202 (2007).

128. Cep97 and CP110 Suppress a Cilia Assembly Program. *Cell* **130,** 678–690 (2007).

129. Majumder, S. & Fisk, H. A. VDAC3 and Mps1 negatively regulate ciliogenesis. *Cell Cycle* **12,** 849–858 (2013).

130. Goetz, S. C. & Anderson, K. V. The primary cilium: a signalling centre during vertebrate development. *Nat. Rev. Genet.* **11,** 331–344 (2010).

131. Kuhns, S. *et al.* The microtubule affinity regulating kinase MARK4 promotes axoneme extension during early ciliogenesis. *J. Cell Biol.* **200,** 505–22 (2013).

132. Centriolar Kinesin Kif24 Interacts with CP110 to Remodel Microtubules and Regulate Ciliogenesis. *Cell* **145,** 914–925 (2011).

133. Kim, S., Lee, K., Choi, J.-H., Ringstad, N. & Dynlacht, B. D. Nek2 activation of Kif24 ensures cilium disassembly during the cell cycle. *Nat. Commun.* **6,** 8087 (2015).

134. Jang, C.-Y., Coppinger, J. A., Seki, A., Yates, J. R. & Fang, G. Plk1 and Aurora A regulate the depolymerase activity and the cellular localization of Kif2a. *J. Cell Sci.* **122,** 1334–41 (2009).

135. Cilia Disassembly with Two Distinct Phases of Regulation. *Cell Rep.* **10,** 1803–1810 (2015).

136. Miyamoto, T. *et al.* The Microtubule-Depolymerizing Activity of a Mitotic Kinesin Protein KIF2A Drives Primary Cilia Disassembly Coupled with Cell Proliferation. *Cell Rep.* **10,** 664–673 (2015).

137. Kinzel, D. *et al.* Pitchfork Regulates Primary Cilia Disassembly and Left-Right Asymmetry. *Dev. Cell* **19,** 66–77 (2010).

138. HEF1-Dependent Aurora A Activation Induces Disassembly of the Primary Cilium. *Cell* **129,** 1351–1363 (2007).

139. de Diego, A. S., Alonso Guerrero, A., Martínez-A, C. & van Wely, K. H. M. Dido3-dependent HDAC6 targeting controls cilium size. *Nat. Commun.* **5,** 3500 (2014).

140. Kim, M., Kim, M., Lee, M.-S., Kim, C.-H. & Lim, D.-S. The MST1/2-SAV1 complex of the Hippo pathway promotes ciliogenesis. *Nat. Commun.* **5,** 5370 (2014).

141. Zhang, B., Wang, Q. & Pan, X. No Title. **210,** (2007).

142. Corbit, K. C. *et al.* Kif3a constrains β-catenin-dependent Wnt signalling through dual ciliary and non-ciliary mechanisms. *Nat. Cell Biol.* **10,** 70–76 (2008).

143. Saeed, H., Taipaleenmäki, H., Aldahmash, A. M., Abdallah, B. M. & Kassem, M. Mouse Embryonic Fibroblasts (MEF) Exhibit a Similar but not Identical Phenotype to Bone Marrow Stromal Stem Cells (BMSC). *Stem Cell Rev. Reports* **8,** 318–328 (2012).

144. Croyle, M. J. *et al.* Role of epidermal primary cilia in the homeostasis of skin and hair follicles. *Development* **138,** 1675–85 (2011).

145. Tummala, P., Arnsdorf, E. J. & Jacobs, C. R. The Role of Primary Cilia in Mesenchymal Stem Cell Differentiation: A Pivotal Switch in Guiding Lineage Commitment. *Cell. Mol. Bioeng.* **3,** 207–212 (2010).

146. Pazour, G. J., San Agustin, J. T., Follit, J. A., Rosenbaum, J. L. & Witman, G. B. Polycystin-2 localizes to kidney cilia and the ciliary level is elevated in orpk mice with polycystic kidney disease. *Curr. Biol.* **12,** R378-80 (2002).

147. Schneider, L. *et al.* PDGFRalphaalpha signaling is regulated through the primary cilium in fibroblasts. *Curr. Biol.* **15,** 1861–6 (2005).

148. Rohatgi, R., Milenkovic, L. & Scott, M. P. Patched1 regulates hedgehog signaling at the primary cilium. *Science* **317,** 372–6 (2007).

149. Ezratty, E. J. *et al.* A Role for the Primary Cilium in Notch Signaling and Epidermal Differentiation during Skin Development. *Cell* **145,** 1129–1141 (2011).

150. Wallingford, J. B. & Mitchell, B. Strange as it may seem: the many links between Wnt signaling, planar cell polarity, and cilia. *Genes Dev.* **25,** 201–213 (2011).

151. Habbig, S. *et al.* NPHP4, a cilia-associated protein, negatively regulates the Hippo pathway. *J. Cell Biol.* **193,** 633–42 (2011).

152. Hoch, R. V. & Soriano, P. Roles of PDGF in animal development. *Development* **130,** 4769–4784 (2003).

153. Suizu, F. *et al.* Phosphorylation-dependent Akt–Inversin interaction at the basal body of primary cilia. *EMBO J.* **35,** 1346–1363 (2016).

154. Schneider, L. *et al.* Directional Cell Migration and Chemotaxis in Wound Healing Response to PDGF-AA are Coordinated by the Primary Cilium in Fibroblasts. *Cell. Physiol. Biochem.* **25,** 279–292 (2010).

155. Christensen, S. T., Clement, C. A., Satir, P. & Pedersen, L. B. Primary cilia and coordination of receptor tyrosine kinase (RTK) signalling. *J. Pathol.* **226,** 172–184 (2012).

156. Grisanti, L., Revenkova, E., Gordon, R. E. & Iomini, C. Primary cilia maintain corneal epithelial homeostasis by regulation of the Notch signaling pathway. *Development* **143,** 2160–71 (2016).

157. Leitch, C. C., Lodh, S., Prieto-Echagü E, V., Badano, J. L. & Zaghloul, N. A. Basal body proteins regulate Notch signaling through endosomal trafficking. *J. Cell Sci.* doi:10.1242/jcs.130344

158. Harvey, K. & Tapon, N. The Salvador-Warts-Hippo pathway - an emerging tumour-suppressor network. *Nat. Rev. Cancer* **7,** 182–91 (2007).

159. Cisternas, P., Vio, C. P. & Inestrosa, N. C. Role of Wnt Signaling in Tissue Fibrosis, Lessons from Skeletal Muscle and Kidney.

160. Tavares, A., Goncalves, J., Florindo, C., Tavares, A. A. & Soares, H. Mob1: defining cell polarity for proper cell division. *J. Cell Sci.* **125,** 516–527 (2012).

161. Fliegauf, M., Benzing, T. & Omran, H. When cilia go bad: cilia defects and ciliopathies. *Nat. Rev. Mol. Cell Biol.* **8,** 880–893 (2007).

162. Larkins, C. E., Aviles, G. D. G., East, M. P., Kahn, R. A. & Caspary, T. Arl13b regulates ciliogenesis and the dynamic localization of Shh signaling proteins. *Mol. Biol. Cell* **22,** 4694–4703 (2011).

163. Robbins, D. J., Fei, D. L. & Riobo, N. A. The Hedgehog Signal Transduction Network. *Sci. Signal.* **5,** re6-re6 (2012).

164. Attanasio, M. *et al.* Loss of GLIS2 causes nephronophthisis in humans and mice by increased apoptosis and fibrosis. *Nat. Genet.* **39,** 1018–1024 (2007).

165. Yin, A. H. *et al.* AC133, a novel marker for human hematopoietic stem and progenitor cells. *Blood* **90,** 5002–5012 (1997).

166. Miraglia, S. *et al.* A novel five-transmembrane hematopoietic stem cell antigen: isolation, characterization, and molecular cloning. *Blood* **90,** 5013–5021 (1997).

167. Weigmann, A., Corbeil, D., Hellwig, A. & Huttner, W. B. Prominin, a novel microvilli-specific polytopic membrane protein of the apical surface of epithelial cells, is targeted to plasmalemmal protrusions of non-epithelial cells. *Proc Natl Acad Sci U S A* **94,** 12425–12430 (1997).

168. Corbeil, D. *et al.* The Human AC133 Hematopoietic Stem Cell Antigen Is also Expressed in Epithelial Cells and Targeted to Plasma Membrane Protrusions*.

169. Fargeas, C. A. Characterization of Prominin-2, a New Member of the Prominin Family of Pentaspan Membrane Glycoproteins. *J. Biol. Chem.* **278,** 8586–8596 (2003).

170. Han, Z. & Papermaster, D. S. Identification of three prominin homologs and characterization of their messenger RNA expression in Xenopus laevis tissues. *Mol. Vis.* **17,** 1381–96 (2011).

171. Shmelkov, S. V. Alternative promoters regulate transcription of the gene that encodes stem cell surface protein AC133. *Blood* **103,** 2055–2061

(2004).

172. Jaszai, J., Fargeas, C. A., Florek, M., Huttner, W. B. & Corbeil, D. Focus on molecules: prominin-1 (CD133). *Exp Eye Res* **85,** 585–586 (2007).

173. Fargeas, C. A., Florek, M., Huttner, W. B. & Corbeil, D. Characterization of prominin-2, a new member of the prominin family of pentaspan membrane glycoproteins. *J. Biol. Chem.* **278,** 8586–96 (2003).

174. Ohnishi, S. *et al.* Hypoxia-Inducible Factors Activate CD133 Promoter through ETS Family Transcription Factors. *PLoS One* **8,** e66255 (2013).

175. Li, Z. CD133: a stem cell biomarker and beyond. **2,** 1 (2013).

176. Hanahan, D. & Weinberg, R. A. Hallmarks of Cancer: The Next Generation. *Cell* **144,** 646–674 (2011).

177. Gopisetty, G., Xu, J., Sampath, D., Colman, H. & Puduvalli, V. K. Epigenetic regulation of CD133/PROM1 expression in glioma stem cells by Sp1/myc and promoter methylation. *Oncogene* **32,** 3119–3129 (2013).

178. Yi, J. M. *et al.* Abnormal DNA Methylation of CD133 in Colorectal and Glioblastoma Tumors. *Cancer Res.* **68,** 8094–8103 (2008).

179. Tabu, K. *et al.* Promoter hypomethylation regulates CD133 expression in human gliomas. *Cell Res.* **18,** 1037–1046 (2008).

180. Park, E. K. *et al.* Transcriptional repression of cancer stem cell marker CD133 by tumor suppressor p53. *Cell Death Dis.* **6,** e1964 (2015).

181. Miraglia, S., Godfrey, W. & Buck, D. A response to AC133 hematopoietic stem cell antigen: human homologue of mouse kidney prominin or distinct member of a novel protein family? *Blood* **91,** 4390–1 (1998).

182. Corbeil, D., Fargeas, C. A. & Huttner, W. B. Rat prominin, like its mouse and human orthologues, is a pentaspan membrane glycoprotein. *Biochem. Biophys. Res. Commun.* **285,** 939–44 (2001).

183. Fargeas, C. A. *et al.* Identification of novel Prominin-1/CD133 splice variants with alternative C-termini and their expression in epididymis and testis. *J. Cell Sci.* **117,** 4301–11 (2004).

184. Fargeas, C. A., Huttner, W. B. & Corbeil, D. Nomenclature of prominin-1 (CD133) splice variants ? an update. *Tissue Antigens* **69,** 602–606 (2007).

185. Corbeil, D. *et al.* Expression of distinct splice variants of the stem cell marker prominin-1 (CD133) in glial cells. *Glia* **57,** 860–74 (2009).

186. Scadden, D. T. *et al.* The stem-cell niche as an entity of action. *Nature* **441,** 1075–1079 (2006).

187. Fargeas, C. A., Huttner, W. B. & Corbeil, D. Nomenclature of prominin-1 (CD133) splice variants - an update. *Tissue Antigens* **69,** 602–6 (2007).

188. Yu, Y., Flint, A., Dvorin, E. L. & Bischoff, J. AC133-2, a Novel Isoform of Human AC133 Stem Cell Antigen. *J. Biol. Chem.* **277,** 20711–20716 (2002).

189. Jászai, J. *et al.* Distinct and Conserved Prominin-1/CD133–Positive Retinal Cell Populations Identified across Species. *PLoS One* **6,** e17590 (2011).

190. Corbeil, D., Karbanová, J., Fargeas, C. A. & Jászai, J. Prominin-1 (CD133): Molecular and Cellular Features Across Species. *Adv. Exp. Med. Biol.* **777,** 3–24 (2013).

191. Harris, B. Z. & Lim, W. A. Mechanism and role of PDZ domains in signaling complex assembly. *J. Cell Sci.* **114,** (2001).

192. Sheng, M. & Sala, C. PDZ D OMAINS AND THE O RGANIZATION OF S UPRAMOLECULAR C OMPLEXES. *Annu. Rev. Neurosci.* **24,** 1–29 (2001).

193. Peichev, M. *et al.* Expression of VEGFR-2 and AC133 by circulating human CD34(+) cells identifies a population of functional endothelial precursors. *Blood* **95,** 952–8 (2000).

194. Uchida, N. *et al.* Direct isolation of human central nervous system stem cells. *Proc. Natl. Acad. Sci. U. S. A.* **97,** 14720–5 (2000).

195. Richardson, G. D. CD133, a novel marker for human prostatic epithelial stem cells. *J. Cell Sci.* **117,** 3539–3545 (2004).

196. Torrente, Y. *et al.* Human circulating AC133+ stem cells restore dystrophin expression and ameliorate function in dystrophic skeletal muscle. *J. Clin. Invest.* **114,** 182–195 (2004).

197. Maw, M. A. *et al.* A frameshift mutation in prominin (mouse)-like 1 causes human retinal degeneration. *Hum. Mol. Genet.* **9,** 27–34 (2000).

198. Bhatia, M. AC133 expression in human stem cells. *Leukemia* **15,** 1685–1688 (2001).

199. Pfenninger, C. V. *et al.* CD133 Is Not Present on Neurogenic Astrocytes in the Adult Subventricular Zone, but on Embryonic Neural Stem Cells, Ependymal Cells, and Glioblastoma Cells. *Cancer Res.* **67,** 5727–5736 (2007).

200. Wang, L. D. & Wagers, A. J. Dynamic niches in the origination and differentiation of haematopoietic stem cells. *Nat. Rev. Mol. Cell Biol.* **12,** 643–655 (2011).

201. Pasino, M. *et al.* Flow cytometric and functional characterization of AC133+ cells from human umbilical cord blood. *Br J Haematol* **108,** 793–800 (2000).

202. Gallacher, L. *et al.* Isolation and characterization of human CD34(-)Lin(-) and CD34(+)Lin(-) hematopoietic stem cells using cell surface markers AC133 and CD7. *Blood* **95,** 2813–2820 (2000).

203. Matsumoto, K. *et al.* In vitro proliferation potential of AC133 positive cells in peripheral blood. *Stem Cells* **18,** 196–203 (2000).

204. Summers, Y. J. *et al.* AC133+ G0 cells from cord blood show a high incidence of long-term culture-initiating cells and a capacity for more than 100 million-fold amplification of colony-forming cells in vitro. *Stem Cells* **22,** 704–715 (2004).

205. Leor, J. *et al.* Human umbilical cord blood-derived CD133+ cells enhance function and repair of the infarcted myocardium. *Stem Cells* **24,** 772–780 (2006).

206. Stamm, C. *et al.* Autologous bone-marrow stem-cell transplantation for myocardial regeneration. *Lancet* **361,** 45–46 (2003).

207. Jang, Y. K. *et al.* Retinoic acid-mediated induction of neurons and glial cells from human umbilical cord-derived hematopoietic stem cells. *J. Neurosci. Res.* **75,** 573–84 (2004).

208. Kamei, N. *et al.* Ex-vivo expanded human blood-derived CD133+ cells promote repair of injured spinal cord. *J. Neurol. Sci.* **328,** 41–50 (2013).

209. Tamaki, S. *et al.* Engraftment of sorted/expanded human central nervous system stem cells from fetal brain. *J. Neurosci. Res.* **69,** 976–986 (2002).

210. Thill, M. *et al.* A novel population of repair cells identified in the stroma of the human cornea. *Stem Cells Dev.* **16,** 733–45 (2007).

211. Bussolati, B. *et al.* Isolation of Renal Progenitor Cells from Adult Human Kidney. *Am. J. Pathol.* **166,** 545–555 (2005).

212. Ahmadi, H. *et al.* Safety analysis and improved cardiac function following local autologous transplantation of CD133(+) enriched bone marrow cells after myocardial infarction. *Curr. Neurovasc. Res.* **4,** 153–60 (2007).

213. Nikeghbalian, S. *et al.* Autologous transplantation of bone marrow-derived mononuclear and CD133(+) cells in patients with decompensated cirrhosis. *Arch. Iran. Med.* **14,** 12–7 (2011).

214. Noiseux, N. *et al.* The IMPACT-CABG trial: A multicenter, randomized clinical trial of CD133+ stem cell therapy during coronary artery bypass grafting for ischemic cardiomyopathy. *J. Thorac. Cardiovasc. Surg.* **152,** 1582–1588.e2 (2016).

215. Search of: CD133 | Open Studies - List Results - ClinicalTrials.gov. (2017). Available at: https://clinicaltrials.gov/ct2/results?term=CD133&recr=Open. (Accessed: 15th February 2017)

216. Florek, M. *et al.* Prominin-1/CD133, a neural and hematopoietic stem cell marker, is expressed in adult human differentiated cells and certain types of kidney cancer. *Cell Tissue Res.* **319,** 15–26 (2005).

217. Immervoll, H., Hoem, D., Sakariassen, P. Ø., Steffensen, O. J. & Molven, A. Expression of the "stem cell marker" CD133 in pancreas and pancreatic ductal adenocarcinomas. *BMC Cancer* **8,** 48 (2008).

218. Lardon, J., Corbeil, D., Huttner, W. B., Ling, Z. & Bouwens, L. Stem Cell

Marker Prominin-1/AC133 Is Expressed in Duct Cells of the Adult Human Pancreas.

219. Corbeil, D. *et al.* The human AC133 hematopoietic stem cell antigen is also expressed in epithelial cells and targeted to plasma membrane protrusions. *J. Biol. Chem.* **275,** 5512–20 (2000).

220. Corbeil, D., Röper, K., Hannah, M. J., Hellwig, A. & Huttner, W. B. Selective localization of the polytopic membrane protein prominin in microvilli of epithelial cells - a combination of apical sorting and retention in plasma membrane protrusions. *J. Cell Sci.* 1023–33 (1999).

221. Dubreuil, V., Marzesco, A.-M., Corbeil, D., Huttner, W. B. & Wilsch-Bräuninger, M. Midbody and primary cilium of neural progenitors release extracellular membrane particles enriched in the stem cell marker prominin-1. *J. Cell Biol.* **176,** 483–495 (2007).

222. Röper, K., Corbeil, D. & Huttner, W. B. Retention of prominin in microvilli reveals distinct cholesterol-based lipid micro-domains in the apical plasma membrane. *Nat. Cell Biol.* **2,** 582–92 (2000).

223. Marzesco, A.-M. *et al.* Release of extracellular membrane vesicles from microvilli of epithelial cells is enhanced by depleting membrane cholesterol. *FEBS Lett.* **583,** 897–902 (2009).

224. Corbeil, D., Marzesco, A.-M., Fargeas, C. A. & Huttner, W. B. in 399–423 (2010). doi:10.1007/978-90-481-8622-8_14

225. Head, B. P., Patel, H. H. & Insel, P. A. Interaction of membrane/lipid rafts with the cytoskeleton: Impact on signaling and function ☆ Membrane/lipid rafts, mediators of cytoskeletal arrangement and cell signaling. *BBA - Biomembr.* **1838,** 532–545 (2014).

226. Janich, P. & Corbeil, D. GM1 and GM3 gangliosides highlight distinct lipid microdomains within the apical domain of epithelial cells. *FEBS Lett.* **581,** 1783–7 (2007).

227. Muth, T. R., Ahn, J. & Caplan, M. J. Identification of Sorting Determinants in the C-terminal Cytoplasmic Tails of the -Aminobutyric Acid Transporters GAT-2 and GAT-3. *J. Biol. Chem.* **273,** 25616–25627 (1998).

228. György, B. *et al.* Membrane vesicles, current state-of-the-art: emerging role of extracellular vesicles. *Cell. Mol. Life Sci.* **68,** 2667–2688 (2011).

229. Kosodo, Y. *et al.* Asymmetric distribution of the apical plasma membrane during neurogenic divisions of mammalian neuroepithelial cells. *EMBO J.* **23,** 2314–24 (2004).

230. Marzesco, A.-M. *et al.* Release of extracellular membrane particles carrying the stem cell marker prominin-1 (CD133) from neural progenitors and other epithelial cells. *J. Cell Sci.* **118,** (2005).

231. Rossi, F., McNagny, M., Smith, G., Frampton, J. & Graf, T. Lineage

commitment of transformed haematopoietic progenitors is determined by the level of PKC activity. *EMBO J.* **15,** 1894–901 (1996).

232. Zweibaum, A. [Differentiation of human colon cancer cells: a new approach to colon cancer]. *Bull. Acad. Natl. Med.* **177,** 63-71; discussion 71–3 (1993).

233. Nunukova, A. *et al.* Atypical nuclear localization of CD133 plasma membrane glycoprotein in rhabdomyosarcoma cell lines. *Int. J. Mol. Med.* (2015). doi:10.3892/ijmm.2015.2210

234. Cantile, M. *et al.* Nuclear localization of cancer stem cell marker CD133 in triple-negative breast cancer: a case report. *Tumori* **99,** e245-50

235. Huang, M., Zhu, H., Feng, J., Ni, S. & Huang, J. High CD133 Expression in the Nucleus and Cytoplasm Predicts Poor Prognosis in Non-Small Cell Lung Cancer. *Dis. Markers* **2015,** 1–8 (2015).

236. Zacchigna, S. *et al.* Loss of the cholesterol-binding protein prominin-1/CD133 causes disk dysmorphogenesis and photoreceptor degeneration. *J Neurosci* **29,** 2297–2308 (2009).

237. Liu, F. *et al.* Wnt/β-catenin signaling directs multiple stages of tooth morphogenesis. *Dev. Biol.* **313,** 210–224 (2008).

238. Zhang, Q. *et al.* Severe retinitis pigmentosa mapped to 4p15 and associated with a novel mutation in the PROM1 gene. *Hum. Genet.* **122,** 293–299 (2007).

239. Pras, E. *et al.* Cone-rod dystrophy and a frameshift mutation in the PROM1 gene. *Mol. Vis.* **15,** 1709–16 (2009).

240. Permanyer, J. *et al.* Autosomal Recessive Retinitis Pigmentosa with Early Macular Affectation Caused by Premature Truncation in *PROM1*. *Investig. Opthalmology Vis. Sci.* **51,** 2656 (2010).

241. Yang, Z. *et al.* Mutant prominin 1 found in patients with macular degeneration disrupts photoreceptor disk morphogenesis in mice. *J. Clin. Invest.* **118,** 2908–16 (2008).

242. Michaelides, M. *et al.* The PROM1 mutation p.R373C causes an autosomal dominant bull's eye maculopathy associated with rod, rod-cone, and macular dystrophy. *Invest. Ophthalmol. Vis. Sci.* **51,** 4771–80 (2010).

243. Rattner, A. *et al.* A photoreceptor-specific cadherin is essential for the structural integrity of the outer segment and for photoreceptor survival. *Neuron* **32,** 775–86 (2001).

244. Bonnet, D. & Dick, J. E. Human acute myeloid leukemia is organized as a hierarchy that originates from a primitive hematopoietic cell. *Nat. Med.* **3,** 730–7 (1997).

245. Shackleton, M., Quintana, E., Fearon, E. R. & Morrison, S. J. Heterogeneity in cancer: cancer stem cells versus clonal evolution. *Cell* **138,** 822–9 (2009).

246. Shackleton, M. *et al.* Generation of a functional mammary gland from a single stem cell. *Nature* **439,** 84–88 (2006).

247. Medema, J. P. Cancer stem cells: The challenges ahead. *Nat. Cell Biol.* **15,** 338–344 (2013).

248. Singh, S. K. *et al.* Identification of a cancer stem cell in human brain tumors. *Cancer Res.* **63,** 5821–8 (2003).

249. Chiou, S.-H. *et al.* Identification of CD133-Positive Radioresistant Cells in Atypical Teratoid/ Rhabdoid Tumor. *PLoS One* **3,** e2090 (2008).

250. Rappa, G., Fodstad, O. & Lorico, A. The Stem Cell-Associated Antigen CD133 (Prominin-1) Is a Molecular Therapeutic Target for Metastatic Melanoma. *Stem Cells* **26,** 3008–3017 (2008).

251. Hou, Y., Zou, Q., Ge, R., Shen, F. & Wang, Y. The critical role of CD133(+)CD44(+/high) tumor cells in hematogenous metastasis of liver cancers. *Cell Res.* **22,** 259–72 (2012).

252. Horst, D. *et al.* The cancer stem cell marker CD133 has high prognostic impact but unknown functional relevance for the metastasis of human colon cancer. *J. Pathol.* **219,** 427–434 (2009).

253. Kemper, K., Grandela, C. & Medema, J. P. Molecular identification and targeting of colorectal cancer stem cells. *Oncotarget* **1,** 387–95 (2010).

254. Karbanová, J. *et al.* The stem cell marker CD133 (Prominin-1) is expressed in various human glandular epithelia. *J. Histochem. Cytochem.* **56,** 977–93 (2008).

255. Yoshikawa, S. *et al.* Characterization of CD133+ parenchymal cells in the liver: histology and culture. *World J. Gastroenterol.* **15,** 4896–906 (2009).

256. Ogden, A. T. *et al.* Identification of A2B5+CD133- tumor-initiating cells in adult human gliomas. *Neurosurgery* **62,** 505-14; discussion 514–5 (2008).

257. Dong, T.-T. *et al.* Salinomycin Selectively Targets 'CD133+' Cell Subpopulations and Decreases Malignant Traits in Colorectal Cancer Lines. *Ann. Surg. Oncol.* **18,** 1797–1804 (2011).

258. Heavner, W. & Pevny, L. Eye development and retinogenesis. *Cold Spring Harb. Perspect. Biol.* **4,** (2012).

259. Hong, D.-H. *et al.* A retinitis pigmentosa GTPase regulator (RPGR)-deficient mouse model for X-linked retinitis pigmentosa (RP3). *Proc. Natl. Acad. Sci.* **97,** 3649–3654 (2000).

260. Li, T., Snyder, W. K., Olsson, J. E. & Dryja, T. P. Transgenic mice carrying the dominant rhodopsin mutation P347S: Evidence for defective vectorial transport of rhodopsin to the outer segments. *Neurobiology* **93,** 14176–14181 (1996).

261. Anderson, L. H., Boulanger, C. A., Smith, G. H., Carmeliet, P. & Watson,

C. J. Stem cell marker Prominin-1 regulates branching morphogenesis, but not regenerative capacity, in the mammary gland. doi:10.1002/dvdy.22539

262. Wiseman, B. S. *et al.* Site-specific inductive and inhibitory activities of MMP-2 and MMP-3 orchestrate mammary gland branching morphogenesis. *J. Cell Biol.* **162,** 1123–33 (2003).

263. Fargeas, C. A., Huttner, W. B. & Corbeil, D. No Title. **69,** (2007).

264. Wei, Y. *et al.* Activation of PI3K/Akt pathway by CD133-p85 interaction promotes tumorigenic capacity of glioma stem cells. *Proc. Natl. Acad. Sci. U. S. A.* **110,** 6829–34 (2013).

265. Mak, A. B. *et al.* Regulation of CD133 by HDAC6 promotes β-catenin signaling to suppress cancer cell differentiation. *Cell Rep.* **2,** 951–63 (2012).

266. Thesleff, I. The genetic basis of tooth development and dental defects. *Am. J. Med. Genet. Part A* **140A,** 2530–2535 (2006).

267. Järvinen, E., Tummers, M. & Thesleff, I. The role of the dental lamina in mammalian tooth replacement. *J. Exp. Zool. Part B Mol. Dev. Evol.* **312B,** 281–291 (2009).

268. Järvinen, E., Välimäki, K., Pummila, M., Thesleff, I. & Jernvall, J. The taming of the shrew milk teeth. *Evol. Dev.* **10,** 477–86

269. Stock, D. W. Zebrafish dentition in comparative context. *J. Exp. Zool. Part B Mol. Dev. Evol.* **308B,** 523–549 (2007).

270. Francis-West, P., Ladher, R., Barlow, A. & Graveson, A. Signalling interactions during facial development. *Mech. Dev.* **75,** 3–28 (1998).

271. Schneider, R. A. Neural Crest Can Form Cartilages Normally Derived from Mesoderm during Development of the Avian Head Skeleton. *Dev. Biol.* **208,** 441–455 (1999).

272. Mitsiadis, T. A., Chéraud, Y., Sharpe, P. & Fontaine-Pérus, J. Development of teeth in chick embryos after mouse neural crest transplantations. *Proc. Natl. Acad. Sci. U. S. A.* **100,** 6541–5 (2003).

273. Mitsiadis, T. A., Caton, J. & Cobourne, M. Waking-up the sleeping beauty: recovery of the ancestral bird odontogenic program. *J. Exp. Zool. Part B Mol. Dev. Evol.* **306B,** 227–233 (2006).

274. Keränen, S. V, Kettunen, P., Aberg, T., Thesleff, I. & Jernvall, J. Gene expression patterns associated with suppression of odontogenesis in mouse and vole diastema regions. *Dev. Genes Evol.* **209,** 495–506 (1999).

275. Peterková, R., Peterka, M., Viriot, L. & Lesot, H. Development of the vestigial tooth primordia as part of mouse odontogenesis. *Connect. Tissue Res.* **43,** 120–8 (2002).

276. Jernvall, J., Kettunen, P., Karavanova, I. & Martin, L. Evidence for the role of the enamel knot as a control center in mammalian tooth cusp formation:

non-dividing cells express growth stimulating Fgf-4 gene. *Int. J.* (2002).

277. Vaahtokari, A., Aberg, T., Jernvall, J., Keränen, S. & Thesleff, I. The enamel knot as a signaling center in the developing mouse tooth. *Mech. Dev.* **54,** 39–43 (1996).

278. Jernvall, J., Aberg, T., Kettunen, P. & Keranen, S. The life history of an embryonic signaling center: BMP-4 induces p21 and is associated with apoptosis in the mouse tooth enamel knot. (1998).

279. Åberg, T., Wozney, J. & Thesleff, I. Expression patterns of bone morphogenetic proteins (Bmps) in the developing mouse tooth suggest roles in morphogenesis and cell differentiation. *Dev. Dyn.* **210,** 383–396 (1997).

280. Sarkar, L. & Sharpe, P. T. *Expression of Wnt signalling pathway genes during tooth development*. *Mechanisms of Development* **85,** (1999).

281. Laurikkala, J., Pispa, J., Jung, H. & Nieminen, P. Regulation of hair follicle development by the TNF signal ectodysplasin and its receptor Edar. (2002).

282. Wang, X.-P. *et al.* Modulation of activin/bone morphogenetic protein signaling by follistatin is required for the morphogenesis of mouse molar teeth. *Dev. Dyn.* **231,** 98–108 (2004).

283. Lesot, H. *et al.* Mouse molar morphogenesis revisited by three-dimensional reconstruction. II. Spatial distribution of mitoses and apoptosis in cap to bell staged first and second upper molar teeth. *Int. J. Dev. Biol.* **40,** 1017–31 (1996).

284. PETERKOVÁ, R., PETERKA, M. & LESOT, H. The Developing Mouse Dentition. *Ann. N. Y. Acad. Sci.* **1010,** 453–466 (2003).

285. Berkovitz, B. K. B., Holland, G. R. (Graham R. & Moxham, B. J. *Oral anatomy, histology and embryology*. (Mosby/Elsevier, 2009).

286. Tummers, M. & Thesleff, I. Root or crown: a developmental choice orchestrated by the differential regulation of the epithelial stem cell niche in the tooth of two rodent species. *Development* **130,** 1049–57 (2003).

287. Tummers, M., Yamashiro, T. & Thesleff, I. Modulation of epithelial cell fate of the root in vitro. *J. Dent. Res.* **86,** 1063–7 (2007).

288. Pispa, J. & Thesleff, I. Mechanisms of ectodermal organogenesis. *Dev. Biol.* **262,** 195–205 (2003).

289. Tucker, A. & Sharpe, P. The cutting-edge of mammalian development; how the embryo makes teeth. *Nat. Rev. Genet.* **5,** 499–508 (2004).

290. Chai, Y. *et al.* Fate of the mammalian cranial neural crest during tooth and mandibular morphogenesis. *Development* **127,** 1671–9 (2000).

291. Jarvinen, E. *et al.* Continuous tooth generation in mouse is induced by activated epithelial Wnt/beta-catenin signaling. *Proc. Natl. Acad. Sci.* **103,**

18627–18632 (2006).

292. Kuraguchi, M. *et al.* Adenomatous Polyposis Coli (APC) Is Required for Normal Development of Skin and Thymus. *PLoS Genet.* **2,** e146 (2006).

293. Wang, X.-P. *et al.* Apc inhibition of Wnt signaling regulates supernumerary tooth formation during embryogenesis and throughout adulthood. *Development* **136,** 1939–1949 (2009).

294. Mina, M. & Kollar, E. J. The induction of odontogenesis in non-dental mesenchyme combined with early murine mandibular arch epithelium. *Arch. Oral Biol.* **32,** 123–7 (1987).

295. Ruch, J. V. Determinisms of odontogenesis. *Revis. Biol. Celular* **14,** 1–99 (1987).

296. Ahmad, N. & Ruch, J. V. Comparison of growth and cell proliferation kinetics during mouse molar odontogenesis in vivo and in vitro. *Cell Tissue Kinet.* **20,** 319–29 (1987).

297. Viriot, L., PETERKovA, R. & Vonesch, J. Mouse molar morphogenesis revisited by three-dimensional reconstruction. III. Spatial distribution of mitoses and apoptoses up to bell-staged first lower molar teeth. *Int. J.* (2003).

298. Lesot, H., Peterkova, R., Schmitt, R. & Meyer, J. Initial features of the inner dental epithelium histo-morphogenesis in the first lower molar in mouse. *Int. J.* (2002).

299. Rothová, M., Feng, J., Sharpe, P. T., Peterková, R. & Tucker, A. S. Contribution of mesoderm to the developing dental papilla. *Int. J. Dev. Biol.* **55,** 59–64 (2011).

300. Nait Lechguer, A., Kuchler-Bopp, S., Hu, B., Haïkel, Y. & Lesot, H. Vascularization of engineered teeth. *J. Dent. Res.* **87,** 1138–43 (2008).

301. Bloch-Zupan, A., Leveillard, T. & Gorry, P. Expression of p21WAF1/CIP1 during mouse odontogenesis. *Eur. J.* (1998).

302. Mitsiadis, T. A. & Graf, D. Cell fate determination during tooth development and regeneration. *Birth Defects Res. Part C Embryo Today Rev.* **87,** 199–211 (2009).

303. Jussila, M. & Thesleff, I. Signaling networks regulating tooth organogenesis and regeneration, and the specification of dental mesenchymal and epithelial cell lineages. *Cold Spring Harb. Perspect. Biol.* **4,** a008425 (2012).

304. Goldberg, M., Kulkarni, A. B., Young, M. & Boskey, A. Dentin: structure, composition and mineralization. *Front. Biosci. (Elite Ed).* **3,** 711–35 (2011).

305. Simmer, J. P. *et al.* Regulation of Dental Enamel Shape and Hardness. *J. Dent. Res.* **89,** 1024–1038 (2010).

306. Smith, C. E. & Nanci, A. Overview of morphological changes in enamel

organ cells associated with major events in amelogenesis. *Int. J. Dev. Biol.* **39,** 153–61 (1995).

307. Nanci, A. & Ten Cate, A. R. (Arnold R. *Ten Cate's oral histology : development, structure, and function.* (Elsevier, 2013).

308. Fincham, A. G. & Simmer, J. P. Amelogenin proteins of developing dental enamel. *Ciba Found. Symp.* **205,** 118-30; discussion 130–4 (1997).

309. Robinson, C., Brookes, S. J., Shore, R. C. & Kirkham, J. The developing enamel matrix: nature and function. *Eur. J. Oral Sci.* 282–91 (1998).

310. Simmer, J. P. & Fincham, A. G. Molecular mechanisms of dental enamel formation. *Crit. Rev. Oral Biol. Med.* **6,** 84–108 (1995).

311. Duan, X. Ion Channels, Channelopathies, and Tooth Formation. *J. Dent. Res.* **93,** 117–125 (2014).

312. Lu, Y. *et al.* Functions of KLK4 and MMP-20 in dental enamel formation. *Biol. Chem.* **389,** 695–700 (2008).

313. Mucchielli, M. L. & Mitsiadis, T. A. Correlation of asymmetric Notch2 expression and mouse incisor rotation. *Mech. Dev.* **91,** 379–82 (2000).

314. Ohshima, H. *et al.* The eternal tooth germ is formed at the apical end of continuously growing teeth. *Arch. Oral Biol.* **50,** 153–157 (2005).

315. Harada, H. *et al.* Localization of putative stem cells in dental epithelium and their association with Notch and FGF signaling. *J. Cell Biol.* **147,** 105–20 (1999).

316. Zhao, H. *et al.* Secretion of Shh by a Neurovascular Bundle Niche Supports Mesenchymal Stem Cell Homeostasis in the Adult Mouse Incisor. *Cell Stem Cell* **14,** 160–173 (2014).

317. Kaukua, N. *et al.* Glial origin of mesenchymal stem cells in a tooth model system. *Nature* **513,** 551–554 (2014).

318. Sharpe, P. T. Dental mesenchymal stem cells. *Development* **143,** 2273–80 (2016).

319. Tummers, M. & Thesleff, I. The importance of signal pathway modulation in all aspects of tooth development. *J. Exp. Zool. Part B Mol. Dev. Evol.* **312B,** 309–319 (2009).

320. Wang, X.-P. *et al.* An Integrated Gene Regulatory Network Controls Stem Cell Proliferation in Teeth. *PLoS Biol.* **5,** e159 (2007).

321. Cate, A. Ten. The role of epithelium in the development, structure and function of the tissues of tooth support. *Oral Dis.* **2,** 55–62 (2008).

322. Smith, C. E. & Warshawsky, H. Cellular renewal in the enamel organ and the odontoblast layer of the rat incisor as followed by radioautography using3H-thymidine. *Anat. Rec.* **183,** 523–561 (1975).

323. Seidel, K. *et al.* Hedgehog signaling regulates the generation of ameloblast progenitors in the continuously growing mouse incisor. *Development* **137,** 3753–61 (2010).

324. Suomalainen, M. & Thesleff, I. Patterns of Wnt pathway activity in the mouse incisor indicate absence of Wnt/β-catenin signaling in the epithelial stem cells. *Dev. Dyn.* **239,** NA-NA (2009).

325. Harada, H. *et al.* FGF10 maintains stem cell compartment in developing mouse incisors. **129,** 1533–1541 (2002).

326. Parsa, S. *et al.* Signaling by FGFR2b controls the regenerative capacity of adult mouse incisors. *Development* **137,** 3743–52 (2010).

327. Klein, O. D. *et al.* An FGF signaling loop sustains the generation of differentiated progeny from stem cells in mouse incisors. *Development* **135,** 377–85 (2008).

328. Zhao, H., Li, S., Han, D., Kaartinen, V. & Chai, Y. Alk5-mediated transforming growth factor β signaling acts upstream of fibroblast growth factor 10 to regulate the proliferation and maintenance of dental epithelial stem cells. *Mol. Cell. Biol.* **31,** 2079–89 (2011).

329. Yang, G. *et al.* Mesenchymal TGF-β Signaling Orchestrates Dental Epithelial Stem Cell Homeostasis Through Wnt Signaling. *Stem Cells* **32,** 2939–2948 (2014).

330. Plikus, M. V. *et al.* Morphoregulation of teeth: modulating the number, size, shape and differentiation by tuning Bmp activity. *Evol. <html_ent glyph="@amp;" ascii="&"/> Dev.* **7,** 440–457 (2005).

331. Andl, T. *et al.* Epithelial Bmpr1a regulates differentiation and proliferation in postnatal hair follicles and is essential for tooth development. *Development* **131,** 2257–68 (2004).

332. Kratochwil, K., Dull, M., Farinas, I., Galceran, J. & Grosschedl, R. Lef1 expression is activated by BMP-4 and regulates inductive tissue interactions in tooth and hair development. *Genes Dev.* **10,** 1382–94 (1996).

333. Szeto, D. P. *et al.* Role of the Bicoid-related homeodomain factor Pitx1 in specifying hindlimb morphogenesis and pituitary development. *Genes Dev.* **13,** 484–94 (1999).

334. Peters, H., Neubuser, A., Kratochwil, K. & Balling, R. Pax9-deficient mice lack pharyngeal pouch derivatives and teeth and exhibit craniofacial and limb abnormalities. *Genes Dev.* **12,** 2735–2747 (1998).

335. Bei, M. & Maas, R. FGFs and BMP4 induce both Msx1-independent and Msx1-dependent signaling pathways in early tooth development. *Development* **125,** 4325–33 (1998).

336. Hardcastle, Z., Mo, R., Hui, C. C. & Sharpe, P. T. The Shh signalling pathway in tooth development: defects in Gli2 and Gli3 mutants. *Development* **125,** 2803–11 (1998).

337. Oosterveen, T. *et al.* Mechanistic Differences in the Transcriptional Interpretation of Local and Long-Range Shh Morphogen Signaling. *Dev. Cell* **23,** 1006–1019 (2012).

338. Bhardwaj, G. *et al.* Sonic hedgehog induces the proliferation of primitive human hematopoietic cells via BMP regulation. *Nat. Immunol.* **2,** 172–180 (2001).

339. Gao, J. *et al.* Hedgehog Signaling Is Dispensable for Adult Hematopoietic Stem Cell Function. *Cell Stem Cell* **4,** 548–558 (2009).

340. Hofmann, I. *et al.* Hedgehog Signaling Is Dispensable for Adult Murine Hematopoietic Stem Cell Function and Hematopoiesis. *Cell Stem Cell* **4,** 559–567 (2009).

341. Cobourne, M. T., Hardcastle, Z. & Sharpe, P. T. Sonic hedgehog Regulates Epithelial Proliferation and Cell Survival in the Developing Tooth Germ. *J. Dent. Res.* **80,** 1974–1979 (2001).

342. Kumamoto, H. & Ohki, K. Detection of CD133, Bmi-1, and ABCG2 in ameloblastic tumors. *J. Oral Pathol. Med.* **39,** 87–93 (2010).

343. Kamijo, T. Role of stemness-related molecules in neuroblastoma. *Pediatr. Res.* **71,** 511–515 (2012).

344. Jacobs, J. J. L., Kieboom, K., Marino, S., DePinho, R. A. & van Lohuizen, M. The oncogene and Polycomb-group gene bmi-1 regulates cell proliferation and senescence through the ink4a locus. *Nature* **397,** 164–168 (1999).

345. Felszeghy, S., Suomalainen, M. & Thesleff, I. Notch signalling is required for the survival of epithelial stem cells in the continuously growing mouse incisor. *Differentiation* **80,** 241–248 (2010).

346. Avilion, A. A. *et al.* Multipotent cell lineages in early mouse development depend on SOX2 function. *Genes Dev.* **17,** 126–140 (2003).

347. Zhang, L. *et al.* Expression pattern of Sox2 during mouse tooth development. *Gene Expr. Patterns* **12,** 273–281 (2012).

348. Cuylen, S. *et al.* Ki-67 acts as a biological surfactant to disperse mitotic chromosomes. *Nature* **535,** 308–312 (2016).

349. Berbari, N. F., O'Connor, A. K., Haycraft, C. J. & Yoder, B. K. The Primary Cilium as a Complex Signaling Center. *Curr. Biol.* **19,** R526–R535 (2009).

350. Basten, S. G. & Giles, R. H. Functional aspects of primary cilia in signaling, cell cycle and tumorigenesis. *Cilia* **2,** 6 (2013).

351. Perdiz, D., Mackeh, R., Poüs, C. & Baillet, A. The ins and outs of tubulin acetylation: more than just a post-translational modification? *Cell. Signal.* **23,** 763–71 (2011).

352. Piperno, G., LeDizet, M. & Chang, X. J. Microtubules containing acetylated

alpha-tubulin in mammalian cells in culture. *J. Cell Biol.* **104,** 289–302 (1987).

353. Van der Heiden, K. *et al.* Endothelial primary cilia in areas of disturbed flow are at the base of atherosclerosis. *Atherosclerosis* **196,** 542–550 (2008).

354. Besschetnova, T. Y. *et al.* Identification of Signaling Pathways Regulating Primary Cilium Length and Flow-Mediated Adaptation. *Curr. Biol.* **20,** 182–187 (2010).

355. Izawa, I., Goto, H., Kasahara, K. & Inagaki, M. Current topics of functional links between primary cilia and cell cycle. *Cilia* **4,** 12 (2015).

356. Chang, J. Y. F. *et al.* Self-renewal and multilineage differentiation of mouse dental epithelial stem cells. *Stem Cell Res.* **11,** 990–1002 (2013).

357. Houlihan, D. D. *et al.* Isolation of mouse mesenchymal stem cells on the basis of expression of Sca-1 and PDGFR-α. *Nat. Protoc.* **7,** 2103–2111 (2012).

358. Emmert-Buck, M. R. *et al.* Laser capture microdissection. *Science* **274,** 998–1001 (1996).

359. Espina, V., Heiby, M., Pierobon, M. & Liotta, L. A. Laser capture microdissection technology. *Expert Rev. Mol. Diagn.* **7,** 647–657 (2007).

360. Bakondi, B. *et al.* CD133 identifies a human bone marrow stem/progenitor cell sub-population with a repertoire of secreted factors that protect against stroke. *Mol. Ther.* **17,** 1938–47 (2009).

361. Tondreau, T. *et al.* Mesenchymal Stem Cells Derived from CD133-Positive Cells in Mobilized Peripheral Blood and Cord Blood: Proliferation, Oct4 Expression, and Plasticity. *Stem Cells* **23,** 1105–1112 (2005).

362. Gygi, S. P., Rochon, Y., Franza, B. R. & Aebersold, R. Correlation between protein and mRNA abundance in yeast. *Mol. Cell. Biol.* **19,** 1720–30 (1999).

363. Liu, Y., Beyer, A. & Aebersold, R. Leading Edge Review On the Dependency of Cellular Protein Levels on mRNA Abundance. (2016). doi:10.1016/j.cell.2016.03.014

364. Hu, J. C.-C., Chun, Y.-H. P., Al Hazzazzi, T. & Simmer, J. P. Enamel Formation and Amelogenesis Imperfecta. *Cells Tissues Organs* **186,** 78–85 (2007).

365. Millar, S. E. *et al.* Over- and ectopic expression of Wnt3 causes progressive loss of ameloblasts in postnatal mouse incisor teeth. *Connect. Tissue Res.* **44 Suppl 1,** 124–9 (2003).

366. Rappa, G., Mercapide, J., Anzanello, F., Pope, R. M. & Lorico, A. Biochemical and biological characterization of exosomes containing prominin-1/CD133. *Mol. Cancer* **12,** 62 (2013).

367. Zhang, X., Diekwisch, T. G. H. & Luan, X. Structure and function of

ameloblastin as an extracellular matrix protein: adhesion, calcium binding, and CD63 interaction in human and mouse. *Eur. J. Oral Sci.* **119,** 270–279 (2011).

368. Wright, J. T. *et al.* The role of amelogenin during enamel-crystallite growth and organization in vivo. *Eur. J. Oral Sci.* **119 Suppl 1,** 65–9 (2011).

369. Fukumoto, S. *et al.* Ameloblastin is a cell adhesion molecule required for maintaining the differentiation state of ameloblasts. *J Cell Biol* **167,** 973–983 (2004).

370. Katsuta, O., Hoshino, N., Takeda, M., Ono, A. & Tsuchitani, M. A Spontaneous Mutation: Amelogenesis Imperfecta with Cysts in Rats. *Toxicol. Pathol.* **31,** 411–416 (2003).

371. Chavez, M. G. *et al.* Isolation and Culture of Dental Epithelial Stem Cells from the Adult Mouse Incisor. *J. Vis. Exp.* (2014). doi:10.3791/51266

372. Wöltgens, J. H., Lyaruu, D. M., Bronckers, A. L., Bervoets, T. J. & Van Duin, M. Biomineralization during early stages of the developing tooth in vitro with special reference to secretory stage of amelogenesis. *Int. J. Dev. Biol.* **39,** 203–12 (1995).

373. Chen, J., Zhang, Y., Mendoza, J. & DenBesten, P. Calcium-mediated differentiation of ameloblast lineage cells in vitro. *J. Exp. Zool. Part B Mol. Dev. Evol.* **312B,** 458–464 (2009).

374. Babajko, S., de La Dure-Molla, M., Jedeon, K. & Berdal, A. MSX2 in ameloblast cell fate and activity. *Front. Physiol.* **5,** 510 (2015).

375. Franken, N. A. P., Rodermond, H. M., Stap, J., Haveman, J. & van Bree, C. Clonogenic assay of cells in vitro. *Nat. Protoc.* **1,** 2315–2319 (2006).

376. Yang, D. *et al.* Short RNA duplexes produced by hydrolysis with Escherichia coli RNase III mediate effective RNA interference in mammalian cells. *Proc. Natl. Acad. Sci. U. S. A.* **99,** 9942–7 (2002).

377. Brentnall, M., Rodriguez-Menocal, L., De Guevara, R., Cepero, E. & Boise, L. H. Caspase-9, caspase-3 and caspase-7 have distinct roles during intrinsic apoptosis. *BMC Cell Biol.* **14,** 32 (2013).

378. Elledge, S. J. Cell cycle checkpoints: preventing an identity crisis. *Science* **274,** 1664–72 (1996).

379. Sakaue-Sawano, A. *et al.* Visualizing Spatiotemporal Dynamics of Multicellular Cell-Cycle Progression. *Cell* **132,** 487–498 (2008).

380. Scholzen, T. & Gerdes, J. The Ki-67 protein: From the known and the unknown. *J. Cell. Physiol.* **182,** 311–322 (2000).

381. Henderson, L., Lim, C. & Zambon, A. A live-cell reporter that differentiates between quiescent and cycling cells. *FASEB J.* **28,** 1148.14 (2014).

382. Mariani, L. E. *et al.* Arl13b regulates Shh signaling from both inside and

outside the cilium. *Mol. Biol. Cell* **27,** 3780 (2016).

383. Caspary, T., Larkins, C. E. & Anderson, K. V. The graded response to Sonic Hedgehog depends on cilia architecture. *Dev. Cell* **12,** 767–78 (2007).

384. Rimkus, T. K., Carpenter, R. L., Qasem, S., Chan, M. & Lo, H.-W. Targeting the Sonic Hedgehog Signaling Pathway: Review of Smoothened and GLI Inhibitors. *Cancers (Basel).* **8,** (2016).

385. Aldana-Masangkay, G. I. & Sakamoto, K. M. The role of HDAC6 in cancer. *J. Biomed. Biotechnol.* **2011,** 875824 (2011).

386. Waters, A. M. & Beales, P. L. Ciliopathies: an expanding disease spectrum. *Pediatr. Nephrol.* **26,** 1039–1056 (2011).

387. Lam, H. C. *et al.* Histone deacetylase 6–mediated selective autophagy regulates COPD-associated cilia dysfunction. *J. Clin. Invest.* **123,** 5212–5230 (2013).

388. Boyault, C., Sadoul, K., Pabion, M. & Khochbin, S. HDAC6, at the crossroads between cytoskeleton and cell signaling by acetylation and ubiquitination. *Oncogene* **26,** 5468–5476 (2007).

389. Lee, J.-Y. *et al.* HDAC6 controls autophagosome maturation essential for ubiquitin-selective quality-control autophagy. *EMBO J.* **29,** 969–80 (2010).

390. Larkins, C. E., Aviles, G. D. G., East, M. P., Kahn, R. A. & Caspary, T. Arl13b regulates ciliogenesis and the dynamic localization of Shh signaling proteins. *Mol. Biol. Cell* **22,** 4694–703 (2011).

391. Mak, A. B. *et al.* Regulation of CD133 by HDAC6 Promotes β-Catenin Signaling to Suppress Cancer Cell Differentiation. *Cell Rep.* **2,** 951–963 (2012).

392. Cohen, M. *et al.* Ptch1 and Gli regulate Shh signalling dynamics via multiple mechanisms. *Nat. Commun.* **6,** 6709 (2015).

393. Haycraft, C. J. *et al.* Gli2 and Gli3 Localize to Cilia and Require the Intraflagellar Transport Protein Polaris for Processing and Function. *PLoS Genet.* **1,** e53 (2005).

394. Schiapparelli, P. *et al.* Inhibition of the sonic hedgehog pathway by cyplopamine reduces the CD133+/CD15+ cell compartment and the in vitro tumorigenic capability of neuroblastoma cells. *Cancer Lett.* **310,** 222–231 (2011).

395. Dechat, T. *et al.* Nuclear lamins: major factors in the structural organization and function of the nucleus and chromatin. *Genes Dev.* **22,** 832–53 (2008).

396. Marfori, M. *et al.* Molecular basis for specificity of nuclear import and prediction of nuclear localization. *Biochim. Biophys. Acta - Mol. Cell Res.* **1813,** 1562–1577 (2011).

397. Boivin, D. *et al.* The stem cell marker CD133 (prominin-1) is phosphorylated

on cytoplasmic tyrosine-828 and tyrosine-852 by Src and Fyn tyrosine kinases. *Biochemistry* **48,** 3998–4007 (2009).

398. Lee, C. in 401–406 (2007). doi:10.1007/978-1-59745-257-1_31

399. Fredriksson, S. *et al.* Protein detection using proximity-dependent DNA ligation assays. *Nat. Biotechnol.* **20,** 473–477 (2002).

400. Stark, G. R. & Darnell, J. E. The JAK-STAT Pathway at Twenty. *Immunity* **36,** 503–514 (2012).

401. Igaz, P., Tóth, S. & Falus, A. Biological and clinical significance of the JAK-STAT pathway; lessons from knockout mice. *Inflamm. Res.* **50,** 435–441 (2001).

402. O'Shea, J. J., Gadina, M. & Schreiber, R. D. Cytokine signaling in 2002: new surprises in the Jak/Stat pathway. *Cell* **109 Suppl,** S121-31 (2002).

403. O'Shea, J. J., Holland, S. M. & Staudt, L. M. JAKs and STATs in Immunity, Immunodeficiency, and Cancer. *N. Engl. J. Med.* **368,** 161–170 (2013).

404. Babon, J. J., Sabo, J. K., Zhang, J.-G., Nicola, N. A. & Norton, R. S. The SOCS box encodes a hierarchy of affinities for Cullin5: implications for ubiquitin ligase formation and cytokine signalling suppression. *J. Mol. Biol.* **387,** 162–74 (2009).

405. Lou, Y., Xia, D., Yu, M., Tong, J. & Jin, J. Identification of an IRF-1 splicing transcript in APL cells sharing similar transactivation activity of the full length one. *Gene* **605,** 108–113 (2017).

406. Paun, A. & Pitha, P. M. The IRF family, revisited. *Biochimie* **89,** 744–753 (2007).

407. Garcia-Diaz, A. *et al.* Interferon Receptor Signaling Pathways Regulating PD-L1 and PD-L2 Expression. (2017). doi:10.1016/j.celrep.2017.04.031

408. Tsankov, A. M. *et al.* Transcription factor binding dynamics during human ES cell differentiation. *Nature* **518,** 344–349 (2015).

409. Wutz, A. in *Advances in experimental medicine and biology* **786,** 307–328 (2013).

410. Schwartz, Y. B. & Pirrotta, V. A new world of Polycombs: unexpected partnerships and emerging functions. *Nat. Rev. Genet.* **14,** 853–64 (2013).

411. Ding, X., Lin, Q., Ensenat-Waser, R., Rose-John, S. & Zenke, M. Polycomb Group Protein Bmi1 Promotes Hematopoietic Cell Development from Embryonic Stem Cells. doi:10.1089/scd.2010.0539

412. Tian, H. *et al.* A reserve stem cell population in small intestine renders Lgr5-positive cells dispensable. *Nature* **478,** 255–259 (2011).

413. Paranjape, A. N. *et al.* Bmi1 regulates self-renewal and epithelial to mesenchymal transition in breast cancer cells through Nanog. *BMC Cancer*

14, 785 (2014).

414. Siddique, H. R. & Saleem, M. Role of BMI1, a Stem Cell Factor, in Cancer Recurrence and Chemoresistance: Preclinical and Clinical Evidences. *Stem Cells* **30,** 372–378 (2012).

415. Jacobs, J. J. L., Kieboom, K., Marino, S., DePinho, R. A. & van Lohuizen, M. The oncogene and Polycomb-group gene bmi-1 regulates cell proliferation and senescence through the ink4a locus. *Nature* **397,** 164–168 (1999).

416. Pérez-Mancera, P. A., Young, A. R. J. & Narita, M. Inside and out: the activities of senescence in cancer. *Nat. Rev. Cancer* **14,** 547–558 (2014).

417. Hosen, N. *et al.* Bmi-1-green fluorescent protein-knock-in mice reveal the dynamic regulation of bmi-1 expression in normal and leukemic hematopoietic cells. *Stem Cells* **25,** 1635–1644 (2007).

418. Sobecki, M. *et al.* Cell-Cycle Regulation Accounts for Variability in Ki-67 Expression Levels. *Cancer Res.* **77,** 2722–2734 (2017).

419. Seidel, K. *et al.* Resolving stem and progenitor cells in the adult mouse incisor through gene co-expression analysis. *Elife* **6,** (2017).

420. Stone, D. M. *et al.* The tumour-suppressor gene patched encodes a candidate receptor for Sonic hedgehog. *Nature* **384,** 129–134 (1996).

421. Giebel, B. *et al.* Segregation of lipid raft markers including CD133 in polarized human hematopoietic stem and progenitor cells. *Blood* **104,** 2332–2338 (2004).

422. Lewis, P. M. *et al.* Cholesterol modification of sonic hedgehog is required for long-range signaling activity and effective modulation of signaling by Ptc1. *Cell* **105,** 599–612 (2001).

423. Gardner, K., Arnoczky, S. P. & Lavagnino, M. Effect of in vitro stress-deprivation and cyclic loading on the length of tendon cell cilia in situ. *J. Orthop. Res.* **29,** 582–587 (2011).

424. Li, B. *et al.* Increased hedgehog signaling in postnatal kidney results in aberrant activation of nephron developmental programs. *Hum. Mol. Genet.* **20,** 4155–66 (2011).

425. Karavanova, I. D., Dove, L. F., Resau, J. H. & Perantoni, A. O. Conditioned medium from a rat ureteric bud cell line in combination with bFGF induces complete differentiation of isolated metanephric mesenchyme. *Development* **122,** (1996).

426. Lin, Y. *et al.* Induced repatterning of type XVIII collagen expression in ureter bud from kidney to lung type: association with sonic hedgehog and ectopic surfactant protein C. *Development* **128,** (2001).

427. Zhang, F. *et al.* Characterization of Glis2, a novel gene encoding a Gli-related, Krüppel-like transcription factor with transactivation and repressor

functions. Roles in kidney development and neurogenesis. *J. Biol. Chem.* **277,** 10139–49 (2002).

428. Bellusci, S. *et al.* Involvement of Sonic hedgehog (Shh) in mouse embryonic lung growth and morphogenesis. *Development* **124,** (1997).

429. Yu, G.-F., Lin, X., Luo, R.-C. & Fang, W.-Y. *Original Article Nuclear CD133 expression predicts poor prognosis for hepatocellular carcinoma*. *Int J Clin Exp Pathol* **11,** (2018).

430. Timney, B. L. *et al.* Simple rules for passive diffusion through the nuclear pore complex. *J. Cell Biol.* **215,** 57–76 (2016).

431. Cautain, B., Hill, R., de Pedro, N. & Link, W. Components and regulation of nuclear transport processes. *FEBS J.* **282,** 445–462 (2015).

432. Lin, J. & Hu, J. SeqNLS: Nuclear Localization Signal Prediction Based on Frequent Pattern Mining and Linear Motif Scoring. *PLoS One* **8,** e76864 (2013).

433. Seo, H. G. *et al.* Identification of the nuclear localisation signal of O-GlcNAc transferase and its nuclear import regulation. *Sci. Rep.* **6,** 34614 (2016).

434. Smoyer, C. J. & Jaspersen, S. L. Breaking down the wall: the nuclear envelope during mitosis. *Curr. Opin. Cell Biol.* **26,** 1–9 (2014).

435. Wu, Y.-C., Zhu, M. & Robertson, D. M. Novel nuclear localization and potential function of insulin-like growth factor-1 receptor/insulin receptor hybrid in corneal epithelial cells. *PLoS One* **7,** e42483 (2012).

436. Tierney, M. T. *et al.* STAT3 signaling controls satellite cell expansion and skeletal muscle repair. *Nat. Med.* **20,** 1182–1186 (2014).

437. Galoczova, M., Coates, P. & Vojtesek, B. STAT3, stem cells, cancer stem cells and p63. *Cell. Mol. Biol. Lett.* **23,** 12 (2018).

438. Gupta, S., Takebe, N. & Lorusso, P. Targeting the Hedgehog pathway in cancer. *Ther. Adv. Med. Oncol.* **2,** 237–50 (2010).

439. Stalmans, I. *et al.* Arteriolar and venular patterning in retinas of mice selectively expressing VEGF isoforms. *J Clin Invest* **109,** 327–336 (2002).

440. Reya, T., Morrison, S. J., Clarke, M. F. & Weissman, I. L. Stem cells, cancer, and cancer stem cells. *Nature* **414,** 105–111 (2001).

441. Plaks, V., Kong, N. & Werb, Z. The cancer stem cell niche: how essential is the niche in regulating stemness of tumor cells? *Cell Stem Cell* **16,** 225–38 (2015).

442. Gajadhar, A. & Guha, A. A proximity ligation assay using transiently transfected, epitope-tagged proteins: application for in situ detection of dimerized receptor tyrosine kinases. *Biotechniques* **48,** 145–152 (2010).

443. Risnes, S., Septier, D. & Goldberg, M. Accelerated eruption of rat lower

incisor. Relationship between impeded and unimpeded eruption rates, rate of attrition, tooth length, and production of dentin and enamel. *Connect. Tissue Res.* **32,** 183–9 (1995).

444. Risnes, S. Multiangular viewing of dental enamel in the SEM: an apparatus for controlled mechanical specimen preparation. *Scand. J. Dent. Res.* **93,** 135–8 (1985).

445. Risnes, S. Multiangular viewing of dental enamel in the SEM: a simple specimen holder system. *Scand. J. Dent. Res.* **90,** 80–2 (1982).

446. Brewer, G. J. & Cotman, C. W. Survival and growth of hippocampal neurons in defined medium at low density: advantages of a sandwich culture technique or low oxygen. *Brain Res* **494,** 65–74 (1989).

447. DULBECCO, R. & FREEMAN, G. Plaque production by the polyoma virus. *Virology* **8,** 396–7 (1959).

448. HAM, R. G. CLONAL GROWTH OF MAMMALIAN CELLS IN A CHEMICALLY DEFINED, SYNTHETIC MEDIUM. *Proc. Natl. Acad. Sci. U. S. A.* **53,** 288–93 (1965).

449. Chen, X., Shen, Y. Detection of Copy Number Variants Reveals Association of Cilia Genes with Neural Tube Defects. PLOS one. Vol 8. (2013)450.

450. Schuldiner, Benvenisty. Effects of eight growth factors on the differentiation of cells derived from human embryonic stem cells. PNAS. 2000 97 (21) 11307-11312451.

451. van de Wetering, et al.The beta-catenin/TCF-4 complex imposes a crypt progenitor phenotype on colorectal cancer cells. Cell, 111 2002

452. van der Flier, Clevers Stem cells, self-renewal, and differentiation in the intestinal epithelium Annu. Rev. Physiol., 71 2009

453. Barker, Clevers. Lgr5+ve stem/progenitor cells contribute to nephron formation during kidney development. Cell Rep. 2 (3) 2012

454. Sanz-Navarro M., Amendt B.: Plasticity within the niche ensures the maintenance of a Sox2+ stem cell population in the mouse incisor. Development 2018